




Universitat Autònoma de Barcelona

ADVERTIMENT. L'accés als continguts d'aquesta tesi queda condicionat a l'acceptació de les condicions d'ús establertes per la següent llicència Creative Commons:  http://cat.creativecommons.org/?page_id=184

ADVERTENCIA. El acceso a los contenidos de esta tesis queda condicionado a la aceptación de las condiciones de uso establecidas por la siguiente licencia Creative Commons:  <http://es.creativecommons.org/blog/licencias/>

WARNING. The access to the contents of this doctoral thesis it is limited to the acceptance of the use conditions set by the following Creative Commons license:  <https://creativecommons.org/licenses/?lang=en>



From nanoparticles to graphene: architecting novel (bio)sensing platforms and devices

Luis Miguel Baptista Pires

Thesis dissertation to apply for the PhD in Biotechnology

Department of Genetics and microbiology - Faculty of Biosciences

Autonomous University of Barcelona

PhD director

Prof. Arben Merkoçi

ICREA & Nanobioelectronics and Biosensors Group
Institut Català de Nanociència i Nanotecnologia (ICN2)

2016

Acknowledgement for the financial and logistical support

Acknowledgments are given for the financial support from Spanish MINECO under Project grant MAT2011-25870 for BES-2012-056022, the Generalitat de Catalunya for the project 2014SGR-260 and FP7 for projects under number 315653 “POC4PETS”



tion of PTHrP using n
immunoassa



ndwich

e by ICN group as a contribution to the project:

tion of the calcium sensing receptor as a potential new tumor suppressor
gene and therapeutic target in neuroblastoma”.



A mi amor, mi familia, Marta Martínez Suarez, que me inspira, me llena el corazón, y es el sol y la luna de todos mis días. Es un extasíe vivir cada día a tu lado y compartir la emoción de vivir este viaje que es la vida juntos! Que vengan más y más días, muchos, infinitos, para que sigamos cambiando el mundo, poder perderme en tu mirada e juntar nuestros corazones para que sigan charlando en nuestro silencio!

Aos meus pais, Luis Miguel Martins Pires y Rosa Maria dos Santos Baptista Pires, e á minha irma, Marta Baptista Pires. A saudade, esse sentimento tao bonito e tao triste faz parte das nossas vidas, mas a forza e a educacao da vida que me deram fazem-me viver cada dia sentindo que estao aqui ao meu lado, vendo e vivendo cada momento da minha vida. Adoro-vos, amo-vos e tenho um orgulho enorme de fazer parte de uma familia tao bonita como a nossa!

E aos meus avôs e avós, para que nos sigam guiando com os seus sorrisos e maestria...!

Index

Preface	I
Optical abstracts	II
Thesis overview.....	IV
Chapter 1- introduction	1
1. Nanotechnology	2
2. (Bio)sensing systems.....	4
3. Nanomaterials	5
3.1 Gold nanoparticles and Magnetic beads.....	8
3.2 Carbon nanomaterials: the graphene rise.....	10
3.2.1 Graphene materials production.....	12
3.2.1.1 Pristine graphene.....	14
3.2.1.2 Graphene polycrystalline.....	15
3.2.1.3 Graphene oxide.....	17
3.2.1.3.1 Graphene oxide architected materials.....	19
3.2.1.3.1.1 Graphene oxide quantum dots.....	20
3.2.1.3.1.2 Graphene oxide fibers.....	23
3.2.1.3.1.3 Graphene oxide foams.....	25
3.2.1.3.1.4 Graphene oxide scrolls.....	26
3.2.1.3.2 Why graphene oxide? An insight look over graphene oxide applications.	28
3.2.1.3.3 Graphene oxide printing and patterning.....	31

3.2.1.3.4 Graphene oxide morphology over printed methodologies.....	34
3.2.1.3.5 Graphene oxide electrochemical properties and applications.....	36
Chapter 2 – Objectives.....	55
Chapter 3- Electrochemical detection of an immunosandwich using nanoparticles.....	59
Chapter 4- Electrocatalytic tune of screen printed electrodes with graphene oxide.....	91
Chapter 5- Printing graphene oxide using wax printed membranes	113
Chapter 6- General conclusion and future perspective.....	147
Annex A - Compendium of publications.....	151
Acknowledgements	

Preface

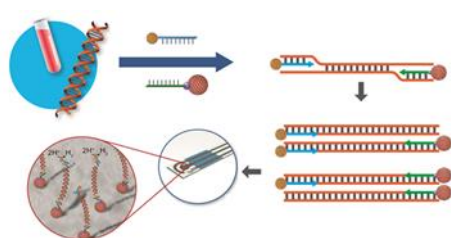
The present PhD thesis has been carried out mainly in the Nanobioelectronics and Biosensors Group of the Catalan Institute of Nanoscience and Nanotechnology (ICN2). According to the decision of the PhD Commission of the Autonomous University of Barcelona, this PhD thesis is presented as a compendium of publications.

All the publications and manuscripts are listed below following their appearance in the thesis:

- 1) Alfredo de la Escosura-Muñiz, Luis Baptista-Pires, Lorena Serrano, Laura Altet, Olga Francino, Armand Sánchez, Arben Merkoçi, Magnetic bead/gold nanoparticle double-labeled primers for electrochemical detection of isothermal amplified Leishmania DNA. *Small*, 2015. **12**(2):p.205-2013
- 2) Luis Baptista-Pires, B. Pérez-López, Carmen C. Mayorga-Martinez, Eden Morales-Narváez , Neus Domingo , Maria Jose Esplandiu , Francesc Alzina , C. M. Sotomayor Torres and A. Merkoçi, Electrocatalytic tuning of biosensing response through electrostatic or hydrophobic enzyme-graphene oxide interactions. *Biosensors & Bioelectronics*, 2014. **61**: p. 655-662.
- 3) Luis Baptista-Pires, Carmen C. Mayorga-Martínez, Mariana Medina-Sánchez, Helena Montón and Arben Merkoçi, Water Activated Graphene Oxide Transfer Using Wax Printed Membranes for Fast Patterning of a Touch Sensitive Device. *Acs Nano*, 2016. **10**(1): p. 853-860.

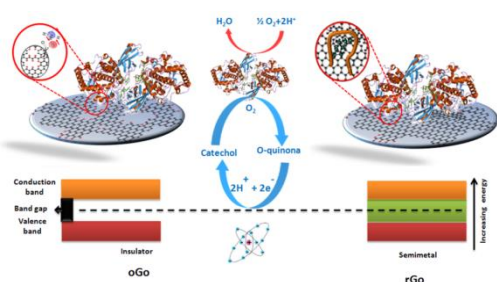
Optical abstracts

- 1) **Alfredo de la Escosura-Muñiz, Luis Baptista-Pires, Lorena Serrano, Laura Altet, Olga Francino, Armand Sánchez, Arben Merkoçi, Magnetic bead/gold nanoparticle double-labeled primers for electrochemical detection of isothermal amplified Leishmania DNA. Small, 2015. 12(2):p.205-2013**



A novel methodology for the isothermal amplification of *Leishmania* DNA using labeled primers combined with the advantages of magnetic purification/preconcentration and the use of gold nanoparticle (AuNPs) tags for the sensitive electrochemical detection of such amplified DNA is developed.

- 2) **Luis Baptista-Pires, B. Pérez-López, Carmen C. Mayorga-Martínez, Eden Morales-Narváez, Neus Domingo, María Jose Esplandiú, Francesc Alzina, C. M. Sotomayor Torres and A. Merkoçi, Electrocatalytic tuning of biosensing response through electrostatic or hydrophobic enzyme-graphene oxide interactions. Biosensors & Bioelectronics, 2014. 61: p. 655-662.**



The influence of graphene oxidative grades, concerning their clear influence on conductivity and hydrophobicity upon biosensing response is studied. Different levels of graphene oxide results on changes of (bio)conjugation properties occurring at enzyme/graphene oxide interface mainly due to the electrostatic or

hydrophobic interactions with biomolecules in comparison with bare screen printing electrodes. Tyrosinase enzyme as a proof of concept receptor with interest for phenolic compounds detection is tested through its direct adsorption onto SPE previously modified with highly oxidized graphene oxide reduced graphene oxide. The electrochemical responses of this reduced graphene oxide have been compared with the responses obtained for graphene oxide and their electrochemical performance has been accordingly discussed with various evidences obtained by optical techniques.

- 3) ***Luis Baptista-Pires, Carmen C. Mayorga-Martínez, Mariana Medina-Sánchez, Helena Montón and Arben Merkoçi, Water Activated Graphene Oxide Transfer Using Wax Printed Membranes for Fast Patterning of a Touch Sensitive Device. ACS Nano, 2016. 10(1): p. 853-860.***



A methodology for fast patterning and transfer graphene oxide using water activated wax printed membranes with infinite shaping capability is presented.

Water activation transfer of patterned GO over flexible substrates using the roll-to-roll mechanism for rapid building of plastic, paper or textile electronic platforms is demonstrated. A touch sensitive device over PET for switching on and off a LED is produced.

Thesis overview

This PhD thesis is divided in 6 chapters where we discuss the importance of nanomaterials for designing novel biosensors and devices. **Chapter 1** is a review about the nanomaterials history, their importance in (bio)sensing strategies and how we applied them in the projects presented in further chapters. A deep study over graphene materials and architectures is presented and their applications are described. In this chapter, we want the reader to be clarified about the importance of nanomaterials such as gold nanoparticles (AuNPs), magnetic beads (MB) and graphene-based materials for the development of portable and wearable devices that might come into day-life in the near future.

In **Chapter 2** the objective of the thesis are explained.

In **Chapter 3** a biosensor using screen printing carbon electrodes (SPCE) as electrical transducer for the detection of leishmania is presented. The manuscript entitled “Magnetic bead/gold nanoparticle double-labeled primers for electrochemical detection of isothermal amplified Leishmania” (Small, 2015. 12(2):p.205-2013) introduces the possibility for low temperature DNA amplification in the presence of labeled AuNPs and MB with primers using isothermal amplification. The AuNPs enable electrochemical detection and the MB for cleaning the excess of unbounded primers opening the opportunity for fast electrochemical detection on the surface of the SPCE.

In **Chapter 4**, the tuning of a SPCE with graphene oxide (GO) and reduced GO (RGO) was performed for the detection of catechol using enzyme immobilized onto the surface of the SPCE. The publication is entitled “Electrocatalytic tuning of biosensing response through electrostatic or hydrophobic enzyme-graphene oxide interactions” (Biosensors & Bioelectronics, 2014. **61**: p. 655-662). GO and RGO were characterized either optically and electrochemically to understand the influence of the materials properties to the electrochemical performance. Enzyme was immobilized by simple drop casting and adsorbed over the

modified SPCE working electrode with GO and RGO and the electrocatalytic tune was obvious in the presence of graphene based materials.

In the **Chapter 5**, a novel GO printing technology is presented using wax printed membranes and the published article entitled: “Water Activated Graphene Oxide Transfer Using Wax Printed Membranes for Fast Patterning of a Touch Sensitive Device, Acs Nano, 2016. **10**(1): p. 853-860). This technology have enabled to print GO over a wide variety of substrates such as plastic, paper or textile. The technique is simple, low cost and doesn't need for personnel with expertise, enabling for rapid prototyping with unlimited shaping capabilities. A touch sensitive device is described for turning on/off a LED.

Finally, in **Chapter 6** the general conclusions and the future perspectives are discussed.

The **Annex A** lists all the publications accepted by the commission (including their supporting informations) for this thesis.

Chapter 1**Introduction**

This introductory chapter aims to give the reader the basis to understand the importance of biosensors and nanomaterials. Particular focus will be done in the evolution of (bio)sensors, the nanomaterials applications in immunosensors that involve gold nanoparticles or magnetic beads and the interest and role of graphene materials in developing novel (bio)sensing applications.

1. Nanotechnology

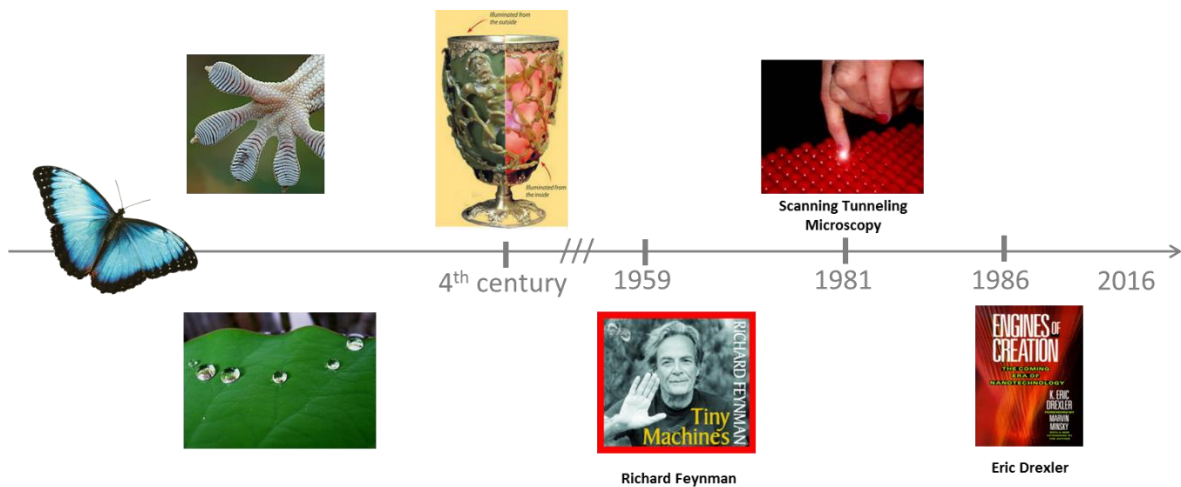


Figure 1. Chronography of the history of nanotechnology.

Feynman in 1959 in a simple after dinner talking has determined the start of a new way of looking at science and gave rise to a new field of research called nowadays nanotechnology. At that time Feynman, simply introduced the concept of “molecular manufacturing” - “I am not afraid to consider the final question as to whether, ultimately – in the great future – we can arrange the way we want , the very atom all the way down!” (*there is a plenty of room at the bottom*). Erix Drexler for instance in 1986 wrote a book (*Engines of Creation: The Coming Era of Nanotechnology*) envisioning that nanoscale managing would change industry and technology as the way we were seeing it before and introduce nanomachines with a billion of nanomachines inside from medicinal robots that help clear capillaries to environmental scrubbers that clear pollutants from the air. We have already got into it in our last living live decade, using transistor and chips in everyday life electronic technology.

Although, nanotechnology is widely present in nature, where the downscale reveals impressive characteristics such as hydrophobic effect of a Lotus which able this plant for self-cleaning; the gecko ability to walk over the walls; the peacock wing or the butterfly wings with their amazing optical patterns. All these are biological features from nature that were reproduced recently in laboratories using nanomaterials or nanopatterns. In ancient times, the nanotechnology

have already been developed by man (possibly without knowing) and were present in glasses of churches which change colors upon the sunrise, or in a cup. This cup, the Lycurgus Cup is a glass from the 4th century which was done using a colloidal nanoparticles (70 nm) suspension of gold and silver which is responsible for the dichroic effect (red/green).

Nowadays, we are able to manipulate single atoms using a technique as simple as Scanning Tunneling Microscopy (STM). The question is how to establish an end to our nanoscale managing and which direct research fields should focus. From nanotechnology advances we got nanomedicine, nanoelectronics, nanobiosensing, nanomechanics, nanophotonics, nanoionics and recently quantum nanoelectronics giving rise to quantum computers and the management of quarks. All this research areas are of most importance and the creation of nanomaterials have created tools to re-arrange old techniques where the use of carbon based nanomaterials, gold nanoparticles, nanocore-shell particles and quantum dots for example have been identified to have manufacturers. Forward in this work, we will discuss how the nanomaterials like gold nanoparticles (AuNPs), magnetic beads (MBs) or graphene can produce novel sensing and biosensing systems and discuss material architecture specially in graphene materials for the development of (bio)sensing systems.

2. (Bio)sensing systems

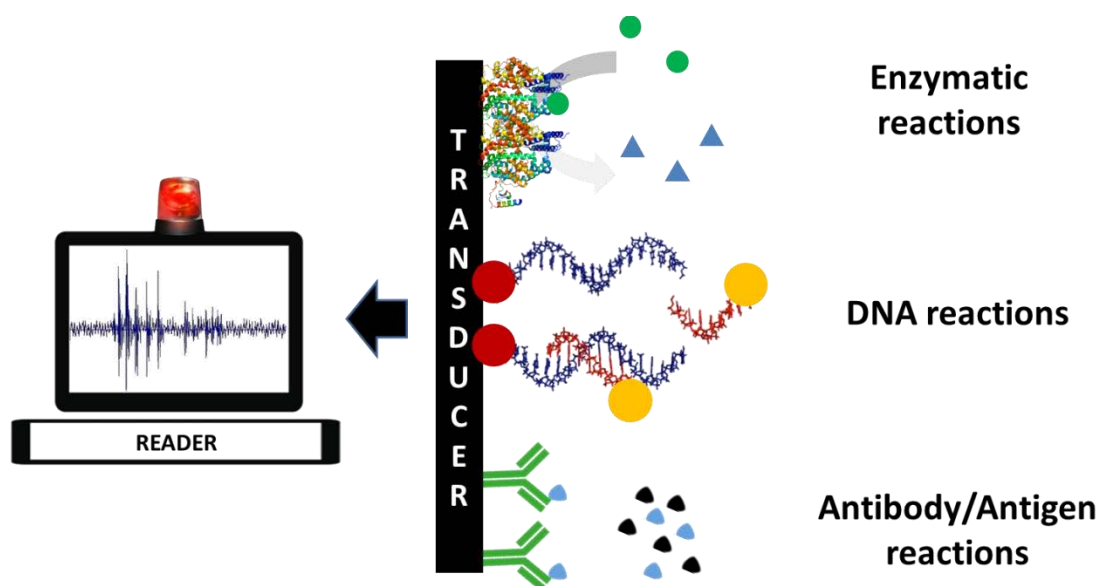


Figure 2. Scheme of the principal components of a biosensor and their functions. The case of an electrochemical biosensor is shown. Optical or mass changes can also be produced leading to other kinds of transducers (i.e. optical, piezoelectric etc.).

Sensors and biosensors are devices formed by a transducer and a receptor. The receptor in the case of biosensors recognizes an analyte, enabling to sense biochemical or chemical compounds through very highly specific (bio)chemical reactions and can be constituted by enzymes, proteins or DNA in between others (figure 2). The transducer transmits the signal produced upon the (bio)chemical recognition event as an electrical, optical or other output. The absence of receptors has also been used for the development of the so-called label free biosensors that take advantage of the transducer affinity to specific molecules.

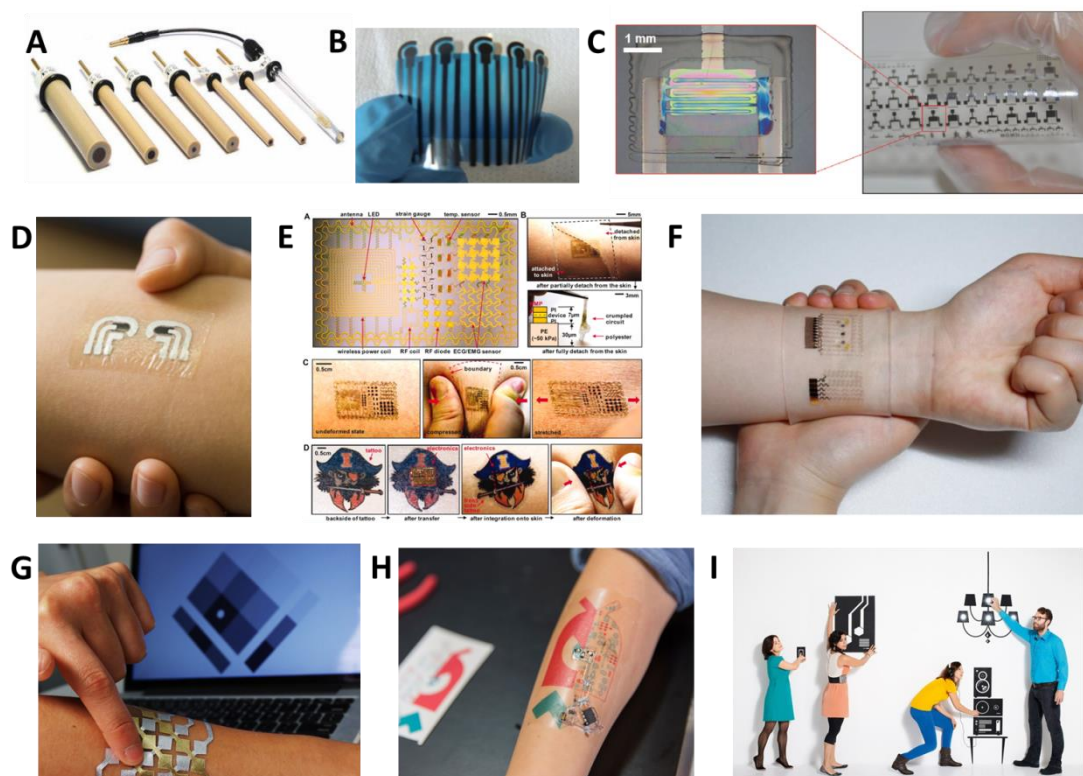


Figure 3. Sensors overview: A) GC electrodes (reprinted with permission from reference [1]) ; B) SPCE; C) inkjet printed transistor (reprinted with permission from reference [2]) ; D) silver pen printed electrodes (reprinted with permission from reference [3]); E) tattoo like sensors (reprinted with permission from reference [4]); F) wearable graphene based electrochemical sensors enabling theranostic (reprinted with permission from reference [5]); G) jewel like sensors (reprinted with permission from reference [6]); H) tattoo like sensor with incorporated traditional electronics (reprinted with permission from reference [7]); I) home touch sensors using carbon paint (reprinted with permission from reference [8]).

Electrochemical biosensors have been widely used in recent years and have undergone through an immense evolution in terms of portability, flexibility, wearability and human-machine interaction. For instance, the glassy carbon electrodes (GCE) represented in figure 3A, one of the most used electrodes for biosensing applications is a rigid electrode composed of a carbon paste normally used in a three electrode system composed of a GCE as working electrode, platinum (Pt) as a counter electrode and a silver(ag)/silver

chloride(AgCl) reference electrode. These electrodes are highly feasible and can be reused by simply polishing the surface[9]. Nevertheless they lack portability and for personal use are quite problematic. In this way screen printing electrodes (SPE) produced using a screen printing technology which is common for printing t-shirts came to innovate in a sense of miniaturization and portability (figure 3B) [10]. These can be printed over a wide variety of substrates: flexible as plastics and non-flexible as ceramics. They are disposable, for example glucose biosensor, one of the most worldwide used biosensor for diabetes control. SPEs are fabricated through a sequential deposition of layers of different conductive or non-conductive inks on a variety of inert substrates. Nowadays, screen-printing microfabrication technology is well-established for the mass production of thick film electrodes and it is widely applied to build biological or chemical sensors. The need for smaller and more tiny electrodes have attracted much attention in the electrode field for biosensing in which photolithography or inkjet printing have played an important role[2]. Field effect transistors have been developed for biosensing proposes also over flexible or rigid substrates reducing even more the volume of analyte or the receptor concentration which have important advantages in the price or the sample volume (ex. blood) extracted from a patient for instance (figure 3C). These techniques in between others somehow have made biosensors and sensors to perform better, use less sample volumes, to be flexible and disposable. Some other techniques have been used such as simply drawing with a pen a carbon or a silver paste as represented in figure 3D [3]. This has introduced the ability for the absence of laboratory facilities or specialized people with specific printing know how. Another important advance was the development of novel substrates that can be stretched and are transparent that were able to have skin like appearance [4, 11, 12]. The formation of electronic devices over these substrates has permitted to develop tattoo like sensors (figure 3E) [4]. This is a quite big change in how we see biosensors and a direction that envisions the wearability of these devices performing in day-life. The addition of extra electronic capabilities in these sensors such as wireless communication or near field communication (NFC) makes a step forward in human-machine interface with automatic responses such as the in-situ therapy enabling theranostic (figure 3F) [4, 5]. Reorganizing components of biosensing platform is still a

challenge, ethical aspects also are and how to prove the need of real time sensors or biosensors without medical observation is still a challenge. Despite this, sensing technologies are getting in fields like design or architecture; communities such as do-it-yourself (DiY) or internet-of-things (IOT) are coming into play for sensors and biosensors making these more connected. The beauty of the devices are upcoming with jewel like tattoos (figure 3G), the coolness in wearing an electronic tattoo with LED incorporated being there (figure 3H) and the human-machine interface at home is no more a promise (figure 3I) [6-8]. Biosensors are changing, are more attractive and effective, communicative, and can already take automatic decisions leading to a society that can be more responsible for their medical problems encouraging for a better life quality and personal knowledge of their body.

.

3. Nanomaterials

3.1 Gold nanoparticles and magnetic beads

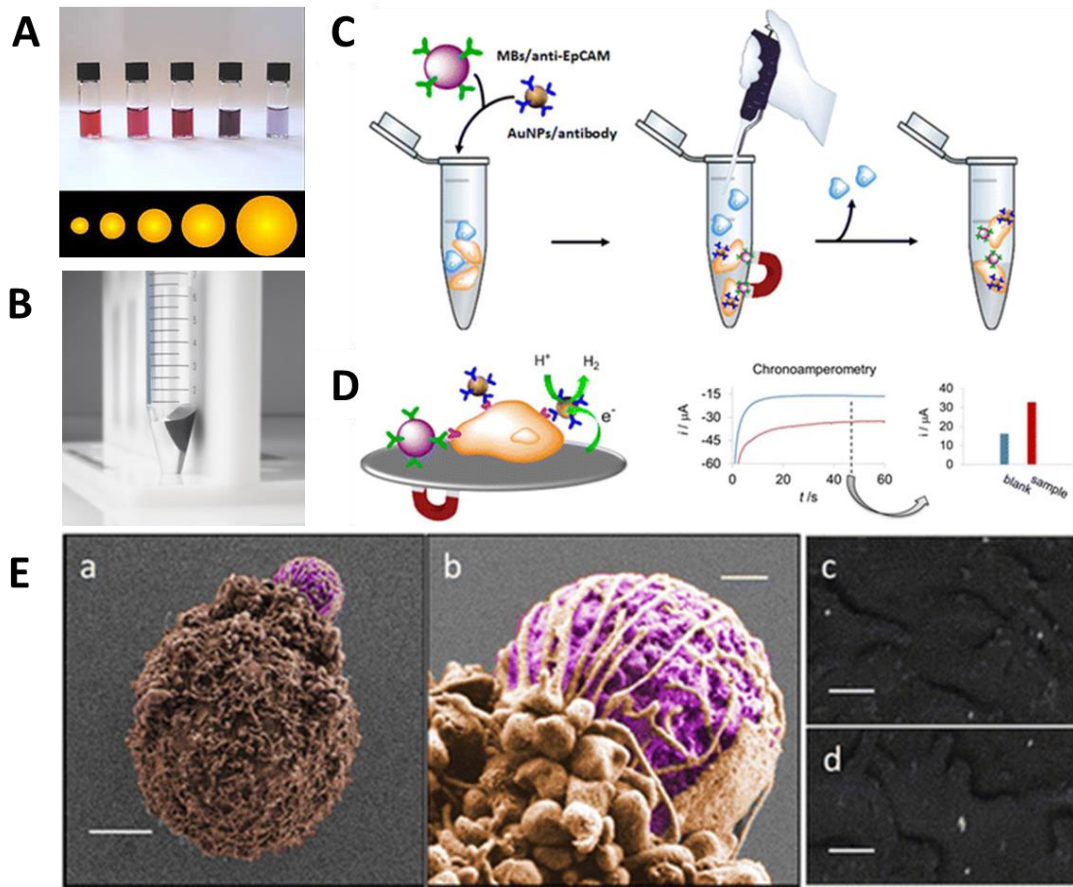


Figure 4. Biosensing using AuNP and MB. A) AuNP influence of size in colour absorbed (reprinted with permission from reference [13]); B) MB under applied magnetic field (reprinted with permission from reference [14]); C) schematics of magnetosandwich incubation and separation for the capture of Caco2 cells (reprinted with permission from reference [15]); D) electrochemical detection of magnetosandwich using SPCE and chronoamperometry ; E) Scanning electron microscopy. (a–d) Caco2 cells captured with MB/anti-EpCAM and simultaneously labeled with AuNPs/anti-EpCAM, in the presence of THP-1 cells. (a, b) SEM images of a Caco2 cell captured by MBs/anti-EpCAM. (c, d) Higher magnification backscattered images of the Caco2 cell surface showing AuNPs distributed along the cell plasma membrane. Scale bars, 3 μm (a), 400 nm (b), and 200 nm (c, d) (reprinted with permission from reference [15]).

AuNPs are nanoparticles that are of easy preparation in comparison with other nanoparticles such as CdSe quantum dots mainly due to the Turkevich method which introduced single phase water based reduction of gold by citrate [16]. This enabled to have a suspension of AuNPs with tunable sizes with unique electronic, optical, and catalytic properties (figure 4A). These are easily modified (with biological compounds for instance) and highly biocompatible which have raised research in fields such as immunocytochemistry and cell biology. According to this, their properties and biocompatibility have raised a variety of analytical and sensing applications, including DNA and immuno-sensing. Electrochemical sensing using DNA assays were explored by our and other groups and can be detected using two different strategies: one direct and one indirect. The direct approach consists of three steps: first the adsorption of the AuNPs on the surface of the electrotransducer, then the electro-oxidation of the AuNPs to Au(III), and finally the reverse electroreduction to Au(0) this last step generates a well-defined cathodic peak, which constitutes the analytical signal [17]. In the indirect step, the AuNPs catalyze the hydrogen formation in acidic solution (1M HCl) producing a current that can be measured by chronoamperometry holding the working electrode at a potential of +1.35V for 1min followed by a negative potential of -1V for 100s or the time it needs to be constant [18]. The current intensity is directly proportional to the amount of AuNPs. The last methodology was the one applied in the following chapter of this PhD thesis. In our proposed biosensing system, we bring also into play MBs represented in figure 4B). This magnetosandwich immunoassay is a system where the AuNPs are used as labels and the MBs as immobilization platforms. This enables attraction using a magnetic field (a permanent magnet for instance), of all the AuNPs that are labeled to the surface of the electrode enhancing the signal and cleaning the unbonded AuNPs that could give a false positive (figure 4C and D). This strategy has been widely used by our group for biosensing systems where efforts were made to optimize and characterize the AuNP and MBs size studying their importance in practical biosensors.

3.2 Carbon nanomaterials: the graphene rise

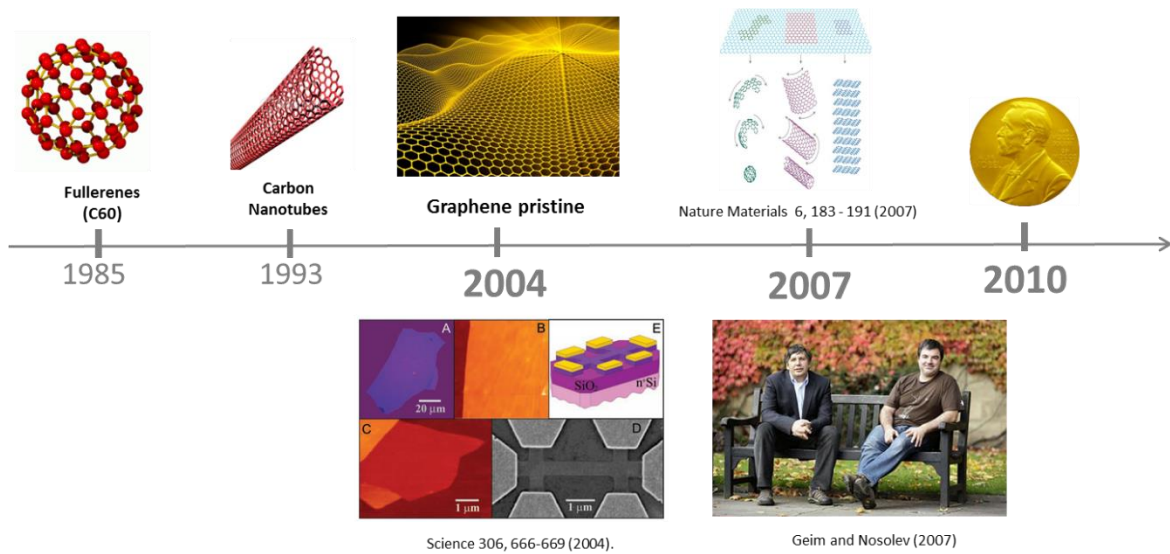


Figure 5. Chronology of carbon materials history.

Carbon nanomaterials are a wide range of materials that due to the nanometric size give rise to electric and optical properties that are not present on the initial graphite. Fullerenes ($C_{60}H_{60}$) “buckyballs” which have a spherical (0D) structure composed only by carbon atoms are of most importance, highly present in nature and can be present as a cylindrical nanometric structure denominated as Carbon Nanotubes (CNT). CNT (1D) have generated great interest due to their field emission and electronic transport properties, their chemical properties and their high mechanical strength. This material is also a semiconductor and can be an insulator or conductor at the same time applying nanoelectronics to reduce size mostly on transistors fabrication. When wrapping CNT sp^2 bonds cylindrical structure a completely new structure called graphene appears. This 2D single sheet was first found in 2004, using a simple scotch tape method to exfoliate bulk graphite [19]. This hexagonal packed carbon atoms structure have even stronger properties in comparison to CNT, is highly transparent and has charge carriers behave as massless relativistic particles or Dirac Fermions and under ambient conditions they can move with little scattering. “Golden rush” or “the rise of graphene” were the words described by Geim and Nosolev in 2007 that couldn’t fit better with what was coming on. This way, graphene was called as the “wonder material” of our generation and many graphene materials have raised. Graphene oxide (GO), graphene

polycrystalline, graphene quantum dots, graphene fibers, graphene foams, graphene ribbons or graphene scrolls are some of the type of family materials we have seen during last years and have invaded all fields of technology, from energy, sensing or medicine in between others.

3.2.1 Graphene materials production

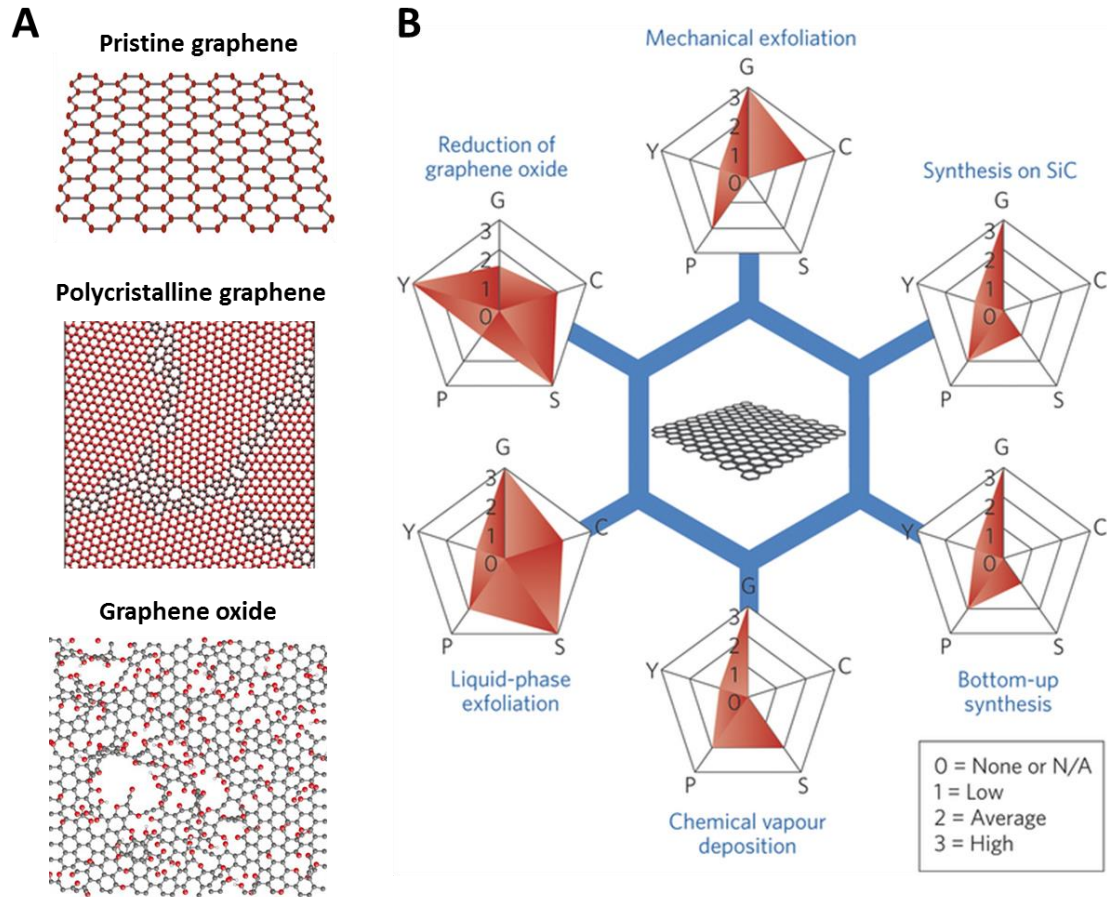


Figure 6. Graphene production properties. A) graphene materials structure (reprinted with permission from reference [20-22]). B) Each method has been evaluated in terms of graphene quality (G), cost aspect (C); a low value corresponds to high cost of production), scalability (S), purity (P) and yield (Y) of the overall production process structure (reprinted with permission from reference [23]).

Graphene materials are different from each other depending on their production methodology (figure 6). Each material has inherent characteristics such as defects, functional groups and impurities. These characteristics can change from material to material, but a balance between cost of production and performance is of major importance for industrial applications and to implement graphene based devices in day-life technologies. For instance, pristine

graphene found in 2004 has remarkable properties based on their perfect crystalline structure [19]. Although its production is tedious, with limited scalability and with high production cost. In this way, mechanical exfoliation is similar with growing techniques with this characteristic such as epitaxial growth on SiC and bottom up synthesis from structurally defined organic precursors [24, 25]. Chemical vapour deposition (CVD) for instance seem rather unsuitable for mass production due to their high cost, low yield and moderate purity. On the other hand, liquid phase exfoliation of graphite seems promising due to its low cost and high scalability making it promising for the production of high quality graphene in bulk quantities [26]. Nevertheless this technique lacks from high yield due to the presence of unexfoliated graphite particles that need to be removed. Chemical exfoliation of graphite and posterior reduction of the obtained GO seems to be cost effective for mass production with high yield but has demonstrated production of structures with plenty of defects and with the presence of impurities [23]. Although it has demonstrated to be effective in a wide range of applications performing similarly or even better than pristine or CVD graphene. In the following, we will describe technologies from production to printing and a study in the electrochemical behavior of these materials that have been one of the main focuses of this PhD thesis.

3.2.1.1 Pristine graphene

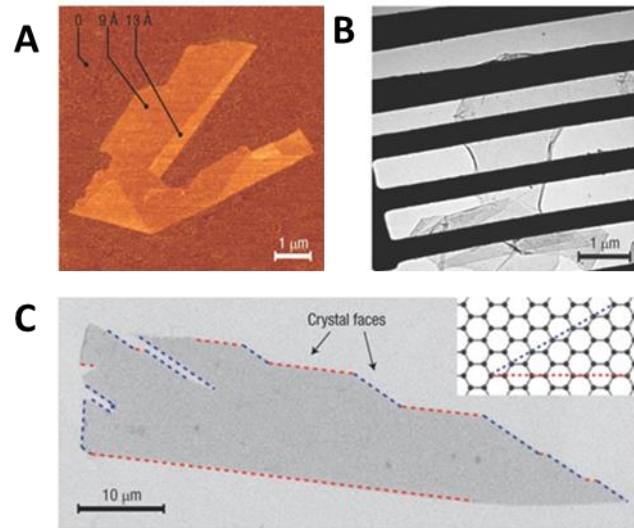


Figure 7: Pristine graphene. A) Graphene visualized by atomic force microscopy; B) TEM image of graphene sheet freely suspended on a micrometre-size metallic scaffold; C) SEM of a relatively large graphene crystal. (reprinted with permission from reference [19])

Pristine graphene can be produced using top down methodologies such as mechanical exfoliation of graphite or solution based exfoliation of graphite. Mechanical exfoliation, also known as the “scotch tape method”, was the first proposed methodology known to isolate graphene as a single layer form[27]. Successive “peeling off” of graphene layers from highly oriented pyrolytic graphite (HOPG) using adhesive tape enabled to isolate and deposit over a SiO₂ substrate a single graphene layer. This mechanical methodology enabled to experimentally measure the extraordinary electronic, mechanical and thermal conductivity properties of graphene [27-32]. This is the method for achieving the highest graphene quality so far in terms of impurities and defects. Solution-based exfoliation of graphite consists in trying to achieve a comparable material to pristine graphene by the chemical route. In this way, HOPG is submersed in organic solvents and subjected to ultrasonication in order to facilitate the separation between sheets although breaking them into very small flakes [33-

38]. Despite high quality graphene flakes are achieved, the high quantity of multilayer and unbroken graphite is huge, in addition to the defect containing in the edges by the ultrasonication. Impurities have also been addressed especially when added surfactants[39].

3.2.1.2 Polycrystalline graphene

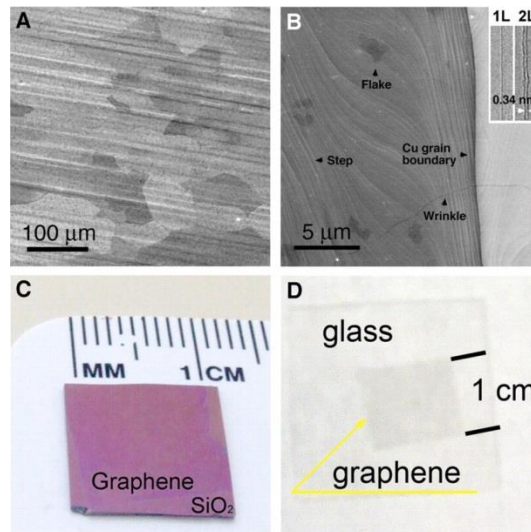


Figure 8. Polycrystalline graphene. A) SEM image of graphene on a copper foil; B) High-resolution SEM image showing a Cu grain boundary and steps, two- and three-layer graphene flakes, and graphene wrinkles. Inset in (B) shows TEM images of folded graphene edges; C) and D) Graphene films transferred onto a SiO₂/Si substrate and a glass plate, respectively. Reprinted with permission from reference [40].

Bottom up approaches to produce polycrystalline graphene are based on chemical synthesis, epitaxial growth on SiC, chemical vapor deposition, arc discharge and open/unzipping of carbon nanotubes. Chemical synthesis consists on the synthesis of small polycyclic aromatic molecules that combine into larger structures to form graphene. They have very well defined structure and edge shape (it have been demonstrated in performing a 30nm length nanoribbon) [41-43]. In epitaxial growth on SiC, graphene is grown over SiC substrate by heat treatment at very high temperatures under ultra-high vacuum

(UHV) conditions where the Si atoms sublime to leave an exposed layer of carbon atoms that will rearrange to form graphitic layers (epitaxial graphene) [44-46]. CVD is one of the most promising techniques for the production of large area graphene films with high quality structure (figure 8) [25]. Single, double and multilayer graphene have already been produced using this technique. The methodology consists in the high temperature decomposition of a carbon source in the presence of transition metal catalyst on which carbon atoms will deposit and rearrange into sp^2 like structures. It has been grown in metals such as ruthenium, platinum, iridium, nickel or copper [40, 47-50]. Nickel and copper in the last years have been the mostly used due to their high availability and low cost in comparison with the others mentioned above. Despite the great success in recent developments, the production of a total monocrystalline film is still a gap, whereas the presence of polycrystalline sites is common in few areas of the film. This comes across due to the fact that carbon atoms starts from different nucleation sites during the cooling process and then crystal growth laterally with specific lattice orientations until the entire metal substrate surface is covered. This results in the appearances of grain boundaries - intrinsic defects in the carbon structure. These boundaries have been widely studied due to their reactivity to molecules and to the possibility of performing spin theoretical physics opening fields in graphene sensing research. The possibility to have large films with boundary defect control could be a major advantage in graphene applications. The appearance of graphitic regions or islands has also been reported, and can have great implications in sensing or biosensing technologies. Apart from the growth of graphene which represent an issue in order to achieve a perfect atomic ordered structure, CVD also faces the problem of transferring the graphene film without contamination once the methodologies involve chemical etching of the copper or nickel over polymer support such as PMMA or PDMS, resulting in wrinkled graphene films or structural damage from tearing and ripping [47, 51]. Fe, Ni and Cu are common impurities that transform mostly the electronic properties of the graphene film [39]. Top down approaches are based on opening/unzipping carbon nanotubes and arc discharge [52, 53].

3.2.1.3 Graphene oxide

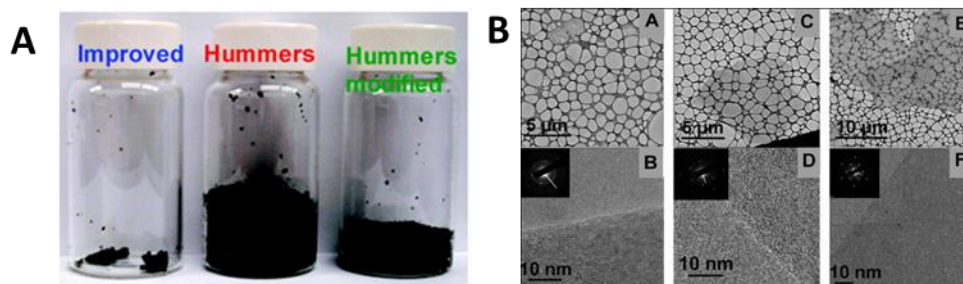


Figure 9. Graphene oxide. A) GO powders resulting from 3 different production methodologies. B) TEM images for the 3 different production methodologies. Reprinted with permission from reference [54].

GO like pristine graphene is produced by top down approaches and as his name suggests contains oxygen functional groups. It can be produced by electrochemical exfoliation of graphite or chemical oxidation. Electrochemical exfoliation consists in immersing a HOPG as a working electrode in a typical 3 electrode system: auxiliary (usually Pt) and reference (SPCE, Ag/AgCl, etc...) and applying a cathodic (reduction) or anodic (oxidation) potential or current in aqueous or organic electrolytes [55, 56]. When a positive potential is applied the HOPG is oxidized and the negatively charged ions from the solution are intercalated onto the graphitic layers. This is followed by the application of a negative potential that facilitates the exfoliation process. The use of high anodic potentials produces GO rich in oxygen functional groups and structural defects [56]. The sheet size varies a lot as well as the layer distribution and structure is also damaged. The chemical oxidation of graphite is a well-known methodology that in recent years was developed for a less hazard methodology by Tour and coworkers (2010) due to the recent interest in graphene materials. Although, it has already been successfully developed in 1898 by Staudenmaier, 1937 by Hofman and Konig and in 1958 by Hummers and Offeman to obtain that time called graphite oxide [39, 57]. This terminology has been substituted in recent years for GO and is associated with a high content of oxygen functional groups on the basal plane and edges of the graphene sheet and innumerous structural defects on the honeycomb structure. It consists in oxidative intercalation using

strong oxidation agents such as concentrated sulfuric and nitric acids for the exfoliation of graphite. The last developments changed the addition of potassium chlorate by potassium permanganate avoiding the formation of ClO_2 gas (figure 9). This GO sheets can be suspended in water offering the possibility for large scale production [23]. It is a highly resistive material due to the high presence of oxygen functional groups although their presence can be advantageous for the functionalization of biomolecules. It also exhibits photoluminescence due to the band gap opening as a result of quantum confinement effect from small sp^2 domains. It is an excellent fluorescent quencher which in addition with their bio functionality (sp^2 and sp^3 sites) can result in advanced sensors. The versatility of this material is also ascribed to the possibility of the elimination of the oxygen content called reduced GO (RGO). Although the total removal has not been achieved, highly effective methods such as hydrazine, thermal, sodium borohydrate or more ecofriendly such as ascorbic acid, tea extract or even bacteria procedures have been highly effective for GO reduction [58]. In recent published articles even the use of camera flash or laser scribe from commercial optical drive were used for reducing GO [59].

3.2.1.3.1 Graphene oxide architected materials

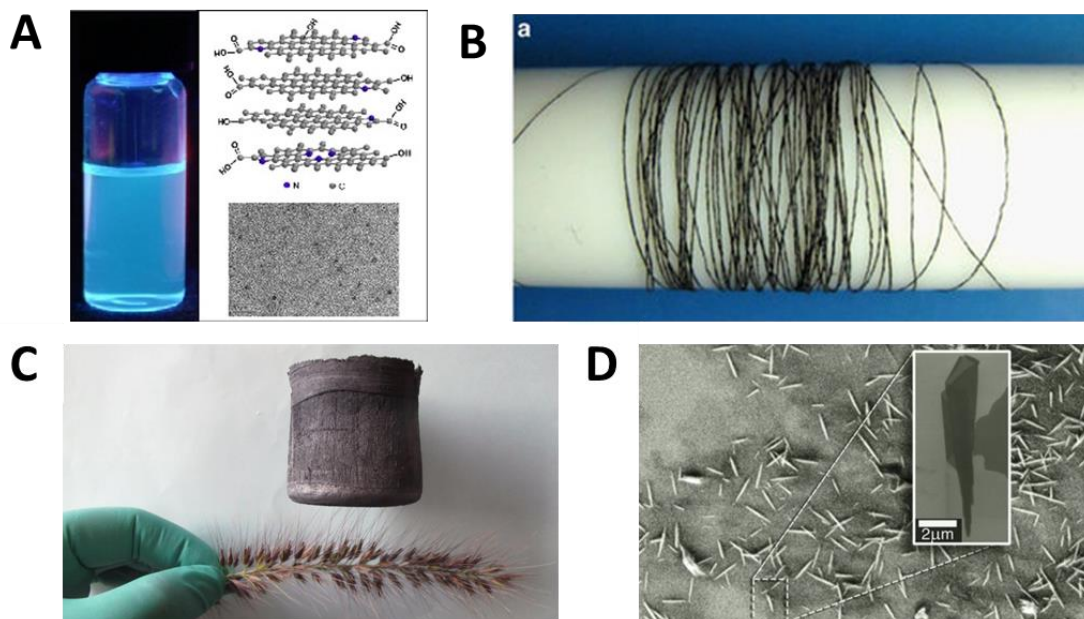


Figure 10. GO materials. A) GOQDs (Reprinted with permission from reference [60]); B) GO fibers (Reprinted with permission from reference [61]; C) GO foam (Reprinted with permission from reference [62]; D) GO scrolls (Reprinted with permission from reference [63]).

Playing with the GO architecture has demonstrated to produce novel materials that can be shaped in different forms and one could state “all dimensions” shape like structures. In the following, we will discuss how to produce these and their applications. In the special case of biosensors, GO quantum dots (GOQD) are making a step forward in applications, whereas GO fibers or GO foams are mainly used for energy storage. The GO scrolls applications are not clear in our opinion, and still need to be proved their superior performance in a niche sector.

3.2.1.3.1.1 Graphene oxide quantum dots

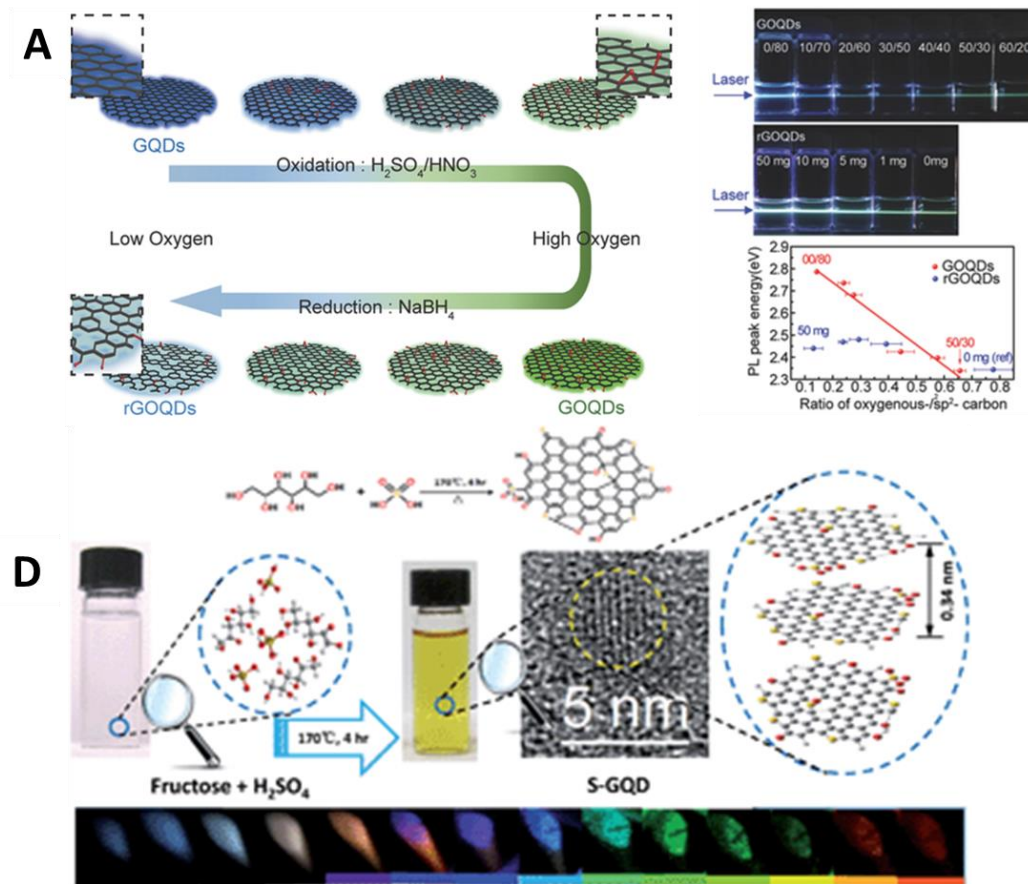


Figure 11. GO quantum dots. A) Effect of the ratio between oxidation degree and sp^2 carbon bonds in the emission wavelength (Reprinted with permission from reference[64]); B) Sulfur functionalization for tuning the emission wavelength. (Reprinted with permission from reference [65]).

GOQDs are considered a 0D material which properties are a synergy between GO and traditional quantum dots. This material has been produced using a wide variety of procedures that are common for GO production. In some sense, they are present in GO produced solutions that have a wide range of lateral dimensions materials. Although, their properties can be hidden upon the high rate of big GO flakes that have a near infrared (NIR) emission. Either top-down and bottom up approaches have been used to produce this kind of materials. From the top-down approach there is acidic oxidation, hydrothermal or

solvothermal microwave assisted, sonicated assisted, electrochemical exfoliation, photo-Fenton reaction and chemical exfoliation [66]. In the bottom up synthesis, they have been processed using benzenes as starting material using solution step chemistry methods; carbonization as starting materials through microwave assisted hydrothermal reduction; and unsubstituted hexaperihexabenzocoronene as starting material followed by carbonization, oxidization, surface functionalization, and reduction successively [66]. When reducing the GO lateral size from approximately 100nm down to 1.5 with a thickness of 0.5 to 5nm the edge effects and the quantum confinement assume the properties that are characteristic of semiconductor quantum dots. According to this, tuning the properties of this materials such as size, shape, excitation wavelength, pH, concentrations, surface oxidation degree or surface functionalization enable to vary the PL emission color. Until now, deep UV, blue, green, yellow and red PL emission has been reported. The PL emission exhibited by this material has been explored for the development of photoluminescence (PL) sensors for the detection of many analytes. The detection systems consists in the fluorescent quenching of the GOQDs or fluorescence recover upon the presence of target analytes either by charge transfer (ions or cations); energy transfer; or luminescence resonance energy transfer (by surface passivation (or distruction of this) using electrostatic interaction, π - π stacking or hydrogen bonding); and excited state electron transfer (resulting from the formation of a ground state complex). This have enabled the detection of Fe^{3+} , chlorine, TNT, pyrocatechol, Eu^{3+} , glucose, ATP, IgG. In addition, due to their biocompatibility, these GOQDs have been investigated for biology and medical imaging, intercellular sensors and drug delivery. In electrochemical sensors, GOQDs have been widely used for the detection of DNA due to their high affinity by π - π stacking. Similarly to GO, this single strand tends to release in the presence of the target DNA strand. According to this, cyclic voltammetry and differential pulse voltammetry measurements where used to detect the electrochemical behavior of ssDNA-GOQD-graphite modified electrode using $[\text{Fe}(\text{CN})_6]^{3-}$ as an electroactive specie. The GOQDs tend to block via electrostatic repulsion resulting in a drastic decrease of the electrochemical signal. Once in presence of the target DNA or target protein, the electrostatic repulsion disappears and the resulting peak

current increases. Glucose oxidase has also been immobilized in GOQD modified carbon ceramic electrode. In this strategy, the hydrophobic plane of GOQDs and the hydrophilic edges enhanced the enzyme absorption on the electrode surface enabling for direct electrochemistry. GOQDs have also been used for the modification of gold electrodes taking advantage of their good electron transporters and acceptors, showing peroxidase like activity which is a characteristic of GO too. These assemble was done with enriched periphery carboxylic groups on an gold electrode. The fast amperometric response was also tested in living cells for the detection of H_2O_2 [66].

Despite the great efforts for producing GOQDs materials for high performance sensors or biosensors or other devices the low quantum yield of this material (maximum is 73% reported till now) is a disadvantage in comparison with semiconductor quantum dots. Although we believe that the ease of processing, the low toxicity and the reactive active sites provided by the nature of this materials can be a real feature when balancing the advantages/disadvantages in the biosensing field

3.2.1.3.1.2 Graphene oxide fibers

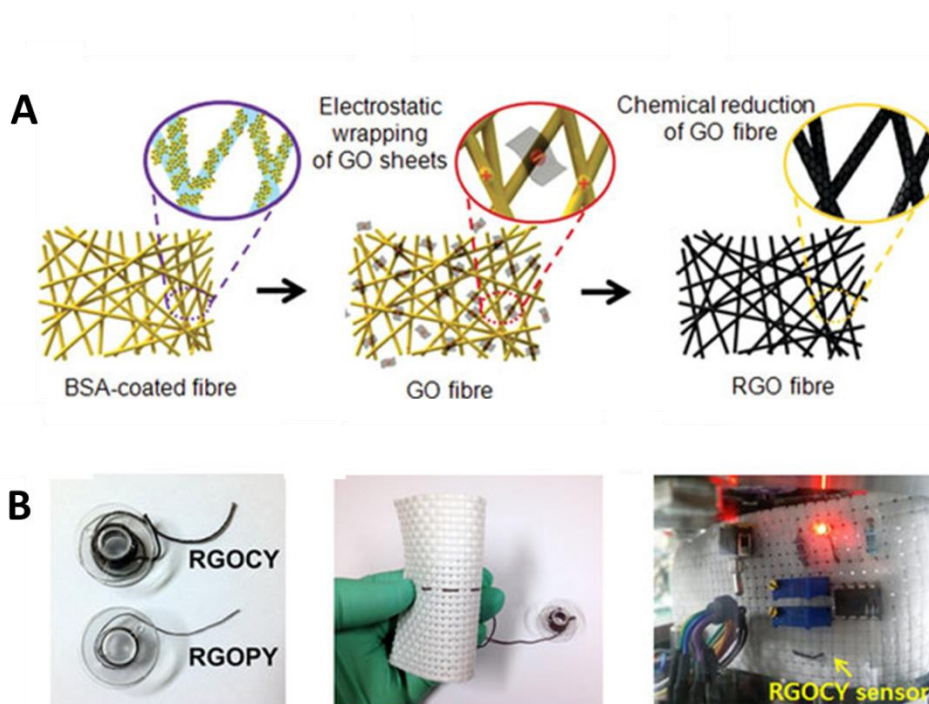


Figure 12. A) Process for coating fibers using BSA pretreatment. B) RGO fibers used as a wearable sensor. Reprinted with permission from reference [69].

GO based fibers are making a disruption in wearability enabling the production of wires that can be bent, knotted or woven into flexible electronic textiles. The applications have a lot in common with foam like structures such as energy storage and conversion, solid phase microextraction, spring, catalysis and sensors. They can be produced using wet spinning, dry spinning, dry jet, electrophoretic self-assembly, and film shrinkage or spinning in between others. [61, 67-71]. In figure 12 a distinct approach from other GO based fiber is such as simple as wrapping a normal textile fiber using bovine serum albumin (BSA) self-assembly which serves as a universal self-assembly to GO followed by low thermal reduction[69]. Most of these fibers follow reducing methodologies described before such as chemical, thermal or laser scribing. The last exposed coating technology could be simply integrated into textile industry as a post treatment of cotton, nylon or polyester in contrast with others that are 100% GO based. The fabrication of a bendable and washable gas sensor using this methodology also was reported. The developed sensor possesses chemical

durability, mechanical stability, and a high response to NO₂ gas. Most notable is its ultra-sensitivity as a gas sensor even at room temperature, which is made possible through robustly wrapping the yarn with RGO, and by the large accessible surface area of yarn. This could take advantage in the marriage between existing textiles and graphene. The possibility to have graphene or GO based in a wire form changes the sense of applications and open venues for innovative technologies for the upcoming years. The aligned structure or the porous structure change their properties where a planar structure can be more smooth to touch and able for the increasing field of wearable technologies.

3.2.1.3.1.3 Graphene oxide foams

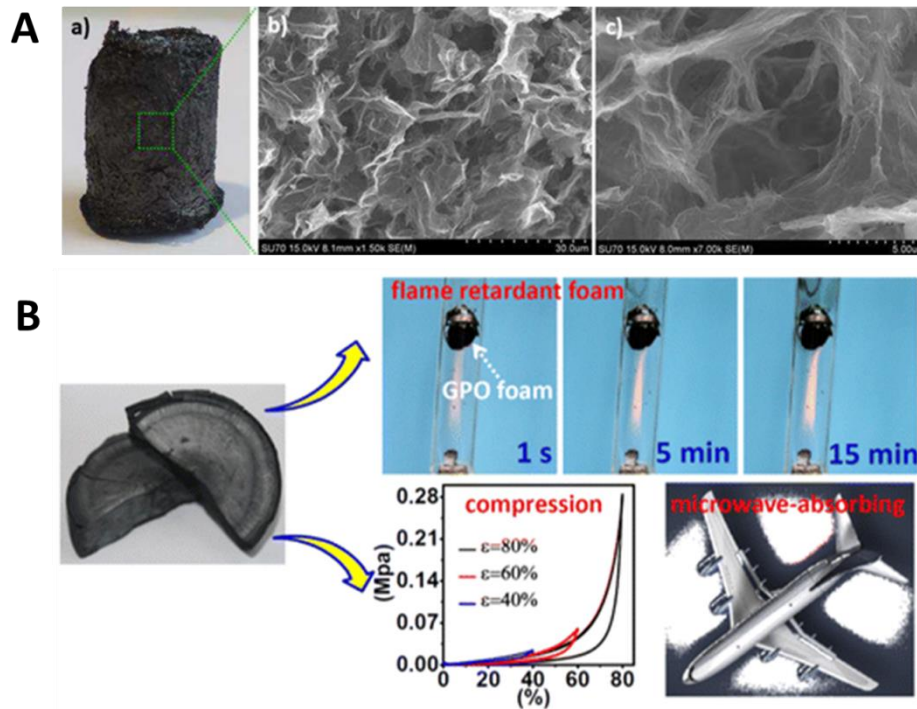


Figure 13. GO foam. A) Photograph of the GO based foam a) and SEM characterization in b) and c). Reprinted with permission from reference [72]. B) applications of GO based foam such as flame retardancy, compression and recover, and microwave absorption (Reprinted with permission from reference [73]).

GO foams are porous structure films with highly enhanced surface area, conductive properties and flexibility. This can be achieved by simple vacuum filtration and posterior reduction in hydrazine solution by autoclave at 90°C for 10 hours resulting in a horizontal porous network from sub micrometer to micrometer that is cross linked and not totally separated (this enabled to maintain electrical resistance in 100ohm\sqare) [74]. In a different approach mixing 1M KOH into a GO suspension and heating at 100°C under constant stirring is applied until a paste is obtained. This paste can be simply filtered in vacuum and additionally reduced. The obtained porous structure of the film is flexible, highly conductive and can be cut into desired shapes. The KOH concentration seems to be the trivial step for obtaining homogeneous films [75,

76]. Another reduction methodology using vacuum filtration for the production of thin films have been reported using the direct laser writing [77, 78]. This reduction enables the production of porous like structures in the reduction process that enhanced the surface area. GO foam composites have also been developed for extreme characteristics such as ultralight weight using hydrogel/GO mixture , fire retardancy using nanocelulose/GO mixture, microwave absorption, or mercury brew [79]. Surprisingly, in accordance with their high active surface area in addition to the GO or RGO properties such as binding sites or biocompatibility, the applications of this RGO foams are scarcely reported in biosensing systems.

3.2.1.3.1.4 Graphene oxide scrolls

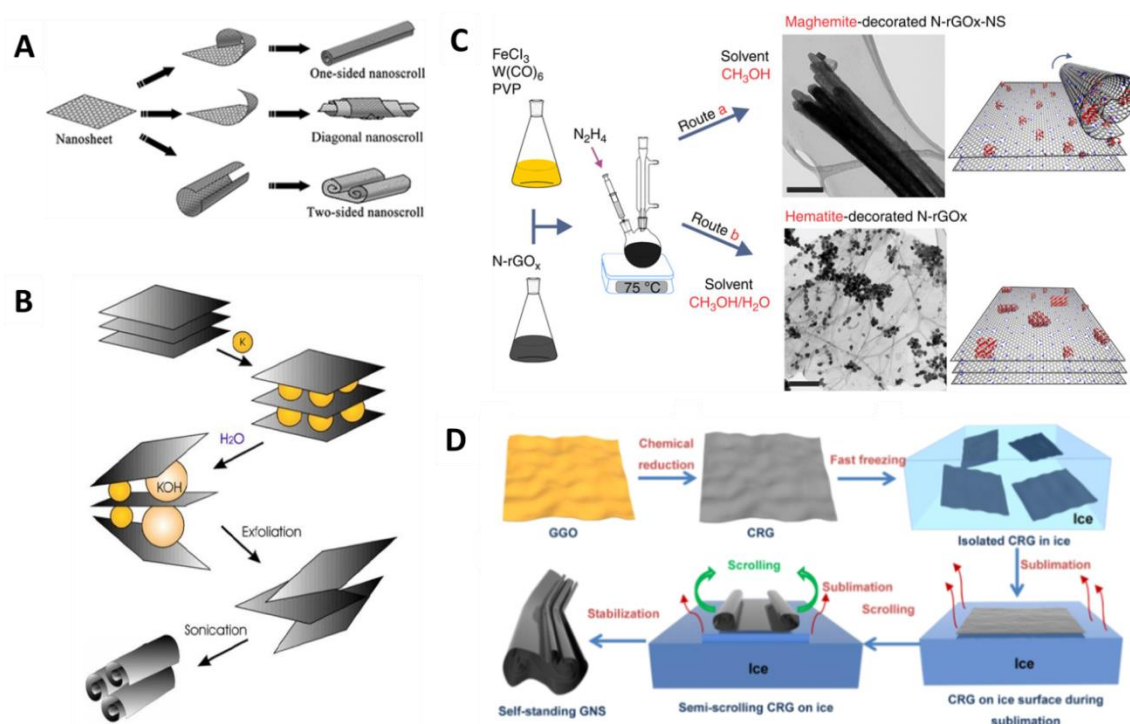


Figure 14. GO scrolls properties. A) typical shape of GO based scrolls Reprinted with permission from reference [80]. B) schematic of GO scrolls production using sonication methodology. Reprinted with permission from reference [81]. C) schematic of GO modification with magnetic nanoparticles for

the formation of GO based scrolls Reprinted with permission from reference [82]. D) Schematic of the production of GO based scrolls using sublimation. Reprinted with permission from reference [83]

Another material shape in graphene family is graphene or GO scrolls (figure 14A). The GO scrolls formation occurs upon external energy forming a papyrus like shape. GO scrolls are a quite weird material, and despite their similarity with carbon nanotubes their open ended structure and spacing between sheets typically differs from his carbon far cousin. The GO scrolls have been processed mainly using sonication (figure 14B), chemical microexplosion, sublimation (figure 14C), microwave radiation, or using Fe_2O_3 maghemite (figure 14D) [81-86]. These GO scrolls have the ability to open again into a 2D structure by simple charge tuning (theoretically) or chemical modification. Somehow these methodologies have characteristics in common with micromotors or nanomotors rolling fabrication. Although, micromotors have in addition photolithographic processes in order to shape the initial 2D structure. Remarkably, GO scrolls have been applied in various applications such as electroactuators, gas storage, supercapacitors, batteries, catalysis and sensors. Recently, graphene nanoscroll formation over diamonds have displayed extreme macroscale superlubricity [87].

3.2.1.3.2 Why graphene oxide? An insight over graphene oxide applications.

Playing with the planar structure of graphene and GO sheets enabled unlimited applications in fields as important as membranes for desalination and water purification; sensing and biosensing; energy storage and production; or optical devices [88-99]. The high surface area exhibited by graphene is the rock soul for the infinite research in graphene manufacturing and shape ordering. It should be noticed that due to the nature of the graphene materials they are differently processed for the control of their structure. Once GO is a water soluble suspension, its use facilitates applications due to the high yield obtained upon exfoliation in contrast with their pristine cousin[23].

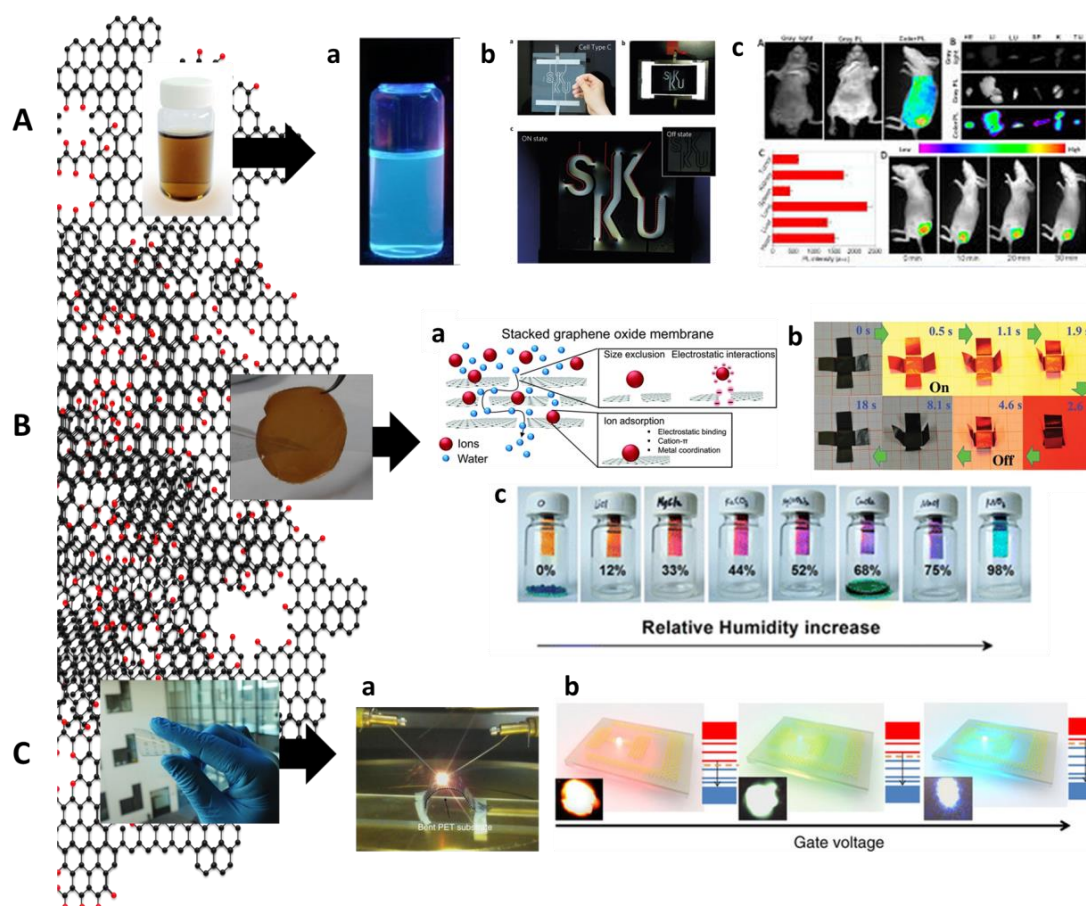


Figure 15. GO applications using GO solutions (A), GO membranes (B) and GO printed (C). A) GO solutions applications such as fluorescence (a), screen display (b) and phototherapy (c). Reprinted with permission from reference [60, 100, 101]. B) GO membranes applications such as molecular sieving (a),

actuators (b) and optical humidity sensor (c) [102-104]. C) Printed GO applications such spectrally tunable field-effect light emitting device (a) with tunable luminescence (b). Reprinted with permission from reference [89].

The oxygen content resulting from graphite exfoliation either chemical or electrochemical spreads oxygen functional groups all over the surface and the edges. These groups can be epoxy, carbonyl, carboxyl, ethanol, ketone etc. being the surface groups present on the edges the most difficult to remove upon reduction and the ones in the basal plane the easiest [105]. The atomic structure of GO is highly disordered and has few in common with graphene pristine. The typical hexagonal honeycomb structure of graphite is destroyed upon exfoliation and gives rise to the appearance of pentagons, triangles in between others, disorderly distributed over the GO sheet. This might look like a disadvantage in comparison with pristine graphene applications although it might be naive to think in this direction for the following reasons:

- i) The presence of oxygen functional groups leads to high stability in water solutions and opens the door to easy immobilization by covalent or Van der Waals interactions in addition to the π - π interactions. This has been used for the functionalization with polymers, biomolecules, drugs, carbon nanoallotropes, magnetic structures, quantum dots in between others [106]. Depending on the lateral size of the GO sheets these functionalization can be used for biotherapeutics, due to the high NIR light absorbance of GO (vital for phototherapy) [107, 108] and the GO enzymatic degradation [109, 110]. In addition the electro-optical switch of a GO solution with very low concentration is an extreme example of its versatile nature, where controlling the axis direction of the GO sheets enables revealing of the liquid crystal nature of this material for the development of a screen display [100].
- ii) The presence of high oxygen content ($C/O=1$) in GO films has a d-spacing between sheets of approximately 8Å in a 50% humidity environment. This separation has enabled the development of well aligned GO membranes using vacuum filtration technique for

desalination or gas separation in between other application. These GO membranes have been studied for the separation of copper sulfate and rhodamine B, Na^+ , Mg^{2+} , K^+ ; Ca^{2+} , Ba^{2+} , Cl^- and Mg^{2+} blocking all solutes with hydrated radius bigger than 4.5\AA [94, 111-113]. The GO modified with a polyamide chain have also been reported for the CO_2 capture [112]. This d-spacing highly dependent on the humidity due to high water permeability of the oxygen functional has been experimentally tested using X-ray diffraction and noticed that the oxygen content channels open and close upon humidity addition [114, 115]. This mechanism has been used for the detection of humidity either optically with a calorimetric device using deep coated GO paper film or electrochemically with a gold interdigitated modified with spray coated GO [102, 103]. GO paper is also commonly used in actuators highly dependent to humidity or light [116]. This separation has also enabled the production of supercapacitors taking advantage of the localized water of GO as ionic conductor and an electrical insulator, allowing it to serve as both an electrolyte and an electrode separator with ion transport characteristics observer for Nafion membranes [78]. The tune of this separation with other compounds, and the possibility to have adjustable d-spacing between sheets have also been described for future personalized biomedical or pharmaceutical separation [93].

- iii) Electrically, GO can transit between an insulator to a metal depending on their oxygen content. This tunable band gap have been used for the production of an all GO/RGO field effect light emitting device reduced using laser scribing technique and exhibited tunable electroluminescence [89]. It has been experimentally reported that RGO electroactivity to typical electroactive species due to the presence of defects and biofunctional groups increase in comparison with polycrystalline graphene or pristine graphene [39]. The biocompatibility of solution based GO and RGO devices and the possibility to manage their 3D architecture has already proved to be multifaceted. In the cellular field, GO functionalization of surfaces for capturing circulating tumor cells for instance or for the cell growth and differentiation is also described [117, 118]. RGO 3D structures printed using 3D printer have

also been reported for implant applications, and RGO scaffolds are also a constant for cell imaging and cell growth [119, 120].

3.2.1.3.3 Graphene oxide printing and patterning

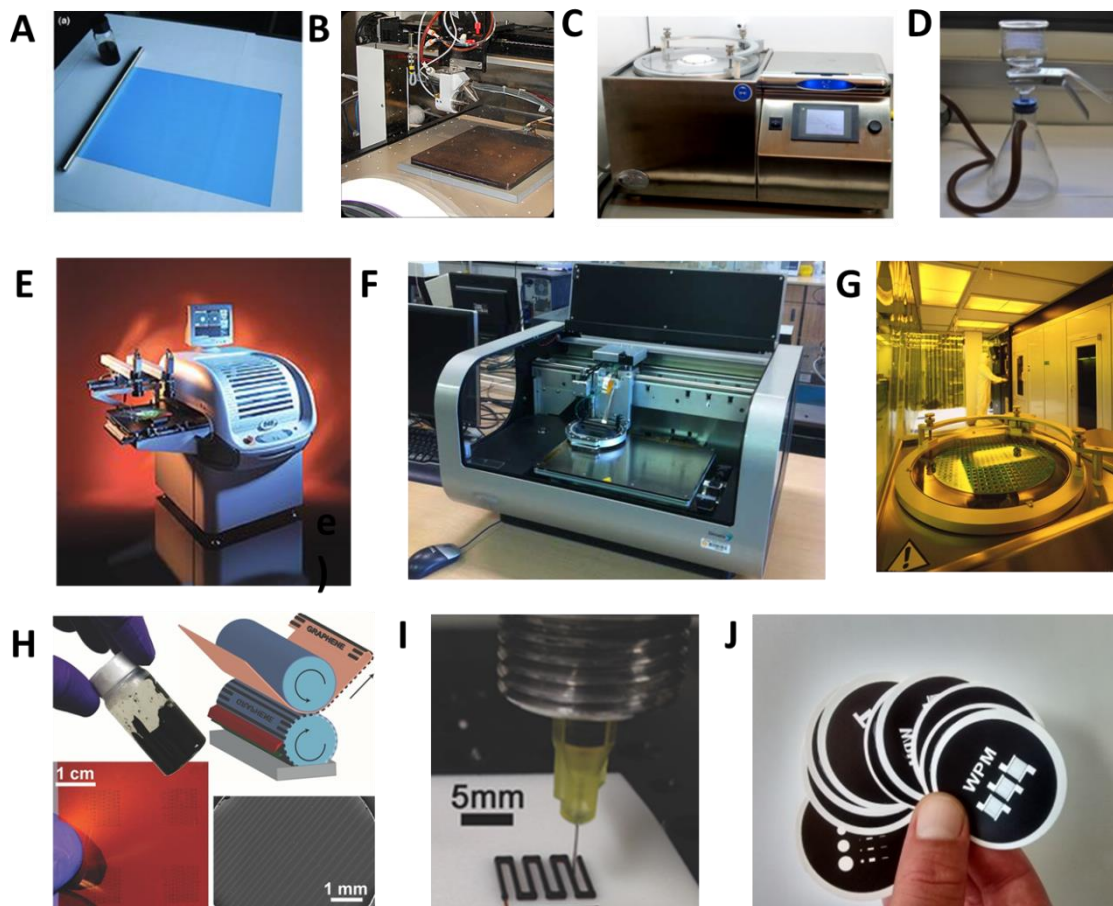


Figure 16. GO printing and patterning. A) Rod coating ; B) spray coating; C) spin coating; D) vacuum filtration; E) screen printing; F) inkjet printing; G) photolithographic processes; H) Gravure; I) 3D printing and J) wax printed membranes. Reprinted with permission from references [6, 119, 121-123]

The production of GO thin films is of major importance to a wide variety of applications. Their price and the low need for expertise could improve the fast integration and abundance of GO devices with interest not only for research but

for a variety of applications as well. Several methods have been described to produce GO films (figure 16A-D) such as rod coating [121], spin coating [88], drop casting [125], layer-by-layer assembly [126], spray coating [127] and vacuum filtration [124]. These methodologies vary in terms of energy/time consuming beside others. For instance layer by layer assembly can produce highly ordered films but it need small size sheets for efficiency coming up with a very high energy/time consuming. For instance, vacuum filtration, also reports the production of very well aligned and ordered GO films but is size limited which enhances the energy/time consuming. Although this technique has been widely studied due to their simplicity nature, no need for know-how or chemical interfaces. A continuous film formation set-up was proposed using this technology which could change dramatically the long filtration rate. Despite this, the control over the thickness, the simplicity, the cost, and the possibility of making GO based composites have brought a wide variety of applications. This have enabled, the production of either free standing films by simple peeling of the GO film from the membrane (made of fluorinated polymer or anodized alumina) [93, 94] or the production of films that can be transferred to the target substrate either rigid or flexible by acetone chemical etching of nitrocellulose membranes [124]. Recently from our group, we were able to couple this technology with wax printing mode and avoid the use of chemicals such as acetone for transferring a patterned GO film onto target substrates [128]. We reported a simple way to transfer GO patterned structures to target substrates by simple water activation and pressure. In this work, the wax that clogs the membrane pores (of a 25nm commercial nitrocellulose membrane) enables to direct the GO solution to desiring unclogged regions. Once the wax printing technology is cheap and versatile technology, one can produce unlimited shapes and structures and the control over the thickness provided by the vacuum filtration enables to print nanometer vertically sized films. This came as a solution to existing patterning technologies (figure 16E-H) such as screen printing [129], gravure [123], inkjet [130] and lithography (also as developers of microcontact stamps) [88, 131]. For instance, lithography and gravure techniques have high set-up costs and are advantageous only for high production rates. Apart, lithography is mainly a chemical or photochemical method process with the need for clean room facilities and consumable and

expensive photoresists and developers. Our technique also avoids the preparation of inks which is an issue for inkjet and screen printing in terms of viscosity and polymerizations and in the particular case of inkjet one needs to sum the substrate treatment and printing temperature. In addition, the presence of surfactants or polymers can affect the device optoelectronic performance. As so, for the development of a single and simple electronic device, one has to pass a lot of issues in addition with the knowhow need. In this way, the water activated wax printed membranes (figure 16J) for the patterning of GO devices is quite simple, effective, versatile and low cost, and in the future could surpass the disadvantages of size limitation and time consuming for the production of GO devices at the industrial level by simple introductions in the process of fabrication while maintaining its main characteristics and the features related to it.

3.2.1.3.4 Graphene oxide morphology over printed methodologies

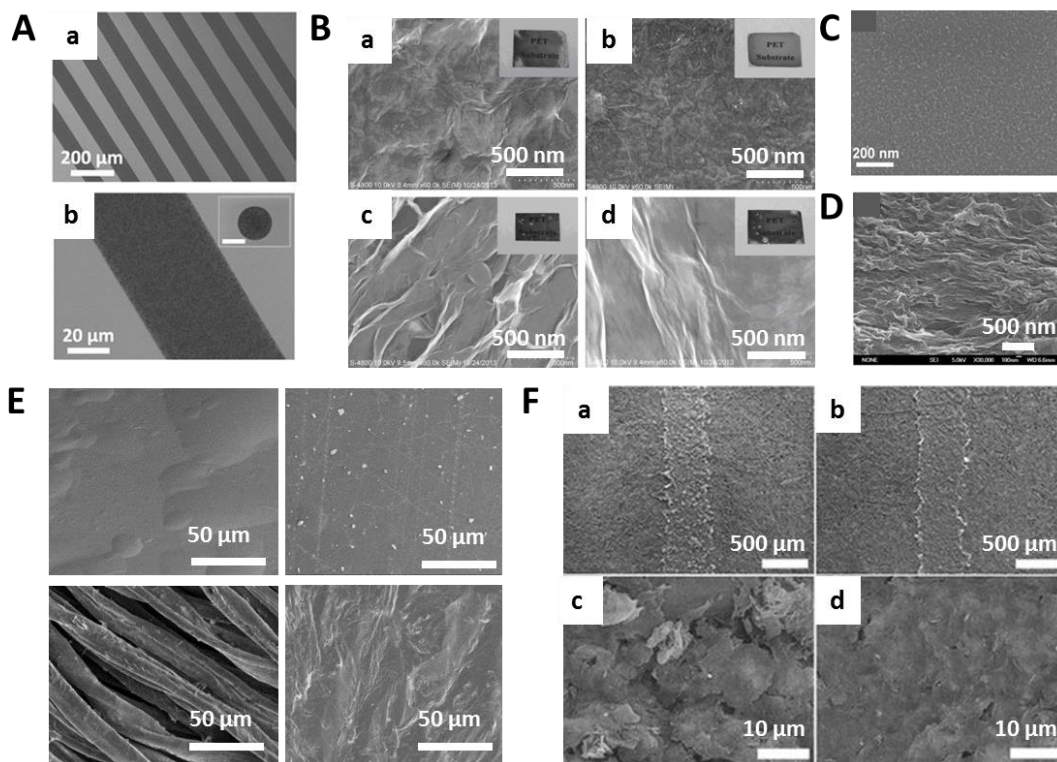


Figure 17. Morphology of GO based films. A) SEM image of inkjet printed at different magnifications (a,b) reprinted with permission of reference [130]. B) SEM image of drop-casted GO films at different concentrations reprinted with permission of reference [125]. C) SEM image of a spin coated GO film reprinted with permission of reference[88]. D) SEM image of a electrodeposited GO film reprinted with permission of reference [132]. E) SEM image of GO based films using wax printed membranes in PET, adhesive film, textile and paper (from left to right, up to down). F) SEM image of RGO directly printed over paper using a pencil at two different concentrations (a and b) with magnified images on the down part (c and d) (reprinted with permission of reference [133])

While GO based electrodes can be printed in different ways (as described before) nevertheless the surface roughness and consequent edge site available and defects such as wrinkles or open sites differs from technique to technique (figure 17). Vacuum filtration [124, 128] can produce very well aligned GO sheet films due to the alignment of the sheets in solution upon filtration and deposition

over the membrane. On the same way, spin coating [88] and self-assembly [126] are also venues for producing homogeneous coated thin films. Ink jet printing [130] for instance shows similar results as simple drop-casting [125], spray coating [127] or PDMS based stamp patterning [134] where a random confinement and aggregation of GO or RGO are responsible for non-uniform depositions, cracks or unaligned GO sheet deposition. Additionally, electrochemical deposition over conductive substrates has been described for the production of RGO wavy like structures [132] or even nanowalls [135]. Another important aspect to take in account for film formation is the structure of the substrate where GO seems to shape concerning the structure [128]. On the other hand, printing GO or RGO also seem to change the structure due to the change in sheets behavior. For instance in vacuum filtration the shape of the printed films changes when using RGO based ink, forming more edge like sites [133]. Regarding conductivity it is also tricky to compare thickness of different films as these depend on the reducing methodology; although it is worth to mention that GO printed films may lack the conductivity due to the unreduced areas on the bottom of the GO film where the reducing agent for instance cannot actuate [124]. In this way, reduction of GO in solution seems to be much more advantageous for high conductive thin films. In the following section, we will describe how shape can have an important role in the electrochemical behavior over pristine, polycrystalline graphene and RGO.

The printing or growth technologies have a major importance in the electrochemical behavior of graphene materials. For instance, in pristine graphene the sheet shape can induce variable edge active sites in comparison with the basal plane depending on the sheet size and quality. The appearance of cracks in the structure can also change the electrochemical behavior. In the case of polycrystalline graphene, the growth for instance can induce graphitic islands in addition to the polycrystalline structure. In GO films, which in the majority of the cases are formed by simple drop casting, problems in the uniformity of the films are reported [98, 99, 136-138]. The uniformity in the GO film structure is of major importance because in addition to the structural defects, the active edge like sites play an important role in the electrochemical behavior. In GO modified electrodes, an inhomogeneous film can induce a

response that is not related to graphene modification but from the adjacent electrode. As so, the study over the influence of controlled structures in electrochemical performance will be widely studied in the following section.

3.2.1.3.5 Graphene oxide electrochemical properties and applications

Heterogeneous electron transfer (HET) that is the exchange of electrons between graphene and molecules is correlated not only with the type of molecules in question but also importantly with the oxygen content and functional groups, the amount of defects, the edge like architecture, the thickness and the impurities most of the times dependent on the production methodology [139, 140].

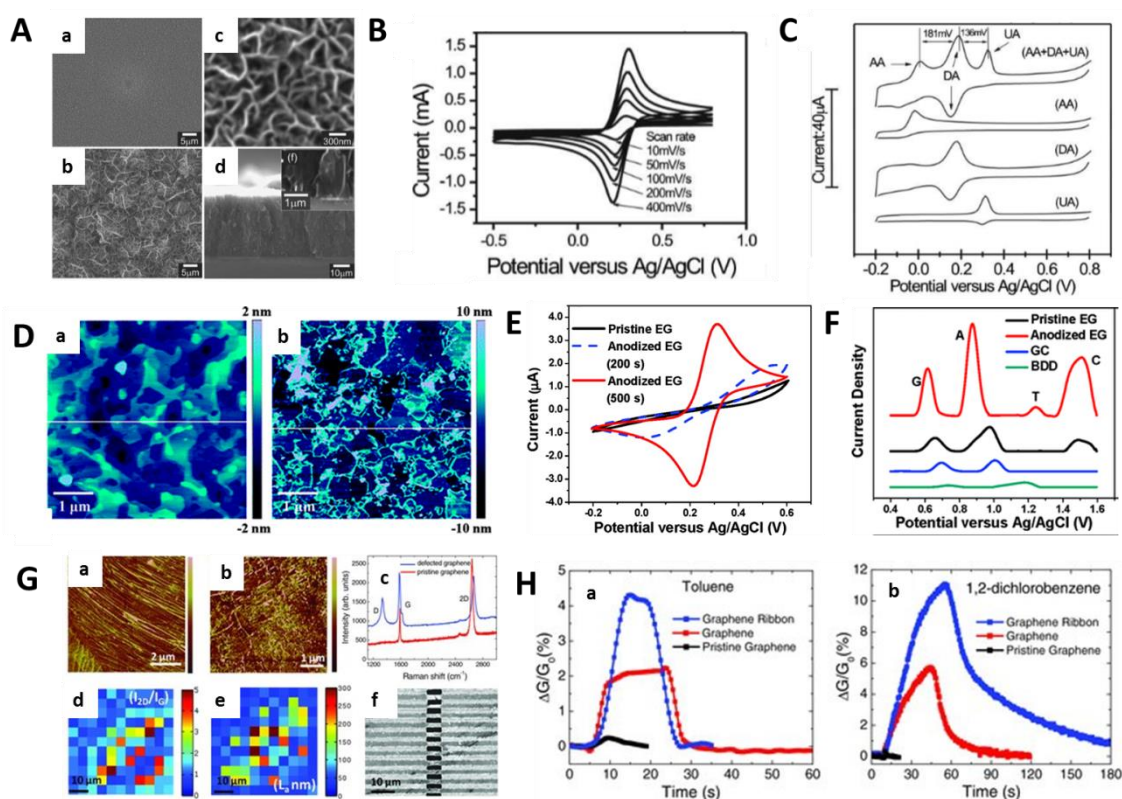


Figure 18. Electrochemistry of graphene materials. A) SEM images of graphene film deposited for 30 min (a) ; b) and c) are an enlarged image of (a); d) lateral view. B) CV profiles of the graphene electrode in 5 mM ferrocouple with different scan rates from 10–400 mV s⁻¹ ; C) C–V profiles of the graphene films for the detection of AA, DA and UA. D) Topographical images and cross

sections for a) pristine EG and b) anodized epitaxial grown (EG) graphene; E) CVs for pristine EG, anodized EG (200 s), and anodized EG (500 s) at 1.0 mM $\text{Fe}(\text{CN})_6^{3-/4-}$ in 1 M KCl; F) DPV profiles for pristine EG, anodized EG, GC, and BDD electrodes in 30 μM equimolar mixture of G, A, T, and C; G) AFM images of polycrystalline graphene used for sensors, color scales are 10 in a) and 5 nm in b). c) Raman spectra of pristine and CVD-based “defective” graphene samples; d) map of I_{2D}/I_G ratio; e) map of crystallite size ; f) SEM image of CVD graphene ribbons; H) Ratio of conductance to initial conductance (G/G_0) response of CVD-grown defective graphene, CVD graphene microribbon, and 5 μm wide pristine (exfoliated) graphene sensors to 10^{14} molecules of toluene and 10^{15} molecules of 1,2-dichlorobenzene, a) and b) respectively. Reprinted with permission from [97, 141, 142]

HET of graphene is widely compared with the case of HOPG where the HET of $[\text{Fe}(\text{CN})_6]^{3-}$ at the edges is very fast and in the basal plane is very slow or limited to near-zero [143]. In order to understand how this affect graphene Banks and coworkers [144] have compared CVD graphene electrodes to GCE, edge-plane-pyrolytic graphite and basal plane pyrolytic graphite showing that the electrocatalytic properties of CVD graphene are due to the presence of graphitic islands over the graphene surface resembling edge like sites. Electrochemical actuation has also been demonstrated in CVD graphene sheet with grown graphitic islands as active sites [145]. Shang grew multilayer graphene nanoflakes by microwave plasma enhanced CVD technique to obtain a very high density of edge like exposed planes and tuned the electrochemical behavior (figure 18A-C) [141]. In addition, it has also been reported that a large amount of defects either mechanically or chemically on the basal plane can induce a faster HET for mechanically exfoliated graphene or CVD graphene [145-147]. In an epitaxially grown graphene film, the application of an anodizing potential enabled the increase on the density of defects and introduce oxygen functional groups enhancing electrochemical properties, enabling to detect simultaneous DNA bases and resolved signals from DA, UA, and AA (figure 18 D-F). They were able to detect DA with a limit of detection 0.17 μM in the presence of UA and AA [142]. Amin and co-workers have studied the influence

of low concentrations of randomly distributed defects on pristine graphene and graphene grown by CVD to the absorption of gases (figure 18G,H) [97]. Firstly they have determined that nearly pristine graphene is less sensitive to analytes because adsorbates bind to point defects which have low resistance pathways around them [97, 148]. They have determined that the gas detection is easily short circuited given the 2D nature of current flow in graphene always searching for low resistance pathways. This was solved by micrometer sized line defects or continuous lines of point defects where no easy conduction paths exist around such defects, so the resistance change after adsorption is significant. In this way, the engineering of the line defects and edges are proposed by the authors for ultrasensitive graphene chemiresistors. Despite this, pristine graphene have been widely used in gas sensors with high sensitivity such as the one described for single molecule detection [96]. Gas detection could be performed in pristine graphene using FET [149], chemical resistors [96] or graphene/semiconductor Schottky diodes. In our group, we have developed a pristine graphene Schottky diode using AC for the detection of various vapors fingerprint [150]. This enabled to distinguish between chloroform, phenol and methanol using impedance spectroscopy change.

Unlike pristine graphene or CVD graphene, GO is highly disordered and contain functional groups from production. RGO reduced from either chemically, thermal or electrochemically can still contain oxygen functional groups and can suffer from a higher level of disorder or defect areas due to the reduction. It is reported that the increase in C/O ratio, the HET increases [39]. But in the electrochemical biosensing field using GO the search for increased surface areas and edge like sites for increasing HET and LOD is still ongoing. For instance a biosensor was developed taking advantage of the edge like sites by electrodeposition over the surface of a graphite electrode of GO. They were able to build nanowalls and improve the LOD to 9.4zM [135]. Apart from edge active sites or defects, the search for increasing surface area while maintaining or even increasing the edge like active sites have also been performed. RGO micropillars have been used for chemical sensors in a search for new architectures with enhanced limits of detection in comparison with planar ones[151] . Electrochemistry have been used for etching GO into controlled

mesoporous structures with micrometric channels [152]. In other work, they studied the electrochemical performance of RGO foam, edge-plane pyrolytic graphite /basal-plane pyrolytic graphite and single layer CVD graphene [59]. It is clear the high electron transfer and the outstanding performance of a printed RGO foam electrode in its own right without summative effects being used as a disposable printed 3 electrode system.

Although as referred by Katie Griffiths and co-authors [59], a plethora of scientific literature on graphene electrochemistry is based in GO based solutions which are drop-casted or electrodeposited onto underlying electrodes which in essence the graphene derivatives are acting in concert with the underlying electrodes, producing summative electrochemical effects [153-155]. This have been achieved also for a wide myriad of electrochemical sensors or biosensors that are graphene modified using SPCE, GCE , Au or ITO for the detection of biomarkers, proteins, DNA analysis, or heavy metal detection[39, 57]. In our group we have also developed similar sensors reaching advantageous tunable electrochemical properties in a carbon SPCE modified with GO and RGO for enzyme immobilization [10]. The sensors that use only graphene as a transducer are few although they exhibit good performance (Figure 19).

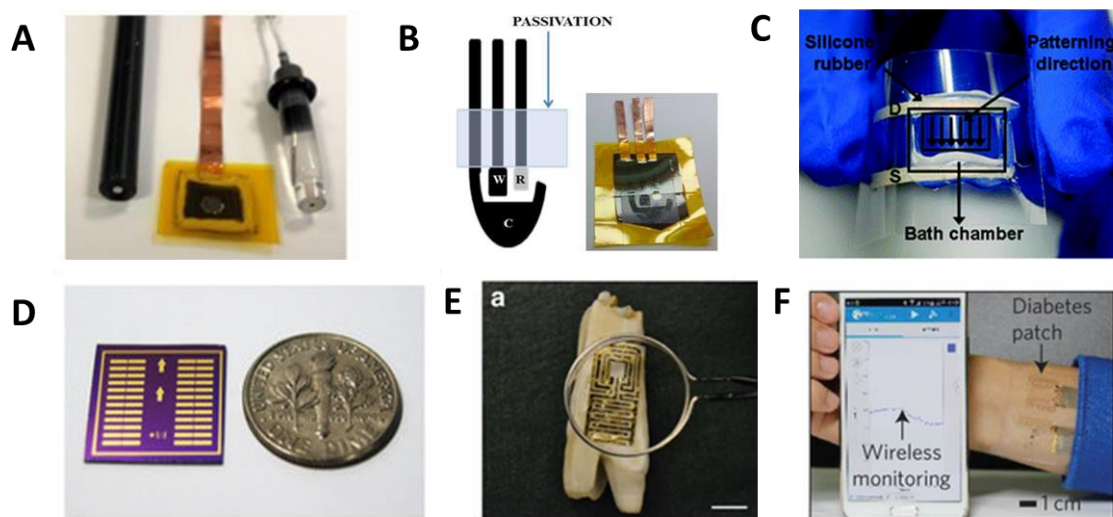


Figure 19. GO/RGO devices. A) photograph of all the electrodes required in the setup with the working RGO electrode in the centre. B) schematic of the planar three electrode system on the left and the RGO patterned. C) Photograph of rGO pattern-based sensing device on PET film. D) photograph of RGO

patterned over Si/SiO₂ wafer. E) Optical image of the graphene wireless sensor biotransferred onto the surface of a tooth. Scale bar is 1 cm. F) Optical image of the integrated wearable diabetes monitoring and therapy system connected to a portable electrochemical analyser. Reprinted with permission from [59, 131, 134, 156, 157].

SPCE was fabricated electrode by a drop casted RGO working electrode in the absence of the underlying carbon paste for the detection of H₂O₂. This RGO ink was tuned with ferrocene molecule and chitosan for advanced electrochemical behavior [158]. In a PDMS stamped GO [159] the authors were able to produced GO thin film transistors for the detection of fibronectin with a LOD of 0.5nM and avidin in physiological buffer. This transistors where flexible and transparent with performances comparable with pristine graphene [95]. The same authors reported FETs based on RGO patterns that abled the label-free detection of hormonal catecholamine molecules and their dynamic secretion from living cells [134]. In a different approach, using dry etching methodologies, the authors where able to pattern RGO resistors at the wafer scale with a resolution of 5µm up to hundred µm. They were able to detect amyloid beta (pathological hallmark of alzheimer's disease) in plasma of a transgenic mice, studying the changes in resistance of the device modified with biomarkers. they achieved a limit of detection as low as 100fg ml⁻¹ [156]. A recent study using the laser scribed portable electrodes described by Katie before in this work[59], in addition with copper nanocubes were able to detect glucose with a LOD of 250 nM [160]. It is clear that increasing edge shape volume and surface area enables to tune the electrochemical behavior of graphene materials and probably in the biosensing field the disruption with existing technologies is a major priority for the development of new type of biosensors. RGO foams, RGO fibers or even RGO scrolls could bring characteristics such as wearability or actuation that are not present in typical RGO devices. In this sense, CVD graphene sensors are making one step forward for portable and wearable biosensors that one cannot observe in GO or RGO electrochemical bio devices [5, 157].

References

1. Available from: <http://www.als-japan.com/1408.html>.
2. Medina-Sanchez, M., et al., *An Inkjet-Printed Field-Effect Transistor for Label-Free Biosensing*. Advanced Functional Materials, 2014. **24**(40): p. 6291-6302.
3. Bandodkar, A.J., et al., *Tattoo-Based Noninvasive Glucose Monitoring: A Proof-of-Concept Study*. Analytical Chemistry, 2015. **87**(1): p. 394-398.
4. Kim, D.H., et al., *Epidermal Electronics*. Science, 2011. **333**(6044): p. 838-843.
5. Lee, H., et al., *A graphene-based electrochemical device with thermoresponsive microneedles for diabetes monitoring and therapy*. Nature Nanotechnology, 2016. **11**(6): p. 566.
6. Available from: <http://www.als-japan.com/1408.html>.
7. Available from: <http://www.chaoticmoon.com/>.
8. Available from: <http://www.bareconductive.com/>.
9. Musameh, M., et al., *Low-potential stable NADH detection at carbon-nanotube-modified glassy carbon electrodes*. Electrochemistry Communications, 2002. **4**(10): p. 743-746.
10. Baptista-Pires, L., et al., *Electrocatalytic tuning of biosensing response through electrostatic or hydrophobic enzyme-graphene oxide interactions*. Biosensors & Bioelectronics, 2014. **61**: p. 655-662.
11. Yu, B., et al., *An elastic second skin*. Nature materials, 2016. **15**(8): p. 911-8.
12. Kaltenbrunner, M., et al., *An ultra-lightweight design for imperceptible plastic electronics*. Nature, 2013. **499**(7459): p. 458-+.
13. Available from: https://en.wikipedia.org/wiki/Colloidal_gold.
14. Available from: <http://www.sigmaaldrich.com/life-science/proteomics/recombinant-protein-expression/purification-detection/his-select/magnetic-agarose-beads.html>.
15. Maltez-da Costa, M., et al., *Simple Monitoring of Cancer Cells Using Nanoparticles*. Nano Letters, 2012. **12**(8): p. 4164-4171.

16. Kimling, J., et al., *Turkevich method for gold nanoparticle synthesis revisited*. Journal of Physical Chemistry B, 2006. **110**(32): p. 15700-15707.
17. Pumera, M., et al., *Direct voltammetric determination of gold nanoparticles using graphite-epoxy composite electrode*. Electrochimica Acta, 2005. **50**(18): p. 3702-3707.
18. Dequaire, M., C. Degrand, and B. Limoges, *An electrochemical metalloimmunoassay based on a colloidal gold label*. Analytical Chemistry, 2000. **72**(22): p. 5521-5528.
19. Geim, A.K. and K.S. Novoselov, *The rise of graphene*. Nature Materials, 2007. **6**(3): p. 183-191.
20. Tuan, D.V., et al., *Scaling Properties of Charge Transport in Polycrystalline Graphene*. Nano Letters, 2013. **13**(4): p. 1730-1735.
21. Bagri, A., et al., *Structural evolution during the reduction of chemically derived graphene oxide*. Nature Chemistry, 2010. **2**(7): p. 581-587.
22. Available from:
<https://www.sciencenews.org/article/%E2%80%98impermeable%E2%80%99-graphene-yields-protons>.
23. Raccichini, R., et al., *The role of graphene for electrochemical energy storage*. Nature Materials, 2015. **14**(3): p. 271-279.
24. Warner, J.H., et al., *Graphene: Fundamentals and Emergent Applications*. Graphene: Fundamentals and Emergent Applications. 2013, Amsterdam: Elsevier Science Bv. 1-450.
25. Novoselov, K.S., et al., *A roadmap for graphene*. Nature, 2012. **490**(7419): p. 192-200.
26. Tour, J.M., *LAYERED MATERIALS Scaling up exfoliation*. Nature Materials, 2014. **13**(6): p. 545-546.
27. Novoselov, K.S., et al., *Electric field effect in atomically thin carbon films*. Science, 2004. **306**(5696): p. 666-669.
28. Balandin, A.A., et al., *Superior thermal conductivity of single-layer graphene*. Nano Letters, 2008. **8**(3): p. 902-907.
29. Lee, C., et al., *Measurement of the elastic properties and intrinsic strength of monolayer graphene*. Science, 2008. **321**(5887): p. 385-388.

30. Guinea, F., M.I. Katsnelson, and A.K. Geim, *Energy gaps and a zero-field quantum Hall effect in graphene by strain engineering*. Nature Physics, 2010. **6**(1): p. 30-33.
31. Wu, J., W. Pisula, and K. Muellen, *Graphenes as potential material for electronics*. Chemical Reviews, 2007. **107**(3): p. 718-747.
32. Novoselov, K.S., et al., *Two-dimensional atomic crystals*. Proceedings of the National Academy of Sciences of the United States of America, 2005. **102**(30): p. 10451-10453.
33. Englert, J.M., et al., *Soluble Graphene: Generation of Aqueous Graphene Solutions Aided by a Perylenebisimide-Based Bolaamphiphile*. Advanced Materials, 2009. **21**(42): p. 4265-+.
34. Lotya, M., et al., *High-Concentration, Surfactant-Stabilized Graphene Dispersions*. Acs Nano, 2010. **4**(6): p. 3155-3162.
35. Lotya, M., et al., *Liquid Phase Production of Graphene by Exfoliation of Graphite in Surfactant/Water Solutions*. Journal of the American Chemical Society, 2009. **131**(10): p. 3611-3620.
36. Li, X., et al., *Highly conducting graphene sheets and Langmuir-Blodgett films*. Nature Nanotechnology, 2008. **3**(9): p. 538-542.
37. Blake, P., et al., *Graphene-based liquid crystal device*. Nano Letters, 2008. **8**(6): p. 1704-1708.
38. Hernandez, Y., et al., *High-yield production of graphene by liquid-phase exfoliation of graphite*. Nature Nanotechnology, 2008. **3**(9): p. 563-568.
39. Ambrosi, A., et al., *Electrochemistry of Graphene and Related Materials*. Chemical Reviews, 2014. **114**(14): p. 7150-7188.
40. Li, X., et al., *Large-Area Synthesis of High-Quality and Uniform Graphene Films on Copper Foils*. Science, 2009. **324**(5932): p. 1312-1314.
41. Cai, J.M., et al., *Atomically precise bottom-up fabrication of graphene nanoribbons*. Nature, 2010. **466**(7305): p. 470-473.
42. Yang, X.Y., et al., *Two-dimensional graphene nanoribbons*. Journal of the American Chemical Society, 2008. **130**(13): p. 4216-+.
43. Chen, L., et al., *From Nanographene and Graphene Nanoribbons to Graphene Sheets: Chemical Synthesis*. Angewandte Chemie-International Edition, 2012. **51**(31): p. 7640-7654.

44. Emtsev, K.V., et al., *Towards wafer-size graphene layers by atmospheric pressure graphitization of silicon carbide*. Nature Materials, 2009. **8**(3): p. 203-207.
45. Berger, C., et al., *Electronic confinement and coherence in patterned epitaxial graphene*. Science, 2006. **312**(5777): p. 1191-1196.
46. Berger, C., et al., *Ultrathin epitaxial graphite: 2D electron gas properties and a route toward graphene-based nanoelectronics*. Journal of Physical Chemistry B, 2004. **108**(52): p. 19912-19916.
47. Kim, K.S., et al., *Large-scale pattern growth of graphene films for stretchable transparent electrodes*. Nature, 2009. **457**(7230): p. 706-710.
48. Reina, A., et al., *Large Area, Few-Layer Graphene Films on Arbitrary Substrates by Chemical Vapor Deposition*. Nano Letters, 2009. **9**(1): p. 30-35.
49. Coraux, J., et al., *Structural coherency of graphene on Ir(111)*. Nano Letters, 2008. **8**(2): p. 565-570.
50. Sutter, P.W., J.I. Flege, and E.A. Sutter, *Epitaxial graphene on ruthenium*. Nature Materials, 2008. **7**(5): p. 406-411.
51. Li, X., et al., *Transfer of Large-Area Graphene Films for High-Performance Transparent Conductive Electrodes*. Nano Letters, 2009. **9**(12): p. 4359-4363.
52. Wu, Y., et al., *Efficient and large-scale synthesis of few-layered graphene using an arc-discharge method and conductivity studies of the resulting films*. Nano Research, 2010. **3**(9): p. 661-669.
53. Kosynkin, D.V., et al., *Longitudinal unzipping of carbon nanotubes to form graphene nanoribbons*. Nature, 2009. **458**(7240): p. 872-U5.
54. Marcano, D.C., et al., *Improved Synthesis of Graphene Oxide*. Acs Nano, 2010. **4**(8): p. 4806-4814.
55. Wang, G., et al., *Highly efficient and large-scale synthesis of graphene by electrolytic exfoliation*. Carbon, 2009. **47**(14): p. 3242-3246.
56. Su, C.-Y., et al., *High-Quality Thin Graphene Films from Fast Electrochemical Exfoliation*. Acs Nano, 2011. **5**(3): p. 2332-2339.
57. Chen, D., H.B. Feng, and J.H. Li, *Graphene Oxide: Preparation, Functionalization, and Electrochemical Applications*. Chemical Reviews, 2012. **112**(11): p. 6027-6053.

58. Thakur, S. and N. Karak, *Alternative methods and nature-based reagents for the reduction of graphene oxide: A review*. Carbon, 2015. **94**: p. 224-242.
59. Griffiths, K., et al., *Laser-scribed graphene presents an opportunity to print a new generation of disposable electrochemical sensors*. Nanoscale, 2014. **6**(22): p. 13613-13622.
60. Li, Y., et al., *Nitrogen-Doped Graphene Quantum Dots with Oxygen-Rich Functional Groups*. Journal of the American Chemical Society, 2012. **134**(1): p. 15-18.
61. Xu, Z. and C. Gao, *Graphene chiral liquid crystals and macroscopic assembled fibres*. Nature Communications, 2011. **2**.
62. Hu, H., et al., *Ultralight and Highly Compressible Graphene Aerogels*. Advanced Materials, 2013. **25**(15): p. 2219-2223.
63. Amadei, C.A., et al., *Fabrication and morphology tuning of graphene oxide nanoscrolls*. Nanoscale, 2016. **8**(12): p. 6783-6791.
64. Jang, M.H., et al., *Is the Chain of Oxidation and Reduction Process Reversible in Luminescent Graphene Quantum Dots?* Small, 2015. **11**(31): p. 3773-3781.
65. Li, X., et al., *Sulphur doping: a facile approach to tune the electronic structure and optical properties of graphene quantum dots*. Nanoscale, 2014. **6**(10): p. 5323-5328.
66. Sun, H., et al., *Recent advances in graphene quantum dots for sensing*. Materials Today, 2013. **16**(11): p. 433-442.
67. Cheng, H.H., et al., *Graphene fiber: a new material platform for unique applications*. Npg Asia Materials, 2014. **6**.
68. Jost, K., G. Dion, and Y. Gogotsi, *Textile energy storage in perspective*. Journal of Materials Chemistry A, 2014. **2**(28): p. 10776-10787.
69. Yun, Y.J., et al., *A Novel Method for Applying Reduced Graphene Oxide Directly to Electronic Textiles from Yarns to Fabrics*. Advanced Materials, 2013. **25**(40): p. 5701-+.
70. Meng, F.C., et al., *Graphene-Based Fibers: A Review*. Advanced Materials, 2015. **27**(35): p. 5113-5131.
71. Xin, G.Q., et al., *Highly thermally conductive and mechanically strong graphene fibers*. Science, 2015. **349**(6252): p. 1083-1087.

72. Henriques, B., et al., *Optimized graphene oxide foam with enhanced performance and high selectivity for mercury removal from water*. Journal of Hazardous Materials, 2016. **301**: p. 453-461.
73. Hu, C., et al., *Scalable Preparation of Multifunctional Fire-Retardant Ultralight Graphene Foams*. Acs Nano, 2016. **10**(1): p. 1325-1332.
74. Niu, Z.Q., et al., *A Leavening Strategy to Prepare Reduced Graphene Oxide Foams*. Advanced Materials, 2012. **24**(30): p. 4144-4150.
75. Zhang, L.L., et al., *Highly Conductive and Porous Activated Reduced Graphene Oxide Films for High-Power Supercapacitors*. Nano Letters, 2012. **12**(4): p. 1806-1812.
76. Zhu, Y.W., et al., *Carbon-Based Supercapacitors Produced by Activation of Graphene*. Science, 2011. **332**(6037): p. 1537-1541.
77. Peng, Z.W., et al., *Flexible Boron-Doped Laser-Induced Graphene Microsupercapacitors*. Acs Nano, 2015. **9**(6): p. 5868-5875.
78. Gao, W., et al., *Direct laser writing of micro-supercapacitors on hydrated graphite oxide films*. Nature Nanotechnology, 2011. **6**(8): p. 496-500.
79. Wicklein, B., et al., *Thermally insulating and fire-retardant lightweight anisotropic foams based on nanocellulose and graphene oxide*. Nature Nanotechnology, 2015. **10**(3): p. 277-283.
80. Zeng, F., et al., *Supercapacitors based on high-quality graphene scrolls*. Nanoscale, 2012. **4**(13): p. 3997-4001.
81. Viculis, L.M., J.J. Mack, and R.B. Kaner, *A chemical route to carbon nanoscrolls*. Science, 2003. **299**(5611): p. 1361-1361.
82. Sharifi, T., et al., *Formation of nitrogen-doped graphene nanoscrolls by adsorption of magnetic gamma-Fe₂O₃ nanoparticles*. Nature Communications, 2013. **4**.
83. Xu, Z., et al., *Highly Efficient Synthesis of Neat Graphene Nanoscrolls from Graphene Oxide by Well-Controlled Lyophilization*. Chemistry of Materials, 2014. **26**(23): p. 6811-6818.
84. Zhang, Z. and T. Li, *Carbon nanotube initiated formation of carbon nanoscrolls*. Applied Physics Letters, 2010. **97**(8).
85. Shioyama, H. and T. Akita, *A new route to carbon nanotubes*. Carbon, 2003. **41**(1): p. 179-181.

86. Roy, D., et al., *Synthesis and Raman spectroscopic characterisation of carbon nanoscrolls*. Chemical Physics Letters, 2008. **465**(4-6): p. 254-257.
87. Berman, D., et al., *Macroscale superlubricity enabled by graphene nanoscroll formation*. Science, 2015. **348**(6239): p. 1118-1122.
88. Wu, Z.S., et al., *Graphene-based in-plane micro-supercapacitors with high power and energy densities*. Nature Communications, 2013. **4**.
89. Wang, X.M., et al., *A spectrally tunable all-graphene-based flexible field-effect light-emitting device*. Nature Communications, 2015. **6**.
90. Acik, M., et al., *Unusual infrared-absorption mechanism in thermally reduced graphene oxide*. Nature Materials, 2010. **9**(10): p. 840-845.
91. Konstantatos, G., et al., *Hybrid graphene-quantum dot phototransistors with ultrahigh gain*. Nature Nanotechnology, 2012. **7**(6): p. 363-368.
92. Kolmakov, A., et al., *Graphene oxide windows for in situ environmental cell photoelectron spectroscopy*. Nature Nanotechnology, 2011. **6**(10): p. 651-657.
93. Mi, B.X., *Graphene Oxide Membranes for Ionic and Molecular Sieving*. Science, 2014. **343**(6172): p. 740-742.
94. Joshi, R.K., et al., *Precise and Ultrafast Molecular Sieving Through Graphene Oxide Membranes*. Science, 2014. **343**(6172): p. 752-754.
95. Ohno, Y., et al., *Electrolyte-Gated Graphene Field-Effect Transistors for Detecting pH Protein Adsorption*. Nano Letters, 2009. **9**(9): p. 3318-3322.
96. Schedin, F., et al., *Detection of individual gas molecules adsorbed on graphene*. Nature Materials, 2007. **6**(9): p. 652-655.
97. Salehi-Khojin, A., et al., *Polycrystalline Graphene Ribbons as Chemiresistors*. Advanced Materials, 2012. **24**(1): p. 53-+.
98. Zhou, M., Y. Zhai, and S. Dong, *Electrochemical Sensing and Biosensing Platform Based on Chemically Reduced Graphene Oxide*. Analytical Chemistry, 2009. **81**(14): p. 5603-5613.
99. Wang, X., L. Zhi, and K. Muellen, *Transparent, conductive graphene electrodes for dye-sensitized solar cells*. Nano Letters, 2008. **8**(1): p. 323-327.

100. Shen, T.Z., S.H. Hong, and J.K. Song, *Electro-optical switching of graphene oxide liquid crystals with an extremely large Kerr coefficient*. Nature Materials, 2014. **13**(4): p. 394-399.
101. Nurunnabi, M., et al., *Photoluminescent Graphene Nanoparticles for Cancer Phototherapy and Imaging*. Acs Applied Materials & Interfaces, 2014. **6**(15): p. 12413-12421.
102. Borini, S., et al., *Ultrafast Graphene Oxide Humidity Sensors*. Acs Nano, 2013. **7**(12): p. 11166-11173.
103. Chi, H., et al., *Highly Sensitive and Fast Response Colorimetric Humidity Sensors Based on Graphene Oxides Film*. Acs Applied Materials & Interfaces, 2015. **7**(36): p. 19882-19886.
104. An, D., et al., *Separation Performance of Graphene Oxide Membrane in Aqueous Solution*. Industrial & Engineering Chemistry Research, 2016. **55**(17): p. 4803-4810.
105. Aunkor, M.T.H., et al., *The green reduction of graphene oxide*. Rsc Advances, 2016. **6**(33): p. 27807-27828.
106. Georgakilas, V., et al., *Noncovalent Functionalization of Graphene and Graphene Oxide for Energy Materials, Biosensing, Catalytic, and Biomedical Applications*. Chemical Reviews, 2016. **116**(9): p. 5464-5519.
107. Shang, J.Z., et al., *The Origin of Fluorescence from Graphene Oxide*. Scientific Reports, 2012. **2**.
108. Loh, K.P., et al., *Graphene oxide as a chemically tunable platform for optical applications*. Nature Chemistry, 2010. **2**(12): p. 1015-1024.
109. Kurapati, R., et al., *Dispersibility-Dependent Biodegradation of Graphene Oxide by Myeloperoxidase*. Small, 2015. **11**(32): p. 3985-3994.
110. Kotchey, G.P., et al., *The Enzymatic Oxidation of Graphene Oxide*. Acs Nano, 2011. **5**(3): p. 2098-2108.
111. Sun, P.Z., et al., *Selective Trans-Membrane Transport of Alkali and Alkaline Earth Cations through Graphene Oxide Membranes Based on Cation- π Interactions*. Acs Nano, 2014. **8**(1): p. 850-859.
112. Shen, J., et al., *Membranes with Fast and Selective Gas-Transport Channels of Laminar Graphene Oxide for Efficient CO₂ Capture*. Angewandte Chemie-International Edition, 2015. **54**(2): p. 578-582.

113. Sun, P.Z., et al., *Selective Ion Penetration of Graphene Oxide Membranes*. *Acs Nano*, 2013. **7**(1): p. 428-437.
114. Lerf, A., et al., *Hydration behavior and dynamics of water molecules in graphite oxide*. *Journal of Physics and Chemistry of Solids*, 2006. **67**(5-6): p. 1106-1110.
115. Nair, R.R., et al., *Unimpeded Permeation of Water Through Helium-Leak-Tight Graphene-Based Membranes*. *Science*, 2012. **335**(6067): p. 442-444.
116. Park, S., et al., *Graphene-Based Actuators*. *Small*, 2010. **6**(2): p. 210-212.
117. Kim, T.H., et al., *Controlling Differentiation of Adipose-Derived Stem Cells Using Combinatorial Graphene Hybrid-Pattern Arrays*. *Acs Nano*, 2015. **9**(4): p. 3780-3790.
118. Yoon, H.J., et al., *Sensitive capture of circulating tumour cells by functionalized graphene oxide nanosheets*. *Nature Nanotechnology*, 2013. **8**(10): p. 735-741.
119. Serrano, M.C., et al., *3D free-standing porous scaffolds made of graphene oxide as substrates for neural cell growth*. *Journal of Materials Chemistry B*, 2014. **2**(34): p. 5698-5706.
120. Garcia-Tunon, E., et al., *Printing in Three Dimensions with Graphene*. *Advanced Materials*, 2015. **27**(10): p. 1688-+.
121. Wang, J., et al., *Rod-Coating: Towards Large-Area Fabrication of Uniform Reduced Graphene Oxide Films for Flexible Touch Screens*. *Advanced Materials*, 2012. **24**(21): p. 2874-2878.
122. Available from: <http://www.sono-tek.com/graphene-coatings/>.
123. Secor, E.B., et al., *Gravure Printing of Graphene for Large-Area Flexible Electronics*. *Advanced Materials*, 2014. **26**(26): p. 4533-+.
124. Eda, G., G. Fanchini, and M. Chhowalla, *Large-area ultrathin films of reduced graphene oxide as a transparent and flexible electronic material*. *Nature Nanotechnology*, 2008. **3**(5): p. 270-274.
125. Zhao, C.L., et al., *Formation of uniform reduced graphene oxide films on modified PET substrates using drop-casting method*. *Particuology*, 2014. **17**: p. 66-73.

126. Takami, T., T. Ito, and T. Ogino, *Self-Assembly of a Monolayer Graphene Oxide Film Based on Surface Modification of Substrates and its Vapor-Phase Reduction*. Journal of Physical Chemistry C, 2014. **118**(17): p. 9009-9017.
127. Shi, H.F., et al., *Transparent conductive reduced graphene oxide thin films produced by spray coating*. Science China-Physics Mechanics & Astronomy, 2015. **58**(1).
128. Baptista-Pires, L., et al., *Water Activated Graphene Oxide Transfer Using Wax Printed Membranes for Fast Patterning of a Touch Sensitive Device*. Acs Nano, 2016. **10**(1): p. 853-860.
129. Karuwan, C., et al., *A disposable screen printed graphene-carbon paste electrode and its application in electrochemical sensing*. Rsc Advances, 2013. **3**(48): p. 25792-25799.
130. Secor, E.B., et al., *Inkjet Printing of High Conductivity, Flexible Graphene Patterns*. Journal of Physical Chemistry Letters, 2013. **4**(8): p. 1347-1351.
131. Lee, J.S., et al., *Wafer-Scale Patterning of Reduced Graphene Oxide Electrodes by Transfer-and-Reverse Stamping for High Performance OFETs*. Small, 2013. **9**(16): p. 2817-2825.
132. Chen, L.Y., et al., *Direct electrodeposition of reduced graphene oxide on glassy carbon electrode and its electrochemical application*. Electrochemistry Communications, 2011. **13**(2): p. 133-137.
133. Hyun, W.J., O.O. Park, and B.D. Chin, *Foldable Graphene Electronic Circuits Based on Paper Substrates*. Advanced Materials, 2013. **25**(34): p. 4729-4734.
134. He, Q., et al., *Centimeter-Long and Large-Scale Micropatterns of Reduced Graphene Oxide Films: Fabrication and Sensing Applications*. Acs Nano, 2010. **4**(6): p. 3201-3208.
135. Akhavan, O., E. Ghaderi, and R. Rahighi, *Toward Single-DNA Electrochemical Biosensing by Graphene Nanowalls*. Acs Nano, 2012. **6**(4): p. 2904-2916.
136. Chen, M. and X. Ma, *Electrochemical determination of ethyl maltol on a glassy carbon electrode modified with graphene*. Journal of the Chilean Chemical Society, 2013. **58**(3): p. 1918-1920.

137. Li, X., et al., *Graphene Films with Large Domain Size by a Two-Step Chemical Vapor Deposition Process*. Nano Letters, 2010. **10**(11): p. 4328-4334.
138. Ma, X.Y., M.Y. Chao, and Z.X. Wang, *Electrochemical detection of dopamine in the presence of epinephrine, uric acid and ascorbic acid using a graphene-modified electrode*. Analytical Methods, 2012. **4**(6): p. 1687-1692.
139. Brownson, D.A.C., et al., *Electrochemical properties of CVD grown pristine graphene: monolayer- vs. quasi-graphene*. Nanoscale, 2014. **6**(3): p. 1607-1621.
140. Pumera, M., *Graphene-based nanomaterials and their electrochemistry*. Chemical Society Reviews, 2010. **39**(11): p. 4146-4157.
141. Shang, N.G., et al., *Catalyst-Free Efficient Growth, Orientation and Biosensing Properties of Multilayer Graphene Nanoflake Films with Sharp Edge Planes*. Advanced Functional Materials, 2008. **18**(21): p. 3506-3514.
142. Lim, C.X., et al., *Direct Voltammetric Detection of DNA and pH Sensing on Epitaxial Graphene: An Insight into the Role of Oxygenated Defects*. Analytical Chemistry, 2010. **82**(17): p. 7387-7393.
143. Davies, T.J., M.E. Hyde, and R.G. Compton, *Nanotrench arrays reveal insight into graphite electrochemistry*. Angewandte Chemie-International Edition, 2005. **44**(32): p. 5121-5126.
144. Brownson, D.A.C., M. Gomez-Mingot, and C.E. Banks, *CVD graphene electrochemistry: biologically relevant molecules*. Physical Chemistry Chemical Physics, 2011. **13**(45): p. 20284-20288.
145. Brownson, D.A.C. and C.E. Banks, *CVD graphene electrochemistry: the role of graphitic islands*. Physical Chemistry Chemical Physics, 2011. **13**(35): p. 15825-15828.
146. Bowling, R.J., R.T. Packard, and R.L. McCreery, *activation of highly ordered pyrolytic-graphite for heterogeneous electron-transfer - relationship between electrochemical performance and carbon microstructure*. Journal of the American Chemical Society, 1989. **111**(4): p. 1217-1223.

147. Tan, C., et al., *Reactivity of Monolayer Chemical Vapor Deposited Graphene Imperfections Studied Using Scanning Electrochemical Microscopy*. *Acs Nano*, 2012. **6**(4): p. 3070-3079.
148. An, J., et al., *Domain (Grain) Boundaries and Evidence of "Twinlike" Structures in Chemically Vapor Deposited Grown Graphene*. *Acs Nano*, 2011. **5**(4): p. 2433-2439.
149. Rumyantsev, S., et al., *Selective Gas Sensing with a Single Pristine Graphene Transistor*. *Nano Letters*, 2012. **12**(5): p. 2294-2298.
150. Fattah, A., et al., *Graphene/Silicon Heterojunction Schottky Diode for Vapors Sensing Using Impedance Spectroscopy*. *Small*, 2014. **10**(20): p. 4193-4199.
151. Le Thai, D., et al., *High Performance Three-Dimensional Chemical Sensor Platform Using Reduced Graphene Oxide Formed on High Aspect-Ratio Micro-Pillars*. *Advanced Functional Materials*, 2015. **25**(6): p. 883-890.
152. Favaro, M., et al., *Shaping graphene oxide by electrochemistry: From foams to self-assembled molecular materials*. *Carbon*, 2014. **77**: p. 405-415.
153. Wang, Z., et al., *Direct Electrochemical Reduction of Single-Layer Graphene Oxide and Subsequent Functionalization with Glucose Oxidase*. *Journal of Physical Chemistry C*, 2009. **113**(32): p. 14071-14075.
154. Kang, X., et al., *Glucose Oxidase-graphene-chitosan modified electrode for direct electrochemistry and glucose sensing*. *Biosensors & Bioelectronics*, 2009. **25**(4): p. 901-905.
155. Zhou, K., et al., *Electrocatalytic Oxidation of Glucose by the Glucose Oxidase Immobilized in Graphene-Au-Nafion Biocomposite*. *Electroanalysis*, 2010. **22**(3): p. 259-264.
156. Kim, J., et al., *Wafer-scale high-resolution patterning of reduced graphene oxide films for detection of low concentration biomarkers in plasma*. *Scientific Reports*, 2016. **6**.
157. Mannoor, M.S., et al., *Graphene-based wireless bacteria detection on tooth enamel*. *Nature Communications*, 2012. **3**.

158. Rabti, A., et al., *Ferrocene-functionalized graphene electrode for biosensing applications*. *Analytica Chimica Acta*, 2016. **926**: p. 28-35.
159. He, Q., et al., *Transparent, Flexible, All-Reduced Graphene Oxide Thin Film Transistors*. *Acs Nano*, 2011. **5**(6): p. 5038-5044.
160. Tehrani, F. and B. Bavarian, *Facile and scalable disposable sensor based on laser engraved graphene for electrochemical detection of glucose*. *Scientific Reports*, 2016. **6**.

Chapter 2**Objectives**

In this chapter the general objectives of the thesis are presented.

The general objective of this PhD thesis is the development of new biosensing platforms and devices using nanomaterials such as gold nanoparticles, magnetic beads and graphene oxide. More in detail the objectives of this thesis can be summarized as following:

- The study of a novel biosensor using primer labeled gold nanoparticles and magnetic bead and their influence in the isothermal amplification of Leishmania DNA for a direct electrochemical detection using screen printed carbon electrode (SPCE).
- The study and characterization of the optical, electrochemical and electrocatalytic properties of graphene oxide (GO) and reduced GO modified SPCE for the detection of catechol using Tyrosinase as proof-of-concept enzyme.
- The development of a novel printing technology for GO using wax printed membranes for a versatile and low-cost methodology with infinite shaping capability.

Chapter 3**Electrochemical detection of an immunosandwich using nanoparticles**

In this chapter a novel methodology for the isothermal amplification of *Leishmania* DNA using labeled primers combined with the advantages of magnetic purification/preconcentration and the use of gold nanoparticle (AuNPs) tags for the sensitive electrochemical detection of such amplified DNA is developed.

Related publication

- 1) Alfredo de la Escosura-Muñiz, Luis Baptista-Pires, Lorena Serrano, Laura Altet, Olga Francino, Armand Sánchez, Arben Merkoçi, Magnetic bead/gold nanoparticle double-labeled primers for electrochemical detection of isothermal amplified *Leishmania* DNA. *Small*, 2015. 12(2):p.205-2013

1. Introduction

Diseases transmitted by blood-feeding vectors (parasites) are a growing threat to world human health, particularly those affecting pets and transmitted by fleas, ticks, sandflies or mosquitoes (Vector Borne Diseases, VBD).^{1,2,3} One of the most important VBD is visceral leishmaniasis which is endemic in 88 countries on 4 continents.^{4,5,6} Zoonotic visceral leishmaniasis, caused by the protozoan *Leishmania infantum* and transmitted by sandfly vectors, is a fatal disease of domestic dogs, wild canids and humans.⁷ Different methods for the detection and diagnosis of Canine Leishmaniasis (CanL) including parasitological,⁸⁻¹⁰ serological^{11,12} and molecular techniques¹³⁻¹⁹ have been reported, suffering of limitations related to the need of skilled workers, the high cost and the fact that samples must be send to a reference lab. Lateral-flow assay (LFA) strips for specific CanL antigen are commercially available for detection of visceral leishmaniasis.²⁰⁻²³ However, the presence of low antibody levels is not necessarily indicative of disease and further work-up is necessary to confirm it by DNA-based diagnostic methods, being PCR the gold standard. In this context, a dipstick format was developed for the detection of PCR amplified CanL DNA.²⁴ A qualitative real-time PCR (Leish PCR assay)²⁵ is also commercially available for diagnosing cutaneous leishmaniasis. However, both systems did not overcome the limitations of PCR for which sophisticated and expensive equipment is needed to perform the precise and repeated heating cycles required. Therefore, there is still a need for further point-of-care (POC) diagnostic methods for the detection of infections by pathogens, particularly for leishmaniasis.

Isothermal amplification is an alternative approach to the traditional PCR which overcomes many of the complications related to the thermocycling since it is performed at a constant temperature thanks to the use of enzymes. There are many different isothermal amplification methods, depending on the enzymes and the temperature used. The variation called Recombinase Polymerase Amplification (RPA) commercialized by Twist (TwistDx's®)²⁶ employs recombinase enzymes which are capable of pairing oligonucleotide primers with homologous sequence in duplex DNA typically within 5 - 10 minutes. However, in most cases DNA purification and detection after amplification still requires

hazardous, time consuming and expensive equipment, giving only qualitative information, so alternative methodologies overcoming such problems are required. In this context, the integration of nanoparticle (NP) tags during the amplification process combined with the very sensitive electrocatalytic^{27,28} detection of such a tag would overcome most of these limitations. The outstanding properties of different nanomaterials have been extensively approached in DNA biosensing systems. NPs have been used in a high extent as both optical and electrochemical tags in DNA hybridization biosensors²⁹⁻³⁷ while magnetic beads (MBs) have been extensively used as platforms of such and other bioassays.^{38,39} Gold nanoparticles (AuNPs)^{40,41} and in a minor extent silver nanoparticles (AgNPs)⁴² and quantum dots (QDs)⁴³ have been also introduced in the cocktail of reagents of the PCR, taking advantage of their properties as catalyzers of the DNA amplification reaction, constituting the so-called nanoPCR⁴⁴ in some cases after MB-based DNA extraction.⁴⁵ Only a report on AuNPs-labeled primers for optical detection of PCR amplified DNA is found in the bibliography⁴⁶ while few examples of PCR amplification using MB-labeled primers⁴⁷⁻⁴⁹ have been published, but the integration of both MBs and AuNPs-labeled primers have not ever been reported, probably due to the high temperature reached during the PCR cycle which is a serious limitation for preserving the labeled primer integrity. Regarding the isothermal DNA amplification, AuNPs have been used as reporters in optical approaches based on AuNPs addition after DNA amplification followed by colorimetric⁵⁰⁻⁵⁵ or surface plasmon resonance-based^{56,57} detection, in some cases taking also advantage of MBs after the amplification reaction for pre-concentration/purification purposes.⁵⁸ In a similar way, AuNPs have been used as electrochemical reporters in DNA hybridization biosensors for the detection of isothermal amplified DNA⁵⁹ taking also advantage of the use of MBs platforms.^{60,61} All these approaches are based on the addition of the micro/nanoparticles after the DNA amplification and in most cases require the performance of further DNA hybridization assays, which increase the analysis time and also involve more irreproducibility, loss of sensitivity and false positives due to unspecific absorptions.

In this work, we present a novel design of *Leishmania* DNA isothermal amplification using for the first time primers labeled with both AuNPs and MBs.

The low and constant temperature of the isothermal amplification procedure is ideal for preserving the integrity of the nanoparticle-primer conjugates during the amplification step. The double-labeled product resulting from such amplification is ready for a rapid magnetic separation/pre-concentration and direct electrocatalytic detection in a very sensitive and quantitative way. A general scheme of the whole experimental procedure from the DNA extraction to the final electrochemical detection is shown in figure 1.

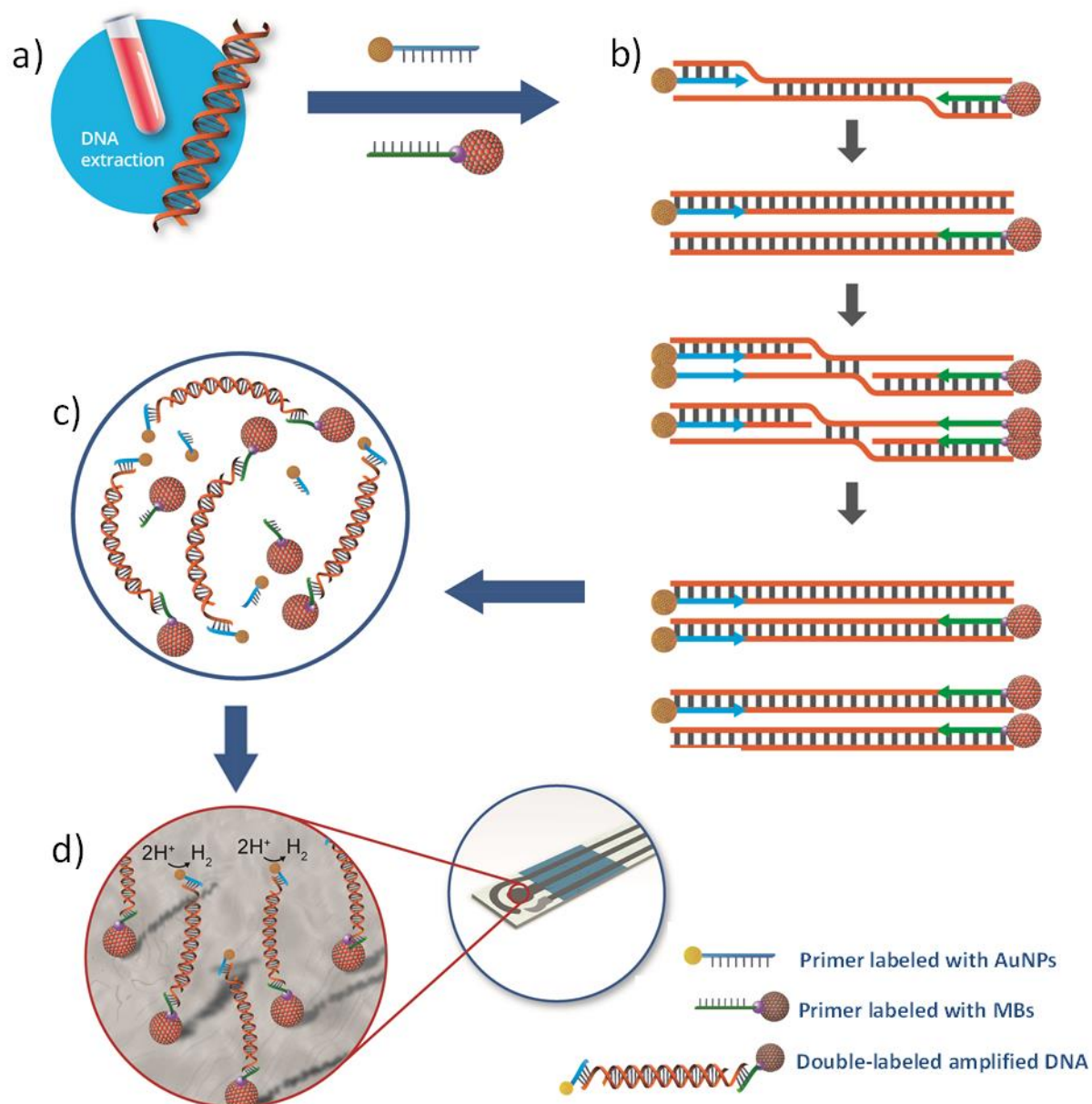


Figure 1: Scheme of the experimental procedure for the detection of isothermal amplified DNA using primers labeled with AuNPs and MBs. DNA is extracted from dog blood (a) and a kinetoplast specific region is isothermal amplified by RPA cycle using primers labeled with AuNPs and MBs (b). The double-labeled amplified product (MB/amplified DNA/AuNP complex) (c) is captured by the magnet placed on the reverse side of the working electrode of the SPCE and AuNPs tags are detected through the electrocatalytic Hydrogen Evolution Reaction (HER) (d).

2. Results and discussion

Design and screening of primer sets for Leishmania assay and endogenous control

3 candidate primers for kinetoplast and 8 candidate primers for Intergenic Spacer region (ITS1) of *Leishmania* were designed following recommended conditions (Appendix to the TwistAmpTM reaction kit manuals²⁶). All possible combinations of primers were tested using standard conditions of TwistAmp (37°C of reaction temperature; Magnesium-Acetate concentrations of 14 mM; shaking 4' after initiation of the reaction; 480 nM of each primer). Parameters that can be modified by the user (temperature, magnesium concentration, stirring regime and primer concentrations) were adjusted to obtain the best performance. This first step generates 4 sets of primers used in simplified standard conditions (37°C of reaction temperature; at 14 mM of Magnesium concentration, 480 nM of primer concentration, without agitation 4' after starting the reaction and with a reaction time of 20'). To improve the performance of the *Leishmania* assay a 'second generation' of primers was designed by creating variants of the best primer set identified in the first step (moving 1 base pair around the initial primer) and re-screening the new candidates to improve amplification performance. Finally, with definitive ones, primer concentration was adjusted to 300 nM and reaction time was decreased up to 10' (figure 2a and b).

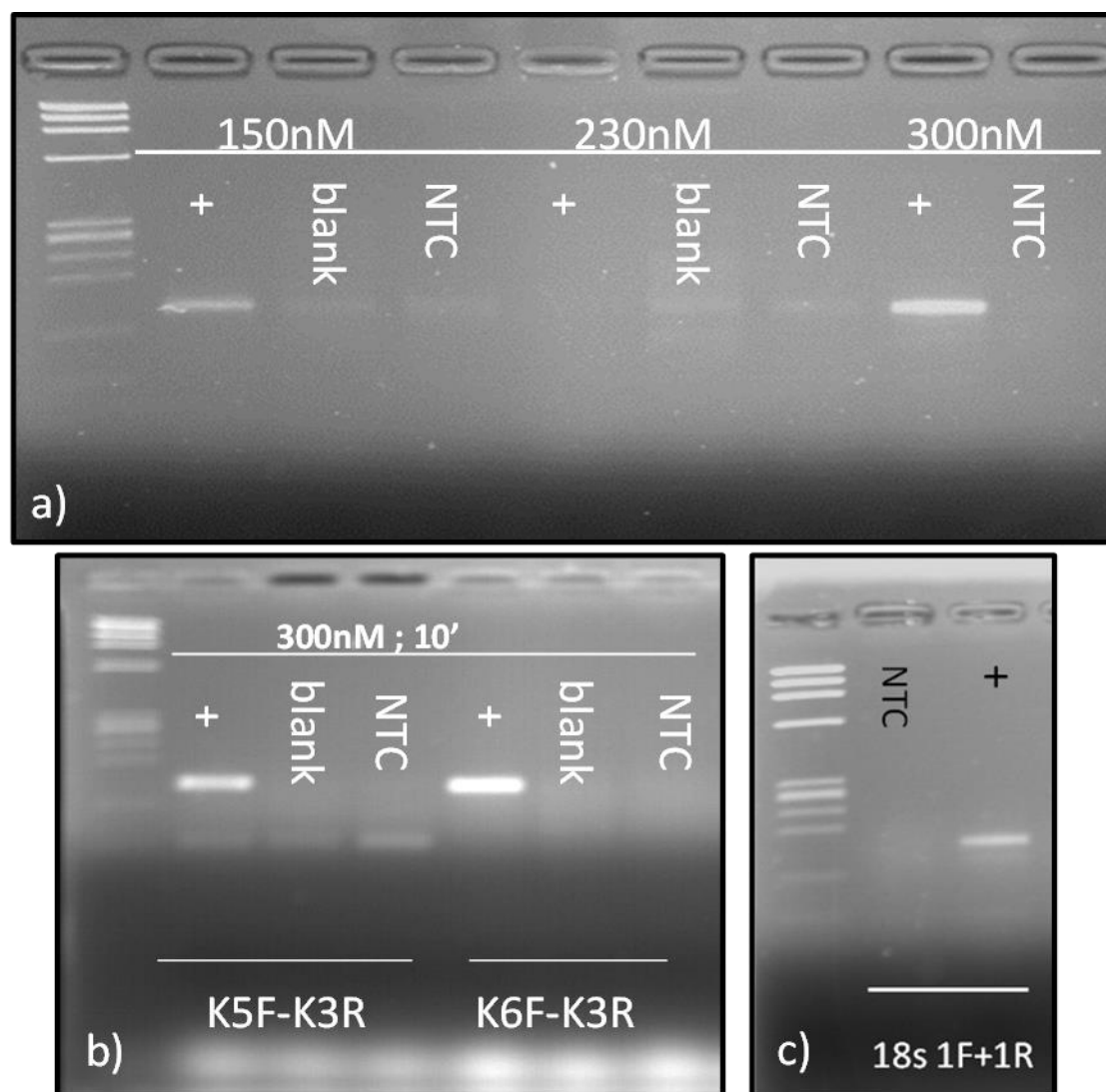


Figure 2. Isothermal assay optimization evaluation by gel electrophoresis. (a) Optimization of primer concentration of *Leishmania* assay.; (b) Example of the "second generation" screening of *Leishmania* primers: K6F-K3R are the chosen ones for its best performance; (c) Definitive endogenous control assay used. +, positive sample (DNA of a dog with *Leishmania* infection); blank, (DNA of a dog without *Leishmania* infection); NTC, negative template control. Line 1 of each gel: Phi-X 174/HaeIII Marker (1353/1078/872/603/310/(281,271)/234/194/118/72). Bands size: 140 bp for *Leishmania* and 168 for 18S.

An endogenous control was incorporated to avoid the generation of artifacts that were detected in no-template controls and samples of very low target copy number. To optimize the endogenous control RPA amplification 6 candidate primers for 18S ribosomal RNA gene were screened (figure 2c).

The assay presented based on isothermal co-amplification of *Leishmania* parasite and 18S as an endogenous control exhibits similar results than the real time used as a gold standard,⁶² with a limit of detection of <1 parasite in the reaction. It is possible since both assays target a conserved region of the *Leishmania* kinetoplast minicircle DNA that is present in about 10.000 copies for parasite.⁶³⁻⁶⁵ Multiplex isothermal has been optimized with an endogenous control primer concentration limited to 150 nM to avoid a loss of sensitivity when low targets of *Leishmania* were present.

Characterization of AuNP/amplified DNA

The performance of the isothermal amplification procedure using primers labeled with AuNPs was evaluated by both Zeta potential and electrochemical measurements. Zeta potential is well known as an efficient tool for the monitoring and analysis of modifications on the surface of NPs, with minimal sample preparation.⁶⁶ It has been used to obtain information concerning the particle surface charge, chemical modifications and also stability of colloid suspensions. A high zeta potential (positive or negative; typically higher than 10 mV) confers stability since the dispersion resists aggregation. Since ssDNA is negatively charged, the conjugation of AuNPs with ssDNA should give rise to negative charged conjugates which would shift the Z potential to more negative values. All these characteristics make zeta potential an ideal technique for the characterization of both the primers and the final amplified DNA labeled with AuNPs.

As can be observed in figure 3a, a gradual shift to more negative values was observed in the Zeta potential of AuNPs when higher was the coverage degree by ssDNA. This suggests that AuNPs were being loaded with negative charged molecules such as ssDNA. First, a shift from the value of the non-modified AuNPs (a) was observed for the AuNP/primer (b) indicating that the primer was correctly connected with the AuNP. After the amplification, a shift of up to 25 mV was observed (d), suggesting the covering of the AuNPs with the amplified

dsDNA (that has more negative charges). No significant shift was observed for a control amplification assay performed with a blank sample (c), also corroborating the specificity of the system.

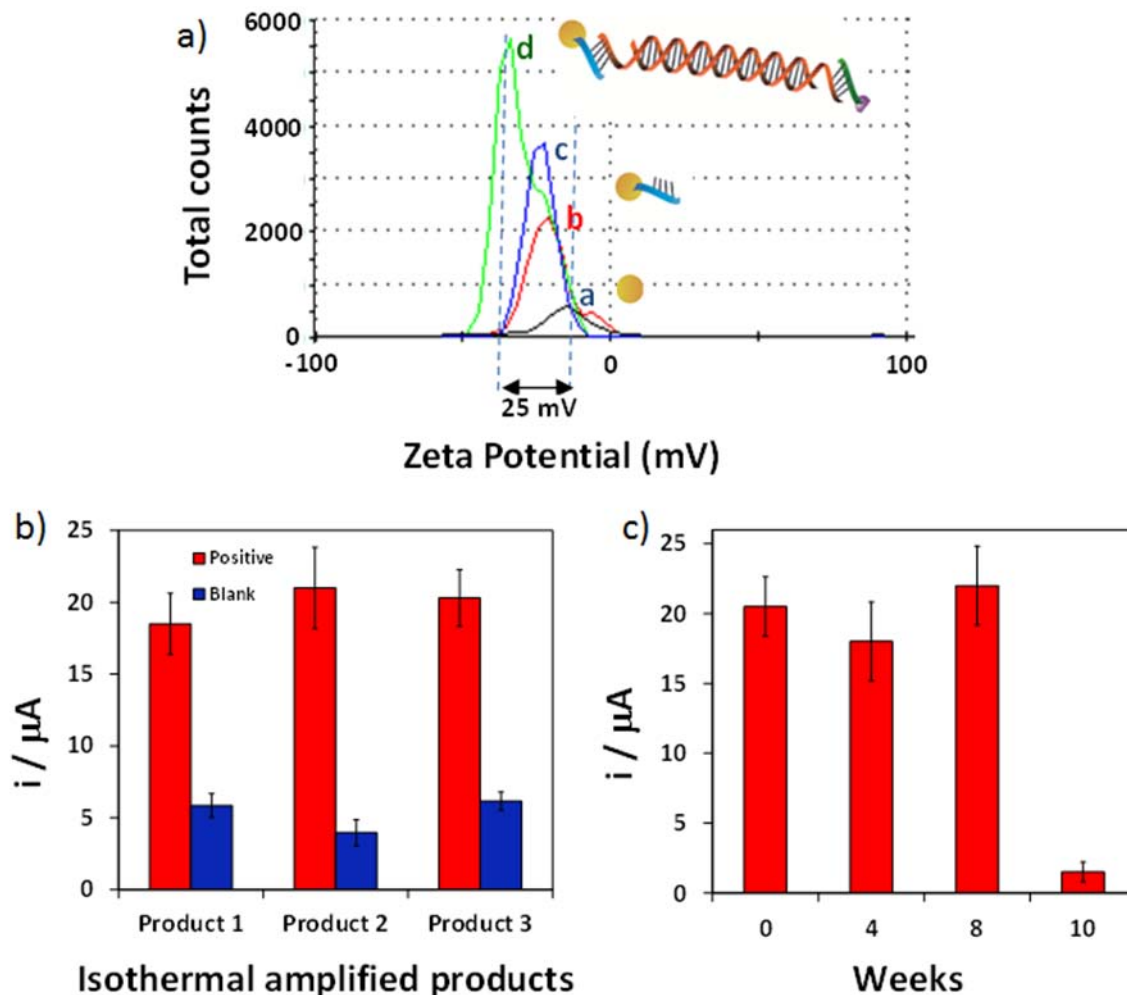


Figure 3. Characterization of AuNP/amplified DNA. (a) Diagram for the zeta potential as a distribution versus total counts for a dispersion of AuNPs before (a curve) and after (b curve) the conjugation with the primer and for amplified DNA using the AuNP-labeled primer for a positive (d curve) and a blank (c curve) sample. (b) Comparison of the analytical signals obtained for different “positive” and “blank” samples after DNA amplification using AuNP-labeled primers. (c) Analytical signals obtained for different isothermal amplifications performed several weeks after the preparation of the conjugate of AuNP/primer.

These evidences were also corroborated by electrochemical measurements. Three different “positive” and “blank” samples were analyzed for this purpose. The AuNP/amplified DNA product was purified by incubation with streptavidin-modified MBs which capture the amplified products through the biotin present in the primer and finally detected taking advantage of the electrocatalytic activity of AuNPs toward the hydrogen evolution reaction (HER). Briefly, this well-known methodology is based on the fact that the presence of AuNP connected to MBs on the SPCE surface shifts the potential for hydrogen ion reduction toward less negative potentials. Fixing a reductive potential of -1.00 V, the intensity of the current recorded in chronoamperometric mode during the stage of hydrogen ion electroreduction at 60 seconds (chosen as analytical signal) is related to the quantity of AuNPs on the SPCE and consequently to the amount of tagged analyte.^{27,28}

As observed in figure 3b, “positive” and “blank” samples can be perfectly discriminated in the three samples, suggesting the specific presence of AuNPs in the amplified products and consequently the good performance of the isothermal amplification in the presence of such tags. The signals of the “blank” samples are at the normal levels of background of the HER in absence of catalyzer (around 5-7 μA), so the specificity of the amplification is demonstrated.

Furthermore, it was observed that the life-time of AuNP/primer conjugates was of up to 8 weeks when stored at 4°C and protected from light, as shown in figure 3c where different amplifications for “positive” samples were performed at different times after the preparation of the AuNP/primer conjugate. The dramatic decrease in the analytical signal observed after 8 weeks suggests the damaging of the AuNP/primer, probably due to either breaking of the binding or AuNPs agglomeration. Further studies will be focused on alternative AuNP/primer storage conditions, such as freezing or lyophilization.

Evaluation of double labeled MB-AuNP/amplified DNA

Once demonstrated the good performance of the isothermal amplification procedure using AuNP-labeled primers, the experimental procedure was significantly simplified by also introducing the MB-labeled primer in the amplification reagents mixture as illustrated in figure 1. In this case, the

experimental procedure for the measurement after the amplification is enormously simplified since the MB/amplified DNA/AuNP complex is directly placed onto the SPCE surface and captured by the magnet placed on the reverse side of the working electrode immediately before the electrochemical measurement.

MBs of two different sizes (2.8 μm and 1 μm) and two different kind of primers were evaluated: the K3R detailed in the experimental section and also a longer one that includes a spacer of (AT)₇ in the 5' tail. This tail of oligonucleotides helps to keep the magnetic bead far from the amplification zone.

The results shown in figure 4a seem to indicate that the amplification doesn't work properly using the bigger MBs in combination with the short primer since the recorded currents are in the levels of the background. The results improved a little bit when the use of longer primers (containing a spacer oligonucleotides sequence) was introduced. When the smaller MBs and the short primer were tested, the amplification worked in a higher extent, and this was highly improved when it was used in combination with the primers containing a spacer. This suggests that the bigger MBs are hindering the amplification, probably due to the beads deposition during the amplification procedure. Furthermore, the procedure takes advantage in this case of the fact that the amplification sequence of the primer is not in direct contact with the bead, which probably facilitates the DNA amplification.

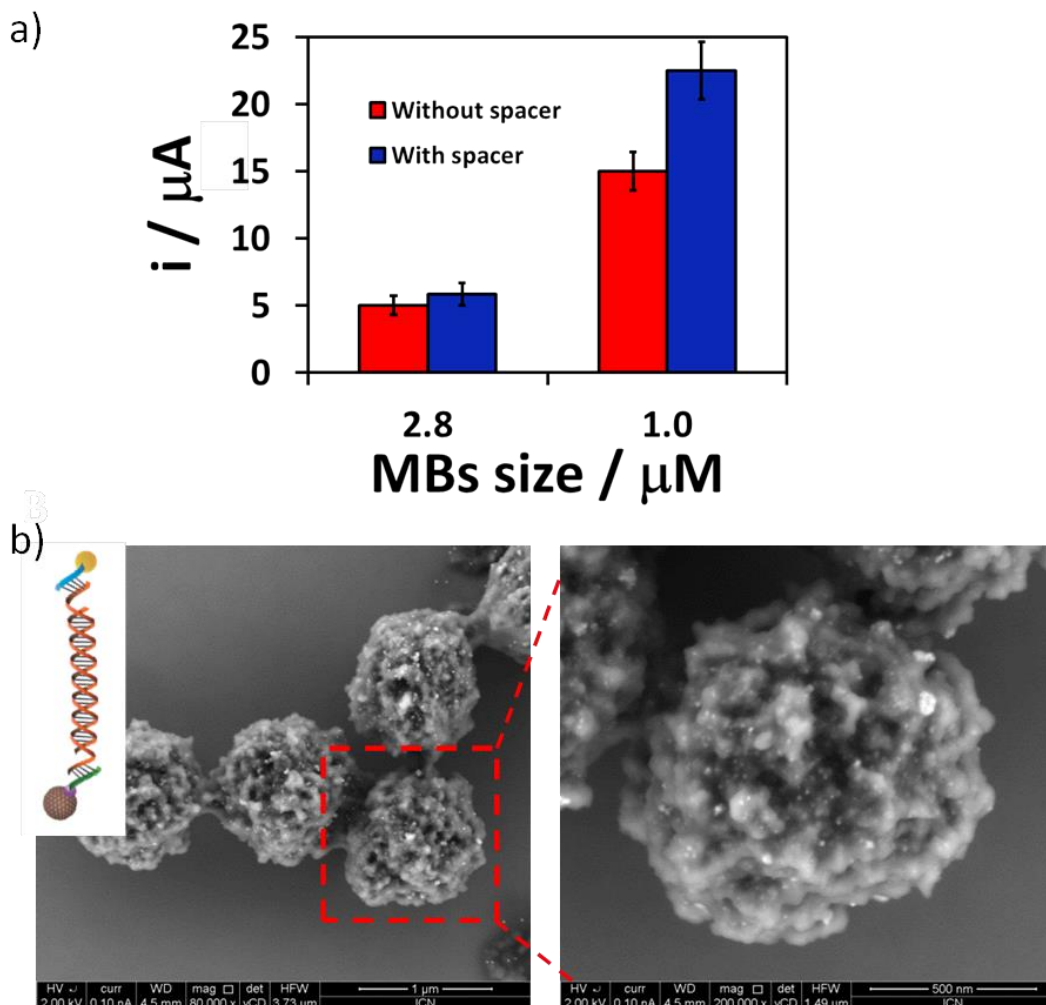


Figure 4. Evaluation of double labeled MB-AuNP isothermal amplified DNA. (a) Analytical signals obtained for MBs of two different sizes (2.8 μm and 1 μm) and reverse primers with and without spacer. (b) SEM characterization of the MBs after the DNA isothermal amplification. In both cases, forward primers are labeled with AuNPs. Experimental conditions as detailed in the text.

The good performance of the amplification procedure as well as the integrity of the double-labeled amplified products was evaluated by SEM analysis. As shown in figure 4b, AuNPs (observed as small white spots) are connected to the MBs (big microspheres in the image) after the amplification procedure, evidencing the formation of the MB-AuNP/amplified DNA (a control image after amplification of DNA without *Leishmania* parasite is shown at the Supporting Information).

Quantitative assays: evaluation of products with different parasite concentration

The optimized methodology was applied for the evaluation of amplified DNA prepared from samples containing different quantities of spiked parasite. Chronoamperograms recorded for the assayed samples are shown in the inset of Figure 5a, where the values of the analytical signals (current at 60 seconds) after subtracting the background (current in 1M HCl, in the absence of catalyzer) are represented for a better understanding.

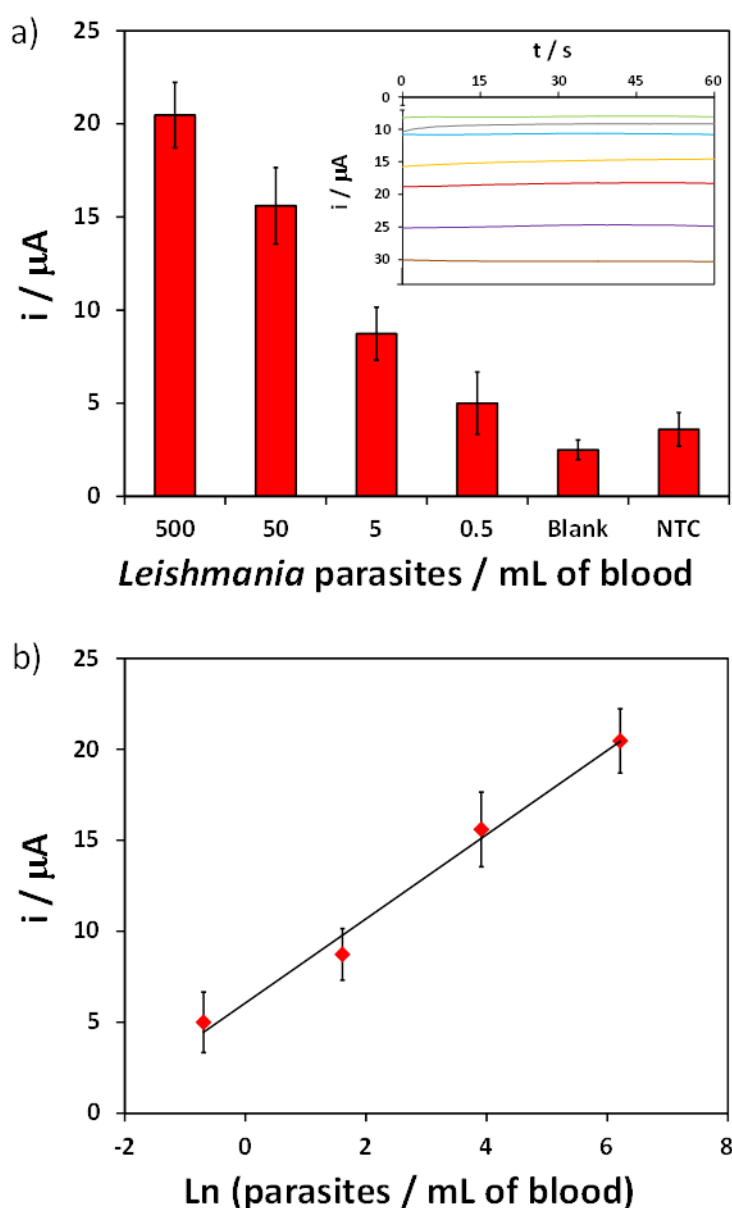


Figure 5. Quantitative *Leishmania infantum* parasite determination. (a) Analytical signals obtained for double labeled MB-AuNP isothermal amplified DNA products prepared from different quantities of parasite, after subtracting the background current. Inset graphic corresponds to the chronoamperograms recorded at -1V. Lower current curve (green curve) corresponds to a 1M HCl solution (background signal). (b) Logarithmic relationship between the number of *Leishmania* parasites and the value of the analytical signal, after subtracting the background. Experimental conditions as detailed in the text.

As shown in Figure 5b, a linear relationship between the analytical signal (after subtracting the background current) and the logarithm of parasite concentration in the range 500 to 0.5 parasites per mL of blood (samples prepared as detailed in the experimental section) was obtained. A limit of detection (LOD) of 0.8 parasites per mL of blood (8×10^{-3} parasites per DNA amplification reaction) was estimated, as the parasite number giving a signal equal to the blank signal plus three times its standard deviation. The reproducibility of responses for 5 parasites per mL of blood was also studied, obtaining a relative standard deviation (RSD) of 7%.

Our AuNP/MBs based electrochemical approach results are quite better to those obtained by other POC tests using nucleic acid sequence based amplification (NASBA) and coupled to oligochromatography (OC) for *Leishmania* detection⁶⁷ and even much better than the 1 parasite per PCR detection limit offered by the OligoC-test®.²⁴

3. Conclusions

In summary, a novel design of isothermal amplification using for the first time primers labeled with both AuNPs and MBs for obtaining of double labeled amplified products has been successfully developed for a DNA sequence characteristic of *Leishmania infantum* kinetoplast tested in dogs, chosen as model. The double label allows the rapid magnetic purification/preconcentration of the product followed by direct AuNP electrocatalytic detection, avoiding DNA hybridization procedures. The electrochemical method exhibits a good

reproducibility and sensitivity, allowing to detect 0.8 parasites per mL of blood (8×10^{-3} parasites per DNA amplification reaction). Furthermore, amplified DNA from dogs without *Leishmania* can be perfectly discriminated, demonstrating the specificity of both the amplification procedure and the electrochemical detection. In addition to the advantages of simplicity and one-step detection of the amplified product, the performance of the proposed approach is better than the obtained with other point-of-care tests for *Leishmania* detection, offering also a quantitative tool for parasite determination.

Furthermore, our technique provides a valuable proof of concept since the double MB/AuNP-label approach is a universal methodology that could be applied for any RPA isothermal DNA amplification design.

4. Experimental section

DNA samples

The present study includes samples of dogs received in Vetgenomics (www.vetgenomics.com) to perform *Leishmania* detection by real time PCR. DNA was isolated from 400 μ L of EDTA- blood samples using the Genelute blood Genomic DNA Kit (Sigma, Spain) following manufacturer instructions. DNA was re-suspended in 200 μ L of elution buffer. A *Leishmania* positive DNA was used to perform the different isothermal amplifications and a negative DNA (without *Leishmania*) was used as blank.

To perform the calibration curve a negative blood (400 μ L) was spiked with 2 μ L of *Leishmania* culture at different concentrations, ranging from 10^5 to 10^2 promastigotes/mL. Samples assayed consequently range from 500 to 0.5 parasites per mL of blood (from 5 to 5×10^{-3} parasites per isothermal amplification reaction in a tenfold dilution).

Chemicals and equipment

Primers labeled with biotin and thiol were purchased from Sigma (Spain). TwistAmp® Basic Kit containing all enzymes and reagents necessary for the amplification of DNA – was supplied by TwistDx Ltd (UK). 16 nm-sized AuNPs were prepared following the Turkevich's method (see detailed preparation

procedure, TEM characterization and electrocatalytic quantification of AuNPs at the Supporting Information). High monodisperse 1 μm and 2.8 μm sized streptavidin-coated magnetic beads (MBs) were purchased from Dynal Biotech (MyOne and M-280 respectively, Invitrogen, Spain) (see SEM characterization of both beads at the Supporting Information). Hydrogen tetrachloroaurate (III) trihydrate ($\text{HAuCl}_4 \cdot 3\text{H}_2\text{O}$, 99.9%) and trisodium citrate ($\text{Na}_3\text{C}_6\text{H}_5\text{O}_7$), used in the synthesis of AuNPs and tris (2-carboxyethyl) phosphine (TCEP) used for thiolated primer pretreatment were purchased from Sigma-Aldrich (Spain). Washing solutions of the MB-labeled conjugates consisted of: (i) Phosphate buffer solution (PBS buffer): 0.01 M phosphate-buffered saline, 0.137 M NaCl and 0.03 M KCl (pH 7.4), (ii) Binding and washing buffer (B&W): PBS buffer solution with added 0.05% (w/v) Tween 20; (iii) Blocking buffer solution: 5 % (v/v) bovine serum albumin (BSA) in PBS buffer. A TS-100 ThermoShaker (Biosan, Latvia) was used for the incubations with agitation at a controlled temperature. A Dynal MPCTM-S Magnetic Particle Concentrator (Invitrogen, Spain) was used for the magnetic separations.

The electrochemical transducers used were homemade screen-printed carbon electrodes (SPCEs), consisting of three electrodes: carbon working electrode (WE), Ag/AgCl reference electrode (RE) and carbon counter electrode (CE) in a single strip fabricated with a semi-automatic screen-printing machine DEK248 (DEK International, Switzerland) (see Supporting Information). The materials and reagents used for this process were: Autostat HT5 polyester sheet (McDermid Autotype, UK), Electrodag 423SS carbon ink, Electrodag 6037SS silver/silver chloride ink and Minico 7000 Blue insulating ink (Acheson Industries, The Netherlands). The experimental procedure for SPCEs fabrication is detailed at the Supporting Information. A neodymium magnet (3 mm in diameter), inserted under the WE, was also used to accumulate the MB-labeled amplified product during the electrochemical measurements. The electrochemical measurements were performed in analytical grade 1 M HCl solution (Merck, Spain) at room temperature using a $\mu\text{Autolab II}$ (Echo Chemie, The Netherlands) potentiostat/galvanostat connected to a PC and controlled by Autolab GPES 4.9007 software (General Purpose Electrochemical System). Unless otherwise stated, all reagents and other inorganic chemicals were supplied by Sigma-Aldrich or Fluka (Spain).

All chemicals were used as received and all aqueous solutions were prepared in milli-Q water (Millipore purification system, 18.2 MOhm cm).

Conjugation of AuNPs and magnetic beads (MBs) to DNA primers

First of all, a reduction step to remove the protecting disulfide group from the thiolated primer was performed before using, following the protocol recommended by the manufacturer. Briefly, 200 μ L of 10 mM Tris (2-carboxyethyl) phosphine (TCEP) were added to the lyophilized primer and the solution was shaken 60 min at room temperature. Then it was precipitated by adding 150 μ L of 3M NaAc and 750 μ L of EtOH and incubating 20 min at -20°C. After that, it was spun for 5 min at 13000 rpm and the supernatant was discarded. The pellet was dried at room temperature.

The conjugation of self-synthesized 16 nm-sized AuNPs to the primer modified with thiol group was performed adapting the procedure pioneered by Mirkin et al.⁶⁸ 190 μ L of AuNPs suspension were mixed with 10 μ L of 1500 μ g/mL thiolated primer solution and incubated for 20h at 25 °C with agitation (250 rpm) (final concentration of primer: 75 μ g/mL). After that, this solution was added to 50 μ L of 10 mM phosphate buffer (pH 7) / 0.1M NaCl and allowed to stand for 44h. Finally, a centrifugation at 14000 rpm for 20 min at 4°C was carried out, and AuNPs/ primer conjugate were reconstituted in 200 μ L of milli-Q water, being stable for up to 8 weeks.

Streptavidin-modified MBs (1 μ m and 2.8 μ m-sized) were connected with the primers through the streptavidin-biotin interaction by mixing 50 μ L of 1 mg/mL MBs suspension with 15 μ L of 100 μ M biotinylated primer during 30 min at 25°C. The MBs/ primer conjugate was washed and re-suspended in 15 μ L of water.

Primer sets for Leishmania amplification and endogenous control

Primers set selected after optimization were (5'-3'):

- K6F: [ThiC6]CTTTTCTGGTCCTCCGGGTAGGGGCGTTCTG
- K3R: [Btn]CCACCCGGCCCTATTTTACACCAACCCCCAGTTTCCC

that amplified a fragment of approximately 140 base pair length of the Kinetoplast.

For the endogenous control, optimum primers were (5'-3'):

- Primer 18s 1F: CTGCGAATGGCTCATTAATCAGTTATGGTTCC

- Primer 18s 1R: CTGACCGGGTTGGTTTTGATCTGATAAATGCACGC that amplified a fragment of 168 base pair length of the 18S ribosomal RNA gene.

Analysis of RPA amplification was performed on 2% agarose-gel stained with ethidium bromide after purification of the reactions with the DNA Clean & Concentrator Kit (Zymo research).

Isothermal amplification assay conditions

Multiplex amplification with primers K6-F and K3R for *Leishmania* and 18S-F1 and 18S-R1 for endogenous control was performed using 14mM of magnesium, 300 nM of *Leishmania* primers, 150nM of 18s primers, 5 μ L of DNA and 37°C of reaction temperature during 10 minutes without agitation.

The same experimental procedure was followed for K6F/AuNPs and K3R/MBs labeled primers (prepared as stated before) so as to obtain the double-labeled amplified product. A preliminary evaluation of the amplification using K6F/AuNPs and free K3R (only modified with biotin) was also performed. In this case, the AuNP/amplified DNA was purified by incubation with MBs under the same conditions than the described for the conjugation of MBs with biotin-labeled primers.

A sample without DNA was used in each isothermal amplification as a Negative Template Control (NTC).

Zeta potential measurements

A 1 μ L suspension of AuNPs, K6F/AuNPs and of AuNPs/amplified DNA was diluted in 1 mL of PBS buffer, vortexed, and transferred into a 4 mL polystyrene cuvette (FB55143, Fisher Scientific). The data were collected and analysed with the Dispersion Technology software 4.20 (Malvern) producing diagrams for the zeta potential as a distribution versus total counts.

Electrochemical detection of MB/AuNP-labeled amplified DNA

25 μ L of the MBs/amplified DNA/AuNPs complex suspension were placed on the working area of the SPCE, where it was previously attached a magnet on the reverse side. After 30 seconds, 25 μ L of 2M HCl solution were added and a

potential of +1.35 V was applied during 1 min (electrochemical pre-treatment). After that, a potential of -1.00 V was applied during 60 seconds in chronoamperometric mode. Under these conditions, the H^+ ions were reduced to H_2 thanks to the catalytic effect of the AuNPs labels.^{27,28} The absolute value of the current registered at 60 seconds was considered as the analytical signal, being this value proportional to the quantity of AuNPs and, consequently, to the concentration of isothermal amplified product. For the quantitative study shown in **figure 5**, the values of the analytical signals (current at 60 seconds) after subtracting the background (current in 1M HCl) are plotted for a better understanding.

5. References

- (1) <http://www.who.int/mediacentre/factsheets/fs387/en/>.
- (2) Rascalou, G. ; Pontier, D. ; Menu, F. ; Gourbière. S. *PLoS One*. **2012**, 7(5), e36858.
- (3) Beugnet, F. ; Marie, J.L. *Vet. Parasito*. **2009**, 163, 298-305.
- (4) Maia, C.; Campino, L. *Vet. Parasitol*. **2008**, 158, 274-287.
- (5) Dantas-Torres, F.; Solano-Gallego, L.; Baneth, G.; Ribeiro, V. M.; de Paiva-Cavalcanti, M.; Otranto, D. *Trends Parasitol*. **2012**, 28, 531-538.
- (6) World Heal. Organ. WHO, Tech. Rep. Ser. 949 **2010**, 1–186.
- (7) Chappuis, F.; Sundar, S.; Hailu, A.; Ghalib, H.; Rijal, S.; Peeling, R. W.; Alvar, J.; Boelaert, M. *Nat. Rev. Microbiol*. **2007**, 5, 873-882.
- (8) Solano-Gallego, L.; Fernández-Bellon, H.; Morell, P.; Fondevila, D.; Alberola, J.; Ramis, A.; Ferrer, L. *J. Comp. Pathol*. **2004**, 130, 7-12.
- (9) De Fátima Madeira, M.; de O Schubach, A.; Schubach, T.M.P.; Pereira, S.; Figueiredo, F.; Baptista, C.; Leal, C.; Melo, C.X.; Confort, E.M.; Marzochi, M.C. *Vet. Parasitol*. **2006**, 138, 366-370.
- (10) Xavier, S.C.; de Andrade, H.M.; Monte, S.J.H.; Chiarelli, I.M.; Lima, W.G.; Michalick, M.S.M.; Tafuri, W.L.; Tafuri, W.L. *BMC Vet. Res*. **2006**, 2-17.
- (11) Figueiredo, F.B.; Madeira, M.F.; Menezes, R.C.; Pacheco, R.S.; Pires, M.Q.; Furtado, M.C.; Pinto, G.; Schubach, T.M. P. *Vet. J*. **2010**, 186, 123-124.
- (12) Marcondes, M.; Biondo, W.; Gomes, D.; Silva, R.S.; Vieira, R.F.C.; Camacho, A.; Quinn, J.; Chandrashekar, R. *Vet. Parasitol*. **2011**, 175, 15-19.
- (13) Reithinger, R.; Dujardin, J.C. *J. Clin. Microbiol*. **2007**, 45, 21-25.

- (14) Srividya, G.; Kulshrestha, A.; Singh, R.; Salotra, P. *Parasitol. Res.* **2012**, *110*, 1065-1078.
- (15) Deborggraeve, S.; Laurent, T.; Espinosa, D.; Van der Auwera, G.; Mbuchi, M.; Wasunna, M.; El-Safi, S.; Al-Basheer, A.A.; Arévalo, J.; Miranda-Verástegui, C.; Leclipteux, T.; Mertens, P.; Dujardin, J.C.; Herdewijn, P.; Büscher, P. *J. Infect. Dis.* **2008**, *198*, 1565-1572.
- (16) Lombardo, G.; Pennisi, M. G.; Lupo, T.; Migliazzo, A.; Caprì, A.; Solano-Gallego, L. *Vet. Parasitol.* **2012**, *184*, 10-17.
- (17) Naranjo, C.; Fondevila, D.; Altet, L.; Francino, O.; Ríos, J.; Roura, X.; Peña, T. *Vet. J.* **2012**, *193*, 168-173.
- (18) Van der Meide, W.; Guerra, J.; Schoone, G.; Farenhorst, M.; Coelho, L.; Faber, W.; Peekel, I.; Schallig, H. *J. Clin. Microbiol.* **2008**, *46*, 73-78.
- (19) Rodríguez-Cortés, A.; Ojeda, A.; López-Fuertes, L.; Timón, M.; Altet, L.; Solano-Gallego, L.; Sánchez-Robert, E.; Francino, O.; Alberola, J. *Int. J. Parasitol.* **2007**, *37*(6), 683-693.
- (20) Salotra, P.; Sreenivas, G.; Ramesh, V.; Sundar, S. *Br. J. Dermatol.* **2001**, *145*, 630-632.
- (21) Chappuis, F.; Mueller, Y.; Nguimfack, A.; Rwakimari, J. B.; Couffignal, S.; Boelaert, M.; Cavailler, P.; Loutan, L.; Piola, P. *J. Clin. Microbiol.* **2005**, *43*, 5973-5977.
- (22) Sundar, S.; Maurya, R.; Singh, R. K.; Bharti, K.; Chakravarty, J.; Parekh, A.; Rai, M.; Kumar, K.; Murray, H.W. *J. Clin. Microbiol.* **2006**, *44*, 251-253.
- (23) Welch, R.J.; Anderson, B.L.; Litwin, C.M. *Clin. Vaccine Immunol.* **2008**, *15*, 1483-1484.

(24) CorisBioconcept. Leishmania spp..
<http://www.corisbio.com/Products/Molecular-Field/Leishmania.php> (accessed July 19, 2015).

(25) Cepheid. <http://www.cephheid.com/us/> ((accessed July 19, 2015).

(26) TwistDx Ltd.. Revolutionary DNA detection. http://www.twistdx.co.uk/our_technology/ (accessed July 19, 2015).

(27) [Maltez-da Costa, M.; de la Escosura-Muniz, A.; Merkoçi, A. *Electrochem. Comm.* **2010**, 12\(11\), 1501-1504.](#)

(28) Maltez-da Costa, M.; de la Escosura-Muniz, A.; Nogues, C. Barrios, L.; Ibáñez, E.; Merkoçi, A. *Nano Lett.* **2012**, 12, 4164–4171.

(29) de la Escosura-Muñiz, A.; Ambrosi, A.; Merkoçi, A. Electrochemical analysis with nanoparticle-based biosystems. *Trends Anal. Chem.*, **2008**, 27(7), 568-584.

(30) Merkoçi, A. *Biosens. Bioelectron.* **2010**, 26(4), 1164-1177.

(31) de la Escosura-Muñiz, A.; Merkoçi, A. *Chem. Commun.*, **2010**, 46, 9007-9009.

(32) Andreadou, M.; Liandris, E.; Gazouli, M.; Taka, S.; Antoniou, M.; Theodoropoulos, G.; Tachtsidis, G.; Goutas, N.; Vlachodimitropoulos, D.; Kasampalidis, I.; Ikonopoulou, J. *Journal of Microbiological Methods*, **2014**, 96, 56-61.

(33) Wang, CH.; Chang, CH.; Wu, JJ.; Lee, GB. *Nanomedicine: Nanotechnology, Biology, and Medicine* **2014**, 10, 809-818.

(34) Saha, K.; Agasti, S.S.; Kim, C.; Li, X.; Rotello, V.M. *Chem Rev.* **2012**, 112(5), 2739-2779.

- (35) Zhao, J.; Liu, T.; Fan, Q.; Li, G. *Chem. Commun.* **2011**, 47, 5262-5264.
- (36) Fan, Q.; Zhao, J.; Li, H.; Zhu, L.; Li, G. *Biosens. Bioelectron.* **2012**, 33(1), 211–215.
- (37) Yang, Y.; Li, C.; Yin, L.; Liu, M.; Wang, Z.; Shu, Y.; Li, G. *ACS Appl. Mater. Interfaces*, **2014**, 6(10), 7579–7584.
- (38) Pumera, M.; Castañeda, M.T.; Pividori, M.I.; Eritja, R.; Merkoçi, A.; Alegret, S. *Langmuir* **2005**, 21, 9625-9629.
- (39) Zhu, X.; Feng, C.; Ye, Z.; Chen, Y.; Li, G. *Sci Rep.* **2014**, 4:4169.
- (40) Lou, X.; Zhang, Y. *ACS Appl. Mater. Interfaces* **2013**, 5, 6276–6284.
- (41) Yang, W.; Li, X.; Sun, J.; Shao, Z. *ACS Appl. Mater. Interfaces* **2013**, 5, 11520–11524.
- (42) Bansod, S.; Bonde, S.; Tiwari, V.; Bawaskar, M.; Deshmukh, S.; Gaikwad, S.; Gade, A.; Rai, M. *Journal of Biomedical Nanotechnology*, **2013**, 9, 1-10.
- (43) Wang, L.; Zhu, Y.; Jiang, Y.; Qiao, R.; Zhu, S.; Chen, W.; Xu, C. *J. Phys. Chem. B* **2009**, 113, 7637–7641.
- (44) Pan, D.; Mi, L.; Huang, Q.; Hu, J.; Fan, C. *Integr. Biol.* **2012**, 4, 1155–1163.
- (45) Huang, Y.; Zhang, X.; Du, Q.; Wang, F.; Zhao, X.; Zhang, W.; Tong, D. *PLOS One*. **2014**, 9(5), e97869.
- (46) Kuang, H.; Zhao, S.; Chen, W.; Ma, W.; Yong, Q.; Xu, L.; Wang, L.; Xu, C. *Biosens. Bioelectron.* **2011**, 26(5), 2495-2499.

- (47) Zhu, X.; Zhou, X.; Xing, D. *Biosens. Bioelectron.* **2012**, *31*, 463-468.
- (48) Liu, H.; Li, S.; Wang, Z.; Hou, P.; He, Q.; He, N. *Biotechnol. J.* **2007**, *2*(4), 508-511.
- (49) Lermo, A.; Campoy, S.; Barbé, J.; Hernández, S.; Alegret, S.; Pividori, Ml. *Biosens Bioelectron.* **2007**, *22*(9-10), 2010-2017.
- (50) Nikbakht, H.; Gill, P.; Tabarraei, A.; Niazi, A. *RSC Adv.*, **2014**, *4*, 13575–13580.
- (51) Veigas, B.; Pedrosa, P.; Couto, I.; Viveiros, M.; Baptista, P.V. *Journal of Nanobiotechnology* **2013**, 11:38.
- (52) Wong, J.K.F.; Yip, S.P.; Lee, T.M.H. *Small* **2014**, *10*(8), 1495-1499.
- (53) Fu, Z.; Zhou, X.; Xing, D. *Methods* **2013**, *64*, 260-266.
- (54) Tan, E.; Wong, J.; Nguyen, D.; Zhang, Y.; Erwin, B.; Van Ness, L.K.; Baker, S.M.; Galas, D.J.; Niemz, A. *Anal. Chem.* **2005**, *77*, 7984-7992.
- (55) Tan, E.; Erwin, B.; Dames, S.; Voelkerding, K.; Niemz, A. *Clin. Chem.* **2007**, *53*(11), 2017-2019.
- (56) Shi, D.; Huang, J.; Chuai, Z.; Chen, D.; Zhu, X.; Wang, H.; Peng, J.; Wu, H.; Huang, Q.; Fu, W. *Biosens. Bioelectron.* **2014**, *62*, 280-287.
- (57) Xiang Y.; Deng, K.; Xia, H.; Yao, C.; Chen, Q.; Zhang, L.; Liu, Z.; Fu, W. *Biosens. Bioelectron.* **2013**, *49*, 442-449.
- (58) Valentini, P.; Fiammengo, R.; Sabella, S.; Gariboldi, M.; Maiorano, G.; Cingolani, R.; Pompa, P.P. *ACS Nano* **2013**, *7*(6), 5530-5538.

- (59) Yang, A.K.L.Y.; Lub, H.; Wu, S.Y.; Kwok, H.C.; Ho, H.P.; Yu, S.; Cheung, AKL.; Kong, S.K. *Anal. Chim. Acta* **2013**, 782, 46-53.
- (60) Torres-Chavolla, E.; Alocilja, E.C. *Biosens. Bioelectron.* **2011**, 26, 4614-4618.
- (61) Chih-Hung, W.; Kang-Yi, L.; Jiunn-Jong, W.; Gwo-Bin, Lee. *Lab Chip*, **2011**, 11, 1521-1531.
- (62) Francino, O; Altet L; Sanchez-Robert, E; Rodríguez, A. ; Solano-Gallego, L.; Ferrer, L.; Sánchez, A.; Roura, X. *Vet. Parasitol.* **2006**, 137(3-4), 214-221.
- (63) Rodgers, MR; Popper, SJ; Wirth, DF. *Exp Parasitol.* **1990**, 71(3), 267-275.
- (64) Weiss, JB. *Clin Microbiol Rev.* **1995**, 8(1), 113-130.
- (65) Wilson, SM. *Ann Trop Med Parasitol.* **1995**, 89, 95-100.
- (66) Thielbeer, F.; Donaldson, K.; Bradley, M. *Bioconj. Chem.* **2011**, 22, 144-150.
- (67) Mugasa, C.M.; Laurent, T.; Schoone, G.J.; Basiye, F.L.; Saad, A.; El Safi, S.; Kager, P.; Schallig, H.D. *Parasit. Vectors* **2010**, 3, 13.
- (68) Mirkin, CA.; Letsinger, RL.; Mucic, RC, Storhoff, JJ. *Nature* **1996**, 382, 607-609.

Supporting Information

Synthesis of gold nanoparticles

16 nm gold nanoparticles (AuNPs) were synthesized by reducing tetrachloroauric acid with trisodium citrate, a method pioneered by Turkevich [Turkevich et al., 1953]. Briefly, 200 mL of 0.01% HAuCl_4 solution (25 mM) were boiled with vigorous stirring. 5 mL of 1% trisodium citrate solution were added quickly to the boiling solution. When the solution turned deep red, indicating the formation of AuNPs 16 nm sized, the solution was left stirring and cooling down.

Fabrication of screen-printed carbon electrodes (SPCEs)

The electrochemical transducers were homemade screen-printed carbon electrodes (SPCEs) consisting of three electrodes in a single strip: working electrode (WE), reference electrode (RE) and counter electrode (CE). The full size of the sensor strip was 29mm x 6.7mm, and the WE diameter was 3mm. The fabrication of the SPCEs was carried out in three steps in the semi-automatic screen-printing machine DEK248 (DEK International, Switzerland), using a different stencil, with the corresponding patterns, for each layer. First, a graphite layer (Electrodag 423SS carbon ink for WE and CE) was printed onto the polyester sheet (Autostat HT5, McDermid Autotype, UK). After curing for 30 min at 95°C, a second layer was printed with silver/silver chloride ink (Electrodag 6037SS for the RE). After another curing for 30 min at 95°C, the insulating layer was printed using insulating ink (Minico 7000 Blue, Acheson Industries, The Netherlands) to protect the contacts and define the sample interaction area. Finally, the SPCEs were cured again at 95°C for 20 min.

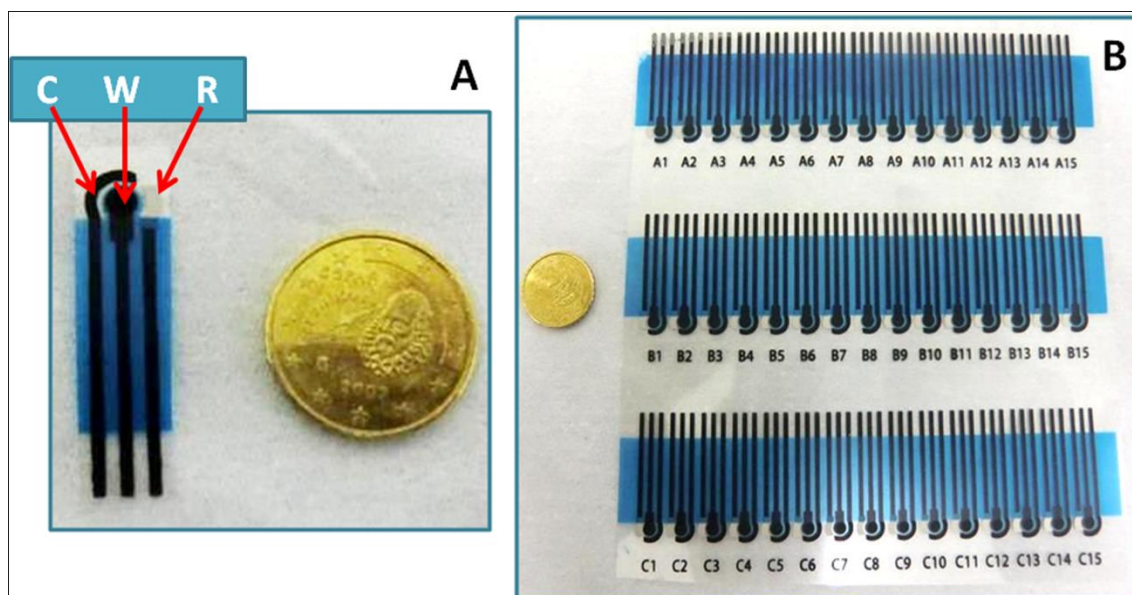


Figure SM-1: (A) Detail of one SPCE, containing the three electrodes in the working area; R- Ag/AgCl reference electrode, W- carbon working electrode and C- carbon counter electrode. (B) Images of the 45 SPCE sensors sheet obtained following the experimental procedure.

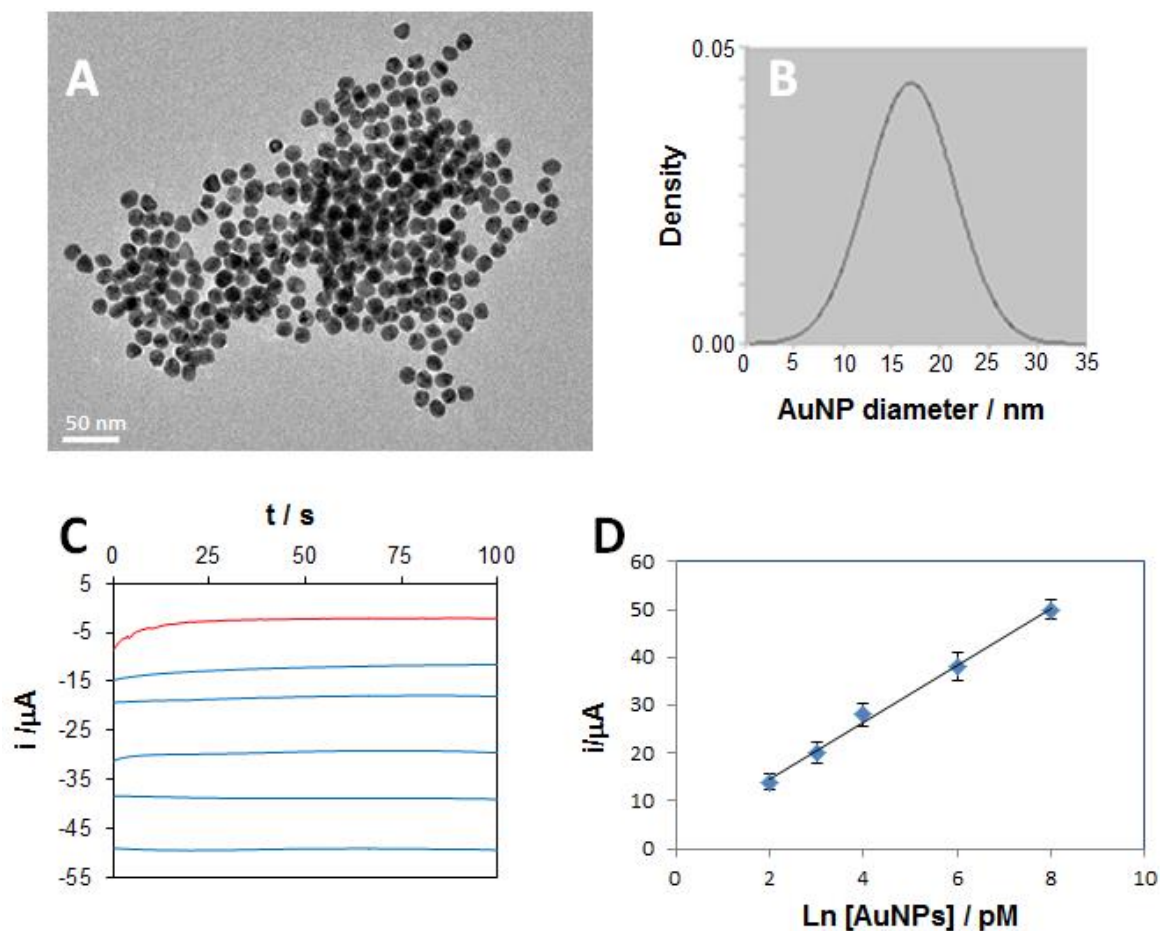


Figure SM-2: (A) TEM image of the self-synthesized AuNPs and (B) the corresponding size-distribution diagram. (C) Chronoamperograms recorded at -1V in 1M HCl for different concentrations of AuNPs suspensions, from up to bottom: 0, 2, 3, 4, 6 and 8 pM and (D) the corresponding relationship between the absolute value of the cathodic current at 60 s and the concentration of AuNPs.

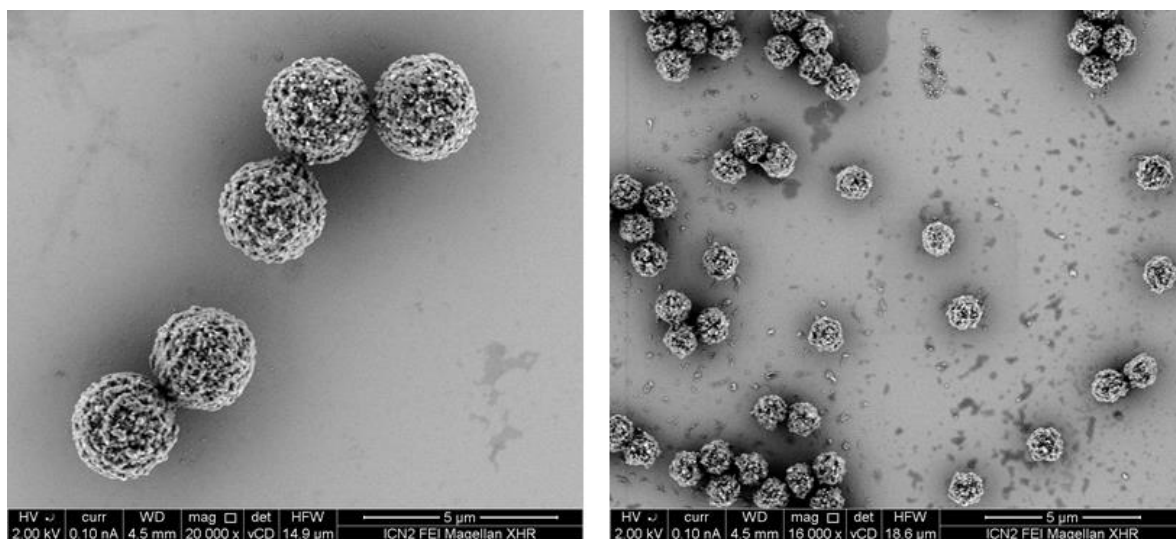


Figure SM-3: SEM images of monodisperse magnetic beads of 2.8 μm (DynaM-280®) (left) and 1 μm (DynaM-MyOne®) (right) .

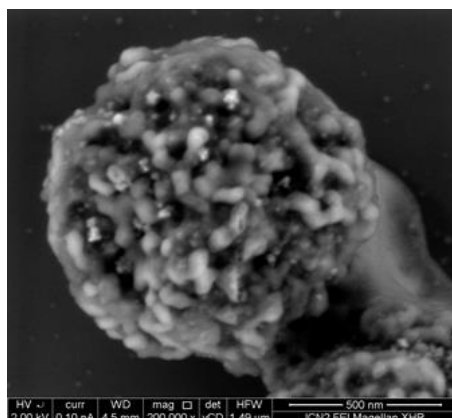


Figure SM-4: SEM image of a 1 μm MB after amplification of DNA without *Leishmania* parasite. Experimental conditions as detailed in the main text.

REFERENCES

Turkevich, J.; Stevenson, P. C.; Hillier, J. J. *Phys. Chem.* 1953, 57, 670.

Chapter 4

Electrocatalytic tune of screen printed electrodes with graphene oxide

In this chapter the influence of graphene oxidative grades, concerning their clear influence on conductivity and hydrophobicity upon biosensing response is studied. Different levels of graphene oxide results on changes of (bio)conjugation properties occurring at enzyme/graphene oxide interface mainly due to the electrostatic or hydrophobic interactions with biomolecules in comparison with bare screen printing electrodes. Tyrosinase enzyme as a proof of concept receptor with interest for phenolic compounds detection is tested through its direct adsorption onto SPE previously modified with highly oxidized graphene oxide reduced graphene oxide. The electrochemical responses of this reduced graphene oxide have been compared with the responses obtained for graphene oxide and their electrochemical performance has been accordingly discussed with various evidences obtained by optical techniques.

Related Publication

- 2) *Luis Baptista-Pires, B. Pérez-López, Carmen C. Mayorga-Martinez, Eden Morales-Narváez, Neus Domingo, Maria Jose Esplandiu, Francesc Alzina, C. M. Sotomayor Torres and A. Merkoçi*, Electrocatalytic tuning of biosensing response through electrostatic or hydrophobic enzyme-graphene oxide interactions. *Biosensors & Bioelectronics*, 2014. **61**: p. 655-662.

1. Introduction

Since the discovery of graphene in the last years (Geim and Novoselov 2007) and with the great progress made in nanoscience and nanotechnology, its integration with biomolecules has received increased attention due to its physical, optical and chemical properties which are not available in other materials, such as its interesting molecular structure, high active surface area and high conductivity capacity that improves the electron transfer (Shao, Wang et al. 2010). Since then, many graphene materials such as graphene oxide (Shen, Hu et al. 2009, Marcano, Kosynkin et al. 2010), graphene quantum dots (Peng, Gao et al. 2012) or graphene nanoribbons have been reported (Martin-Fernandez, Wang et al. 2012).

Graphene oxide (GO) with different oxidized grades, exhibits different defects levels due to the distribution of the oxygen atoms all over the graphene surface. The versatility of oxidative grades of graphene leads to transitions from insulator to semimetallic mainly after reducing processes (Mathkar, Tozier et al. 2012). The reduction modes such as reduction using hydrazine (Marcano, Kosynkin et al. 2010), thermal annealing (Gao, Jang et al. 2010) or bacterial treatment (Salas, Sun et al. 2010) results in highly reasonable methods for the reconstruction of the carbon sp^2 bonds on GO sheet. The reduction of graphene oxide removes the oxygen groups and rehybridize the sp^3 carbon atoms to sp^2 carbon atoms (Cheng, Yang et al. 2012). Epoxy and hydroxyl groups lie above and below each graphene layer and the carboxylic groups are mostly located at the edges (Zhu, Murali et al. 2010). In highly oxidized Graphene oxide (oGO) the presence of the oxygen groups onto the surface of the graphene sheet results in a highly hydrophilic character, which strongly affects the density of electronic states (DOS) and consequently the chemical reactivity and conductivity tuning its properties either to insulator or semimetallic (Eda, Mattevi et al. 2009). Enzymes can be immobilized through electrostatic interaction. However, electrostatic interaction as the driving force for enzyme binding to oGO severely affects the activity of the enzyme and present low stability. This immobilization is not suitable for biosensor application. On the other hand, Zhang et al. have demonstrated that reduced

graphene oxide (rGO) represent a interesting plattform with high affinity for enzyme immobilization. This high affinity is due to the adsorption of enzyme on rGO through hydrophobic interaction and the lack of surface functional groups of rGO that may impart less perturbation to the enzyme (Zhang, Zhang et al. 2012).

According to their properties, the reduced graphene oxide opens the door for biofunctionalization with enzymes. Therefore, due to the biofunctionalization capabilities combined with interesting electrochemical (Shao, Wang et al. 2010) and optical properties (Morales-Narvaez and Merkoci 2012) reduced graphene oxide has greatly stimulated research interest for applications in (bio)sensing systems.

This work presents a new catechol biosensor based on an assembly of GO-Tyrosinase conjugates through electrostatic interactions in the case of oGO or through hydrophobic interaction onto SPE modified with rGO. The characterization of oGO and rGO sheets on screen-printing electrodes, one of the most interesting platforms for electrochemical biosensors were thoroughly discussed. For this study we have used oGO which have been reduced afterwards with hydrazine (Marcano, Kosynkin et al. 2010) for his de-oxygenation. The electrochemical responses of this rGO have been compared with the responses obtained for oGO and their performance has been accordingly discussed with various evidences obtained by optical techniques. The use of reduced graphene-based biosystems improves the detection levels (Wang, Wan et al. 2010), being a great promise for routine sensitive, selective, rapid, and cost-effective analysis making them suitable for environmental, food safety and security and medical applications.

2. Materials and methods

2.1 Preparation of rGO. Oxidized graphene oxide (oGO) was provided from Angstrom Materials, Inc. (Product: N002-PS) and the reduction step to produce reduced graphene oxide (rGO) was made using reported literature (Marcano, Kosynkin et al. 2010) where 100.00 mL of oGO (1mg/mL) was mixed with 1.00 mL of hydrazine hydrate. The mixtures were heated at 95 °C using a water bath

for 45 min; a black solid precipitated from the reaction mixture. Products were isolated by filtration (PTFE 20 μ m pore size) and washed with DI water (50 mL, 3 times) and methanol (20 mL, 3 times).

2.2 Optical measurements and sample characterization. The samples were prepared by drop casting our solution on silicon sample older. X-ray photoelectron spectroscopy (XPS) experiments were performed in a PHI 5500 Multitechnique System (from Physical electronics) with a monochromatic X-ray source (Aluminium Kalfa line of 1486.6 eV energy and 350 W), placed perpendicular to the analyzer axis and calibrated using the 3d5/2 line of Ag with a full width at half maximum (FWHM) of 0.8 eV. Raman spectras were acquired at room temperature with a Horiba T64000 spectrometer operated in single mode configuration with spectral resolution of 4 cm⁻¹. The excitation source was the 514.5 nm line of an argon ion laser. The laser was focused to a spot with diameter of about 560 nm using a 100X objective lens and the intensity was kept below 200 μ w to avoid any damage of the sample. UV-visible absorbance spectra were explored through SpectraMax M2^e multimode reader (Molecular Devices, California, USA) and fluorescence determined using an UV lamp with 345nm excitation wavelength. AFM measurements were done using a Dimension 3100 AFM Machine (Veevo metrology group, digital instruments). Easy drop contact angle measuring instrument was used to perform contact angle of modified graphene surfaces.

2.3 SPE modification and electrochemical characterization. SPE were fabricated using a previously optimized technology by our lab. A graphite layer is printed by using the screen-printing machine (DEK 248) with the stencil (where it is the electron pattern) and graphite ink onto the polyester sheet. Polyester sheet is cured during 15 minutes at 95°C. Silver/silver chloride layer is printed as reference electrode. Polyester sheet is cured during 15 minutes at 95°C. Insulating ink is deposited. Curing during 20 minutes at 95°C was performed. SPE were modified with 10 μ L of 1mg/mL oGO and rGO by drop casting and let dry overnight at room temperature. For exploring

electrochemical behavior of modified electrodes, cyclic voltammetry was done using 50 μL of 1mM Ferricyanide ($[\text{Fe}(\text{CN})_6]^{3-/4-}$) in 1M sodium chloride (KCl) that was deposited onto the SPE by drop casting. Tyrosinase was immobilized onto the electrode surface by physical adsorption. Tyrosinase was solved in 0.1 M phosphate buffer (PBS) at pH 6.5. The concentration of Tyrosinase for SPE modification was 1mg/50 μL in PBS. SPE, SPE-oGO and SPE-rGO electrodes have been modified with 5 μL of 1mg/50 μL Tyrosinase and let it dry overnight in the fridge at 4°C.

Amperometric measurements were performed applying a potential of -0.1 V in a system composed by a 5 mL electrolytic cell containing 0.1M PBS. PBS is necessary to be used in controlled-potential experiments as a supporting electrolyte. It decreases the resistance of the solution, eliminates electro migration effects and maintains a constant ionic strength. Cyclic voltammetry (CV) and amperometric experiments were performed using an electrochemical (CH instrument, model CHI 600C).

3. Results and discussion

3.1 Optoelectronic properties

X-ray photoelectron spectroscopy (XPS) and Raman spectroscopy (Raman) were firstly used to evidence the level of oxidation and correspondent oxygen bonds so as to determine the structural changes occurring during the chemical reduction process mainly affected by the presence of oxygen atoms onto the graphene structure.

The study of the efficiency of graphene reduction using hydrazine method was followed by x-ray photoelectron spectroscopy (XPS). Figure 1a shows the C1s signal of oGO powder. The signal was fitted by four components: C=C & C-C (42.1%, 284.6 eV), C-O (47.9%, 286.7 eV), C=O (7%, 288.0 eV) and O=C-OH (3%, 288.9 eV). The estimated C/O ratio is ~ 1.07 . The same study was pursued for rGO represented in Figure 1b with values for C=C & C-C (60.1%, 284.6 eV), C-O (32.1%, 286.7 eV), C=O (5.1%, 288.0 eV) and O=C-OH (2.7%, 288.9 eV) and a C/O ratio ~ 1.53 . The efficiency of hydrazine reduction is clear and the

improvement of the C/O ratio is quantified. In the case of Raman, in Figure 1c the D and G bands are localized at 1345 cm^{-1} and 1590 cm^{-1} respectively for oGo and rGO (Park, An et al. 2008). However, an increase in D/G intensity ratio (I_D/I_G) is observed for rGO ($I_D/I_G = 1.26$) in comparison with oGO ($I_D/I_G = 0.92$) suggesting a decrease in the average size of the sp^2 domains upon reduction and can be explained by the formation of new graphitic domains that are smaller in size but more numerous (Stankovich, Dikin et al. 2007). According to this study, the modified screen printing electrodes (SPE) with these two kinds of graphene, possess levels of oxidation and carbon networks completely different, and consequently different electrocatalytic responses can be previewed. In order to get insights of the electronic properties of the obtained platform, UV-Visible spectrum was performed and is represented on Figure 1d. For the oGO sample, a maximum peak at 231 nm is ascribed to $\pi \rightarrow \pi^*$ transition of aromatic C–C bonds, and a shoulder at 300 nm is attributed to $n \rightarrow \pi^*$ transition of C=O bonds. In the case of the rGO, the maximum peak was red-shifted to 254 nm after reduction and the absorbance was significantly increased at wavelengths above 233 nm, which indicates that electronic conjugation has been restored, at least to some extent (Cuong, Pham et al. 2010). The defect at 350 nm on the visible spectra is due to the UV lamp change on the device. The fact that under excitation of 350nm UV-light, the oGO presents fluorescence (inset Figure 1d) in detriment of rGO can make us think about the transitions presented on the UV-Visible absorbance spectra which are in line with similar data of an oxidized graphene material (Shang, Ma et al. 2012) for which the appearance of a band gap has been also reported.

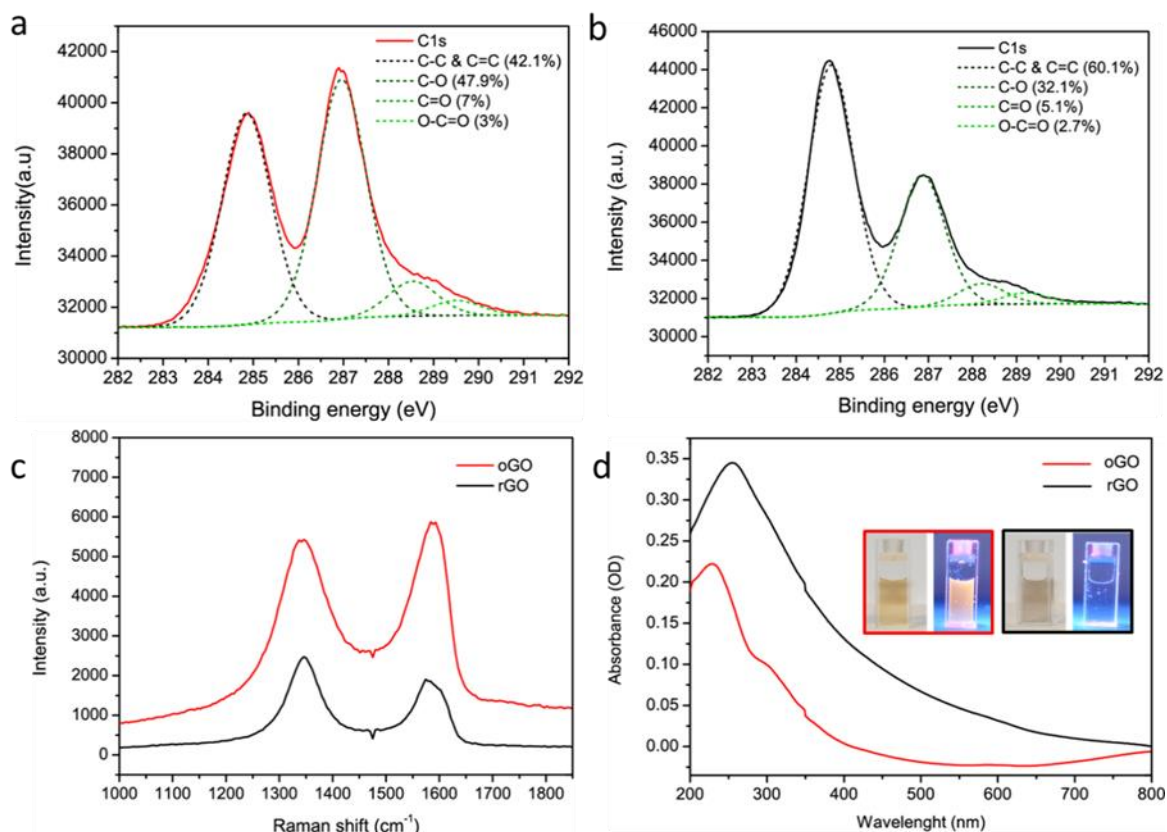


Figure 1. Optical characterization of graphene oxide materials. C1s XPS data of oGO (a) and rGO (b). (c) Raman spectra and (d) UV-visible steady state spectroscopy. Inset: images of oGO and rGO suspensions under UV lamp excitation.

3.2 Morphology characterization

To accurately determine the oGO and rGO morphology at the nanoscale, the sheets were characterized by Atomic Force Microscopy (AFM), as shown in Figure 2. Completely different morphologies were observed between these two nanomaterials. oGO flakes show a high non-uniform surface with high degree of porosity. The average diameter of graphene holes is in the range of tens of nanometers, and the flakes show a thickness of about 2.5 nm. The presence of this topographical defects observed in this sample is explained by the high level of oxidation (Cheng, Yang et al. 2012). Indeed, Figure 2b shows the

topography of rGO flakes in which homogeneous double, triple and multilayer flakes of graphene are observed, (Geim and Novoselov 2007) which is characteristic of reduced graphene oxide materials due to the π - π stacking of aromatic rings after the reduction of oxidized groups. The average thickness of each flake for this sample is around 3 nm. It becomes clear that the reduction process of oGO flakes results onto bigger layers of rGO after reduction of oGO, mostly due to the rearrangement of sp^2 carbon bonds (Gao, Jang et al. 2010).

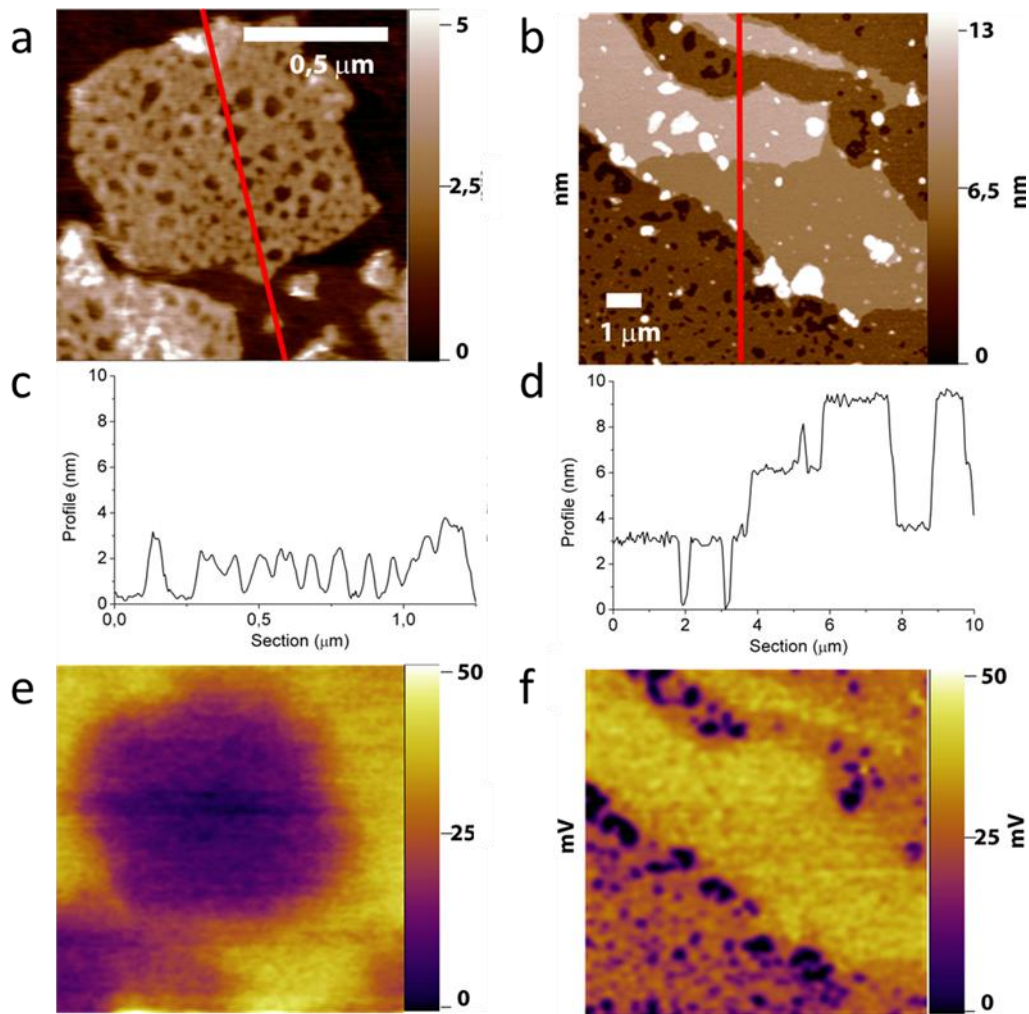


Figure 2. Graphene oxide morphology at the nanoscale. Topography AFM images of oGO (a) and rGO (b) flakes. The red lines correspond to the sections (c) and (d) shown below for each image. KPFM images of oGO (e) and rGO (f) of the same area as (a) and (b).

The different levels of oxidation of the oGO and rGO films are confirmed by Kelvin Probe Force Microscopy (KPFM). In KPFM, the direct measurements of the contact potential difference between the oGO and rGO flakes and the tip of the AFM are obtained and mapped. As shown in Figure 2c and 2d, the KPFM image of the oGO flakes shows a dark contrast with respect to the surrounding substrate, indicating the presence of negative dipoles on the surface of the oGO flakes dominated by the oxygen groups. Instead, for rGO, the flakes show a more positive contrast with respect to the substrate observed through the holes, in agreement with the presence of less negative dipoles on the surface of these samples which are arisen from the reconstruction of the sp^2 carbon network.

In order to evaluate the electrocatalytic properties of the graphene forms we used SPE (Figure 3a) as testing platforms. Screen-printing microfabrication technology is well-established for the mass production of thick film electrodes and it is widely applied to build biological or chemical sensors (Fanjul-Bolado, Lamas-Ardisana et al. 2009). SPE represents one of the most important products of this technology. The main objective of this work is to improve their capabilities in biosensing applications by using graphene oxide modification and to clarify the obtained performance. A simple strategy in which SPE's were modified with 10 μ L of 1 mg/mL oGO and rGO was used. Under this methodology a total coverage of the SPE is achieved and a completely new electrode platform is built.

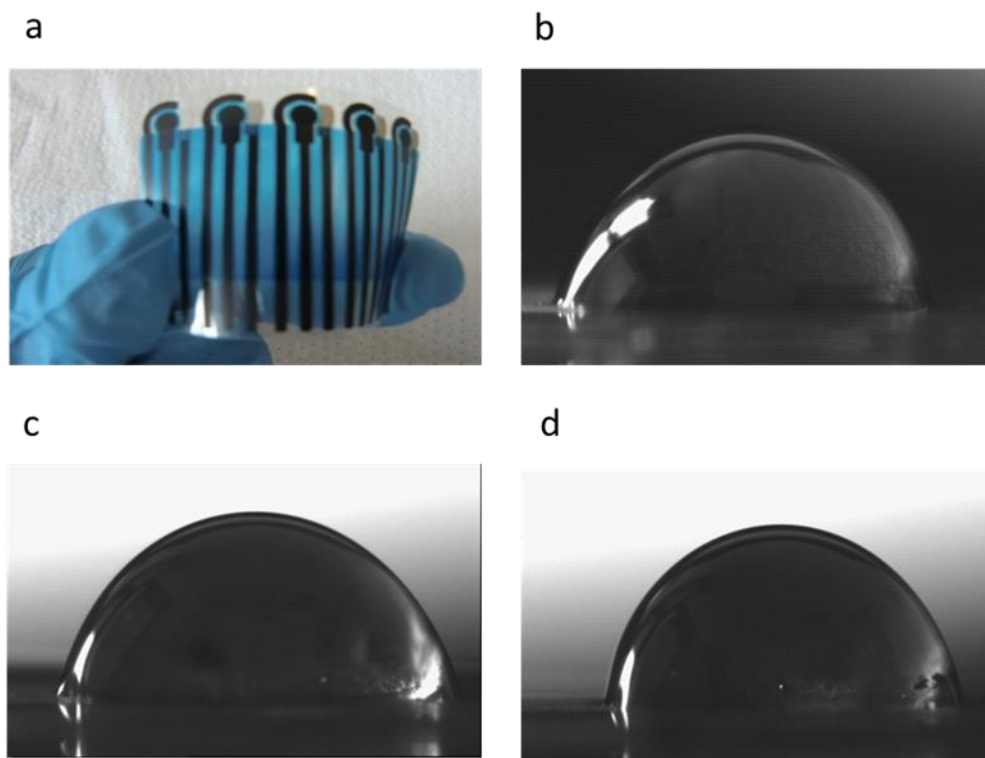


Figure 3. Surface hydrophobicity study. SPE flexible technology (a). Water contact angles for SPE (b), SPE-oGO (c) and SPE-rGO (d).

Surface hydrophobicity of the modified SPE was evaluated due to the fact that adsorption processes have a direct influence on the electrochemical response through the electrocatalytic behavior of the adsorbed enzyme. As shown in Figure 3b, the contact angle to water of typical SPE is 62.2° . After modification with graphene oxide materials, the surface suffers visible changes on its hydrophobicity. In the case of SPE modified with oGO (SPE-oGO) in Figure 3c, the surface changed to a value of 52.6° and in the SPE modified with rGO (SPE-rGO) the contact angle was 73.4° as reported in Figure 3d. These results are also in agreement with the level of oxidation of the graphene materials that is proportional to the hydrophobicity of the modified SPE surface (Zhang, Zhang et al. 2012). In the case of SPE-oGO the surface seems to be much more hydrophilic in comparison with SPE-rGO due to the presence of oxide groups. The consequent removal of these oxygen binding sites for rGO-SPE induced stronger hydrophobicity on these electrodes due to π - π interactions.

3.3 Electrocatalytic properties

To explore electrocatalytic behavior of the modified SPE electrodes, a drop of 50 μL of 1mM Ferricyanide ($[\text{Fe}(\text{CN})_6]^{3-/4-}$) solution was deposited and cyclic voltammetry technique was performed to evaluate electrochemical response of SPE-oGO and SPE-rGO to this redox couple. Figure 4 shows that the presence of graphene materials has an important effect on the electrochemical response of the SPEs. While the presence of oGO decreases the conductivity or the current on the SPE-oGO, the SPE-rGO shows a higher current response to $[\text{Fe}(\text{CN})_6]^{3-/4-}$ (Figure 4a). From these results, one can state that rGO is the most conductive material and oGO the most resistive one. As a matter of comparison, the electrochemical behavior of the free graphene SPE electrode (Figure 4b) together with a zoom of the electrochemical response of the SPE-oGO (Figure 4c) and SPE-rGO (Figure 4d) is also depicted. In the SPE-oGO a very low current redox wave whose possible origin will be addressed later on was also captured.

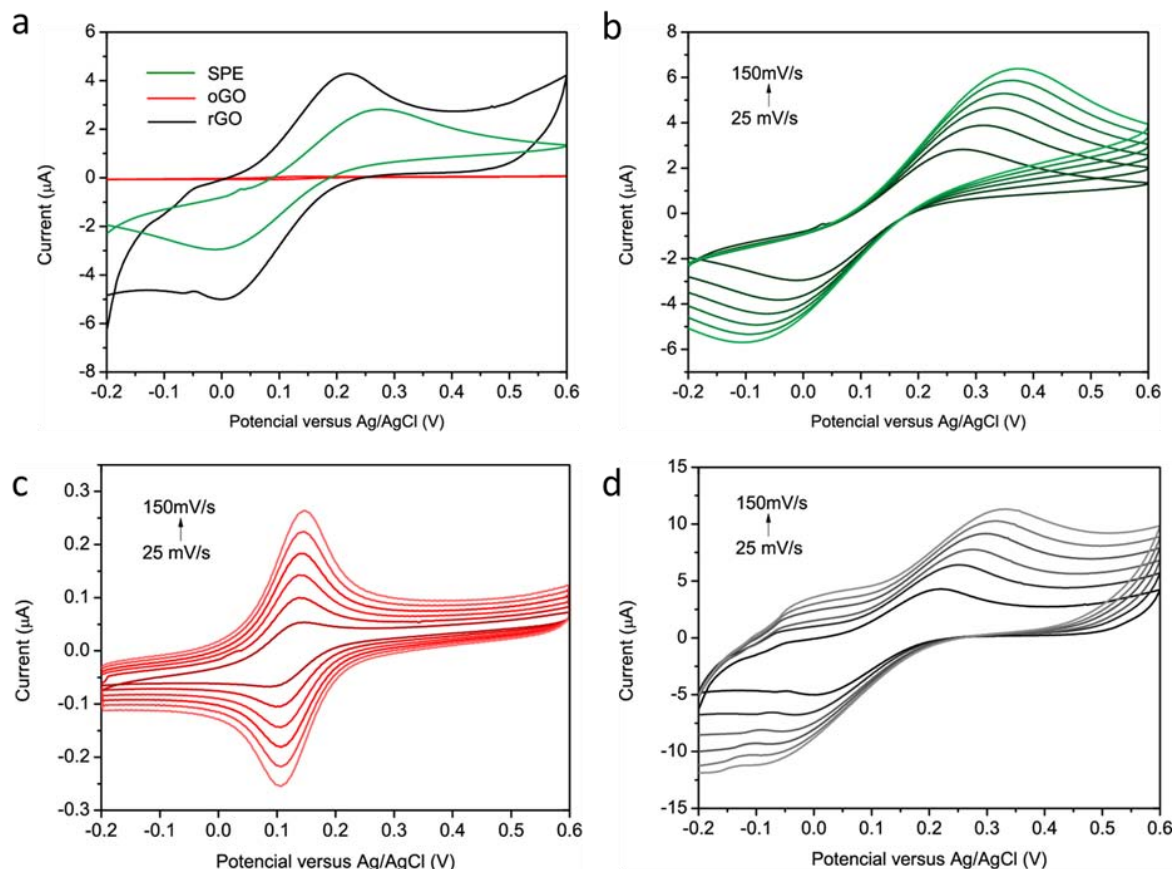


Figure 4. Electrochemical properties. Cyclic voltammetry for SPE, SPE-oGO and SPE-rGO at a scan rate of 25 mV/s (a). Non-modified SPE (b), SPE-oGO (c) and SPE-rGO (d) at scan rates from 25 mV/s to 150 mV/s. All samples were tested in 1 mM $[\text{Fe}(\text{CN})_6]^{3-/4-}$ in 1 M KCl.

The electrochemical reactivity of the SPE-oGO and SPE-rGO can be explained under the light of the density of electronic states which is a very important parameter that controls the electrode kinetics. According to Gerischer-Marcus theory, the heterogeneous electron transfer rate is dependent on DOS of the electrode and on their overlap with the electronic states of the electroactive species (Belding, Campbell et al. 2010). An electron transfer can take place from any occupied energy state that is matched in energy with an occupied receiving state. Thus in metallic electrodes the high density of DOS increases the possibility that an electron of the correct energy is available for the electrode

to transfer to an electroactive species. However if the material exhibits a band gap the probability of matching available states for the electron exchange between electrode and electroactive species is very low decreasing dramatically the electrochemical activity. Therefore in the case of SPE-oGO and in accordance with the fluorescence observations, it is very reasonable to ascribe the low electrochemical performance to the opening of band gap with the oxidation process.

High graphene oxidation is known for instance to remove states close to the Fermi level, thus producing an insulator (Acik, Lee et al. 2010). It is therefore expected that excessive oxygen moieties on graphene in any chemical form (epoxide, hydroxyl, carboxyl and ketonic-type functional groups) both on the basal plane (Cai, Piner et al. 2008) and at the edges (Park, Lee et al. 2008) reduces electronic states at the Fermi level and consequently its conductivity as probed experimentally (Eda, Mattevi et al. 2009). As described before in Figure 1d, the reduction of oGO results on the decrease of $n \rightarrow \pi^*$ transitions, responsible for C=O bonds in sp^3 hybrid regions and responsible for fluorescence emission in graphene oxide (Shang, Ma et al. 2012). It is also reported that graphene reduction using hydrazine decreases the band gap to values almost negligible (Mathkar, Tozier et al. 2012). The conductivity increase after reduction, passing from an insulator material to a more semimetallic conductive one is clear in Figure 4d and consistent with literature reported elsewhere about this transition behavior upon reduction (Acik, Lee et al. 2010).

Redox peak currents increase around sixty times upon reduction as can be observed in Table 1. The table also reports the peak separation voltages (ΔV_p) for the different electrodes. It can be observed that the ΔV_p of SPE-rGO is smaller than in the case of the carbon based SPE evidencing the favourable electrode kinetics of the reduced graphene. The table also reports the ΔV_p value for the case of SPE-oGO ascribed to the very low current oxidation/reduction wave which is captured when zooming in the electrochemical current of the oxidized graphene. The origin of such small redox wave and its surprising low value of ΔV_p cannot be analyzed in the same context as in the case of SPE and SPE-rGO electrodes. We believe that such redox wave in the SPE-oGO is coming from the response of the bottom carbon

support of the SPE and not from the oxidized and insulating graphene. The surprising reversibility of such wave can be explained under the light of the thin layer diffusion model which is applicable when the electrolyte is trapped in porous layers (Belding, Campbell et al. 2010). Indeed, AFM images have shown the porous nature of oxidized graphene. Therefore the electrochemical response is compatible with a passivating oxidized graphene layer with a number of pits (pores) through which the electrolyte penetrates and keeps confined, inducing a kinetically and thermodynamically favourable electron transfer with the base carbon material of the SPE. Accordingly, the peak-to-peak separation in this scenario is expected to be smaller than in the case of the semi-infinite diffusion model in agreement with our findings.

Table 1. Cyclic Voltammetry data for SPE, SPE-oGO and SPE-rGO

	ΔV_p	$\Delta I(\mu A)$
SPE	0.3945	4.72
SPE-oGO	0.0244	0.12
SPE-rGO	0.3297	7.75

The influence of the two explored graphene materials with different levels of oxidation on the attachment of Tyrosinase enzyme has been also studied. The enzymatic activity of the Tyrosinase-graphene oxide modified SPE platform using catechol can be observed through the formation of *o*-Quinone as shown in Figure 5.

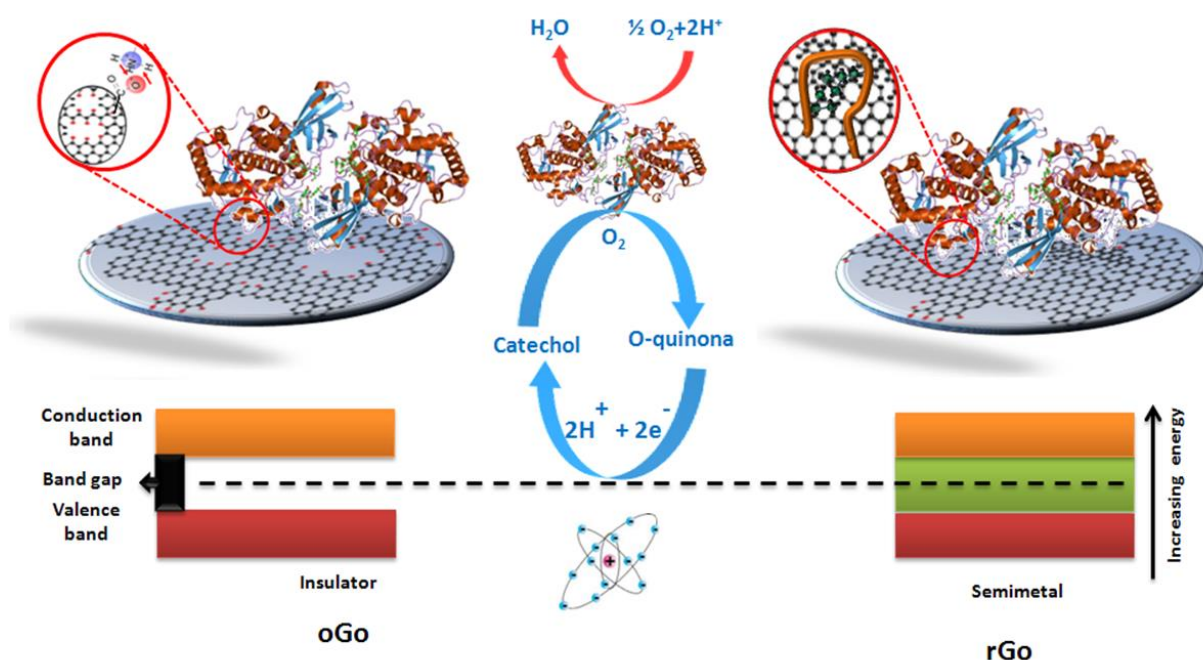


Figure 5: Schematic diagram (not in scale) displaying the enzyme (Tyrosinase) and reactions involved in the catechol detection at the SPE modified with oGO acting as an insulator and rGO as a semimetallic compound.

The voltamperometric evaluation (Figure 6a) shows the comparison of the SPE modified with Tyrosinase (SPE/Tyr), oGO plus tyrosinase (SPE/oGO/Tyr) and rGO plus tyrosinase on the electrocatalytic detection of catechol. All modifications were done under strictly identical conditions. As expected, the reduction signal was improved when GO was present. Moreover, remarkably higher response of SPE/rGO/Tyr was observed, showing fairly well the advantages predicted for this type of biosensor configuration, commented in the introduction section. The enzymatic reaction involves the catalytic oxidation of the catechol to o-quinones, at the expense of reducing oxygen to water. The electrochemical reduction of o-quinones, by transferring two electrons and two protons, was employed to monitor this reaction (Fig. 5). In this case, o-quinone can be reduced back to catechol at low applied potentials (-0.1V). The generation of electrons in this step leads to a change in the current that can be measured. The coupling between the catalytic oxidation (catechol to o-quinone) and the electrochemical reduction (o-quinone to catechol) shuttles the catechol into a cycle with the possibility of signaling amplification (see Figure 6b).

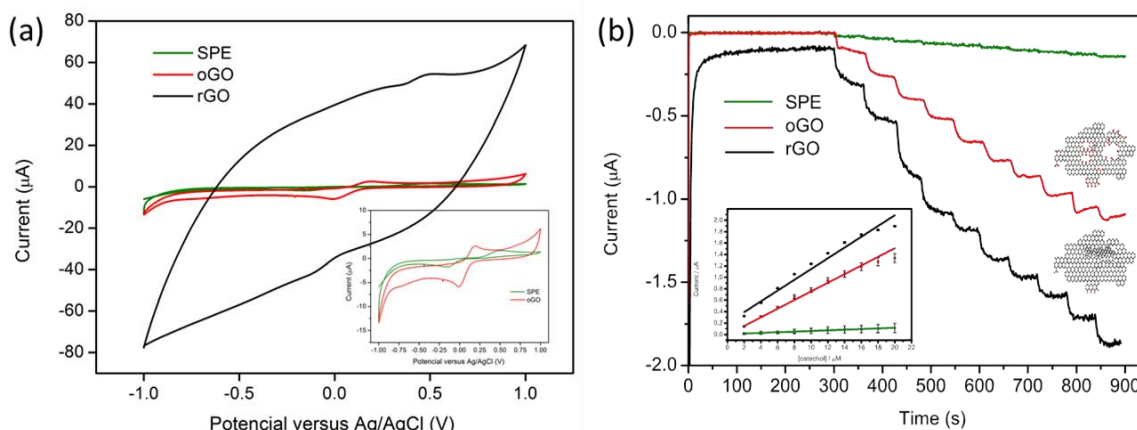


Figure 6. Electrocatalytic properties of SPE/Tyr, SPE/oGO/Tyr and SPE/rGO/Tyr. (a) Cyclic voltammetry response in presence of 20 μM Catechol at 100 mVs^{-1} . (b) Typical current-time curves for the successive additions of 2 μM catechol solution, to a 5mL electrocatalytic cell containing 0.1M PBS (pH 6.5) during stirring conditions under a working potential of -0.1V. Inset: corresponding calibration curves for the graphene modified SPEs.

Herein SPE, SPE-oGO and SPE-rGO electrodes have been modified with Tyrosinase by adsorption. Such immobilization strategy and the final enzymatic activity are expected to be very dependent on the hydrophobicity level of the GO-SPE. The enzymatic response has been followed up by amperometric measurements at -0.1 V. We have found a very good electrochemical stability to the addition of catechol for the highly oxidized graphene as can be observed in Figure 6b. This behavior may be related with the binding of the Tyr to oGO by electrostatic interaction (Zhang, Zhang et al. 2012). Thus and despite being an insulator, SPE-oGO results highly beneficial for enzyme biosensing platforms presenting a limit of detection (LOD – signal to noise ratio (S/N) = 3)) of 0.0711nM and a sensitivity of 0.0679 $\mu\text{A}/\mu\text{M}$ as presented on table 2. In the case of SPE-rGO modified with Tyr, the improvement of the electroanalytical performance (based on LOD and sensitivity parameters) was observed. The

presence of hydrophobic aromatic structures observed by XPS spectra (Fig. 1b) and the water contact angles studies (Fig. 3d) suggested that the adsorption of the enzyme onto SPE-rGO should be governed by a hydrophobic interaction instead of electrostatic interaction as onto SPE-oGO. As reported before, this Tyrosine immobilization onto the rGO was more efficient than the immobilization onto the oGO for similar C/O ratios (Zhang, Zhang et al. 2012). This phenomenon is attributed to the fact that the electrostatic interaction as the driving force for enzyme binding to oGO severely affected the activity of the enzyme. Additionally, the higher conductivity of the rGO promotes high charge transfer (Fig. 4a). As reported in table 2, the SPE-rGO presented the best LOD of all graphene materials (0.0103 nM) and was shown to be the most sensitive (0.0898 $\mu\text{A}/\mu\text{M}$).

Table 2. Description of different analytical performance parameters

	Limit of Detection	Sensitivity	Linear Interval	R^2
	(nM)	($\mu\text{A} \cdot \mu\text{M}^{-1}$)	(μM)	
SPE	0.4140	0.0056	2-16	0.9936
SPE-oGO	0.0711	0.0679	2-16	0.9954
SPE-rGO	0.0103	0.0898	2-16	0.9918

4. Conclusions

As experimentally observed in this work, graphene materials changed the electrochemical properties of SPE in terms of current intensities. In addition, the capability for biofunctionalization that in turn might have been effected by the level of oxidation of graphene materials should have contributed in the biosensor performance (better stability due to a better enzyme immobilization)

and the decrease of the limit of detection in comparison to the non-modified SPE. The obtained results clearly show that the SPE modification either with oGO or rGO may tune the biosensing response. The modification with oGO achieves a lowly biofunctional platform for Tyrosinase (although much higher than SPE) while the modification with highly hydrophobic and conductive reduced graphene oxide leads to a high range of biofunctionalization. Figure 5 is a schematic of this tuned biosensing platform using the two graphene nanomaterials. Two different biosensing systems can be obtained: one using insulating oGO that leads to low concentration of Tyrosinase attached to the surface of the SPE arising in lower signaling response and the other one taking advantage of the highly hydrophobic rGO semimetallic structures, which provides a big amount of enzyme to produce the high electrocatalytic signaling, decreasing significantly the detection limits of the bare SPE. Despite of all different properties of graphene materials, it is obvious the influence on biosensing response of the graphene oxide transition from an insulator to semimetallic compound on SPE response. This tuning capability of the biosensor response can be with interest for building several other biosensors including immunosensors and DNA sensors with interest for various applications.

5. References

- Acik, M., G. Lee, C. Mattevi, M. Chhowalla, K. Cho and Y. J. Chabal (2010). "Unusual infrared-absorption mechanism in thermally reduced graphene oxide." Nature Materials **9**(10): 840-845.
- Belding, S. R., F. W. Campbell, E. J. F. Dickinson and R. G. Compton (2010). "Nanoparticle-modified electrodes." Physical Chemistry Chemical Physics **12**(37): 11208-11221.
- Cai, W. W., R. D. Piner, F. J. Stadermann, S. Park, M. A. Shaibat, Y. Ishii, D. X. Yang, A. Velamakanni, S. J. An, M. Stoller, J. H. An, D. M. Chen and R. S. Ruoff (2008). "Synthesis and solid-state NMR structural characterization of (13)C-labeled graphite oxide." Science **321**(5897): 1815-1817.
- Cheng, M., R. Yang, L. C. Zhang, Z. W. Shi, W. Yang, D. M. Wang, G. B. Xie, D. X. Shi and G. Y. Zhang (2012). "Restoration of graphene from graphene oxide by defect repair." Carbon **50**(7): 2581-2587.
- Cuong, T. V., V. H. Pham, Q. T. Tran, S. H. Hahn, J. S. Chung, E. W. Shin and E. J. Kim (2010). "Photoluminescence and Raman studies of graphene thin films prepared by reduction of graphene oxide." Materials Letters **64**(3): 399-401.
- Eda, G., C. Mattevi, H. Yamaguchi, H. Kim and M. Chhowalla (2009). "Insulator to Semimetal Transition in Graphene Oxide." Journal of Physical Chemistry C **113**(35): 15768-15771.
- Fanjul-Bolado, P., P. J. Lamas-Ardisana, D. Hernandez-Santos and A. Costa-Garcia (2009). "Electrochemical study and flow injection analysis of paracetamol in pharmaceutical formulations based on screen-printed electrodes and carbon nanotubes." Analytica Chimica Acta **638**(2): 133-138.
- Gao, X. F., J. Jang and S. Nagase (2010). "Hydrazine and Thermal Reduction of Graphene Oxide: Reaction Mechanisms, Product Structures, and Reaction Design." Journal of Physical Chemistry C **114**(2): 832-842.
- Geim, A. K. and K. S. Novoselov (2007). "The rise of graphene." Nature Materials **6**(3): 183-191.
- Marcano, D. C., D. V. Kosynkin, J. M. Berlin, A. Sinitskii, Z. Z. Sun, A. Slesarev, L. B. Alemany, W. Lu and J. M. Tour (2010). "Improved Synthesis of Graphene Oxide." Acs Nano **4**(8): 4806-4814.

Martin-Fernandez, I., D. B. Wang and Y. G. Zhang (2012). "Direct Growth of Graphene Nanoribbons for Large-Scale Device Fabrication." Nano Letters **12**(12): 6175-6179.

Mathkar, A., D. Tozier, P. Cox, P. J. Ong, C. Galande, K. Balakrishnan, A. L. M. Reddy and P. M. Ajayan (2012). "Controlled, Stepwise Reduction and Band Gap Manipulation of Graphene Oxide." Journal of Physical Chemistry Letters **3**(8): 986-991.

Morales-Narvaez, E. and A. Merkoci (2012). "Graphene Oxide as an Optical Biosensing Platform." Advanced Materials **24**(25): 3298-3308.

Park, S., J. H. An, R. D. Piner, I. Jung, D. X. Yang, A. Velamakanni, S. T. Nguyen and R. S. Ruoff (2008). "Aqueous Suspension and Characterization of Chemically Modified Graphene Sheets." Chemistry of Materials **20**(21): 6592-6594.

Park, S., K. S. Lee, G. Bozoklu, W. Cai, S. T. Nguyen and R. S. Ruoff (2008). "Graphene oxide papers modified by divalent ions - Enhancing mechanical properties via chemical cross-linking." Acs Nano **2**(3): 572-578.

Peng, J., W. Gao, B. K. Gupta, Z. Liu, R. Romero-Aburto, L. H. Ge, L. Song, L. B. Alemany, X. B. Zhan, G. H. Gao, S. A. Vithayathil, B. A. Kaiparettu, A. A. Marti, T. Hayashi, J. J. Zhu and P. M. Ajayan (2012). "Graphene Quantum Dots Derived from Carbon Fibers." Nano Letters **12**(2): 844-849.

Salas, E. C., Z. Z. Sun, A. Luttge and J. M. Tour (2010). "Reduction of Graphene Oxide via Bacterial Respiration." Acs Nano **4**(8): 4852-4856.

Shang, J. Z., L. Ma, J. W. Li, W. Ai, T. Yu and G. G. Gurzadyan (2012). "The Origin of Fluorescence from Graphene Oxide." Scientific Reports **2**.

Shao, Y. Y., J. Wang, H. Wu, J. Liu, I. A. Aksay and Y. H. Lin (2010). "Graphene Based Electrochemical Sensors and Biosensors: A Review." Electroanalysis **22**(10): 1027-1036.

Shen, J. F., Y. Z. Hu, M. Shi, X. Lu, C. Qin, C. Li and M. X. Ye (2009). "Fast and Facile Preparation of Graphene Oxide and Reduced Graphene Oxide Nanoplatelets." Chemistry of Materials **21**(15): 3514-3520.

Stankovich, S., D. A. Dikin, R. D. Piner, K. A. Kohlhaas, A. Kleinhammes, Y. Jia, Y. Wu, S. T. Nguyen and R. S. Ruoff (2007). "Synthesis of graphene-based nanosheets via chemical reduction of exfoliated graphite oxide." Carbon **45**(7): 1558-1565.

Wang, Y., Y. Wan and D. Zhang (2010). "Reduced graphene sheets modified glassy carbon electrode for electrocatalytic oxidation of hydrazine in alkaline media." Electrochemistry Communications **12**(2): 187-190.

Zhang, Y., J. Y. Zhang, X. L. Huang, X. J. Zhou, H. X. Wu and S. W. Guo (2012). "Assembly of Graphene Oxide-Enzyme Conjugates through Hydrophobic Interaction." Small **8**(1): 154-159.

Zhu, Y. W., S. Murali, W. W. Cai, X. S. Li, J. W. Suk, J. R. Potts and R. S. Ruoff (2010). "Graphene and Graphene Oxide: Synthesis, Properties, and Applications." Advanced Materials **22**(35): 3906-3924.

Chapter 5

Printing graphene oxide using wax printed membranes

In this chapter a methodology for fast patterning and transfer graphene oxide using water activated wax printed membranes with infinite shaping capability is presented. Water activation transfer of patterned GO over flexible substrates using the roll-to-roll mechanism for rapid building of plastic, paper or textile electronic platforms is demonstrated. A touch sensitive device over PET for switching on and off a LED is produced.

Related publication

-
1. *Luis Baptista-Pires, Carmen C. Mayorga-Martínez, Mariana Medina-Sánchez, Helena Montón and Arben Merkoçi*, Water Activated Graphene Oxide Transfer Using Wax Printed Membranes for Fast Patterning of a Touch Sensitive Device. *Acs Nano*, 2016. **10**(1): p. 853-860.

1. Introduction

Printed electronics paved the way to a new type of low cost technologies over plastics and organic substrates for building electrical and electronic devices. Using a wide variety of materials conjugations such as inorganic¹ and organic²⁻⁴ semiconductors, metals⁵ or insulators⁶ enabled building devices such as Radio Frequency Identification (RFID) systems, light emitting diodes (LED), supercapacitors, thin film transistors, resistors or solar cells. Industry equipment in this area is mainly based on screen-printing technology, flexography, gravure, inkjet and lithography (also as developers of micro-contact stamps).⁷⁻⁹ More exactly, lithography, flexography and gravure exhibit high set up costs and are advantageous only for high production rates. Additionally, lithography is mainly a chemical or photochemical process with the need for clean room facilities and consumable and expensive photoresists and developers. In the case of screen-printing and ink-jet printing the need for ink development is an issue in terms of viscosity and polymerization. For the singular case of inkjet printing, additionally to the ink development there is the substrate treatment and printing temperature. Despite this, the last two techniques are cost effective for smaller quantities of printed products. All these technologies possess the need of know-how and specialized personal as common characteristic for the development of simple electronics devices.

Fast prototyping rise in the “Maker” or “Do It Yourself” communities have opened venues for fast integration in electronic industry of creative and original devices of all types integrated with the internet of things.¹⁰⁻¹² This process is done mainly using the techniques described below which become hard in terms of versatility and price for low quantities of prototyping production. Despite 3D printing paved the way for a different type of technologies in these areas, great efforts are still needed for the development of new processes for fast printing technologies that can integrate communities making a step forward to knowledge and technology transfer for society.

The importance of graphene oxide (GO) and derivatives such as reduced GO (rGO) have raised in recent years substituting a wide variety of materials for the production of supercapacitors,¹³⁻¹⁸ LED,¹⁹ RFID,²⁰ solar cells²¹ and

(bio)sensors.²²⁻²⁵ The ability to pattern and transfer GO without using of organic toxic compounds (as in lithography), surfactants or polymer based solutions and (as in ink jet or screen printing) is required given the influence that these compounds can have onto the optoelectronic properties.^{8, 9, 26-31} In this way, vacuum filtration makes a step forward in this development and has been used for various applications either for transferring thin films of rGO using liquid-air exfoliation leaving a suspended film that can be “fished” by the target substrate;³² or for transferring thin films with nanometer resolution onto substrates by dissolving the nitrocellulose membrane with acetone when in contact with the target substrate.³³ Despite the great advances over the transfer of GO thin films using vacuum filtration described before, patterning technologies are still the handicap/bottleneck of the whole process. Existing transfer technologies do not solve problems such as GO ink preparation²⁸ or the need for lithographic²⁷ patterning and physical erasure (possibly by PDMS based microcontact stamps).²⁶ Filling this gap that would lead to an automatized process that controls the thickness and enables the direct patterning of controlled GO structures onto various substrates, in a fast and chemically-free transfer mode, without any requirement for ink treatment and being at the same time simple and cost effective is still a challenging objective in GO printing technologies.

Herein we propose a methodology for fast patterning and transfer of GO using water activated wax printed membranes (WPM). Wax printing technology is a green, low cost and versatile technology that can be easily performed using the desired shape or image chose by the user with micrometer resolution.^{34, 35} Its hydrophobic nature enables to drive GO water suspension over the membrane to the desired regions. This technology coupled with the vacuum filtration provides control over the shape and thickness of GO leaving a patterned GO mesh over the nitrocellulose membrane. In this way, we developed a water activated mechanism to transfer patterned GO over flexible substrates. The roll-to-roll mechanism that outfits the wax printer machine makes this technique suitable for rapid building of plastic, paper or textile electronic platforms. We

have used this technique to produce a touch sensitive device over polyethylene terephthalate (PET) for switching on and off a LED.

2. Results and discussion

In Figure 1 is shown how a nitrocellulose membrane (Figure 1a) is patterned onto the desired shape (Figure 1b) using a wax printer machine. To form the GO pattern the inverse pattern is printed onto the membrane surface. The wax clogs the pores of the membrane wherever it is printed leaving the non-wax containing regions (grey in the reverse pattern) unclogged. The WPM is set onto the filtering glass, and the suspension of GO (at a desired concentration) is filtered, leaving a GO mesh on top of the WPM (Figure 1c1). The WPM is left to dry (Figure 1c2), water activated by rewetting in a water bath (Figure 1c3), fast dried using air flow on the back part of the membrane (Figure 1c4) and transferred by pressure (Figure 1d,1e) to the desired target substrate.

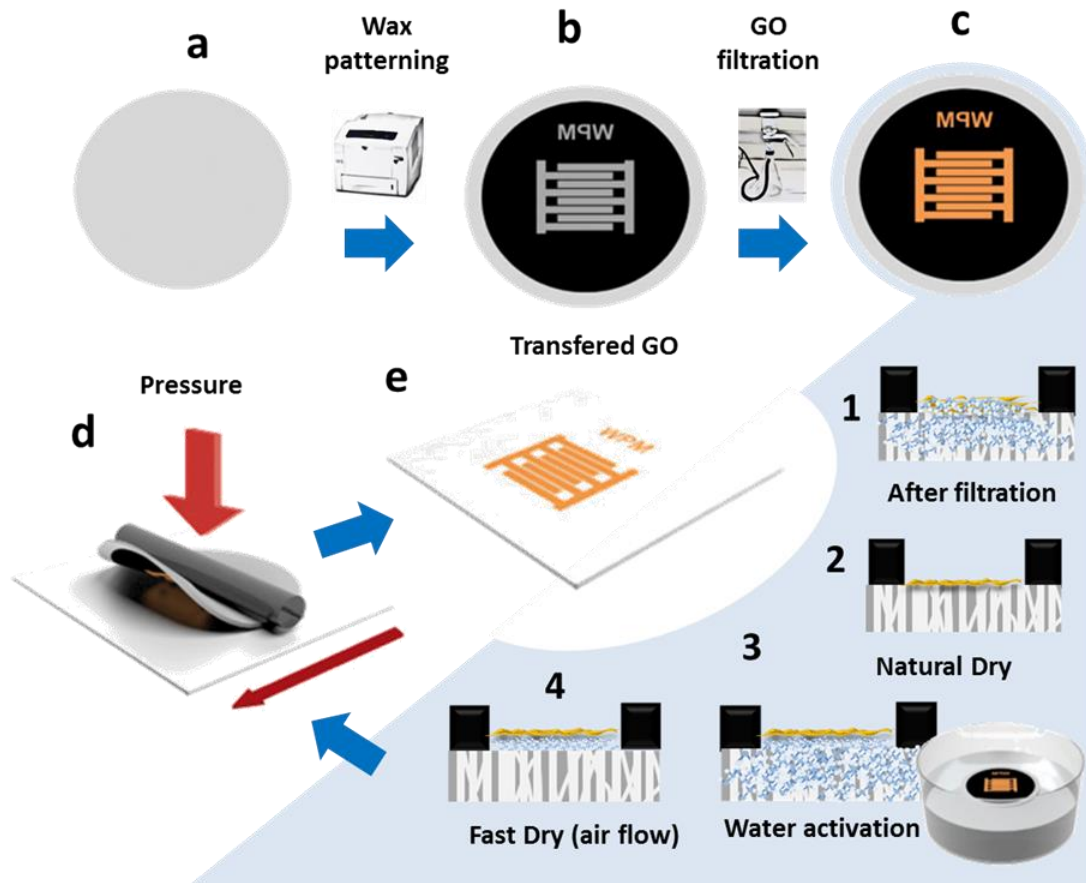


Figure 1. Schematics of the patterning and transfer of GO.(a) nitrocellulose membrane, (b) WPM, (c) WPM modified with GO - (c1) sheets right after filtrations; (c2) after natural dry; (c3) after water activation ; (c4) after fast dry with air flow – (d) transfer of GO by pressure to the substrate, (e) transferred GO pattern.

When the GO mesh over the WPM is dried, which takes between 30-60 min (Figure 1c2), the interactions with the membrane are in their stronger phase which inhibit the transfer of GO. On the other hand, right after filtration (Figure 1c1), the transfer can for instance, spread GO all over the substrate depending on the absorptive properties of the target material.

According to this, we have produced different WPMs through wax printing and modified them with GO (inset Figure 2a,c,e and g). We used the wax printer

which is outfitted with roll-to-roll hardware for fast and automatized transfer of GO over different flexible substrates such as PET, textile t-shirt, paper and adhesive film as demonstrated in Figure 2 using procedure from Figure 1. As proof of concept we transferred a modified WPM using a spatula (Figure S1) where a simple image of the Nobel coin can be transformed into a black and white WPM (Figure S1a,b and c) and transferred over a window glass by simple hand pressure of the spatula (Figure S1d).

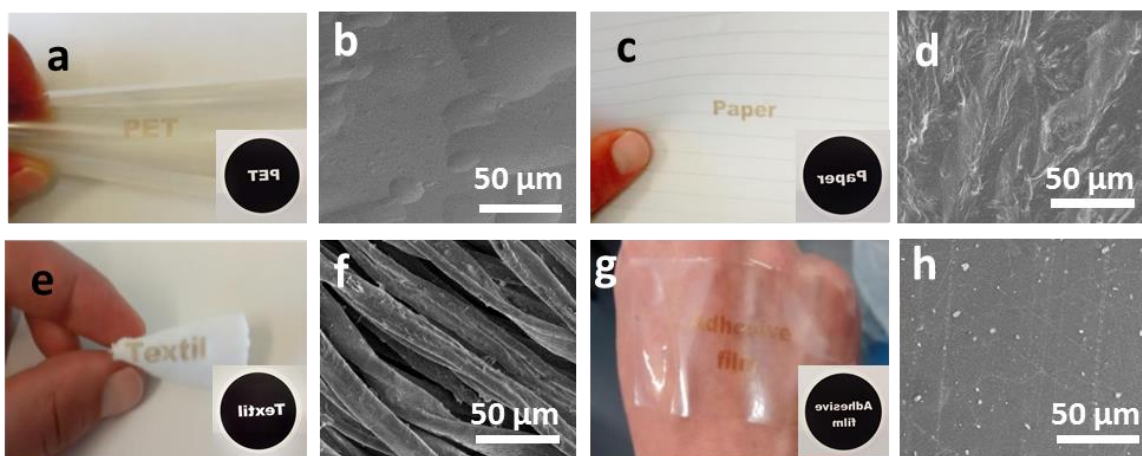


Figure 2. Patterning and transfer over different materials. (a) Patterned GO over PET (inset: WPM for PET); (b) SEM image of patterned rGO over PET; (c) Patterned GO over paper (inset: WPM for paper); (d) SEM image of patterned rGO over paper. (e) Patterned GO over textile t-shirt (inset: WPM for textile); (f) SEM image of patterned rGO over textile. (g) Patterned GO over adhesive film (inset: WPM for adhesive film); (h) SEM image of patterned rGO over the adhesive film.

To determine the resolution we produced different WPMs composed of different geometric forms and lines (Figure 3a). The WPMs shown in Figure 3b, exhibited acceptable designs over a range of 500 μm for circles, once the circle geometry gets degraded over lower size resolutions. The direction of the wax printing (parallel or vertical) was an important parameter to evaluate, as it affects the resolution and the shape of the patterned wax. Figure 3c shows wax lines printed vertically and Figure 3d parallel printed. The wax line, represented in

Figure 3c as the green cross has a minimum resolution of 100 μm which is consistent with literature – values under 100 μm are simply not patterned from the wax printing machine. We investigated the resolution of the unclogged space represented in Figure 3c as the red cross once will be the minimum resolution of the future GO pattern. A resolution of 50 μm (Figure 3e) was obtained when the WPM was printed vertically. For lines parallel printed, the variation in the line size is determined by the bumps and the printing and the resulting width are not consistent. According to this, to define long narrow lines it is better having them printed perpendicular to the printer feed direction (so one avoid poor line to line printer registration issues). According to the technology features described before, the resolution of the WPMs is mainly a hardware characteristic of our printing machine. We believe that hardware evolution will entail advances in resolution factors, and in this way our technique could possibly in the future compete in the microelectronic device fabrication domain. On the other hand, the main principle of our process could be used, and the coupling between photolithography or inkjet printing could produce masks over the nitrocellulose membranes with the technical and cost losses associated with it (as described elsewhere in this work). The ink development such as using smaller GO sheet size should be performed so as to reach better resolution. Despite this, we believe that even the current printing resolution of the WPMs is still efficient for the production of devices such as supercapacitors, solar cells, sensors and biosensors. The lateral spreading of the wax across the WPM at room temperature was studied over 5 months (Figure S2) and any significant deformation or spreading was not observed and therefore we concluded that these WPMs are stable over the long term. Each WPM have a filtration area that is dependent on the patterned design influencing the filtration rate (time) and the vertical size of GO film.

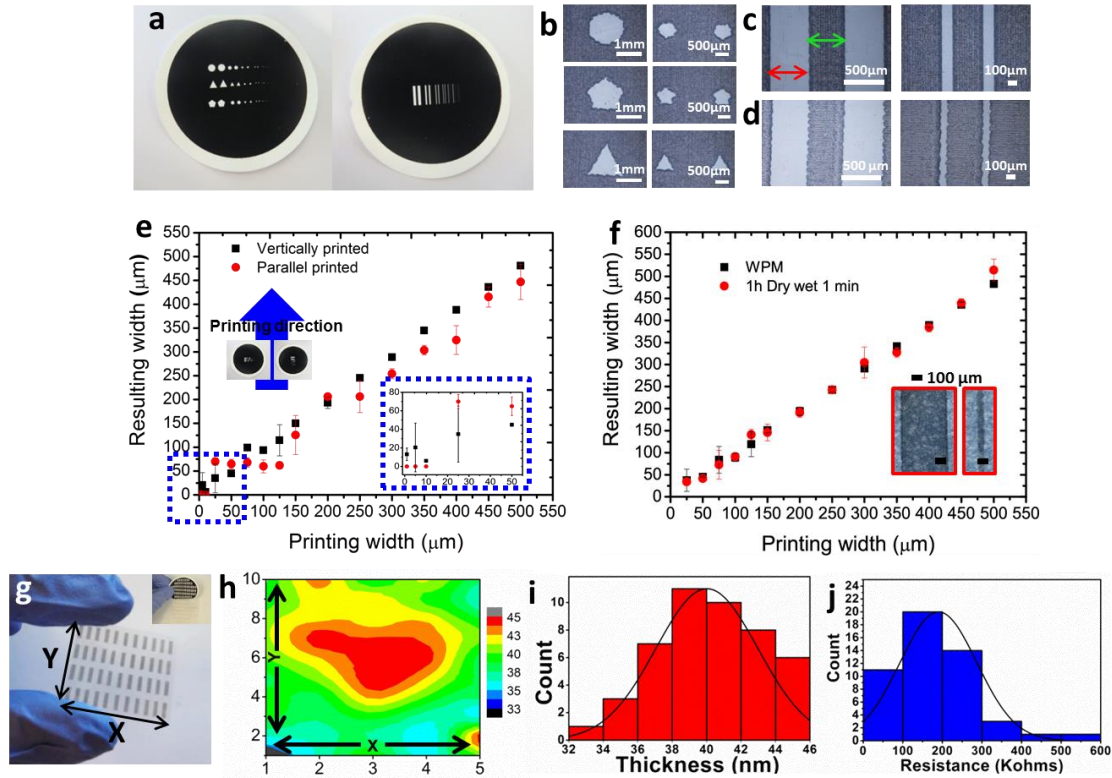


Figure 3. Reproducibility of WPM and transferred patterns. (a) WPM with different forms (left side) and lines (right side). Optical microscope image of the WPM for (b) forms, (c) lines vertically printed, (d) lines parallel printed. (e) Evaluation of vertically and parallel printed WPM of printing width (designed in the computer) and resulting width (patterned onto the NCM). (f) Evaluation of the transferred GO in comparison with WPM widths (inset: optical microscope image of patterned GO lines with 50μm and 300μm). (g) Photo of the patterned lines with 1x4mm (inset: photo of the transferred GO with the WPM). (h) Variation of the thickness of GO over the patterned substrate area. (i) and (j) histogram of the thickness (GO) and resistance (rGO) distribution respectively.

We used vertically printed WPMs (Figure 3a) for studying the transfer process over PET using the roll-to-roll mechanism that outfits the wax printing machine due to the automation that it provides. Accordingly, 5 mL of a GO concentration of 0.01 mg/mL was placed into the filtering flask, filtered and left to dry for 1 hour. After 1h drying followed by 1min wetting and drying process, the WPM

was placed in contact with PET substrate and transferred using the wax printer machine. The transfer efficiency to PET using the mass weight of the WPM before and after the transfer ($n=10$) was calculated obtaining a transfer efficiency of 99.74%. The minimum resolution of GO transferred into PET was 50 μm (Figure 3f) which is in accordance with the resolution of the WPM described before in this work. The transfer mechanism can be understood under the focus of the interlayer distance between GO sheet upon filtration. Filtration of GO layers origins a compressive stacking forming a compact film with low quantity of water molecules in between the layers. According to this, while rewetting, the water is absorbed in the surface of the GO film due to the hydrophilic nature of GO causing the release of the GO film from the membrane. We studied this evolution during one month and the transfer was still effective as reported in Figure S3. The hydrophobicity of GO sheets quickly increased upon drying as determined in Figure S4 and slowed down upon 1 hour to 1 month. It is also known that the reduction of GO is slow at room temperature and normal life conditions which opens to us a big time window to process the transfer. The transfer pressure should be suitable to reach the necessary strength to be applied between GO mesh and the target substrate to avoid the 25 μm wax height (which can be considered as the maximum vertical size that GO film can have – Figure S5) and make direct contact between the GO mesh and the target substrate.

We have built a mask presented in Figure 3g (inset) to address the reproducibility of the transfer in terms of thickness and resistance. In Figure 3h one can see the variation of the thickness of GO over the patterned substrate area. It has shown uniformity of the different lines printed with a medium thickness all over the substrate of 40 ± 3 nm (Figure 3i). The patterned GO films were reduced immersed in 1 mg/mL of ascorbic acid at 30°C for 48h (Figure 3g) and wired using silver ink. The sheet resistance was measured three times using a tester showing a mean distribution of 190.08 ± 97.15 k Ω (Figure 3j). The resistance and thickness variations of our methodology can be related to a myriad of factors such as the nature of our method by itself – the patterned wax should favour the fluidic movement over the membrane upon filtration; the circular filtration area and the round shape of the metallic sieve in the filtration

flask which allows the GO to be filtrated in the central areas rather than in the surrounding areas - and the reduction methodology.³⁶⁻⁴¹ We believe that all these aspects can, in the future, be optimized and developed accordingly and the scalability of the process could diminish and improve these factors. Additionally, we performed an adhesive-tape-peel-off wipe test⁴² in order to determine the stability of the conductive patterns (Figure S6 and Table S1). A different prepared film avoiding silver wiring was used in order to establish maximum contact between the adhesive tape and the rGO tracks area. The same GO concentration (0.01 mg/mL) was used and after 5 peel-off counts the resistance increased from $282.44 \pm 93.02 \text{ k}\Omega$ to $326.75 \pm 129.43 \text{ k}\Omega$ which means an increase of 44.31 k Ω in mean resistance. This can be attributed to the consecutive peeling of few layer graphene⁴³ and the contact stretching of the tester connections with the rGO tracks. According to this, our conductive tracks appear to be stable, avoiding any treatments to substrate or to the patterned conductive tracks.

As reported in Figure 4a we have developed interdigitated electrodes (IDE) using the mask presented in Figure 4b and filtered different concentrations of GO solutions in order to determine the electrical properties dependence on the vertical size of GO film. Accordingly, GO IDEs were fabricated using the procedure developed before using 1h dry and water activation methodology over PET. The GO IDEs (Figure 4c) where reduced (Figure 4d) to improve the electronic properties, using ascorbic acid as a reducing agent. Using four different concentrations - 5mL of 5, 2.5, 1.25, 0.625 $\mu\text{g/mL}$ - (Figure 4e) we studied the evolution in terms of capacitance, resistance and vertical size.

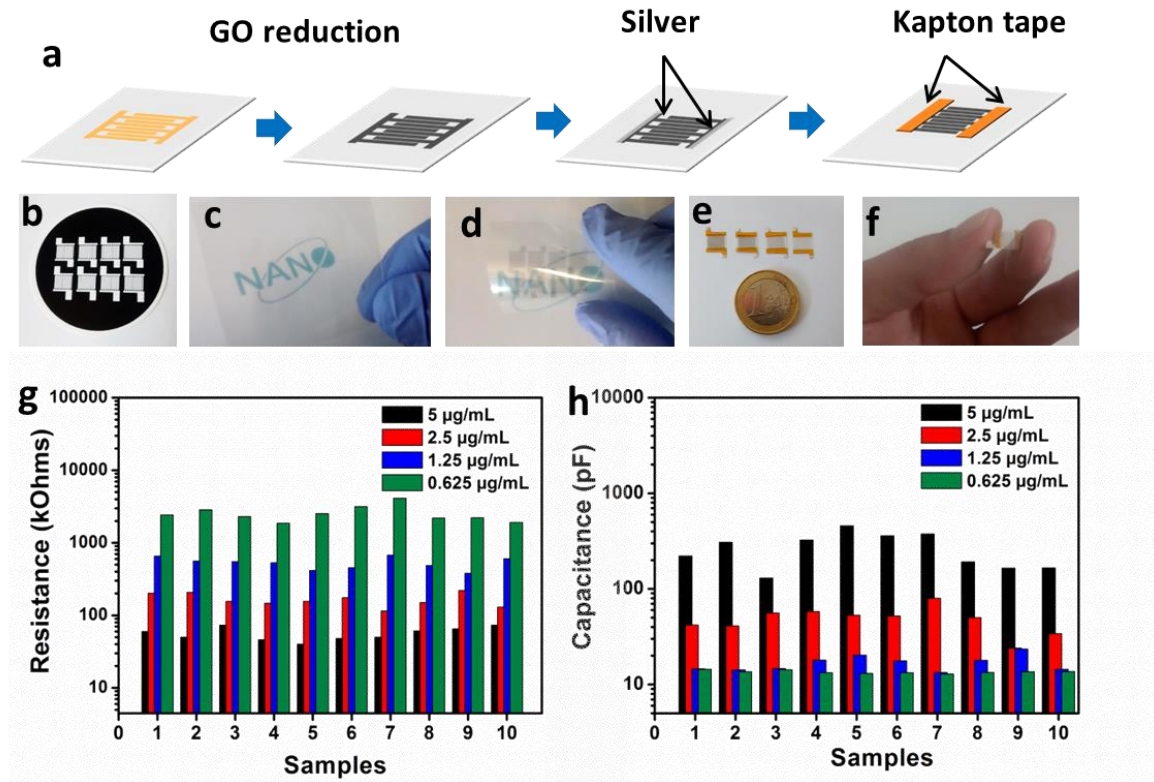


Figure 4. Electrical characterization of the IDE. (a) Schematics of the IDE fabrication. (b) WPM used for the design of GO IDE. (c) IDE tranfered over PET in their oxidized form. (d) IDE transferred over PET in their reduced form. (e) photo of all IDEs with different filtered volumes (5mL of 5, 2.5, 1.25, 0.625 µg/mL – from left to right). (f) IDE with a filtrated volume of 0.625 µg/mL). (g) Resistance of 10 IDEs. (h) Capacitance of 10 IDEs.

According to this, with a decrease of a factor of 2 over the concentration of GO, the thickness was $38.9 \pm 2.3 \text{ nm}$, $24.5 \pm 0.7 \text{ nm}$, $19.8 \pm 0.5 \text{ nm}$, $14.9 \pm 0.8 \text{ nm}$. The resistance varied from 57 ± 12 , 166 ± 34 , 531 ± 98 and $2557 \pm 679 \text{ k}\Omega$ with the decrease of concentration. The capacitance decreased from 270 ± 110 , 49 ± 15 , 17 ± 3 and $13.2 \pm 0.5 \text{ pF}$. We believe that the resistance and capacitance values would reach saturation with the consecutive increase of GO thickness (200nm to 500nm for instance), mainly due to the lack of effectiveness of our reduction methodology to achieve the intrinsic layers in the case of a thicker GO film (being the reduction process only effective on the uppermost layers).^{18, 33} In this

way, the variation of the capacitive properties over different electrodes with similar resistance can be related with the intrinsic properties of GO upon reduction once all the IDE were reduced submerged in ascorbic acid which can possibly alter the intrinsic properties such as the interlayer distance or the surface area exposed to the electrolyte. We expect that these properties can be tuned by the reduction method or either in the in-situ development of GO foam-like materials to develop extreme capacitive characteristics.^{13, 14, 17, 44, 45}

Using the 60nm IDE we measured the resistance and capacitive properties upon the interaction with a human finger. As shown in Figure 5a,b upon touch, the circuit is closed and the resistance changes from $>100\text{ M}\Omega$ (cannot be read in a contact tester) to $\approx 110\text{ k}\Omega$. The capacitance is also changed from 0.25 pF to approximately 0.75 pF . We produced a touch sensing device using an electronic circuit (Figure S7) with interest for real applications making the capacitive\resistive behaviour of this IDE suitable for touch operations such as LED switcher (Figure 5c). Using this we could operate a LED turning it ON (Figure 5d) and OFF (Figure 5d). A movie of the operation of the switcher was additionally obtained (can be seen in Movie S1). The possibility of having GO/rGO interfaces in one single device is also demonstrated. Despite similar circuitry development has been performed by ink-jet printing,⁴⁶ when establishing a comparison with the proposed WPM-based printing, it demonstrates some advantages being a very simple patterning mode, avoiding optimization time of the ink (viscosity, printing temperature, GO concentration used and GO flake size), long chemical substrate treatment and coffee-ring effects. Our technology also can be used in the future for fast patterning of transparent conductive circuitry without the need to develop new GO matrix requested by ink-jet printing or other printing technologies.

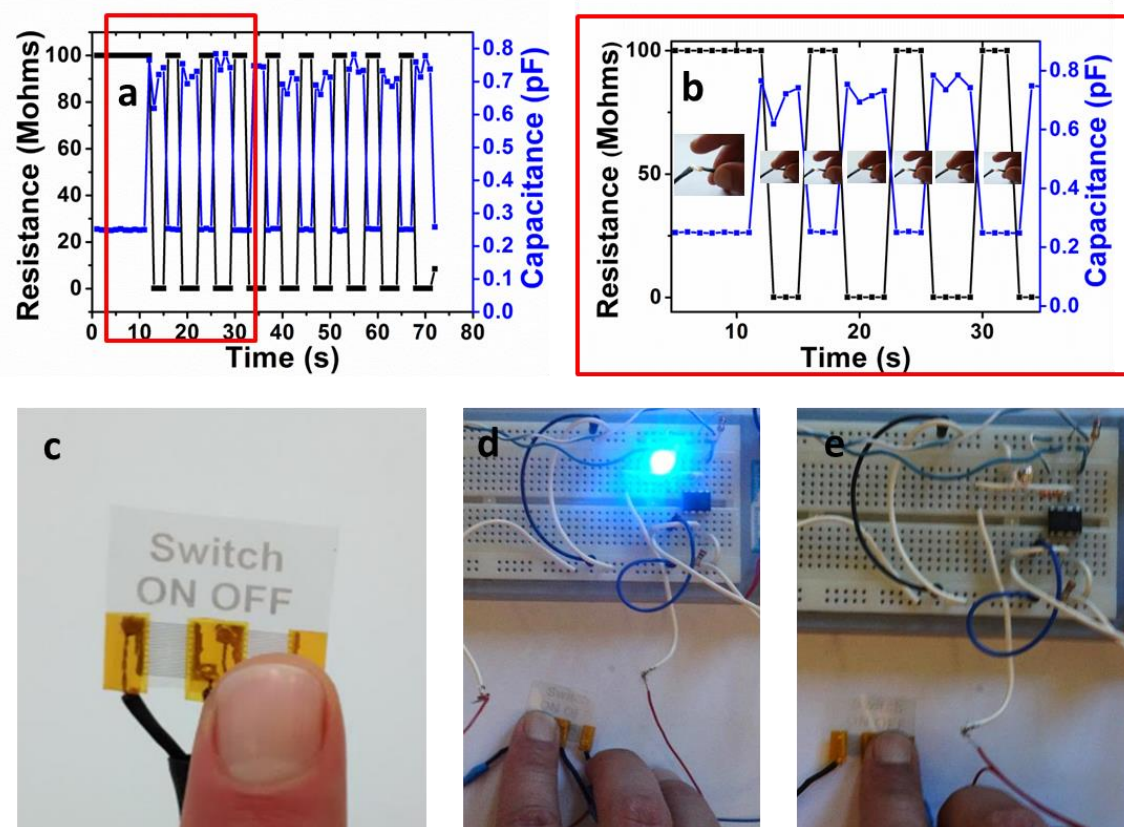


Figure 5. Touch sensitive device. (a) Variation of the resistance/capacitance upon touch. (b) zoom of the initial 30 s of Figure 5(a). (c) IDE used for this experiment. (d) IDE connected to the circuit. (e) IDE turning on a LED upon touch.

The proposed technology opens new venues for direct patterning of GO while filtering using a total green and biological friendly material such as wax and the possibility for long term transfer using the water activation and roll-to-roll pressure. The methodology is automatized, with control over the x, y and z directions and easily scalable. The long term stability that possesses opens the possibility for in-field applications. In addition it can be tuned from a simple patterning methodology (the WPM itself can be turned into simple microfluidic or electronic device made of GO) to a transferring methodology (one could transfer GO without patterning for a wide variety of substrates just by a mechanical actuation using the water activation mechanism). Apart, one can look at this

technology as a non-chemical, clean and polymer free self-adhesive or water activated adhesive for direct patterning of GO devices. We believe a WPM could in the future perform multifunction's that are nowadays applications of lithography such as PDMS stamps molding.

The proposed patterning technique also can be adapted after right optimizations to a wide variety of materials such as silicon nanowires,^{47, 48} carbon nanotubes⁴⁹ or 2D materials⁵⁰ (such as graphene, MOS_2 , WSe_2 or boron nitride). The corresponding matrix of nanomaterial-based inks must avoid the hydrophobic forces of the wax, should not dissolve the membrane and have target substrate affinity. This could be achieved using aqueous solution (as in the current GO printing) or with adequate chemically modified materials, ion intercalated solutions or surfactant suspensions followed by optimization of the transfer process. The possibility to apply the proposed technology to other materials will open the way to fabrication of other devices and many other applications with interest for various fields. Despite the fact that further work will be needed in this area, we believe that the proposed technology will open new opportunities for GO (or other nanomaterials)-based devices. This novel and versatile WPM-based printing technology is advantageous and disruptive in comparison to existing/similar techniques reported earlier.^{32, 33, 51} The WPMs can in a near future open many other application fields taking advantages of each fabrication step of the current technology (presented in Figure 1) either separately or all together.

3. Conclusions

In summary, we have reported a new, versatile, low cost and customisable method for patterning GO onto a myriad of substrates through highly stable, microscale WPMs that can be seen as water activated “adhesives”. The ability and stability of these WPMs in consonance with the properties of GO makes this technique versatile and easy to handle. These masks enable controlled shaped filtration and transfer of different thickness's of GO in various shapes of interest for different applications with a minimum resolution of 50 μm . The GO-printing technology that we report here is advantageous over previously reported methods for fabrication of GO-based devices in terms of ease, versatility, cost and potential end-applications. This long term transfer of GO is promising for actuating in areas that are not suitable to have a laboratory such as underdeveloped countries opening the way for in-field transfer of GO. This could enable future uses such as in-situ transfer of supercapacitor, a solar cell or a LED in between others, for wearable or portable applications. This methodology can pave the way for intuitive soft electronics, fast prototyping in the “maker” community and finally, we believe the step towards to industrial scalability can be easily demonstrated for disposable humanized sensing technologies.

4. Experimental section

Wax printing characterization

The nitrocellulose membranes used are hydrophilic and have a pore size of 0.025 μm and a diameter of 47 mm. The wax was printed with a Xerox ColourQube 8570 printer (which is compatible with WindowsTM, MacOSTM and UNIX). All drawings of the electrode patterns were done on Corel Draw. The high-resolution printing mode was always chosen and the membranes were used 5 min after printing, as a compromise to minimise spreading and maximise drying of the wax. Optical microscopy images of the wax-patterned membranes were obtained on a Nikon Eclipse LV100 microscope with a 20x/0.45 objective lens.

GO characterization

All devices were reduced at the same time to avoid irreproducibilities and to make conductive structures, once GO is highly resistive material. The reduction efficiency was assessed by X-ray Photoelectron Spectroscopy (XPS) (Figure S8) and Scanning Electron Microscopy (SEM) (Figure S9).

The GO was provided by Angstrom Materials. When needed, it was reduced submerging the electrode in ascorbic acid vapour at 30 °C for 48 h. All GO electrodes were reduced at the same time to avoid reduction variations. Aqueous suspensions of GO at various concentrations using a 1 L vacuum-filtering flask, 300 mL glass filter holder and 47 mm SS screen (1/Pk). The WPMs were transferred using the wax printing machine described before. The thickness was determined using a Elipsometer Rudolph AutoEl III.

The samples were electrically characterised using Autolab302 potentiostat/galvanostat/frequency-response analyzer PGST30, controlled by GPES/FRA Version 4.9. The X-ray Photoelectron Spectroscopy (XPS) measurements were performed with a Phoibos 150 analyzer (SPECS GmbH, Berlin, Germany) in ultra-high vacuum conditions (base pressure 1E-10mbar) with a monochromatic aluminium K α x-ray source (1486.74eV). The energy resolution as measured by the FWHM of the Ag 3d_{5/2} peak for a sputtered

silver foil was 0.58 eV. Scanning Electron Microscopy (SEM) was done on a FEI Quanta FEG (pressure: 70Pa; HV: 20kV; and spot: four).

5. References

1. Fang, X.; Bando, Y.; Gautam, U. K.; Ye, C.; Golberg, D. Inorganic Semiconductor Nanostructures and Their Field-Emission Applications. *J. Mater. Chem.* 2008, 18, 509-522.
2. Fenwick, O.; Bozec, L.; Credgington, D.; Hammiche, A.; Lazzerini, G. M.; Silberberg, Y. R.; Cacialli, F. Thermochemical Nanopatterning of Organic Semiconductors. *Nat. Nanotechnol.* 2009, 4, 664-668.
3. Mathijssen, S. G. J.; Smits, E. C. P.; van Hal, P. A.; Wondergem, H. J.; Ponomarenko, S. A.; Moser, A.; Resel, R.; Bobbert, P. A.; Kemerink, M.; Janssen, R. A. J.; de Leeuw, D. M.; et al. Monolayer Coverage and Channel Length Set the Mobility in Self-Assembled Monolayer Field-Effect Transistors. *Nat. Nanotechnol.* 2009, 4, 674-680.
4. Zhang, Q.; Atay, T.; Tischler, J. R.; Bradley, M. S.; Bulovic, V.; Nurmikko, A. V. Highly Efficient Resonant Coupling of Optical Excitations in Hybrid Organic/Inorganic Semiconductor Nanostructures. *Nat. Nanotechnol.* 2007, 2, 555-559.
5. Dong, T.-Y.; Chen, W.-T.; Wang, C.-W.; Chen, C.-P.; Chen, C.-N.; Lin, M.-C.; Song, J.-M.; Chen, I.-G.; Kao, T.-H. One-Step Synthesis of Uniform Silver Nanoparticles Capped by Saturated Decanoate: Direct Spray Printing Ink to Form Metallic Silver Films. *Phys. Chem. Chem. Phys.* 2009, 11, 6269-6275.
6. Sivaramakrishnan, S.; Chia, P.-J.; Yeo, Y.-C.; Chua, L.-L.; Ho, P. K. H. Controlled Insulator-to-Metal Transformation in Printable Polymer Composites with Nanometal Clusters. *Nat. Mater.* 2007, 6, 149-155.
7. Suganuma, K. *Introduction to Printed Electronics*. 1 ed.; Springer-Verlag New York: 2014; p VI, 124.
8. Dua, V.; Surwade, S. P.; Ammu, S.; Agnihotra, S. R.; Jain, S.; Roberts, K. E.; Park, S.; Ruoff, R. S.; Manohar, S. K. All-Organic Vapor Sensor Using Inkjet-Printed Reduced Graphene Oxide. *Angew. Chem., Int. Ed.* 2010, 49, 2154-2157.
9. Lee, J. S.; Kim, N. H.; Kang, M. S.; Yu, H.; Lee, D. R.; Oh, J. H.; Chang, S. T.; Cho, J. H. Wafer-Scale Patterning of Reduced Graphene Oxide Electrodes by Transfer-and-Reverse Stamping for High Performance OFETs. *Small* 2013, 9, 2817-2825.

10. <http://www.nature.com/news/2005/050404/full/news050404-3.html>.
(accessed 04/08/2015).
11. <http://time.com/104210/maker-faire-maker-movement/>. (accessed 04/08/2015).
12. Moorefield-Lang, H. M. Makers in the library: Case Studies of 3D Printers and Maker Spaces in Library Settings. *Library Hi Tech* 2014, 32, 583-593.
13. Zhu, Y.; Murali, S.; Stoller, M. D.; Ganesh, K. J.; Cai, W.; Ferreira, P. J.; Pirkle, A.; Wallace, R. M.; Cychosz, K. A.; Thommes, M.; Su, D.; Stach, E. A.; Ruoff, R. S.; Et, a. Carbon-Based Supercapacitors Produced by Activation of Graphene. *Science* 2011, 332, 1537-1541.
14. Zhang, L. L.; Zhao, X.; Stoller, M. D.; Zhu, Y.; Ji, H.; Murali, S.; Wu, Y.; Perales, S.; Clevenger, B.; Ruoff, R. S.; Et, a. Highly Conductive and Porous Activated Reduced Graphene Oxide Films for High-Power Supercapacitors. *Nano Lett.* 2012, 12, 1806-1812.
15. Niu, Z. Q.; Zhang, L.; Liu, L.; Zhu, B. W.; Dong, H. B.; Chen, X. D. All-Solid-State Flexible Ultrathin Micro-Supercapacitors Based on Graphene. *Advanced Materials* 2013, 25, 4035-4042.
16. Gao, W.; Singh, N.; Song, L.; Liu, Z.; Reddy, A. L. M.; Ci, L.; Vajtai, R.; Zhang, Q.; Wei, B.; Ajayan, P. M.; Et, a. Direct Laser Writing of Micro-Supercapacitors on Hydrated Graphite Oxide Films. *Nat. Nanotechnol.* 2011, 6, 496-500.
17. El-Kady, M. F.; Kaner, R. B. Scalable Fabrication of High-Power Graphene Micro-Supercapacitors for Flexible and On-Chip Energy Storage. *Nat. Commun.* 2013, 4.
18. Wu, Z. S.; Parvez, K.; Feng, X. L.; Mullen, K. Graphene-Based In-Plane Micro-Supercapacitors with High Power and Energy Densities. *Nat. Commun.* 2013, 4, 8.
19. Wang, X.; Tian, H.; Mohammad, M. A.; Li, C.; Wu, C.; Yang, Y.; Ren, T.-L. A Spectrally Tunable All-Graphene-Based Flexible Field-Effect Light-Emitting Device. *Nat. Commun.* 2015, 6, 7767-7767.
20. Lee, J. S.; Oh, J.; Jun, J.; Jang, J. Wireless Hydrogen Smart Sensor Based on Pt/Graphene-Immobilized Radio-Frequency Identification Tag. *ACS Nano* 2015, 9, 7783-7790.

21. Liu, J.; Kim, G.-H.; Xue, Y.; Kim, J. Y.; Baek, J.-B.; Durstock, M.; Dai, L. Graphene Oxide Nanoribbon as Hole Extraction Layer to Enhance Efficiency and Stability of Polymer Solar Cells. *Advanced Materials* 2014, 26, 786-790.
22. Morales-Narvaez, E.; Perez-Lopez, B.; Pires, L. B.; Merkoci, A. Simple Forster Resonance Energy Transfer Evidence for the Ultrahigh Quantum Dot Quenching Efficiency by Graphene Oxide Compared to Other Carbon Structures. *Carbon* 2012, 50, 2987-2993.
23. Mannoor, M. S.; Tao, H.; Clayton, J. D.; Sengupta, A.; Kaplan, D. L.; Naik, R. R.; Verma, N.; Omenetto, F. G.; McAlpine, M. C. Graphene-Based Wireless Bacteria Detection on Tooth Enamel *Nat. Commun.* 2013, 4, 1.
24. Yoon, H. J.; Kim, T. H.; Zhang, Z.; Azizi, E.; Pham, T. M.; Paoletti, C.; Lin, J.; Ramnath, N.; Wicha, M. S.; Hayes, D. F.; Simeone, D. M.; Nagrath, S.; Et, a. Sensitive Capture of Circulating Tumour Cells by Functionalized Graphene Oxide Nanosheets *Nat. Nanotechnol.* 2013, 8, 735-741.
25. Morales-Narvaez, E.; Merkoci, A. Graphene Oxide as an Optical Biosensing Platform. *Advanced Materials* 2012, 24, 3298-3308.
26. He, Q. Y.; Wu, S. X.; Gao, S.; Cao, X. H.; Yin, Z. Y.; Li, H.; Chen, P.; Zhang, H. Transparent, Flexible, All-Reduced Graphene Oxide Thin Film Transistors. *Acs Nano* 2011, 5, 5038-5044.
27. Pang, S. P.; Tsao, H. N.; Feng, X. L.; Mullen, K. Patterned Graphene Electrodes from Solution-Processed Graphite Oxide Films for Organic Field-Effect Transistors. *Advanced Materials* 2009, 21, 3488-+.
28. Lu, G.; Zhou, X. Z.; Li, H.; Yin, Z. Y.; Li, B.; Huang, L.; Boey, F.; Zhang, H. Nanolithography of Single-Layer Graphene Oxide Films by Atomic Force Microscopy. *Langmuir* 2010, 26, 6164-6166.
29. Jeong, H. Y.; Kim, J. Y.; Kim, J. W.; Hwang, J. O.; Kim, J. E.; Lee, J. Y.; Yoon, T. H.; Cho, B. J.; Kim, S. O.; Ruoff, R. S.; Choi, S. Y. Graphene Oxide Thin Films for Flexible Nonvolatile Memory Applications. *Nano Lett.* 2010, 10, 4381-4386.
30. Kim, T.; Kim, H.; Kwon, S. W.; Kim, Y.; Park, W. K.; Yoon, D. H.; Jang, A. R.; Shin, H. S.; Suh, K. S.; Yang, W. S. Large-Scale Graphene Micropatterns via Self-Assembly-Mediated Process for Flexible Device Application. *Nano Lett.* 2012, 12, 743-748.

31. Wang, S.; Ang, P. K.; Wang, Z. Q.; Tang, A. L. L.; Thong, J. T. L.; Loh, K. P. High Mobility, Printable, and Solution-Processed Graphene Electronics. *Nano Lett.* 2010, 10, 92-98.
32. Wang, X.; Xiong, Z.; Liu, Z.; Zhang, T. Exfoliation at the Liquid/Air Interface to Assemble Reduced Graphene Oxide Ultrathin Films for a Flexible Noncontact Sensing Device. *Advanced Materials* 2015, 27, 1370-1375.
33. Eda, G.; Fanchini, G.; Chhowalla, M. Large-Area Ultrathin Films of Reduced Graphene Oxide as a Transparent and Flexible Electronic Material. *Nat. Nanotechnol.* 2008, 3, 270-274.
34. Carrilho, E.; Martinez, A. W.; Whitesides, G. M. Understanding Wax Printing: A Simple Micropatterning Process for Paper-Based Microfluidics. *Anal. Chem.* 2009, 81, 7091-7095.
35. Lu, Y.; Shi, W. W.; Qin, J. H.; Lin, B. C. Fabrication and Characterization of Paper-Based Microfluidics Prepared in Nitrocellulose Membrane By Wax Printing. *Anal. Chem.* 2010, 82, 329-335.
36. Zhang, J.; Yang, H.; Shen, G.; Cheng, P.; Zhang, J.; Guo, S. Reduction of Graphene Oxide via L-Ascorbic Acid. *Chem. Commun.* 2010, 46, 1112-1114.
37. Shin, H. J.; Kim, K. K.; Benayad, A.; Yoon, S. M.; Park, H. K.; Jung, I. S.; Jin, M. H.; Jeong, H. K.; Kim, J. M.; Choi, J. Y.; Lee, Y. H.; Et, a. Efficient Reduction of Graphite Oxide by Sodium Borohydride and Its Effect on Electrical Conductance. *Adv. Funct. Mater.* 2009, 19, 1987-1992.
38. Gao, W.; Alemany, L. B.; Ci, L. J.; Ajayan, P. M. New Insights Into the Structure and Reduction of Graphite Oxide. *Nat. Chem.* 2009, 1, 403-408.
39. Shin, K. H.; Jang, Y.; Kim, B. S.; Jang, J.; Kim, S. H. Highly Conductive Reduced Graphene Oxide Produced via Pressure-Assisted Reduction at Mild Temperature for Flexible and Transparent Electrodes. *Chem. Commun.* 2013, 49, 4887-4889.
40. Ping, J.; Wang, Y.; Fan, K.; Wu, J.; Ying, Y. Direct Electrochemical Reduction of Graphene Oxide on Ionic Liquid Doped Screen-Printed Electrode and its Electrochemical Biosensing Application. *Biosens. Bioelectron.* 2011, 28, 204-209.
41. Feng, H.; Cheng, R.; Zhao, X.; Duan, X.; Li, J. A Low-Temperature Method to Produce Highly Reduced Graphene Oxide. *Nat. Commun.* 2013, 4.

42. Kim, S.-K.; Liu, T.; Wang, X. Flexible, Highly Durable, and Thermally Stable SWCNT/Polyimide Transparent Electrodes. *ACS Appl. Mater. Interfaces* 2015, 7, 20865-20874.
43. Novoselov, K. S.; Fal'ko, V. I.; Colombo, L.; Gellert, P. R.; Schwab, M. G.; Kim, K. A Roadmap for Graphene. *Nature* 2012, 490, 192-200.
44. Gao, W.; Singh, N.; Song, L.; Liu, Z.; Reddy, A. L. M.; Ci, L. J.; Vajtai, R.; Zhang, Q.; Wei, B. Q.; Ajayan, P. M.; Et, a. Direct Laser Writing of Micro-Supercapacitors on Hydrated Graphite Oxide Films. *Nat. Nanotechnol.* 2011, 6, 496-500.
45. Niu, Z.; Chen, J.; Hng, H. H.; Ma, J.; Chen, X. A Leavening Strategy to Prepare Reduced Graphene Oxide Foams. *Advanced Materials* 2012, 24, 4144-4150.
46. Huang, L.; Huang, Y.; Liang, J.; Wan, X.; Chen, Y. Graphene-Based Conducting Inks for Direct Inkjet Printing of Flexible Conductive Patterns and Their Applications in Electric Circuits and Chemical Sensors. *Nano Res.* 2011, 4, 675-684.
47. Peng, C.; Gao, J.; Wang, S.; Zhang, X.; Zhang, X.; Sun, X. Stability of Hydrogen-Terminated Surfaces of Silicon Nanowires in Aqueous Solutions. *J. Phys. Chem. C* 2011, 115, 3866-3871.
48. Heo, K.; Cho, E.; Yang, J.-E.; Kim, M.-H.; Lee, M.; Lee, B. Y.; Kwon, S. G.; Lee, M.-S.; Jo, M.-H.; Choi, H.-J.; Hyeon, T.; Hong, S.; Et, a. Large-Scale Assembly of Silicon Nanowire Network-Based Devices Using Conventional Microfabrication Facilities. *Nano Lett.* 2008, 8, 4523-4527.
49. Wu, Z. C.; Chen, Z. H.; Du, X.; Logan, J. M.; Sippel, J.; Nikolou, M.; Kamaras, K.; Reynolds, J. R.; Tanner, D. B.; Hebard, A. F.; Rinzler, A. G.; Et, a. Transparent, Conductive Carbon Nanotube Films. *Science* 2004, 305, 1273-1276.
50. Nicolosi, V.; Chhowalla, M.; Kanatzidis, M. G.; Strano, M. S.; Coleman, J. N. Liquid Exfoliation of Layered Materials. *Science* 2013, 340, 1420.
51. Hyun, W. J.; Park, O. O.; Chin, B. D. Foldable Graphene Electronic Circuits Based on Paper Substrates. *Advanced materials* 2013, 25, 4729-4734.

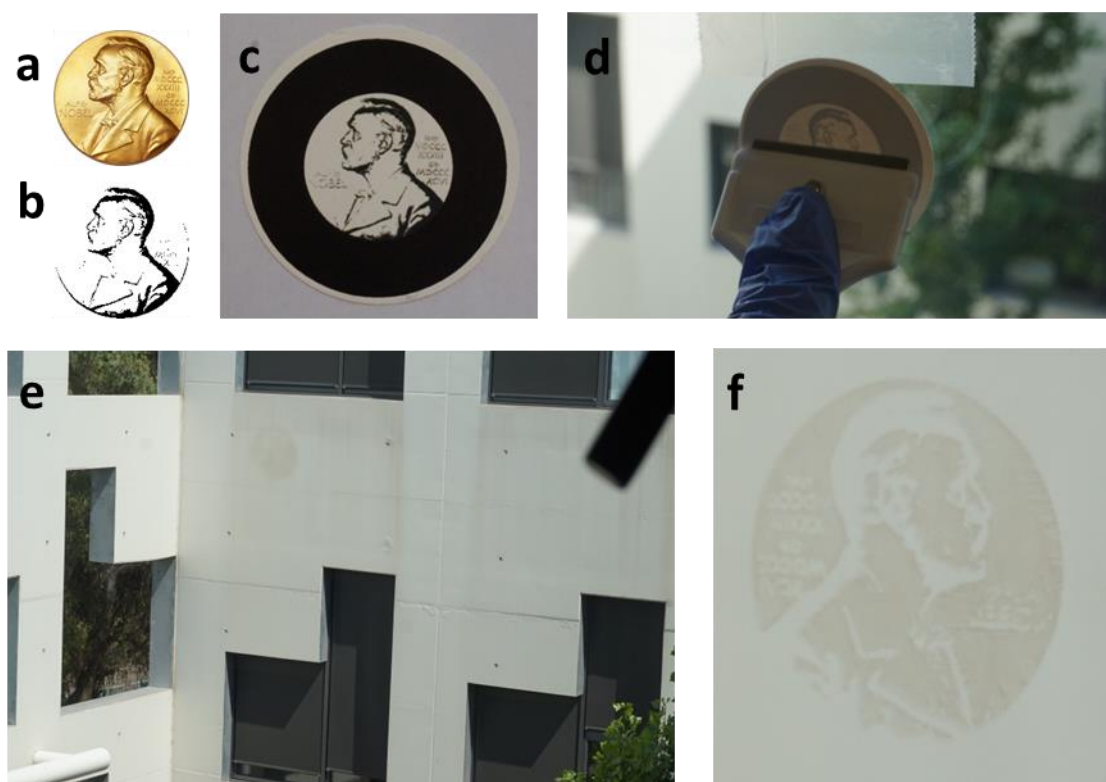
Supporting Information

Figure S1. GO transferred over glass using a spatula.

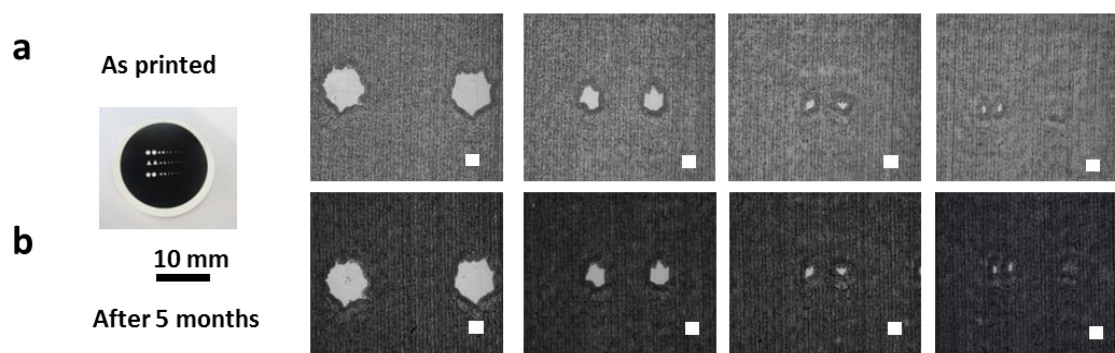


Figure S2. Optical microscopy characterisation of the WPM. a) immediately after printing and b) 5 months after printing.

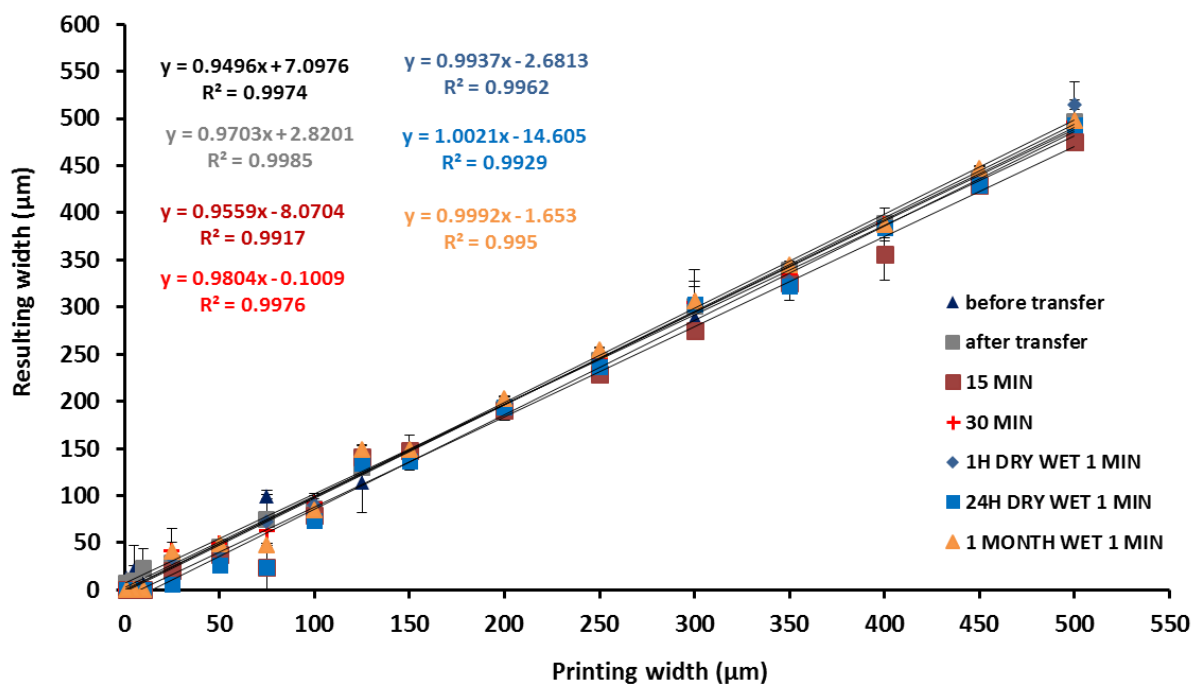


Figure S3. Evaluation of printing and resulting width of the WPM before and after transfer and GO transfer onto PET at different drying time.

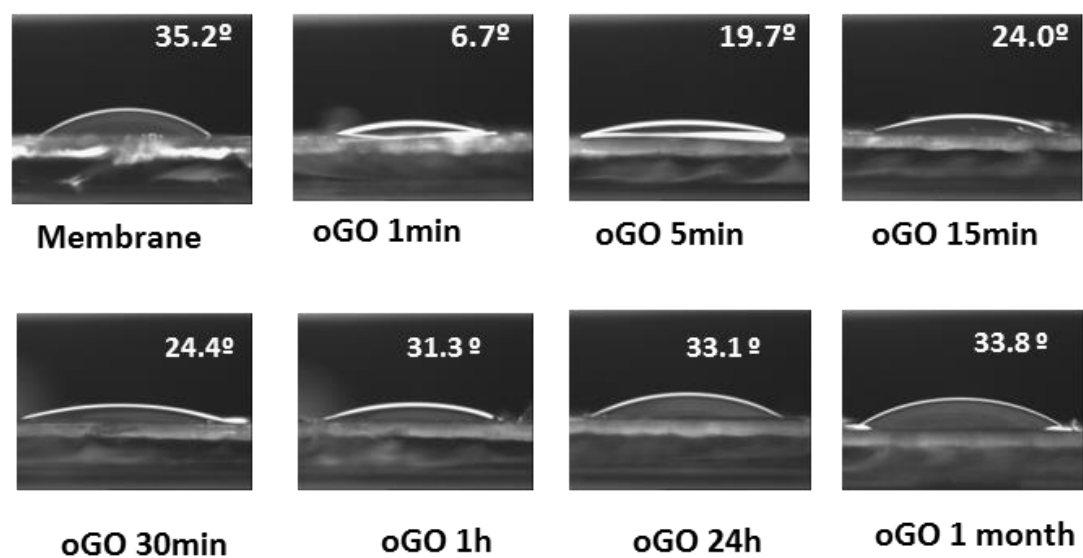


Figure S4. Hydrophobicity of GO film over time filtered on nitrocellulose membrane.

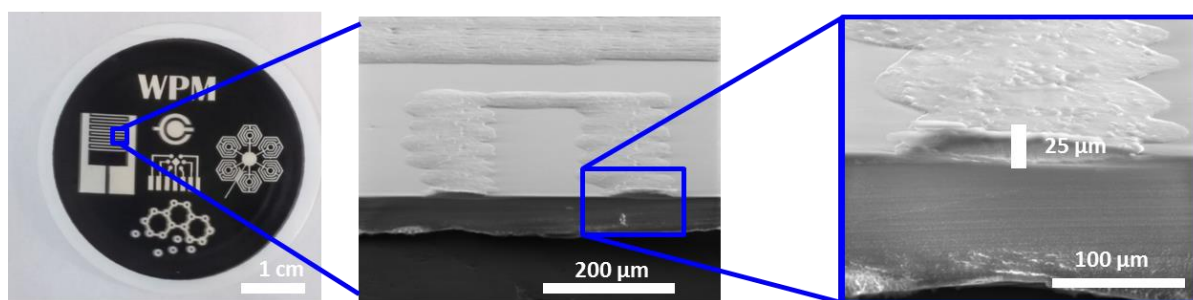


Figure S5. WPM with wax height.

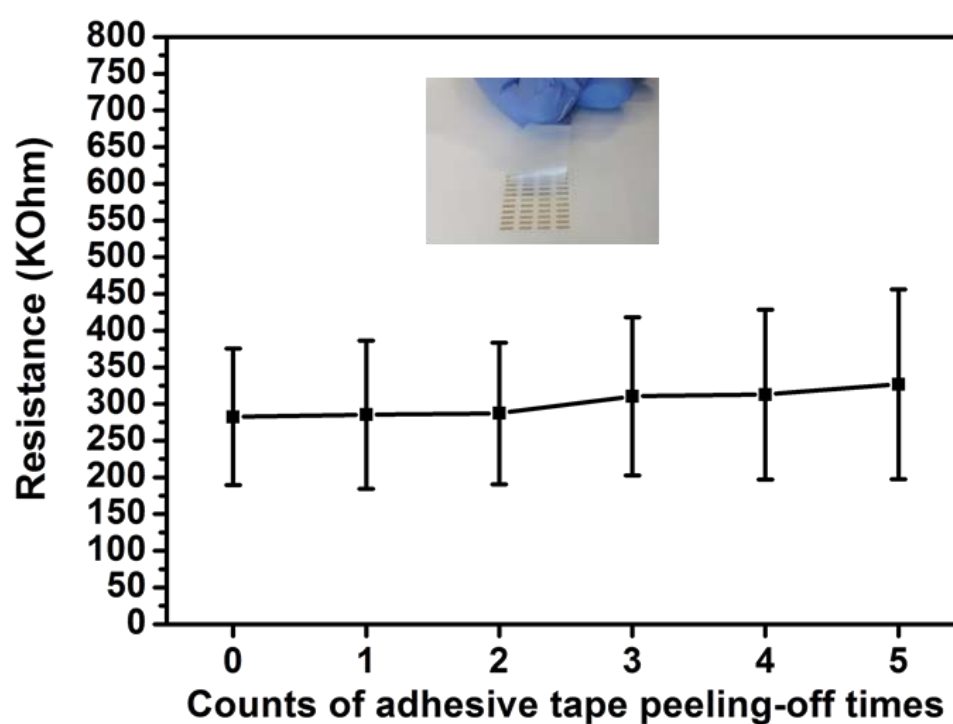


Figure S6. Adhesive peel-off wipe test. Inset: photo of conductive tracks after 5 peel-off counts.

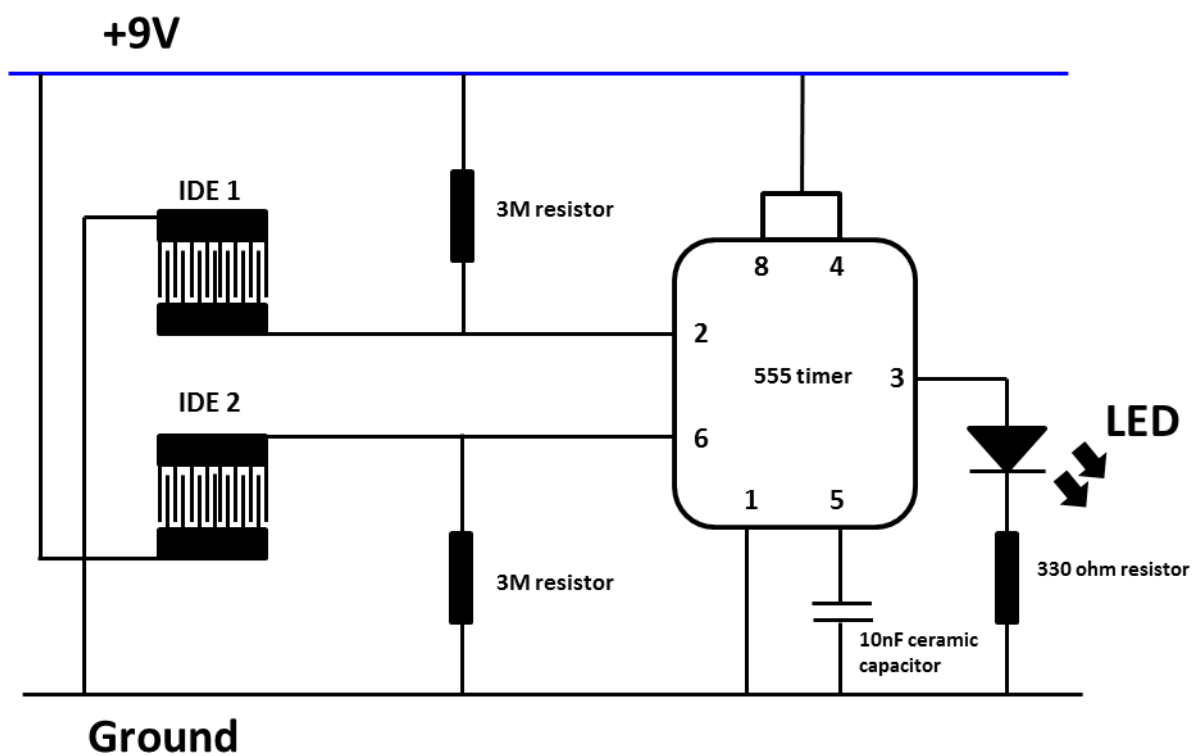


Figure S7. Electronic circuit used for the LED switcher.

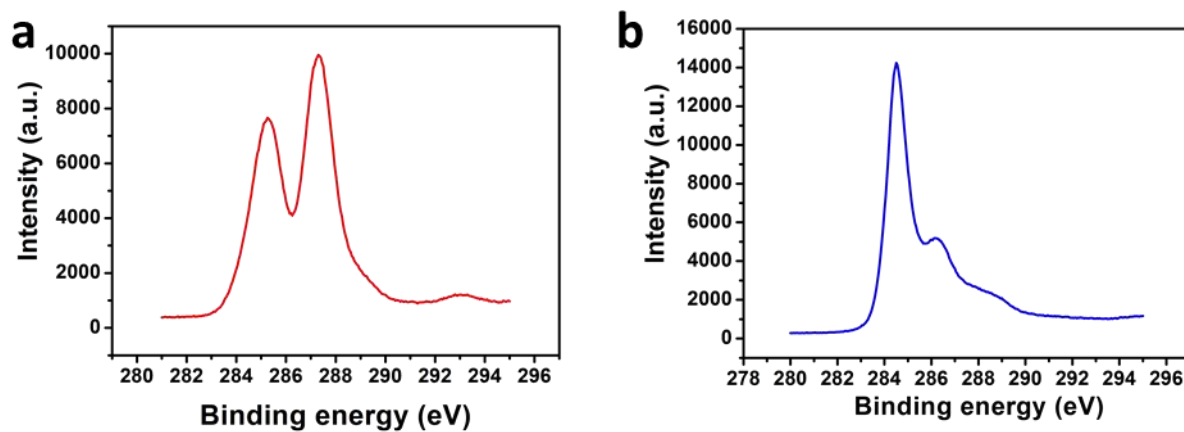


Figure S8. a) C1s spectra of GO and b) C1s spectra of rGO.

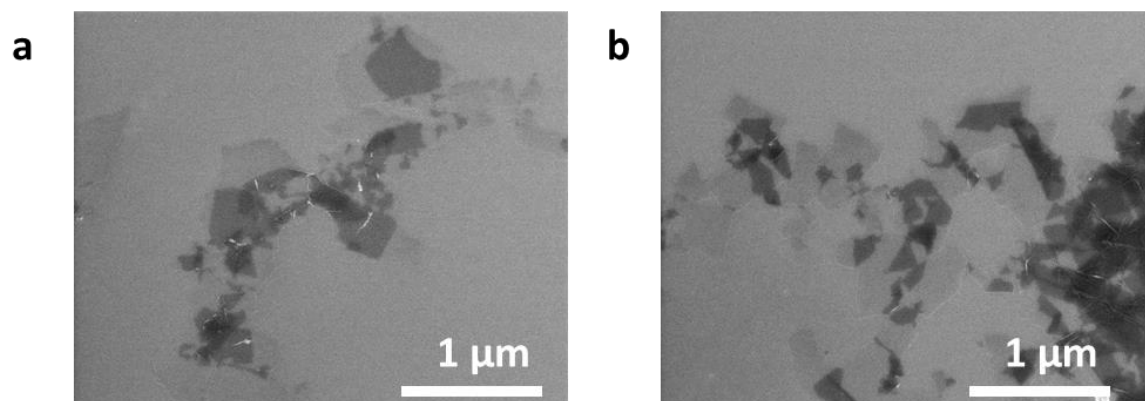


Figure S9. SEM characterization of a) GO and b) rGO.

The GO z-dimension (thickness) of the materials was *ca.* 1.0 to 1.2 nm. The maximum x-y dimensions were 554 nm. These data were provided by Angstrom Materials and are consistent with the SEM results (Figure S8).

Table S1. Resistance values evolution with adhesive peel-off wipe test.

	Initial	1st peel - off	2nd peel - off	3rd peel -off	4th peel -off	5th peel - off
Resistance/square (Kohms)	282.44 ±93.02	285.30 ±100.95	287.16 ±96.64	310.54 ±107.76	312.81 ±115.89	326.75 ±129.43

Chapter 6**General conclusions and future perspectives**

Since the specific conclusions are already written at the end of each chapter, in this paragraph just the general conclusions of the whole thesis are reported and some future perspectives are discussed.

6.1 General conclusions

In this PhD thesis, two biosensing systems were developed using screen printing technology. In the first approach, we took advantage of nanomaterials such as AuNPs or MBs for the in-situ amplification of DNA using isothermal technique as a substitute for PCR. The resulting immunosandwich was ready for electrochemical detection using SPCE and reveals a step-forward in biosensing systems for the detection of leishmania for low cost and portable in-field tests. In a second approach, we tuned the SPCE with GO and RGO and study their influence in the electrochemical and electrocatalytic behavior using a proof-of-concept enzyme such as Tyrosinase. The influence of these materials is clear in terms of performance either for redox indicator or for the detection of catechol. As a continuation of the GO study, was important the development of a technique to print GO for the development of sensors avoiding the effect of SPCE as an underlying layer/platform. In this way, we introduce the printing of patterned GO structures using WPM with thickness control, infinite shaping capability, no need for expertise and low cost. Using this technique we developed a simple touch sensor for turning on and off a LED.

6.2 Future perspectives

As future perspectives, the use of GO based sensors printed using the developed technique could be of major interest for biosensing platforms taking advantage of their thin film structure and transparency enabling simultaneous optical and electrochemical studies. The use of this either for immunosandwich like architectures or enzyme absorption could increase the sensing performance. The use of novel nanomaterials such as the ones described in the introduction for graphene, could make a step forward in the performance for electrochemical sensors and biosensors. The use of novel substrates that can be stretched and knotted with skin-like appearance could be tested using our printing methodology for the production of wearable sensors. In addition, the

introduction of novel capabilities such as wireless or NFC could make the presented biosensors useful for infield applications or in-time monitoring of personal medical activity getting sensors and biosensors in day-life.

Annex A

Compendium of publications

Magnetic Bead/Gold Nanoparticle Double-Labeled Primers for Electrochemical Detection of Isothermal Amplified *Leishmania* DNA

Alfredo de la Escosura-Muñiz, Luis Baptista-Pires, Lorena Serrano, Laura Altet, Olga Francino, Armand Sánchez, and Arben Merkoçi*

A novel methodology for the isothermal amplification of *Leishmania* DNA using labeled primers combined with the advantages of magnetic purification/preconcentration and the use of gold nanoparticle (AuNP) tags for the sensitive electrochemical detection of such amplified DNA is developed. Primers labeled with AuNPs and magnetic beads (MBs) are used for the first time for the isothermal amplification reaction, being the amplified product ready for the electrochemical detection. The electrocatalytic activity of the AuNP tags toward the hydrogen evolution reaction allows the rapid quantification of the DNA on screen-printed carbon electrodes. Amplified products from the blood of dogs with *Leishmania* (positive samples) are discriminated from those of healthy dogs (blank samples). Quantitative studies demonstrate that the optimized method allows us to detect less than one parasite per microliter of blood (8×10^{-3} parasites in the isothermal amplification reaction). This pioneering approach is much more sensitive than traditional methods based on real-time polymerase chain reaction (PCR), and is also more rapid, cheap, and user-friendly.

Dr. A. de la Escosura-Muñiz, L. Baptista-Pires,
Prof. A. Merkoçi
Catalan Institute of Nanoscience and
Nanotechnology (ICN2)
CSIC and Barcelona Institute of Science and Technology
Campus UAB
08193 Barcelona, Spain
E-mail: arben.merkoci@icn.cat

L. Serrano, Dr. L. Altet, Dr. O. Francino
Vetgenomics, Edifici Eureka
Parc de Recerca UAB
08193 Bellaterra (Barcelona), Spain
Dr. O. Francino, Prof. A. Sánchez
Department of Animal and Food Science
Autonomous University of Barcelona
Campus UAB
08193 Bellaterra (Barcelona), Spain
Prof. A. Sánchez
Centre for Research in Agricultural Genomics-CSIC-IRTA-UAB-UB
Campus UAB
08193 Cerdanyola del Valles, Catalonia, Spain
Prof. A. Merkoçi
ICREA—Institució Catalana de Recerca i Estudis Avançats
08010 Barcelona, Spain
DOI: 10.1002/sml.201502350



1. Introduction

Diseases transmitted by blood-feeding vectors (parasites) are a growing threat to world human health, particularly those affecting pets and transmitted by fleas, ticks, sandflies, or mosquitoes (vector-borne diseases, VBDs).^[1–3] One of the most important VBDs is visceral leishmaniasis which is endemic in 88 countries in 4 continents.^[4–6] Zoonotic visceral leishmaniasis, caused by the protozoan *Leishmania infantum* and transmitted by sandfly vectors, is a fatal disease for domestic dogs, wild canids, and humans.^[7] Different methods for the detection and diagnosis of canine leishmaniasis (CanL) including parasitological,^[8–10] serological,^[11,12] and molecular techniques^[13–19] have been reported, suffering from limitations related to the need of skilled workers, the high cost, and the fact that samples must be sent to a reference laboratory. Lateral-flow assay strips for specific CanL antigen are commercially available for detection of visceral leishmaniasis.^[20–23] However, the presence of low antibody levels is not necessarily indicative of disease and further work-up is necessary to confirm it by DNA-based diagnostic methods, polymerase chain reaction (PCR) being the gold standard. In this context, a dipstick format was developed for the detection of

PCR amplified CanL DNA.^[24] A qualitative real-time PCR (Leish PCR assay)^[25] is also commercially available for diagnosing cutaneous leishmaniasis. However, both systems did not overcome the limitations of PCR for which sophisticated and expensive equipment is needed to perform the precise and repeated heating cycles required. Therefore, there is still a need for further point-of-care (POC) diagnostic methods for the detection of infections by pathogens, particularly, for leishmaniasis.

Isothermal amplification is an alternative approach to traditional PCR, which overcomes many of the complications related to the thermocycling since it is performed at a constant temperature thanks to the use of enzymes. There are many different isothermal amplification methods depending on the enzymes and the temperature used. The variation called recombinase polymerase amplification (RPA) commercialized by Twist (TwistDx)^[26] employs recombinase enzymes which are capable of pairing oligonucleotide primers with homologous sequence in duplex DNA typically within 5–10 min. However, in most cases, DNA purification and detection after amplification still requires hazardous, time-consuming and expensive equipment, giving only qualitative information, so alternative methodologies overcoming such problems are required. In this context, the integration of nanoparticle (NP) tags during the amplification process combined with the very sensitive electrocatalytic^[27,28] detection of such a tag would overcome most of these limitations. The outstanding properties of different nanomaterials have been extensively approached in DNA biosensing systems. NPs have been used in a high extent as both optical and electrochemical tags in DNA hybridization biosensors^[29–37] while magnetic beads (MBs) have been extensively used as platforms for such and other bioassays.^[38,39] Gold nanoparticles (AuNPs)^[40,41] and, to a lesser extent, silver nanoparticles^[42] and quantum dots^[43] have been also introduced in the cocktail of reagents of the PCR, taking advantage of their properties as catalyzers of the DNA amplification reaction, constituting the so-called nanoPCR^[44] in some cases after MB-based DNA extraction.^[45] Only a report on AuNP-labeled primers for optical detection of PCR amplified DNA is found in the bibliography^[46] while a few examples of PCR amplification using MB-labeled primers^[47–49] have been published, but the integration of both MBs and AuNP-labeled primers has not ever been reported, probably due to the high temperature reached during the PCR cycle which is a serious limitation for preserving the labeled primer integrity. Regarding the isothermal DNA amplification, AuNPs have been used as reporters in optical approaches based on AuNPs' addition after DNA amplification followed by colorimetric^[50–55] or surface plasmon resonance-based^[56,57] detection, in some cases taking also advantage of MBs after the amplification reaction for preconcentration/purification purposes.^[58] In a similar way, AuNPs have been used as electrochemical reporters in DNA hybridization biosensors for the detection of isothermal amplified DNA^[59] taking also advantage of the use of MB platforms.^[60,61] All these approaches are based on the addition of the micro/nanoparticles after the DNA amplification and, in most cases, require the performance of further DNA hybridization assays, which increase

the analysis time and also involve more irreproducibility, loss of sensitivity, and false positives due to unspecific absorptions.

In this work, we present a novel design of *Leishmania* DNA isothermal amplification using for the first time primers labeled with both AuNPs and MBs. The low and constant temperature of the isothermal amplification procedure is ideal for preserving the integrity of the nanoparticle–primer conjugates during the amplification step. The double-labeled product resulting from such amplification is ready for a rapid magnetic separation/preconcentration and direct electrocatalytic detection in a very sensitive and quantitative way. A general scheme of the whole experimental procedure from the DNA extraction to the final electrochemical detection is shown in **Figure 1**.

2. Results and Discussion

2.1. Design and Screening of Primer Sets for *Leishmania* Assay and Endogenous Control

Three candidate primers for kinetoplast and eight candidate primers for intergenic spacer region (ITS1) of *Leishmania* were designed following recommended conditions (Appendix to the TwistAmp reaction kit manuals^[26]). All possible combinations of primers were tested using standard conditions of TwistAmp (37 °C of reaction temperature; magnesium acetate concentrations of 14×10^{-3} M; shaking 4' after initiation of the reaction; 480×10^{-9} M of each primer). Parameters that can be modified by the user (temperature, magnesium concentration, stirring regime, and primer concentrations) were adjusted to obtain the best performance. This first step generates four sets of primers used in simplified standard conditions (37 °C of reaction temperature; at 14×10^{-3} M of magnesium concentration, 480×10^{-9} M of primer concentration, without agitation 4' after starting the reaction and with a reaction time of 20'). To improve the performance of the *Leishmania* assay a “second generation” of primers was designed by creating variants of the best primer set identified in the first step (moving one base pair around the initial primer) and re-screening the new candidates to improve amplification performance. Finally, with definitive ones, the primer concentration was adjusted to 300×10^{-9} M and the reaction time was decreased up to 10' (**Figure 2a,b**).

An endogenous control was incorporated to avoid the generation of artifacts that were detected in no-template controls and samples of very low target copy number. To optimize the endogenous control RPA amplification, six candidate primers for 18S ribosomal RNA gene were screened (**Figure 2c**).

The assay based on isothermal co-amplification of *Leishmania* parasite and 18S as an endogenous control exhibits similar results than the real time used as a gold standard,^[62] with a limit of detection of <1 parasite in the reaction. It is possible since both assays target a conserved region of the *Leishmania* kinetoplast minicircle DNA that is present in about 10 000 copies for parasite.^[63–65] Multiplex isothermal has been optimized with an endogenous control primer concentration limited to 150×10^{-9} M to avoid a loss of sensitivity when low targets of *Leishmania* were present.

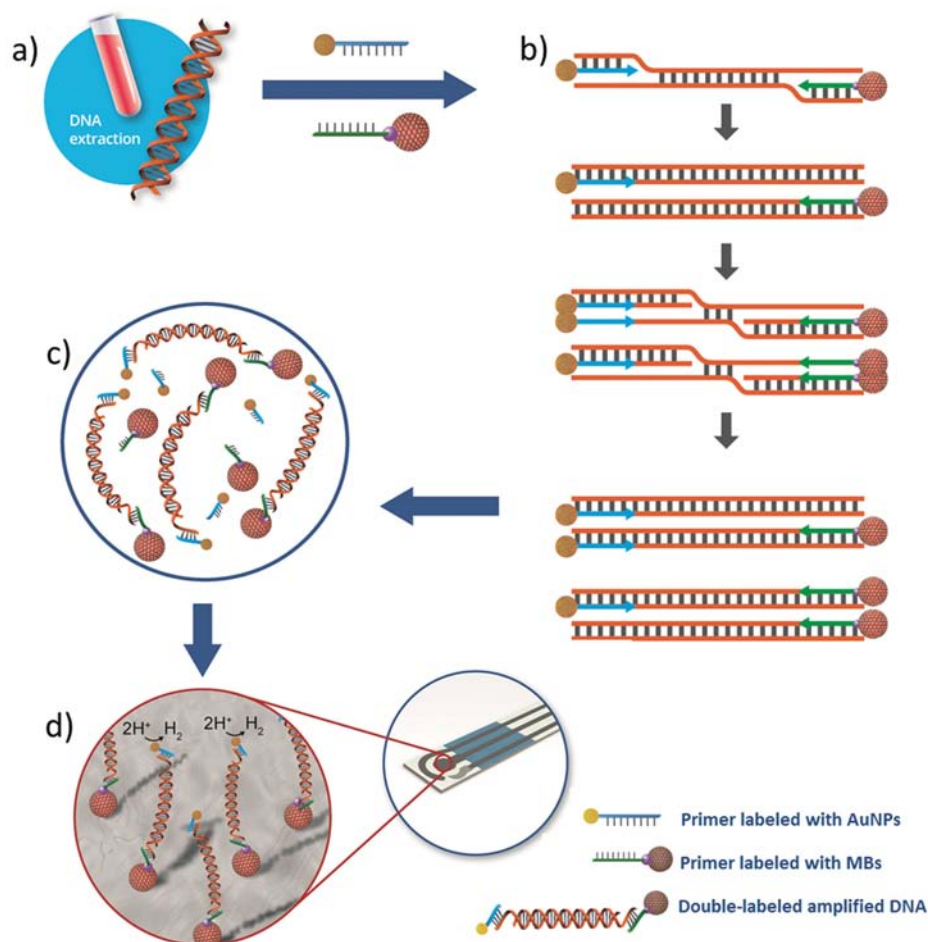


Figure 1. Scheme of the experimental procedure for the detection of isothermal amplified DNA using primers labeled with AuNPs and MBs. a) DNA is extracted from dog blood and b) a kinetoplast specific region is isothermally amplified by an RPA cycle using primers labeled with AuNPs and MBs. c) The double-labeled amplified product (MB/amplified DNA/AuNP complex) is captured by the magnet placed on the reverse side of the working electrode of the SPCE and d) AuNPs tags are detected through the electrocatalytic hydrogen evolution reaction (HER).

2.2. Characterization of AuNP/Amplified DNA

The performance of the isothermal amplification procedure using primers labeled with AuNPs was evaluated by both zeta potential and electrochemical measurements. Zeta potential is well known as an efficient tool for the monitoring and analysis of modifications on the surface of NPs, with minimal sample preparation.^[66] It has been used to obtain information concerning the particle surface charge, chemical modifications, and also stability of colloid suspensions. A high zeta potential (positive or negative; typically higher than 10 mV) confers stability since the dispersion resists aggregation. Since ssDNA is negatively charged, the conjugation of AuNPs with ssDNA should give rise to negative charged conjugates which would shift the zeta potential to more negative values. All these characteristics make zeta potential an ideal technique for the characterization of both the primers and the final amplified DNA labeled with AuNPs.

As can be observed in **Figure 3a**, a gradual shift to more negative values was observed in the zeta potential of AuNPs

when higher was the coverage degree by ssDNA. This suggests that AuNPs were being loaded with negative charged molecules such as ssDNA. First, a shift from the value of the nonmodified AuNPs (a) was observed for the AuNP/primer (b) indicating that the primer was correctly connected with the AuNP. After the amplification, a shift of up to 25 mV was observed (d), suggesting the covering of the AuNPs with the amplified dsDNA (that has more negative charges). No significant shift was observed for a control amplification assay performed with a blank sample (c), also corroborating the specificity of the system.

This evidence was also corroborated by electrochemical measurements. Three different “positive” and “blank” samples were analyzed for this purpose. The AuNP/amplified DNA product was purified by incubation with streptavidin-modified MBs which capture the amplified products through the biotin present in the primer and finally detected taking advantage of the electrocatalytic activity of AuNPs toward the hydrogen evolution reaction (HER). Briefly, this well-known methodology is based

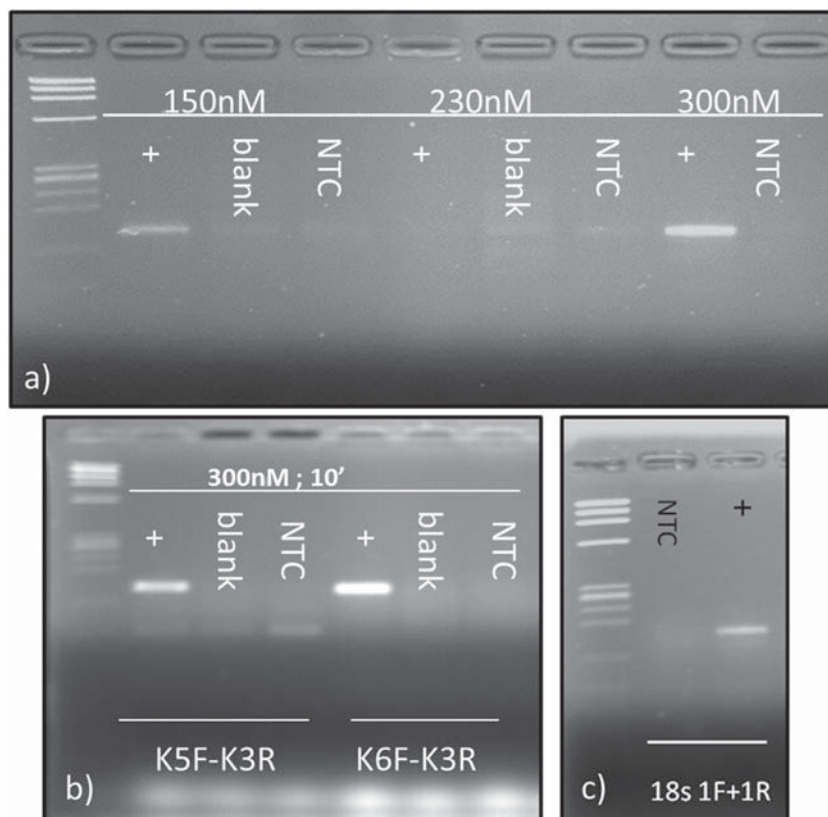


Figure 2. Isothermal assay optimization evaluation by gel electrophoresis. a) Optimization of primer concentration of *Leishmania* assay. b) Example of the “second-generation” screening of *Leishmania* primers: K6F-K3R are selected due to favorable performance. c) Definitive endogenous control assay used. +, positive sample (DNA of a dog with *Leishmania* infection); blank, DNA of a dog without *Leishmania* infection; NTC, negative template control. Line 1 of each gel: Phi-X 174/HaeIII Marker (1353/1078/872/603/310/(281,271)/234/194/118/72). Bands size: 140 bp for *Leishmania* and 168 for 18S.

on the fact that the presence of AuNP connected to MBs on the screen-printed carbon electrode (SPCE) surface shifts the potential for hydrogen ion reduction toward less negative potentials. Fixing a reductive potential of -1.00 V, the intensity of the current recorded in chronoamperometric mode during the stage of hydrogen ion electroreduction at 60 s (chosen as analytical signal) is related to the quantity of AuNPs on the SPCE and consequently to the amount of tagged analyte.^[27,28]

As observed in Figure 3b, “positive” and “blank” samples can be perfectly discriminated in the three samples, suggesting the specific presence of AuNPs in the amplified products and consequently the good performance of the isothermal amplification in the presence of such tags. The signals of the “blank” samples are at the normal levels of background of the HER in absence of catalyzer (around $5\text{--}7$ μA), so the specificity of the amplification is demonstrated.

Furthermore, it was observed that the life-time of AuNP/primer conjugates was of up to 8 weeks when stored at 4 $^{\circ}\text{C}$ and protected from light, as shown in Figure 3c where different amplifications for “positive” samples were performed at different times after the preparation of the AuNP/primer conjugate. The dramatic decrease in the analytical signal observed after 8 weeks suggests the damaging of the AuNP/primer,

probably due to either breaking of the binding or AuNPs’ agglomeration. Further studies will be focused on alternative AuNP/primer storage conditions, such as freezing or lyophilization.

2.3. Evaluation of Double-Labeled MB-AuNP/Amplified DNA

Once demonstrated the good performance of the isothermal amplification using AuNP-labeled primers, the experimental procedure was significantly simplified by also introducing the MB-labeled primer in the amplification reagent mixture as illustrated in Figure 1. In this case, the procedure for the measurement after the amplification is enormously simplified since the MB/amplified DNA/AuNP complex is directly placed onto the SPCE surface and captured by the magnet placed on the reverse side of the working electrode immediately before the electrochemical measurement.

MBs of two different sizes (2.8 and 1 μm) and two different kinds of primers were evaluated: the K3R detailed in the Experimental Section and also a longer one that includes a spacer of $(\text{AT})_7$ in the 5’ tail. This tail of oligonucleotides helps keep the magnetic bead far from the amplification zone.

The results shown in Figure 4a seem to indicate that the amplification does not

work properly using the bigger MBs in combination with the short primer since the recorded currents are in the levels of the background. The results improved a little bit when the use of longer primers (containing a spacer oligonucleotides sequence) was introduced. When the smaller MBs and the short primer were tested, the amplification worked in a higher extent, and this was highly improved when it was used in combination with the primers containing a spacer. This suggests that the bigger MBs are hindering the amplification, probably due to the beads’ deposition during the amplification procedure. Furthermore, the procedure takes advantage in this case of the fact that the amplification sequence of the primer is not in direct contact with the bead, which probably facilitates the DNA amplification.

The good performance of the amplification procedure as well as the integrity of the double-labeled amplified products was evaluated by scanning electron microscopy (SEM) analysis. As shown in Figure 4b, AuNPs (observed as small white spots) are connected to the MBs (big microspheres in the image) after the amplification procedure, evidencing the formation of the MB/amplified DNA/AuNP complex (a control image after amplification of DNA without *Leishmania* parasite is shown in the Supporting Information).

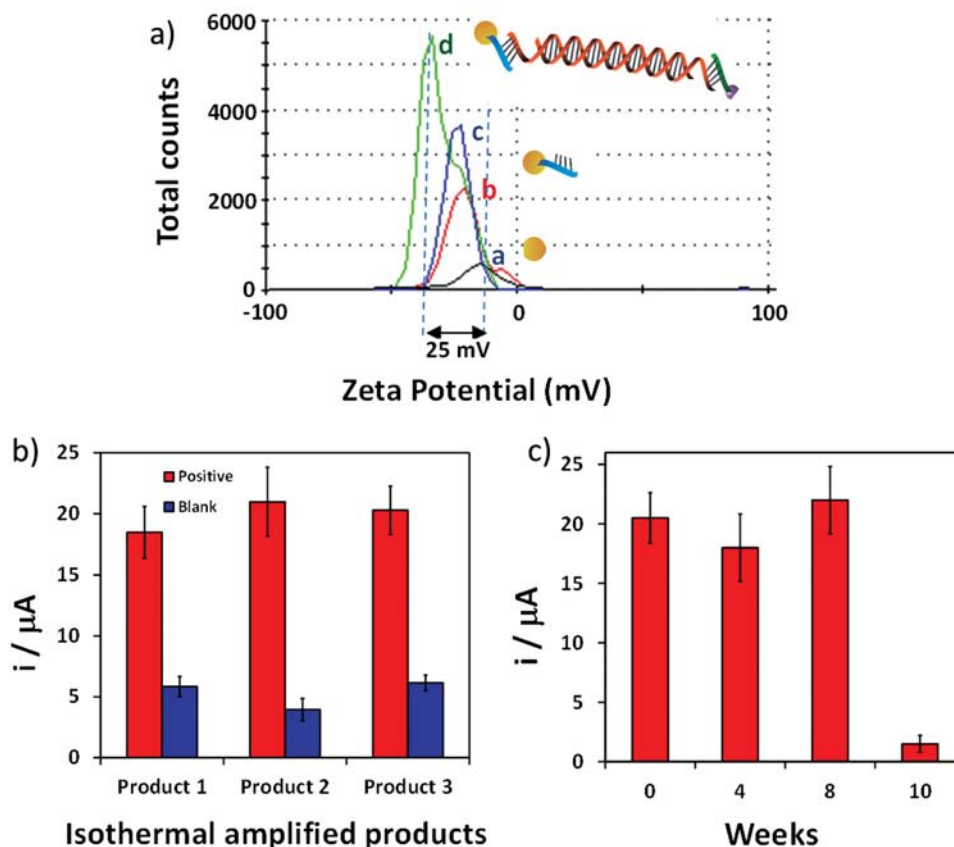


Figure 3. Characterization of AuNP/amplified DNA. a) Diagram for the zeta potential as a distribution versus total counts for a dispersion of AuNPs before (curve a) and after (curve b) the conjugation with the primer and for amplified DNA using the AuNP-labeled primer for a positive (curve d) and a blank (curve c) sample. b) Comparison of the analytical signals obtained for different “positive” and “blank” samples after DNA amplification using AuNP-labeled primers. c) Analytical signals obtained for different isothermal amplifications performed several weeks after the preparation of the conjugate of AuNP/primer.

2.4. Quantitative Assays: Evaluation of Products with Different Parasite Concentrations

The optimized methodology was applied for the evaluation of amplified DNA prepared from samples containing different quantities of spiked parasite. Chronoamperograms recorded for the assayed samples are shown in the inset of Figure 5a, where the values of the analytical signals (absolute value of current at 60 s) after subtracting the background (current in 1 M HCl, in the absence of catalyzer) are represented for a better understanding.

As shown in Figure 5b, a linear relationship between the analytical signal (after subtracting the background current) and the logarithm of parasite concentration in the range 500–0.5 parasites per mL of blood (samples prepared as detailed in the Experimental Section) was obtained. A limit of detection of 0.8 parasites per mL of blood (8×10^{-3} parasites per DNA amplification reaction) was estimated, as the parasite number giving a signal equal to the blank signal plus three times its standard deviation. The reproducibility of responses for 5 parasites per mL of blood was also studied, obtaining a relative standard deviation of 7%.

Our AuNP/MB based electrochemical approach results are better than those obtained by other POC tests using nucleic acid sequence based amplification and coupled to

oligochromatography for *Leishmania* detection,^[67] and even considerably better than the one parasite per PCR detection limit offered by the OligoC-test.^[24]

3. Conclusions

In summary, a novel design of isothermal amplification using for the first time primers labeled with both AuNPs and MBs for obtaining double-labeled amplified products has been successfully developed for a DNA sequence characteristic of *L. infantum* kinetoplast tested in dogs, chosen as the model. The double label allows the rapid magnetic purification/preconcentration of the product followed by direct AuNP electrocatalytic detection, avoiding DNA hybridization procedures. The electrochemical method exhibits a good reproducibility and sensitivity, allowing to detect 0.8 parasites per mL of blood (8×10^{-3} parasites per DNA amplification reaction). Furthermore, amplified DNA from dogs without *Leishmania* can be perfectly discriminated, demonstrating the specificity of both the amplification procedure and the electrochemical detection. In addition to the advantages of simplicity and one-step detection of the amplified product, the performance of the proposed approach is better than that obtained with other point-of-care tests for *Leishmania*

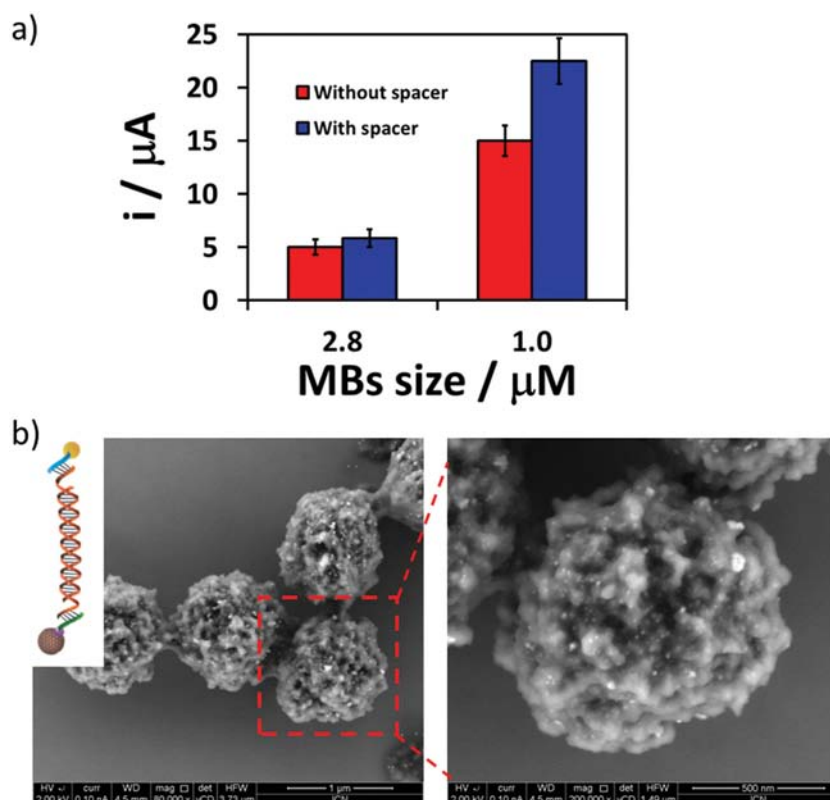


Figure 4. Evaluation of double-labeled MB–AuNP isothermal amplified DNA. a) Analytical signals obtained for MBs of two different sizes (2.8 and 1 μm) and reverse primers with and without spacer. b) SEM characterization of the MBs after the DNA isothermal amplification. In both cases, forward primers are labeled with AuNPs. Experimental conditions as detailed in the text.

detection, offering also a quantitative tool for parasite determination. Furthermore, our technique provides a valuable proof-of-concept since the double MB/AuNP-label approach is a universal methodology that could be applied for any RPA isothermal DNA amplification design.

4. Experimental Section

DNA Samples: The present study included samples of dogs received in Vetgenomics (www.vetgenomics.com) to perform *Leishmania* detection by real-time PCR. DNA was isolated from 400 μL of ethylenediaminetetraacetic acid (EDTA)–blood samples using the Genelute blood Genomic DNA Kit (Sigma, Spain) following the manufacturer instructions. DNA was re-suspended in 200 μL of elution buffer. A *Leishmania* positive DNA was used to perform different isothermal amplifications and a negative DNA (without *Leishmania*) was used as blank.

To perform the calibration curve, a negative blood (400 μL) was spiked with 2 μL of *Leishmania* culture at different concentrations, ranging from 10^5 to 10^2 promastigotes mL^{-1} . Samples assayed consequently range from 500 to 0.5 parasites per mL of blood (from 5 to 5×10^{-3} parasites per isothermal amplification reaction in a tenfold dilution).

Chemicals and Equipment: Primers labeled with biotin and thiol were purchased from Sigma (Spain). TwistAmp Basic Kit containing all enzymes and reagents necessary for the amplification

of DNA was supplied by TwistDx Ltd (UK). The 16 nm sized AuNPs were prepared following the Turkevich's method (see the detailed preparation procedure, transmission electron microscopy (TEM) characterization, and electrocatalytic quantification of AuNPs in the Supporting Information). High monodisperse 1 and 2.8 μm sized streptavidin-coated MBs were purchased from Dynal Biotech (MyOne and M-280, respectively, Invitrogen, Spain) (see SEM characterization of both beads in the Supporting Information). Hydrogen tetrachloroaurate(III) trihydrate ($\text{HAuCl}_4 \cdot 3\text{H}_2\text{O}$, 99.9%) and trisodium citrate ($\text{Na}_3\text{C}_6\text{H}_5\text{O}_7$), used in the synthesis of AuNPs and tris (2-carboxyethyl) phosphine (TCEP) used for thiolated primer pretreatment were purchased from Sigma-Aldrich (Spain). Washing solutions of the MB-labeled conjugates consisted of i) phosphate buffer solution (PBS buffer): 0.01 M phosphate-buffered saline, 0.137 M NaCl, and 0.03 M KCl (pH 7.4); ii) binding and washing buffer: PBS buffer solution with added 0.05% (w/v) Tween 20; iii) blocking buffer solution: 5% (v/v) bovine serum albumin in PBS buffer. A TS-100 ThermoShaker (Biosan, Latvia) was used for the incubations with agitation at a controlled temperature. A Dynal MPC-S Magnetic Particle Concentrator (Invitrogen, Spain) was used for the magnetic separations.

The electrochemical transducers used were homemade SPCEs, consisting of three electrodes: carbon working electrode (W), Ag/AgCl reference electrode (R), and carbon counter electrode (C) in a single strip fabricated with a semiautomatic screen-printing machine DEK248 (DEK International, Switzerland). The materials and reagents used for this process were Autostat HT5 polyester sheet (McDermid Autotype, UK), Electrodeag 423SS carbon ink, Electrodeag 6037SS silver/silver chloride ink and Minico 7000 Blue insulating ink (Acheson Industries, The Netherlands). The experimental procedure for SPCEs fabrication is detailed at the Supporting Information. A neodymium magnet (3 mm in diameter), inserted under the WE, was also used to accumulate the MB-labeled amplified product during the electrochemical measurements. The electrochemical measurements were performed in analytical grade 1 M HCl solution (Merck, Spain) at room temperature using a $\mu\text{Autolab II}$ (Echo Chemie, The Netherlands) potentiostat/galvanostat connected to a PC and controlled by Autolab GPES 4.9007 software (General Purpose Electrochemical System). Unless otherwise stated, all reagents and other inorganic chemicals were supplied by Sigma-Aldrich or Fluka (Spain).

All chemicals were used as received and all aqueous solutions were prepared in milli-Q water (Millipore purification system, 18.2 Mohm cm).

Conjugation of AuNPs and MBs to DNA Primers: First of all, a reduction step to remove the protecting disulfide group from the thiolated primer was performed before using, following the protocol recommended by the manufacturer. Briefly, 200 μL of

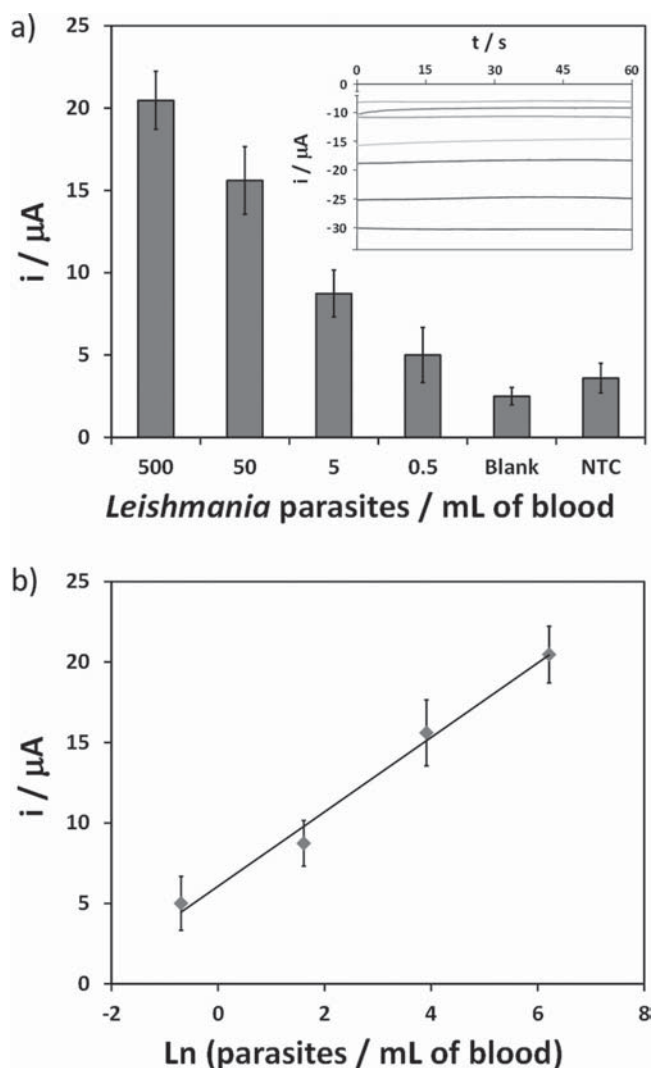


Figure 5. Quantitative *Leishmania infantum* parasite determination. a) Analytical signals obtained for double-labeled MB-AuNP isothermal amplified DNA products prepared from different quantities of parasite, after subtracting the background current. Inset graphic corresponds to the chronoamperograms recorded at -1 V. Lower current curve (green curve) corresponds to a 1 M HCl solution (background signal). b) Logarithmic relationship between the number of *Leishmania* parasites and the value of the analytical signal, after subtracting the background. Experimental conditions as detailed in the text.

10×10^{-3} M TCEP was added to the lyophilized primer and the solution was shaken 60 min at room temperature. Then it was precipitated by adding 150 μ L of 3 M NaAc and 750 μ L of EtOH and incubating 20 min at -20 °C. After that, it was spun for 5 min at 13 000 rpm and the supernatant was discarded. The pellet was dried at room temperature.

The conjugation of self-synthesized 16 nm sized AuNPs to the primer modified with thiol group was performed adapting the procedure pioneered by Mirkin et al.^[68] About 190 μ L of AuNP suspension was mixed with 10 μ L of 1500 μ g mL $^{-1}$ thiolated primer solution and incubated for 20 h at 25 °C with agitation (250 rpm) (final concentration of primer: 75 μ g mL $^{-1}$). After that, this solution was added to 50 μ L of 10×10^{-3} M phosphate buffer (pH 7)/0.1 M NaCl and allowed to stand for 44 h. Finally, a centrifugation of 14 000 rpm for 20 min at 4 °C was carried out, and

AuNPs/ primer conjugate was reconstituted in 200 μ L of milli-Q water, being stable for up to eight weeks.

Streptavidin-modified MBs (1 and 2.8 μ m sized) were connected with the primers through the streptavidin–biotin interaction by mixing 50 μ L of 1 mg mL $^{-1}$ MB suspension with 15 μ L of 100×10^{-6} M biotinylated primer during 30 min at 25 °C. The MBs/ primer conjugate was washed and re-suspended in 15 μ L of water.

Primer Sets for *Leishmania* Amplification and Endogenous Control: Primers set selected after optimization were (5'–3'):

- K6F: [ThiC6]CTTTTCTGGTCTCCGGGTAGGGGCGTCTG
- K3R: [Bttn]CCACCCGGCCCTATTTTACACCAACCCCAAGTTTCCC

that amplified a fragment of ≈ 140 base pair length of the kinetoplast.

For the endogenous control, optimum primers were (5'–3'):

- Primer 18s 1F: CTGCGAATGGCTCATTAAATCAGTTATGGTTCC
- Primer 18s 1R: CTGACCGGGTGGTTTTGATCTGATAATGCACGC

that amplified a fragment of 168 base pair length of the 18S ribosomal RNA gene.

Analysis of RPA amplification was performed on 2% agarose gel stained with ethidium bromide after purification of the reactions with the DNA Clean and Concentrator Kit (Zymo research).

Isothermal Amplification Assay Conditions: Multiplex amplification with primers K6-F and K3R for *Leishmania* and 18S-F1 and 18S-R1 for endogenous control was performed using 14×10^{-3} M of magnesium, 300×10^{-9} M of *Leishmania* primers, 150×10^{-9} M of 18s primers, 5 μ L of DNA, and 37 °C of reaction temperature during 10 min without agitation.

The same experimental procedure was followed for K6F/AuNP and K3R/MB labeled primers (prepared as stated before) so as to obtain the double-labeled amplified product. A preliminary evaluation of the amplification using K6F/AuNPs and free K3R (only modified with biotin) was also performed. In this case, the AuNP/amplified DNA was purified by incubation with MBs under the same conditions as described for the conjugation of MBs with biotin-labeled primers.

A sample without DNA was used in each isothermal amplification as a negative template control (NTC).

Zeta Potential Measurements: About 1 μ L suspension of AuNPs, K6F/AuNPs, and of AuNPs/amplified DNA was diluted in 1 mL of PBS buffer, vortexed, and transferred into a 4 mL polystyrene cuvette (FB55143, Fisher Scientific). The data were collected and analyzed with the Dispersion Technology software 4.20 (Malvern) producing diagrams for the zeta potential as a distribution versus total counts.

Electrochemical Detection of MB/AuNP-Labeled Amplified DNA: About 25 μ L of the MB/amplified DNA/AuNP complex suspension was placed on the working area of the SPCE, where it was previously attached to a magnet on the reverse side. After 30 s, 25 μ L of 2 M HCl solution was added and a potential of +1.35 V was applied during 1 min (electrochemical pretreatment). After that, a potential of -1.00 V was applied during 60 s in chronoamperometric mode. Under these conditions, the H $^{+}$ ions were reduced to H $_2$ thanks to the catalytic effect of the AuNP labels.^[27,28] The absolute value of the current registered at 60 s was considered as the analytical signal, this value being proportional to the quantity of AuNPs and, consequently, to the concentration of isothermal amplified product. For the quantitative study shown in Figure 5, the values of

the analytical signals (current at 60 s) after subtracting the background (current in 1 M HCl) were plotted for a better understanding.

Supporting Information

Supporting Information is available from the Wiley Online Library or from the author.

Acknowledgements

The authors acknowledge EU support under FP7-SME-2012–1 contract number 315653 “POC4PETS.” ICN2 also acknowledges the support of the Spanish MINECO under Project MAT2011–25870 and through the Severo Ochoa Centers of Excellence Program under Grant SEV-2013-0295, and the support from Secretaria d'Universitats i Recerca del Departament d'Economia i Coneixement de la Generalitat de Catalunya (Grant 2014 SGR 260). A patent has been filed (EP14382266.6/P10398EP00 (09/07/14); PCT/EP2015/065742 (09/07/15)) including the results reported in this article.

- [1] World Health Organization, Vector-borne diseases, <http://www.who.int/mediacentre/factsheets/fs387/en/> (accessed: July, 2015).
- [2] G. Rascalou, D. Pontier, F. Menu, S. Gourbière, *PLoS One*. **2012**, *7*, e36858.
- [3] F. Beugnet, J. L. Marie, *Vet. Parasitol.* **2009**, *163*, 298.
- [4] C. Maia, L. Campino, *Vet. Parasitol.* **2008**, *158*, 274.
- [5] F. Dantas-Torres, L. Solano-Gallego, G. Baneth, V. M. Ribeiro, M. de Paiva-Cavalcanti, D. Otranto, *Trends Parasitol.* **2012**, *28*, 531.
- [6] Control of the leishmaniasis, WHO Technical Report Series 949, World Health Organization, Geneva, **2010**, pp. 1–186.
- [7] F. Chappuis, S. Sundar, A. Hailu, H. Ghalib, S. Rijal, R. W. Peeling, J. Alvar, M. Boelaert, *Nat. Rev. Microbiol.* **2007**, *5*, 873.
- [8] L. Solano-Gallego, H. Fernández-Bellón, P. Morell, D. Fondevila, J. Alberola, A. Ramis, L. Ferrer, *J. Comp. Pathol.* **2004**, *130*, 7.
- [9] M. De Fátima Madeira, A. de O Schubach, T. M. P. Schubach, S. Pereira, F. Figueiredo, C. Baptista, C. Leal, C. X. Melo, E. M. Confort, M. C. Marzochi, *Vet. Parasitol.* **2006**, *138*, 366.
- [10] S. C. Xavier, H. M. de Andrade, S. J. H. Monte, I. M. Chiarelli, W. G. Lima, M. S. M. Michalick, W. L. Tafuri, W. L. Tafuri, *BMC Vet. Res.* **2006**, *2*, 17.
- [11] F. B. Figueiredo, M. F. Madeira, R. C. Menezes, R. S. Pacheco, M. Q. Pires, M. C. Furtado, G. Pinto, T. M. P. Schubach, *Vet. J.* **2010**, *186*, 123.
- [12] M. Marcondes, W. Biondo, D. Gomes, R. S. Silva, R. F. C. Vieira, A. Camacho, J. Quinn, R. Chandrashekar, *Vet. Parasitol.* **2011**, *175*, 15.
- [13] R. Reithinger, J. C. Dujardin, *J. Clin. Microbiol.* **2007**, *45*, 21.
- [14] G. Srividya, A. Kulshrestha, R. Singh, P. Salotra, *Parasitol. Res.* **2012**, *110*, 1065.
- [15] S. Deborggraeve, T. Laurent, D. Espinosa, G. M. Van der Auwera, Mbuchi, M. Wasunna, S. El-Safi, A. A. Al-Basheer, J. Arévalo, C. Miranda-Verástegui, T. Leclipteux, P. Mertens, J. C. Dujardin, P. Herdewijn, P. Büscher, *J. Infect. Dis.* **2008**, *198*, 1565.
- [16] G. Lombardo, M. G. Pennisi, T. Lupo, A. Migliazzo, A. Capri, L. Solano-Gallego, *Vet. Parasitol.* **2012**, *184*, 10.
- [17] C. Naranjo, D. Fondevila, L. Altet, O. Francino, J. Ríos, X. Roura, T. Peña, *Vet. J.* **2012**, *193*, 168.
- [18] W. Van der Meide, J. Guerra, G. Schoone, M. Farenhorst, L. Coelho, W. Faber, I. Peekel, H. Schallig, *J. Clin. Microbiol.* **2008**, *46*, 73.
- [19] A. Rodríguez-Cortés, A. Ojeda, L. López-Fuertes, M. Timón, L. Altet, L. Solano-Gallego, E. Sánchez-Robert, O. Francino, J. Alberola, *Int. J. Parasitol.* **2007**, *37*, 683.
- [20] P. Salotra, G. Sreenivas, V. Ramesh, S. Sundar, *Br. J. Dermatol.* **2001**, *145*, 630.
- [21] F. Chappuis, Y. Mueller, A. Nguimfack, J. B. Rwakimari, S. Couffignal, M. Boelaert, P. Cavailler, L. Loutan, P. Piola, *J. Clin. Microbiol.* **2005**, *43*, 5973.
- [22] S. Sundar, R. Maurya, R. K. Singh, K. Bharti, J. Chakravarty, A. Parekh, M. Rai, K. Kumar, H. W. Murray, *J. Clin. Microbiol.* **2006**, *44*, 251.
- [23] R. J. Welch, B. L. Anderson, C. M. Litwin, *Clin. Vaccine Immunol.* **2008**, *15*, 1483.
- [24] CorisBioconcept, *Leishmania* spp., <http://www.corisbio.com/Products/Molecular-Field/Leishmania.php> (accessed: July 2015).
- [25] Cepheid, <http://www.cepheid.com/us/> (accessed: July 2015).
- [26] TwistDx Ltd. Revolutionary DNA detection, http://www.twistdx.co.uk/our_technology/ (accessed: July 2015).
- [27] M. Maltez-da Costa, A. de la Escosura-Muniz, A. Merkoçi, *Electrochem. Commun.* **2010**, *12*, 1501.
- [28] M. Maltez-da Costa, A. de la Escosura-Muniz, C. Nogueira, L. Barrios, E. Ibáñez, A. Merkoçi, *Nano Lett.* **2012**, *12*, 4164.
- [29] A. de la Escosura-Muniz, A. Ambrosi, A. Merkoçi, *Trends Anal. Chem.* **2008**, *27*, 568.
- [30] A. Merkoçi, *Biosens. Bioelectron.* **2010**, *26*, 1164.
- [31] A. de la Escosura-Muniz, A. Merkoçi, *Chem. Commun.* **2010**, *46*, 9007.
- [32] M. Andreadou, E. Liandris, M. Gazouli, S. Taka, M. Antoniou, G. Theodoropoulos, G. Tachtsidis, N. Goutas, D. Vlachodimitropoulos, I. Kasampalidis, J. Ikonopoulos, *J. Microbiol. Methods* **2014**, *96*, 56.
- [33] C. H. Wang, C. H. Chang, J. J. Wu, G. B. Lee, *Nanomedicine* **2014**, *10*, 809.
- [34] K. Saha, S. S. Agasti, C. Kim, X. Li, V. M. Rotello, *Chem. Rev.* **2012**, *112*, 2739.
- [35] J. Zhao, T. Liu, Q. Fan, G. Li, *Chem. Commun.* **2011**, *47*, 5262.
- [36] Q. Fan, J. Zhao, H. Li, L. Zhu, G. Li, *Biosens. Bioelectron.* **2012**, *33*, 211.
- [37] Y. Yang, C. Li, L. Yin, M. Liu, Z. Wang, Y. Shu, G. Li, *ACS Appl. Mater. Interfaces* **2014**, *6*, 7579.
- [38] M. Pumera, M. T. Castañeda, M. I. Pividori, R. Eritja, A. Merkoçi, S. Alegret, *Langmuir* **2005**, *21*, 9625.
- [39] X. Zhu, C. Feng, Z. Ye, Y. Chen, G. Li, *Sci. Rep.* **2014**, *4*, 4169.
- [40] X. Lou, Y. Zhang, *ACS Appl. Mater. Interfaces* **2013**, *5*, 6276.
- [41] W. Yang, X. Li, J. Sun, Z. Shao, *ACS Appl. Mater. Interfaces* **2013**, *5*, 11520.
- [42] S. Bansod, S. Bonde, V. Tiwari, M. Bawaskar, S. Deshmukh, S. Gaikwad, A. Gade, M. Rai, *J. Biomed. Nanotechnol.* **2013**, *9*, 1.
- [43] L. Wang, Y. Zhu, Y. Jiang, R. Qiao, S. Zhu, W. Chen, C. Xu, *J. Phys. Chem. B* **2009**, *113*, 7637.
- [44] D. Pan, L. Mi, Q. Huang, J. Hu, C. Fan, *Integr. Biol.* **2012**, *4*, 1155.
- [45] Y. Huang, X. Zhang, Q. Du, F. Wang, X. Zhao, W. Zhang, D. Tong, *PLoS One* **2014**, *9*, e97869.
- [46] H. Kuang, S. Zhao, W. Chen, W. Ma, Q. Yong, L. Xu, L. Wang, C. Xu, *Biosens. Bioelectron.* **2011**, *26*, 2495.
- [47] X. Zhu, X. Zhou, D. Xing, *Biosens. Bioelectron.* **2012**, *31*, 463.
- [48] H. Liu, S. Li, Z. Wang, P. Hou, Q. He, N. He, *Biotechnol. J.* **2007**, *2*, 508.
- [49] A. Lermo, S. Campoy, J. Barbé, S. Hernández, S. Alegret, M. I. Pividori, *Biosens. Bioelectron.* **2007**, *22*, 2010.
- [50] H. Nikbakht, P. Gill, A. Tabarraei, A. Niazi, *RSC Adv.* **2014**, *4*, 13575.

- [51] B. Veigas, P. Pedrosa, I. Couto, M. Viveiros, P. V. Baptista, *J. Nano-biotechnol.* **2013**, *11*, 38.
- [52] J. K. F. Wong, S. P. Yip, T. M. H. Lee, *Small* **2014**, *10*, 1495.
- [53] Z. Fu, X. Zhou, D. Xing, *Methods* **2013**, *64*, 260.
- [54] E. Tan, J. Wong, D. Nguyen, Y. Zhang, B. Erwin, L. K. Van Ness, S. M. Baker, D. J. Galas, A. Niemz, *Anal. Chem.* **2005**, *77*, 7984.
- [55] E. Tan, B. Erwin, S. Dames, K. Voelkerding, A. Niemz, *Clin. Chem.* **2007**, *53*, 2017.
- [56] D. Shi, J. Huang, Z. Chuai, D. Chen, X. Zhu, H. Wang, J. Peng, H. Wu, Q. Huang, W. Fu, *Biosens. Bioelectron.* **2014**, *62*, 280.
- [57] Y. Xiang, K. Deng, H. Xia, C. Yao, Q. Chen, L. Zhang, Z. Liu, W. Fu, *Biosens. Bioelectron.* **2013**, *49*, 442.
- [58] P. Valentini, R. Fiammengio, S. Sabella, M. Gariboldi, G. Maiorano, R. Cingolani, P. P. Pompa, *ACS Nano* **2013**, *7*, 5530.
- [59] A. K. L. Y. Yang, H. Lub, S. Y. Wu, H. C. Kwok, H. P. Ho, S. Yu, A. K. L. Cheung, S. K. Kong, *Anal. Chim. Acta* **2013**, *782*, 46.
- [60] E. Torres-Chavolla, E. C. Alocilja, *Biosens. Bioelectron.* **2011**, *26*, 4614.
- [61] W. Chih-Hung, L. Kang-Yi, W. Jiunn-Jong, L. Gwo-Bin, *Lab Chip* **2011**, *11*, 1521.
- [62] O. Francino, L. Altet, E. Sanchez-Robert, A. Rodríguez, L. Solano-Gallego, L. Ferrer, A. Sánchez, X. Roura, *Vet. Parasitol.* **2006**, *137*, 214.
- [63] M. R. Rodgers, S. J. Popper, D. F. Wirth, *Exp. Parasitol.* **1990**, *71*, 267.
- [64] J. B. Weiss, *Clin. Microbiol. Rev.* **1995**, *8*, 113.
- [65] S. M. Wilson, *Ann. Trop. Med. Parasitol.* **1995**, *89*, 95.
- [66] F. Thielbeer, K. Donaldson, M. Bradley, *Bioconjug. Chem.* **2011**, *22*, 144.
- [67] C. M. Mugasa, T. Laurent, G. J. Schoone, F. L. Basiye, A. Saad, S. El Safi, P. Kager, H. D. Schallig, *Parasit. Vectors* **2010**, *3*, 13.
- [68] C. A. Mirkin, R. L. Letsinger, R. C. Mucic, J. J. Storhoff, *Nature* **1996**, *382*, 607.

Received: August 5, 2015
Revised: September 26, 2015
Published online: November 18, 2015



Supporting Information

for *Small*., DOI: 10.1002/sml.201502350

Magnetic Bead/Gold Nanoparticle Double-Labeled Primers
for Electrochemical Detection of Isothermal Amplified
Leishmania DNA

*Alfredo de la Escosura-Muñiz, Luis Baptista-Pires, Lorena
Serrano, Laura Altet, Olga Francino, Armand Sánchez, and
Arben Merkoçi**

Supporting Information

Magnetic bead/gold nanoparticle double-labeled primers for electrochemical detection of isothermal amplified Leishmania DNA

*Alfredo de la Escosura-Muñiz, Luis Baptista-Pires, Lorena Serrano, Laura Altet, Olga Francino, Armand Sánchez, Arben Merkoçi**

[*] Prof. Arben Merkoçi
ICN2 – Nanobioelectronics & Biosensors Group, Institut Català de Nanociència i Nanotecnologia, Campus UAB, 08193 Bellaterra (Barcelona), Spain & ICREA – Institutio Catalana de Recerca i Estudis Avançats, 08010 Barcelona, Spain
E-mail: arben.merkoci@icn.cat

Dr. Alfredo de la Escosura-Muñiz, Luis Baptista-Pires
ICN2 – Nanobioelectronics & Biosensors Group, Institut Català de Nanociència i Nanotecnologia, Campus UAB, 08193 Bellaterra (Barcelona), Spain

Lorena Serrano, Dr. Laura Altet, Dr. Olga Francino
Vetgenomics, Edifici Eureka, Parc de Recerca UAB, 08193 Bellaterra (Barcelona), Spain

Dr. Olga Francino, Prof. Armand Sánchez
Autonomous University of Barcelona, Campus UAB, 08193 Bellaterra (Barcelona), Spain.

Prof. Armand Sánchez
Centre for Research in Agricultural Genomics-CSIC-IRTA-UAB-UB, Campus UAB, 08193 Cerdanyola del Valles, Catalonia, Spain

Synthesis of gold nanoparticles

16 nm gold nanoparticles (AuNPs) were synthesized by reducing tetrachloroauric acid with trisodium citrate, a method pioneered by Turkevich [Turkevich et al., 1953]. Briefly, 200 mL of 0.01% H₂AuCl₄ solution (25 mM) were boiled with vigorous stirring. 5 mL of 1% trisodium citrate solution were added quickly to the boiling solution. When the solution turned deep red, indicating the formation of AuNPs **16** nm sized, the solution was left stirring and cooling down.

Fabrication of screen-printed carbon electrodes (SPCEs)

The electrochemical transducers were homemade screen-printed carbon electrodes (SPCEs) consisting of three electrodes in a single strip: working electrode (WE), reference electrode (RE) and counter electrode (CE). The full size of the sensor strip was 29mm x 6.7mm, and the WE diameter was 3mm. The fabrication of the SPCEs was carried out in three steps in the semi-automatic screen-printing machine DEK248 (DEK International, Switzerland), using a different stencil, with the corresponding patterns, for each layer. First, a graphite layer (Electrodag 423SS carbon ink for WE and CE) was printed onto the polyester sheet (Autostat HT5, McDermid Autotype, UK). After curing for 30 min at 95°C, a second layer was printed with silver/silver chloride ink (Electrodag 6037SS for the RE). After another curing for 30 min at 95°C, the insulating layer was printed using insulating ink (Minico 7000 Blue, Acheson Industries, The Netherlands) to protect the contacts and define the sample interaction area. Finally, the SPCEs were cured again at 95°C for 20 min.

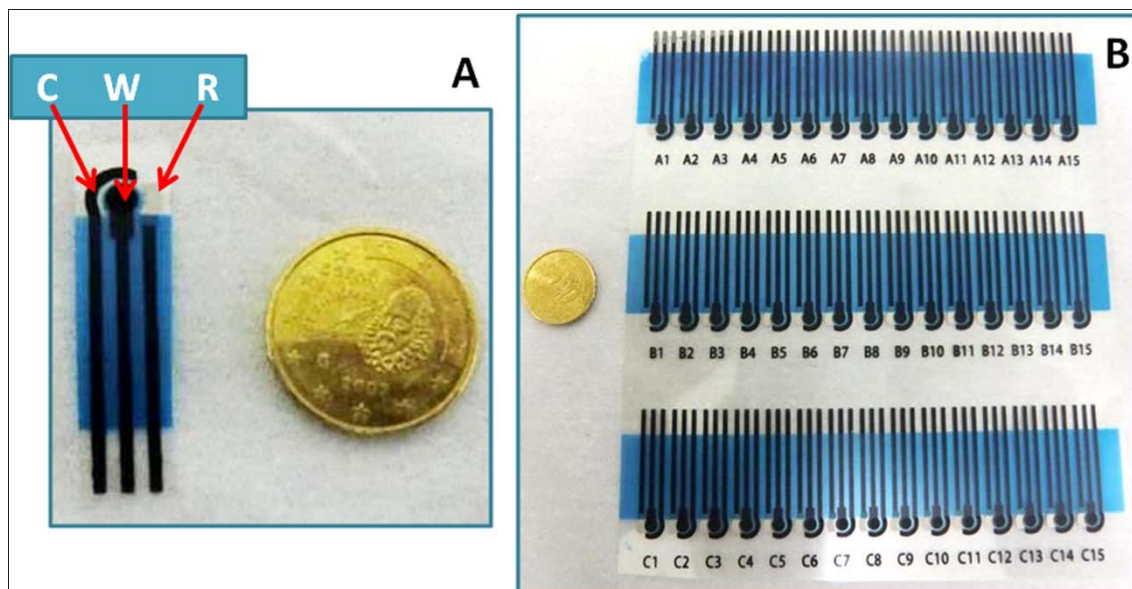


Figure SM-1: (A) Detail of one SPCE, containing the three electrodes in the working area; R- Ag/AgCl reference electrode, W- carbon working electrode and C- carbon counter electrode. (B) Images of the 45 SPCE sensors sheet obtained following the experimental procedure.

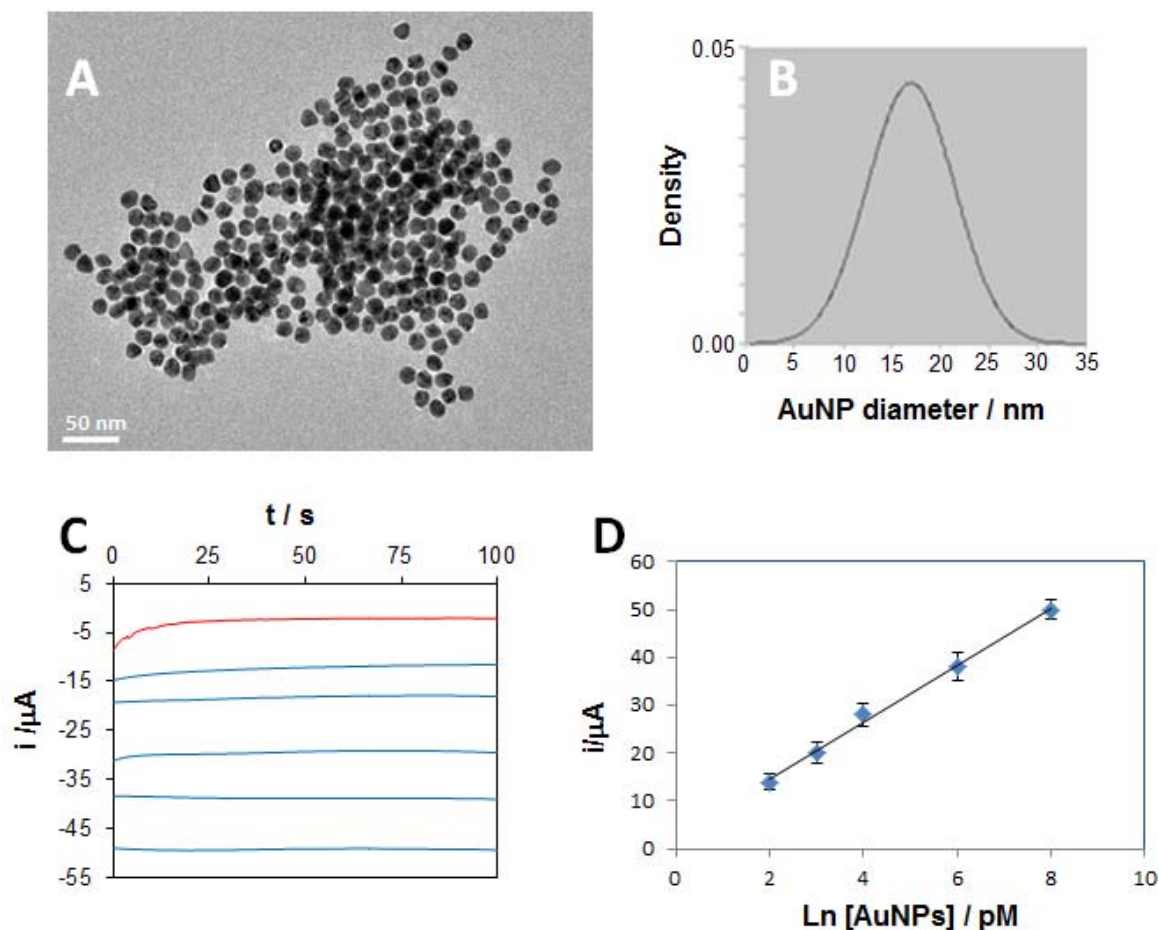


Figure SM-2: (A) TEM image of the self-synthesized AuNPs and (B) the corresponding size-distribution diagram. (C) Chronoamperograms recorded at -1V in 1M HCl for different concentrations of AuNPs suspensions, from up to bottom: 0, 2, 3, 4, 6 and 8 pM and (D) the corresponding relationship between the absolute value of the cathodic current at 60 s and the concentration of AuNPs.

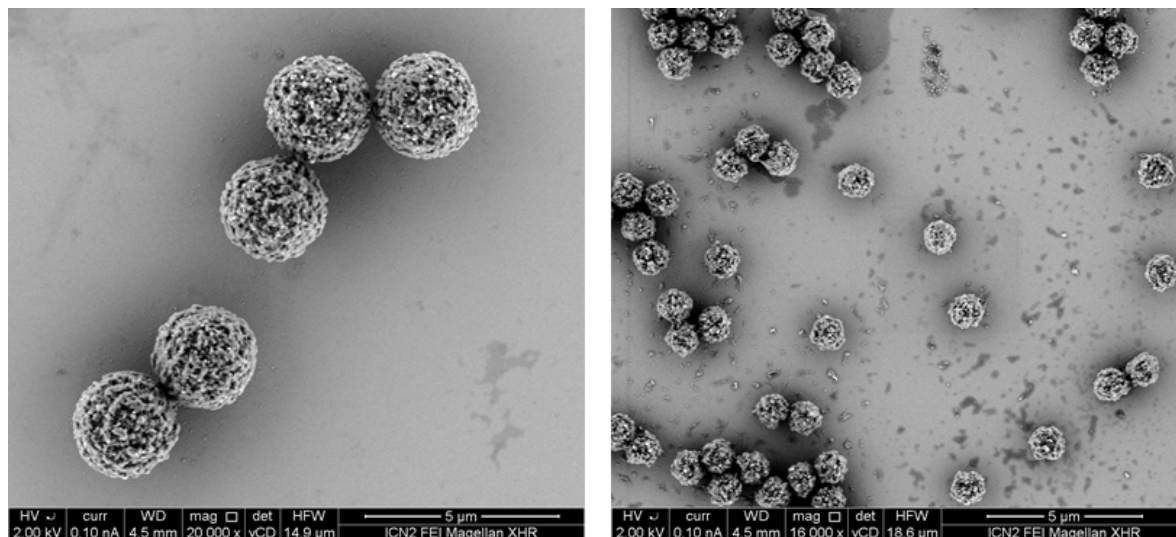


Figure SM-3: SEM images of monodisperse magnetic beads of 2.8 μm (Dynal M-280®) (left) and 1 μm (DynaL MyOne®) (right) .

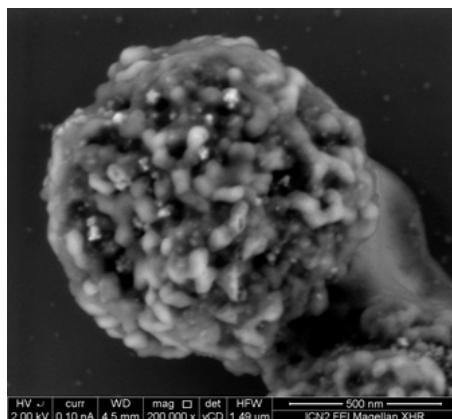


Figure SM-4: SEM image of a 1 μm MB after amplification of DNA without *Leishmania* parasite. Experimental conditions as detailed in the main text.

REFERENCES

Turkevich, J.; Stevenson, P. C.; Hillier, J. J. Phys. Chem. 1953, 57, 670.



Electrocatalytic tuning of biosensing response through electrostatic or hydrophobic enzyme–graphene oxide interactions

Luis Baptista-Pires^a, Briza Pérez-López^b, Carmen C. Mayorga-Martínez^a,
Eden Morales-Narváez^a, Neus Domingo^c, Maria Jose Esplandiú^d, Francesc Alzina^e,
Clivia M. Sotomayor-Torres^{e,f}, Arben Merkoçi^{a,f,*}

^a Nanobioelectronics and Biosensors Group, Catalan Institute of Nanoscience and Nanotechnology, ICN2 Campus de la UAB, 08193 Bellaterra, Barcelona, Spain

^b LEITAT Technological Center, 08225 Terrasa, Spain

^c Oxide Nanoelectronics Group, Catalan Institute of Nanoscience and Nanotechnology, ICN2 Campus de la UAB, 08193 Bellaterra, Barcelona, Spain

^d Catalan Institute of Nanoscience and Nanotechnology, ICN2 Campus de la UAB, 08193 Bellaterra, Barcelona, Spain

^e Phononic and Photonic Nanostructures, Catalan Institute of Nanoscience and Nanotechnology, ICN2 Campus de la UAB, 08193 Bellaterra, Barcelona, Spain

^f ICREA, Institutió Catalana de Recerca i Estudis Avançats, 08010 Barcelona, Spain

ARTICLE INFO

Article history:

Received 7 February 2014

Received in revised form

29 April 2014

Accepted 12 May 2014

Available online 29 May 2014

Keywords:

Oxidized graphene oxide

Reduced graphene oxide

Electrostatic interactions

Hydrophobic interactions

Electrocatalytic tuning

ABSTRACT

The effect of graphene oxidative grades upon the conductivity and hydrophobicity and consequently the influence on an enzymatic biosensing response is presented. The electrochemical responses of reduced graphene oxide (rGO) have been compared with the responses obtained from the oxide form (oGO) and their performances have been accordingly discussed with various evidences obtained by optical techniques. We used tyrosinase enzyme as a proof of concept receptor with interest for phenolic compounds detection through its direct adsorption onto a screen-printed carbon electrode previously modified with oGO or rGO with a carbon–oxygen ratio of 1.07 or 1.53 respectively. Different levels of oGO directly affect the (bio)conjugation properties of the biosensor due to changes at enzyme/graphene oxide interface coming from the various electrostatic or hydrophobic interactions with biomolecules. The developed biosensor was capable of reaching a limit of detection of 0.01 nM catechol. This tuning capability of the biosensor response can be of interest for building several other biosensors, including immunosensors and DNA sensors for various applications.

© 2014 Elsevier B.V. All rights reserved.

1. Introduction

Since the discovery of graphene in the last years (Geim and Novoselov, 2007) and with the great progress made in nanoscience and nanotechnology, its integration with biomolecules has received increased attention due to its physical, optical and chemical properties such as its interesting molecular structure, high active surface area and high conductivity capacity that improves the electron transfer which are not available in other materials (Shao et al., 2010). Since then, many graphene materials such as graphene oxide (Marcano et al., 2010; Shen et al., 2009), graphene quantum dots (Peng et al., 2012) or graphene nanoribbons have been reported (Martin-Fernandez et al., 2012).

Graphene oxide (GO) undergoes transitions from insulator to semimetal mainly after reducing processes (Mathkar et al., 2012). The reduction modes such as reduction using hydrazine (Marcano

et al., 2010), thermal annealing (Gao et al., 2010) or bacterial treatment (Salas et al., 2010) result in highly satisfactory methods for the reconstruction of the carbon sp² bonds on GO sheets. The reduction of GO removes the oxygen groups and rehybridizes the sp³ carbon atoms to sp² carbon atoms (Cheng et al., 2012). Epoxy and hydroxyl groups lie above and below each graphene layer and the carboxylic groups are mostly located at the edges (Zhu et al., 2010). Zhang et al. have demonstrated that reduced graphene oxide (rGO) represents an interesting platform with high affinity for enzyme immobilization. This high affinity is due to the adsorption of enzyme on rGO through hydrophobic interaction and the lack of surface functional groups of rGO that may impart less perturbation to the enzyme (Zhang et al., 2012). Currently different enzymatic biosensors based on graphene for the detection of different analytes such as that reported by Karuwan et al. (Karuwan et al., 2013) that mixes carbon paste and GO for direct manufacturing of screen printing electrodes and Ping et al. (Ping et al., 2011) where GO is directly electrodeposited onto the surface of the electrode and calcium ion-selective membrane is used for tuning the biosensor (Ping et al., 2012) have been developed. On

* Corresponding author. Tel.: +34935868014; fax: +34935868020.

E-mail address: arben.merkoci@icn.cat (A. Merkoçi).

the other hand Song et al. (Song et al., 2011) take advantage of gold nanoparticles, 1-pyrenebutanoic acid and succinimidy ester and Yang et al. (Yang et al., 2013) take advantage of nickel nanoparticles and chitosan.

Due to the biofunctionalization capabilities combined with interesting electrochemical (Shao et al., 2010) and optical properties (Morales-Narvaez and Merkoci, 2012) GO has greatly stimulated research interest for applications in (bio)sensing systems. This work presents a new catechol biosensor based on a GO–Tyrosinase conjugate formation through either electrostatic (case of oGO) or hydrophobic (case of rGO) interactions. For this study we have used oGO reduced with hydrazine (Marcano et al., 2010) so as to achieve its de-oxygenation. The electrochemical responses of this rGO have been compared with the responses obtained for oGO and their performances have been accordingly discussed with various evidences obtained by optical techniques. The use of these GO-based tuning biosystems improves the detection levels compared with similar technologies (Karuwan et al., 2013; Ping et al., 2011, 2012; Song et al., 2011; Yang et al., 2013) and this simple technique does not need the use of any crosslinking agents, surfactants or other materials as reported before.

2. Materials and methods

2.1. Preparation of rGO

Oxidized graphene oxide (oGO) was provided from Angstrom Materials, Inc. (Product: N002-PS) and the reduction step to produce reduced graphene oxide (rGO) was made using reported literature (Marcano et al., 2010), where 100.00 mL of oGO (1 mg/mL) was mixed with 1.00 mL of hydrazine hydrate. The mixtures were heated at 95 °C using a water bath for 45 min; a black solid precipitated from the reaction mixture. Products were isolated by filtration (PTFE 20 µm pore size) and washed with DI water (50 mL, 3 times) and methanol (20 mL, 3 times).

2.2. Optical measurements and sample characterization

The samples were prepared by drop casting our solution on a silicon sample holder. X-ray photoelectron spectroscopy (XPS) experiments were performed in a PHI 5500 Multitechnique System (from Physical electronics) with a monochromatic X-ray source (Aluminum Kalfa line of 1486.6 eV energy and 350 W), placed perpendicular to the analyzer axis and calibrated using the 3d5/2 line of Ag with a full width at half maximum (FWHM) of 0.8 eV. Raman spectra were acquired at room temperature with a Horiba T64000 spectrometer operated in single mode configuration with spectral resolution of 4 cm⁻¹. The excitation source was the 514.5 nm line of an argon ion laser. The laser was focused to a spot with diameter of about 560 nm using a 100 × objective lens and the intensity was kept below 200 µW to avoid any damage of the sample. UV–visible absorbance spectra were explored through a SpectraMax M2^e multimode reader (Molecular Devices, California, USA) and fluorescence was determined using a UV lamp with 345 nm excitation wavelength. AFM measurements were done using a Dimension 3100 AFM Machine (Veeco Metrology Group, Digital Instruments). An easy drop contact angle measuring instrument was used to obtain the contact angle of modified graphene surfaces.

2.3. SPE modification and electrochemical characterization

SPEs were fabricated using a previously optimized technology by our lab. A graphite layer is printed by using a screen-printing

machine (DEK 248) with a stencil (where it is the electron pattern) and graphite ink onto the polyester sheet. The polyester sheet is cured for 15 min at 95 °C. A silver/silver chloride layer is printed as the reference electrode. The polyester sheet is cured for 15 min at 95 °C. Insulating ink is deposited. Curing for 20 min at 95 °C was performed. The SPE was modified with 10 µL of 1 mg/mL oGO and rGO by drop casting and dried overnight at room temperature. For exploring electrochemical behavior of modified electrodes, cyclic voltammetry was done using 50 µL of 1 mM Ferricyanide ([Fe(CN)₆]^{3-/4-}) in 1 M sodium chloride (KCl) that was deposited onto the SPE by drop casting. Tyrosinase was immobilized onto the electrode surface by physical adsorption. Tyrosinase was solved in 0.1 M phosphate buffer (PBS) at pH 6.5. The concentration of Tyrosinase for SPE modification was 1 mg/50 µL in PBS. SPE, SPE–oGO and SPE–rGO electrodes were modified with 5 µL of 1 mg/50 µL Tyrosinase and dried overnight in a fridge at 4 °C.

Amperometric measurements were performed applying a potential of –0.1 V in a system composed of a 5 mL electrolytic cell containing 0.1 M PBS. PBS is necessary to be used in controlled-potential experiments as a supporting electrolyte. It decreases the resistance of the solution, eliminates electromigration effects and maintains a constant ionic strength. Cyclic voltammetry (CV) and amperometric experiments were performed using an electrochemical (CH instrument, model CHI 600C).

3. Results and discussion

3.1. Optoelectronic properties

X-ray photoelectron spectroscopy (XPS) and Raman spectroscopy (Raman) were first used to evidence the level of oxidation and correspondent oxygen bonds so as to determine the structural changes occurring during the chemical reduction process mainly affected by the presence of oxygen atoms on the graphene structure.

The study of efficiency of graphene reduction using the hydrazine method was followed by X-ray photoelectron spectroscopy (XPS). Fig. 1a shows the C1s signal of oGO powder. The signal was fitted by four components: C=C & C–C (42.1%, 284.6 eV), C–O (47.9%, 286.7 eV), C=O (7%, 288.0 eV) and O=C–OH (3%, 288.9 eV). The estimated ratio C/O is ~1.07. The same study was pursued for rGO presented in Fig. 1b with values for C=C & C–C (60.1%, 284.6 eV), C–O (32.1%, 286.7 eV), C=O (5.1%, 288.0 eV) and O=C–OH (2.7%, 288.9 eV) and a C/O ~1.53. The efficiency of hydrazine reduction is clear and the improvement of the C/O is quantified. In the case of Raman, in Fig. 1c the D and G bands are localized at 1345 cm⁻¹ and 1590 cm⁻¹ respectively for oGo and rGO (Park et al., 2008a). However an increase in D/G intensity ratio (ID/IG) is observed for rGO (ID/IG=1.26) in comparison with oGO (ID/IG=0.92), suggesting a decrease in the average size of the sp² domains upon reduction and can be explained by the formation of new graphitic domains that are smaller in size but more numerous (Stankovich et al., 2007). According to this study the modified screen printed electrodes (SPEs) with these two kinds of graphene possess levels of oxidation and carbon networks that are completely different, and consequently different electrocatalytic responses can be previewed. In order to get insights of the electronic properties of the obtained platform, UV–visible spectrum was obtained and is presented in Fig. 1d. For the oGO sample the maximum peak at 231 nm is ascribed to π→π* transition of aromatic C–C bonds, and a shoulder at 300 nm is attributed to n→π* transition of C=O bonds. In the case of the rGO the maximum peak was red-shifted to 254 nm after reduction and the absorbance was significantly increased at wavelengths above 233 nm, which indicates that electronic conjugation has been restored at

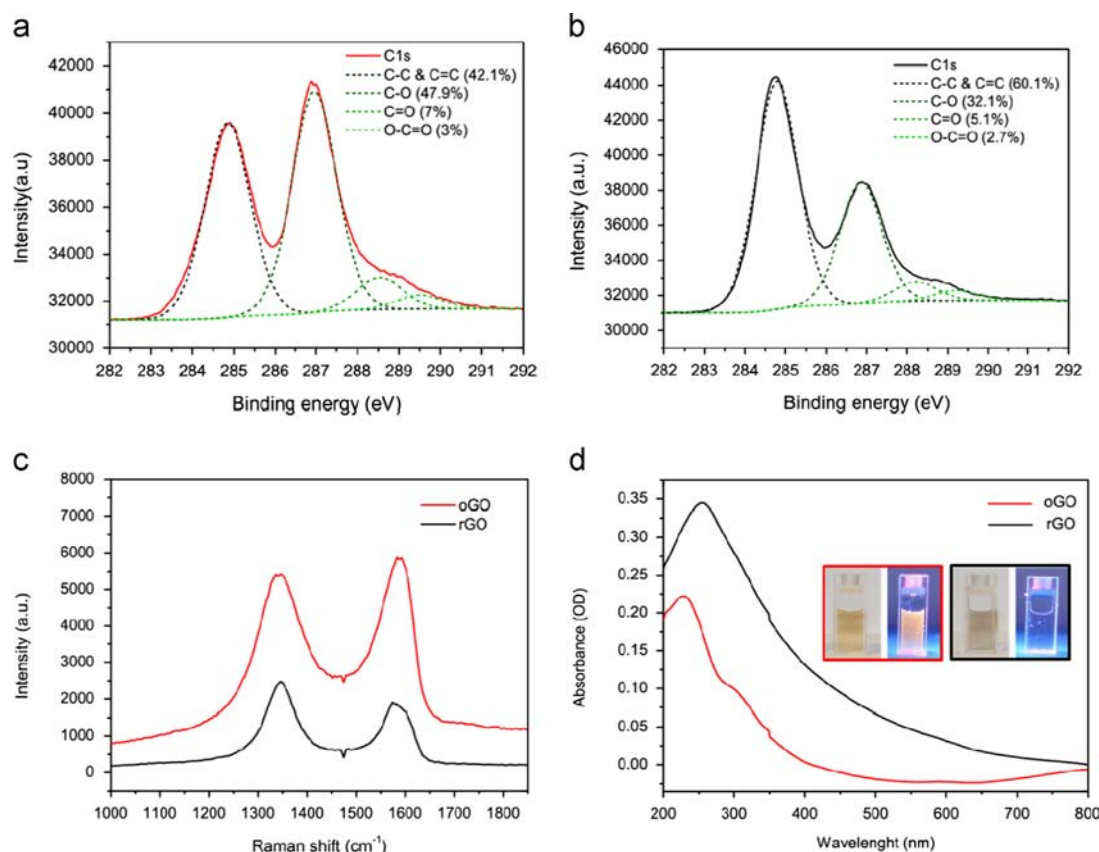


Fig. 1. Optical characterization of graphene oxide materials. C1s XPS data of oGO (a) and rGO (b). (c) Raman spectra and (d) UV-visible steady state spectroscopy. Inset: images of oGO and rGO suspensions under UV lamp excitation.

least to some extent (Cuong et al., 2010). The defect at 350 nm in the visible spectra is due to the UV lamp change in the device. The fact that under excitation of 350 nm UV-light, the oGO presents fluorescence (inset Fig. 1d) in detriment to rGO can make us think about the transitions presented in the UV-visible absorbance spectra which are in line with similar data of an oxidized graphene material (Shang et al., 2012) for which the appearance of a band gap has been also reported.

3.2. Morphology characterization

To accurately determine the oGO and rGO morphology at the nanoscale, the sheets were characterized by Atomic Force Microscopy (AFM), as shown in Fig. 2. Completely different morphologies were observed between these two nanomaterials. oGO flakes show a highly non-uniform surface with high degree of porosity. The average diameter of graphene holes is in the range of tens of nanometers, and the flakes show a thickness of about 2.5 nm. The presence of this topographical defects observed in this sample is explained by the high level of oxidation (Cheng et al., 2012). Indeed, Fig. 2b shows the topography of rGO flakes in which homogeneous double, triple and multilayer flakes of graphene are observed (Geim and Novoselov, 2007). The average thickness of each flake for this sample is around 3 nm. It becomes clear that the reduction process of oGO flakes results in bigger layers of rGO after reduction of oGO, mostly due to the rearrangement of sp^2 carbon bonds (Gao et al., 2010).

The different levels of oxidation of the oGO and rGO films are confirmed by Kelvin Probe Force Microscopy (KPFM) and surface hydrophobicity studies. In KPFM, direct measurements of the contact potential difference between the oGO and rGO flakes and the tip of the AFM are obtained and mapped. As shown in

Fig. 2c and d the KPFM image of the oGO flakes shows a dark contrast with respect to the surrounding substrate, indicating the presence of negative dipoles on the surface of the oGO flakes dominated by the oxygen groups. Instead, for rGO, the flakes show a more positive contrast with respect to the substrate observed through the holes, in agreement with the presence of less negative dipoles on the surface of these samples which arise from the reconstruction of the sp^2 carbon network.

In order to evaluate the surface hydrophobicity and the electrocatalytic properties of the graphene forms we used SPE (Fig. 3a) as testing platforms. Screen-printing microfabrication technology is well-established for the mass production of thick film electrodes and it is widely applied to build biological or chemical sensors (Fanjul-Bolado et al., 2009). SPE represents one of the most important products of this technology. A simple strategy in which SPEs were modified with 10 μ L of 1 mg/mL oGO and rGO was used. Under this methodology a total coverage of the SPE is achieved and a completely new electrode platform is built.

Surface hydrophobicity of the modified SPE was evaluated due to the fact that adsorption processes have a direct influence on the electrochemical response through the electrocatalytic behavior of the adsorbed enzyme. As shown in Fig. 3b, the contact angle to water of typical SPE is 62.2° . After modification with graphene oxide materials, the surface suffers visible changes in its hydrophobicity. In the case of SPE modified with oGO (SPE-oGO) in Fig. 3c, the contact angle changed to a value of 52.6° and in the SPE modified with rGO (SPE-rGO) the contact angle was 73.4° as reported in Fig. 3d (Zhang et al., 2012). In the case of SPE-oGO the surface seems to be much more hydrophilic in comparison with SPE-rGO due to the presence of oxide groups. The consequent removal of these oxygen binding sites for rGO-SPE induced stronger hydrophobicity on these electrodes due to π - π interactions. These results

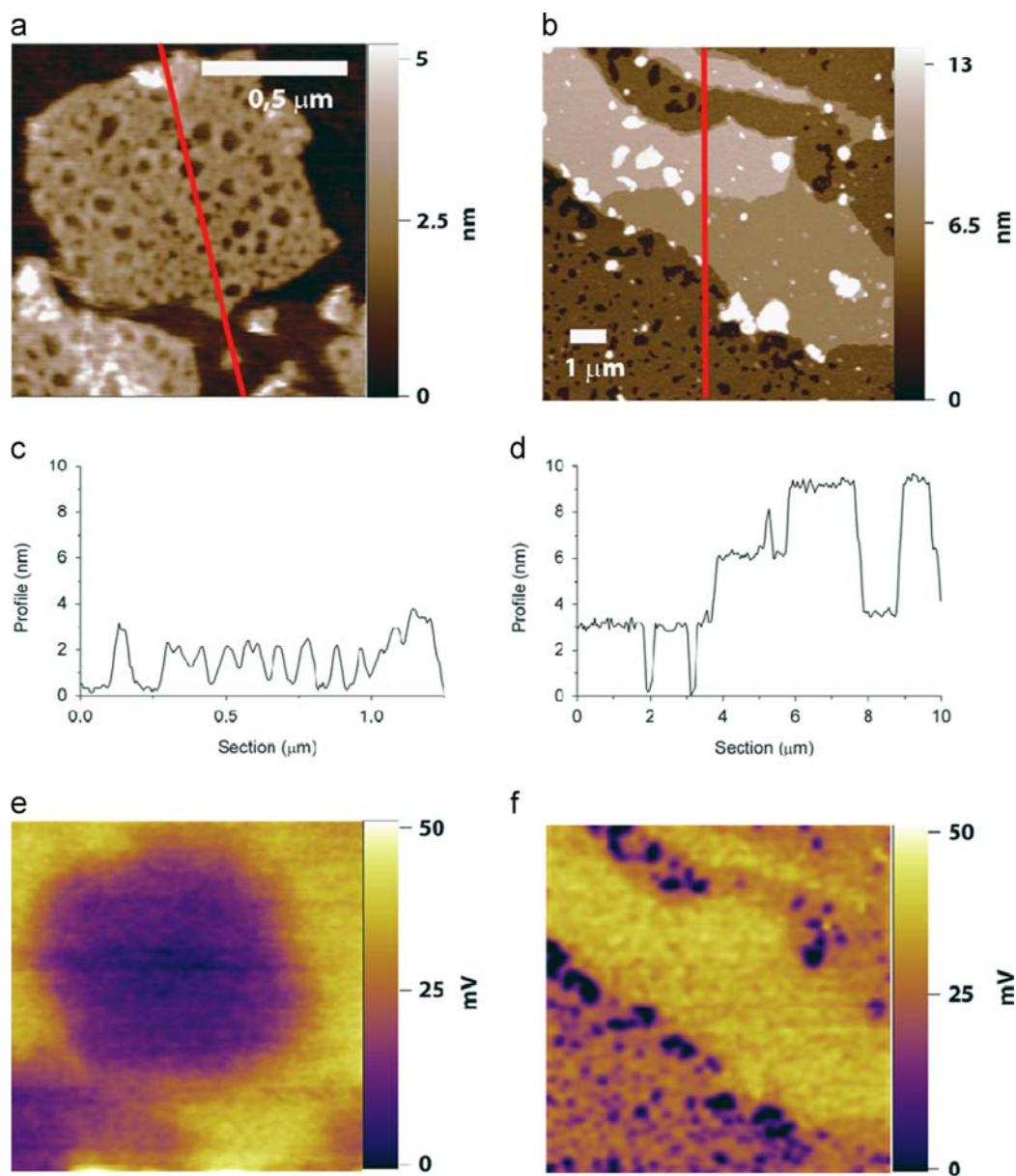


Fig. 2. Graphene oxide morphology at the nanoscale. Topography AFM images of oGO (a) and rGO (b) flakes. The red lines correspond to the sections (c) and (d) shown below for each image. KPFM images of oGO (e) and rGO (f) of the same area as in (a) and (b). (For interpretation of the references to color in this figure legend, the reader is referred to the web version of this article.)

are also in agreement with the level of oxidation of the graphene materials that is proportional to the hydrophobicity of the modified SPE surface and consistent with the AFM measurements.

3.3. Electrocatalytic properties

To explore electrocatalytic behavior of the modified SPE electrodes, a drop of 50 μL of 1 mM Ferricyanide ($[\text{Fe}(\text{CN})_6]^{3-/4-}$) solution was deposited and cyclic voltammetry technique was performed to evaluate electrochemical response of SPE-oGO and SPE-rGO to this redox couple.

Fig. 4 shows that the presence of graphene materials has an important effect on the electrochemical response of the SPEs. While the presence of oGO decreases the conductivity or the current on the SPE-oGO, the SPE-rGO shows a higher current response to $[\text{Fe}(\text{CN})_6]^{3-/4-}$ (Fig. 4a). From these results, one can state that rGO is the most conductive material and oGO the most

resistive one. As a matter of comparison, the electrochemical behavior of the SPE electrode without graphene (Fig. 4b) together with a zoom of the electrochemical response of the SPE-oGO (Fig. 4c) and SPE-rGO (Fig. 4d) is also depicted. In the SPE-oGO a very low current redox wave whose possible origin will be addressed later on was also captured.

The electrochemical reactivity of the SPE-oGO and SPE-rGO can be explained under the light of the density of electronic states which is a very important parameter that controls the electrode kinetics. According to the Gerischer–Marcus theory, the heterogeneous electron transfer rate is dependent on DOS (density of electronic states) of the electrode and on the overlap with the electronic states of the electroactive species (Belding et al., 2010). An electron transfer can take place from any occupied energy state that is matched in energy with an occupied receiving state. Thus in metallic electrodes the high density of DOS increases the possibility that an electron of the correct energy is available for the electrode to transfer to an

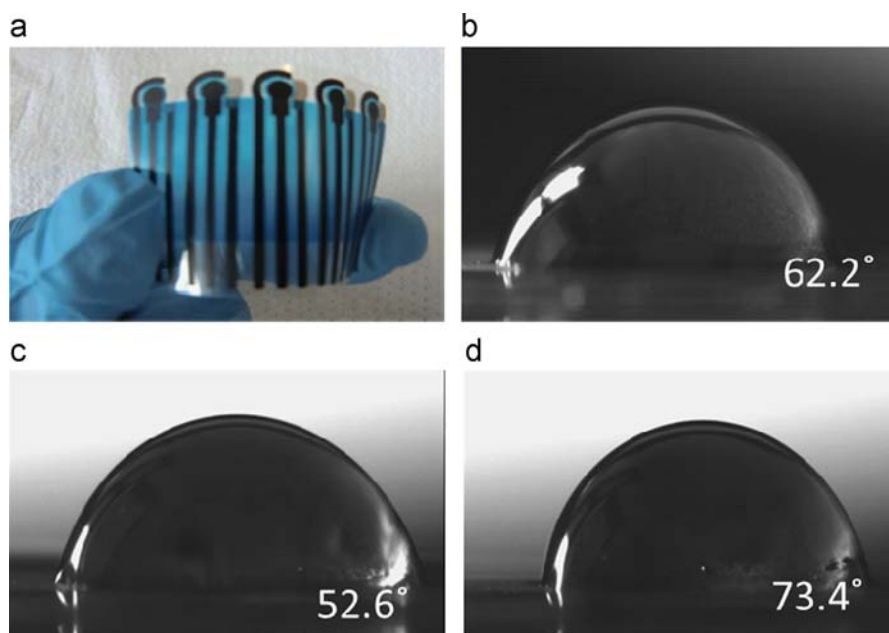


Fig. 3. Surface hydrophobicity study. SPE flexible technology (a). Water contact angles for SPE (b), SPE-oGO (c) and SPE-rGO (d).

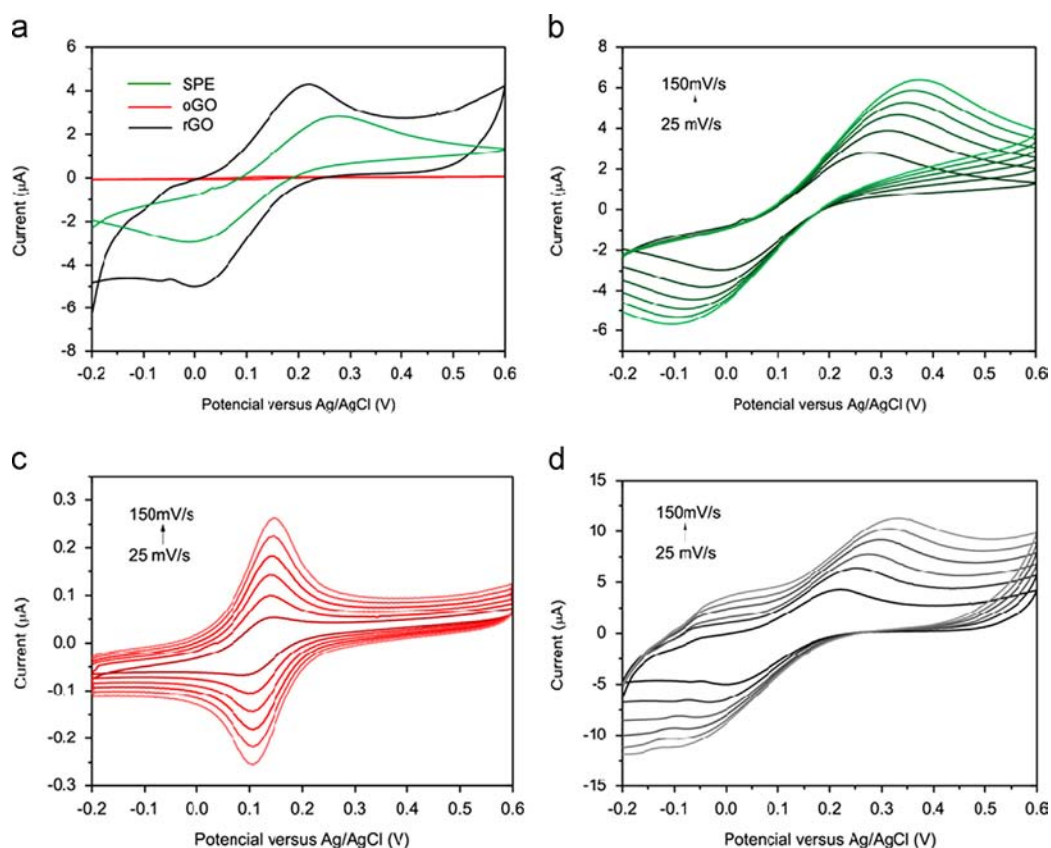


Fig. 4. Electrochemical properties. Cyclic voltammetry for SPE, SPE-oGO and SPE-rGO at a scan rate of 25 mV/s (a). Non-modified SPE (b), SPE-oGO (c) and SPE-rGO (d) at scan rates from 25 mV/s to 150 mV/s. All samples were tested in 1 mM $[\text{Fe}(\text{CN})_6]^{3-/4-}$ and 1 M KCl.

electroactive species. However if the material exhibits a band gap the probability of matching available states for the electron exchange between electrode and electroactive species is very low, decreasing dramatically the electrochemical activity. Therefore in the case of SPE-oGO and in accordance with the fluorescence observations, it is very reasonable to ascribe the low electrochemical performance to the opening of band gap with the oxidation process.

High graphene oxidation is known for instance to remove states close to the Fermi level, thus producing an insulator (Acik et al., 2010). It is therefore expected that excessive oxygen moieties on graphene in any chemical form (epoxide, hydroxyl, carboxyl and ketonic-type functional groups) both on the basal plane (Cai et al., 2008) and at the edges (Park et al., 2008b) reduce electronic states at the Fermi level and consequently its

conductivity as probed experimentally (Eda et al., 2009). As described before in Fig. 1d the reduction of oGO results in the decrease of $n \rightarrow \pi^*$ transitions, responsible for C=O bonds in sp^3 hybrid regions and responsible for fluorescence emission in graphene oxide (Shang et al., 2012). It is also reported that graphene reduction using hydrazine decreases the band gap to almost negligible values (Mathkar et al., 2012). The conductivity increase after reduction, passing from an insulator material to a more semimetallic conductive one, is clear in Fig. 4d and consistent with literature reported elsewhere about this transition behavior upon reduction (Acik et al., 2010).

Redox peak currents increase around 60 times upon reduction as can be observed in Table 1. The table also reports the peak separation voltages (ΔV_p) for the different electrodes. It can be

observed that the ΔV_p of SPE-rGO is smaller than in the case of the carbon based SPE, evidencing the favorable electrode kinetics of the reduced graphene. The table also reports the ΔV_p value for the case of SPE-oGO ascribed to the very low current oxidation/reduction wave which is captured when zooming in the electrochemical current of the oxidized graphene. The origin of such small redox wave and its surprisingly low value of ΔV_p cannot be analyzed in the same context as in the case of SPE and SPE-rGO electrodes. We believe that such redox wave in the SPE-oGO comes from the response of the bottom carbon support of the SPE and not from the oxidized and insulating graphene. The surprising reversibility of such wave can be explained under the light of the thin layer diffusion model which is applicable when the electrolyte is trapped in porous layers (Belding et al., 2010). Indeed, AFM images have shown the porous nature of oxidized graphene. Therefore the electrochemical response is compatible with a passivating oxidized graphene layer with a number of pits (pores) through which the electrolyte penetrates and remains confined, inducing a kinetically and thermodynamically favorable electron transfer with the base carbon material of the SPE. Accordingly, the peak-to-peak separation in this scenario is expected to be smaller than in the case of the semi-infinite diffusion model in agreement with our findings.

Table 1
Cyclic voltammetry data for SPE, SPE-oGO and SPE-rGO.

	ΔE (V)	ΔI (μA)
SPE	0.3945	4.72
SPE-oGO	0.0244	0.12
SPE-rGO	0.3297	7.75

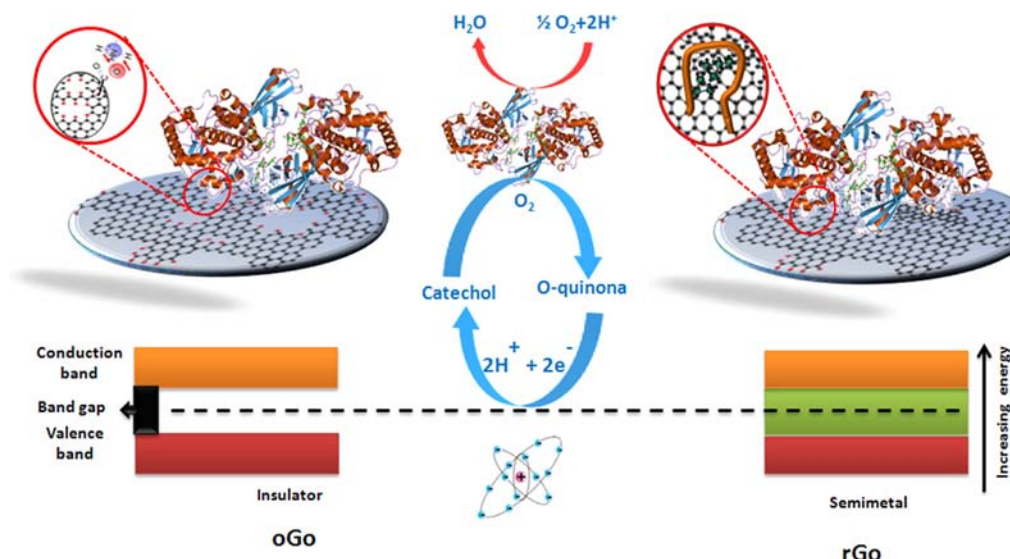


Fig. 5. Schematic diagram (not in scale) displaying the enzyme (Tyrosinase) and reactions involved in the catechol detection at the SPE modified with oGO acting as an insulator and rGO as a semimetallic compound.

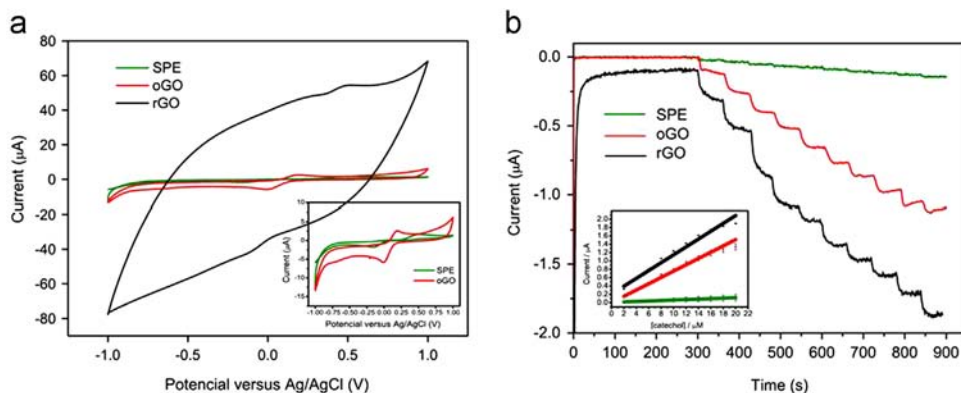


Fig. 6. Electrocatalytic properties of SPE/Tyr, SPE/oGO/Tyr and SPE/rGO/Tyr. (a) Cyclic voltammetry response in the presence of 20 μM catechol at 100 mV/s. (b) Typical current–time curves for the successive additions of 2 μM catechol solution, to a 5 mL electrocatalytic cell containing 0.1 M PBS (pH 6.5) with stirring under a working potential of -0.1 V. Inset: corresponding calibration curves for the graphene modified SPEs.

The influence of the two explored graphene materials with different levels of oxidation on the attachment of Tyrosinase enzyme has been also studied. The enzymatic activity of the Tyrosinase-graphene oxide modified SPE platform using catechol can be observed through the formation of o-quinone as shown in Fig. 5.

The voltamperometric evaluation (Fig. 6a) shows a comparison of the SPE modified with Tyrosinase (SPE/Tyr), oGO plus tyrosinase (SPE/oGO/Tyr) and rGO plus tyrosinase (SPE/rGO/Tyr) on the electrocatalytic detection of catechol. All modifications and measurements with the developed biosensors were done under strictly identical conditions (the total assay time including the SPE modifications through incubations with graphene was around 24 h). As expected, the reduction signal was improved when GO was present. Moreover remarkably higher response of SPE/rGO/Tyr was observed, showing fairly well the advantages predicted for this type of biosensor configuration commented upon in the introduction section. The enzymatic reaction involves the catalytic oxidation of the catechol to o-quinones, at the expense of reducing oxygen to water. The electrochemical reduction of o-quinones, by transferring two electrons and two protons, was employed to monitor this reaction (Fig. 5). In this case, o-quinone can be reduced back to catechol at low applied potentials (-0.1 V). The generation of electrons in this step leads to a change in the current that can be measured. The coupling between the catalytic oxidation (catechol to o-quinone) and the electrochemical reduction (o-quinone to catechol) shuttles the catechol into a cycle with the possibility of signal amplification (see Fig. 6b).

Herein SPE, SPE-oGO and SPE-rGO electrodes have been modified with Tyrosinase by adsorption. Such immobilization strategy and the final enzymatic activity are expected to be very dependent on the hydrophobicity level of the GO-SPE. The enzymatic response has been followed up by amperometric measurements at -0.1 V. We have found a very good electrochemical stability with the addition of catechol for the highly oxidized graphene as can be observed in Fig. 6b. This behavior may be related with the binding of the Tyr to oGO by electrostatic interaction (Zhang et al., 2012). Thus, and despite being an insulator, SPE-oGO is highly beneficial for enzyme biosensing platforms, presenting a limit of detection (LOD – signal to noise ratio ($S/N=3$)) of 0.0711 nM, a limit of quantification (LOQ) of 0.237 nM and a sensitivity of 0.0679 $\mu\text{A}/\mu\text{M}$ as presented in Table 2. In the case of SPE-rGO modified with Tyr, the improvement of the electroanalytical performance (based on LOD and sensitivity parameters) was observed. The presence of hydrophobic aromatic structures observed by XPS spectra (Fig. 1b) and the water contact angles studies (Fig. 3d) suggested that the adsorption of the enzyme onto SPE-rGO should be governed by a hydrophobic interaction instead of electrostatic interaction onto SPE-oGO. As reported before, this Tyrosine immobilization onto the rGO was more efficient than the immobilization onto the oGO for similar C/O (Zhang et al., 2012). This phenomenon is attributed to the fact that the electrostatic interaction as the driving force for enzyme binding to oGO severely affected the activity of the enzyme. Additionally the higher conductivity of rGO promotes high charge transfer (Fig. 4a). As reported in Table 2, the SPE-rGO presented the best LOD of all graphene materials (0.0103 nM), a LOQ of 0.034 nM and was shown to be the most sensitive (0.0898 $\mu\text{A}/\mu\text{M}$).

The obtained results are advantageous when concerning biosensors reported in literature (Karuwan et al., 2013; Ping et al., 2011, 2012; Song et al., 2011; Yang et al., 2013) that use other nanomaterials or a cross-linked agent and longer procedures to immobilize the enzymes and enhance the response. The proposed graphene-based biosensing fabrication is simple, time efficient and does not alter the enzyme structure and its operation yields very good performance.

Table 2

Description of different analytical parameters.

	LOQ (nM)	LOD (nM)	Sensitivity ($\mu\text{A}/\mu\text{M}$)	Linear interval (μM)	R
SPE	1.379	0.4140	0.0056	2–16	0.9968
SPE-oGO	0.237	0.0711	0.0679	2–16	0.9977
SPE-rGO	0.034	0.0103	0.0898	2–16	0.9958

4. Conclusions

As experimentally observed in this work, graphene materials were deeply characterized in terms of morphology and optoelectronic properties. The electrochemical behavior upon the addition of GO over a screen-printed electrode in terms of current responses is described. In addition, it is demonstrated that the biofunctionalization capability might have been affected by the level of oxidation of graphene materials (oGO with a C/O of 1.07 and rGO with a C/O of 1.53). These different C/O levels should have contributed in the biosensor performance (better stability due to a better enzyme immobilization onto SPE modified with rGO by hydrophobic interaction) and the decrease of the limit of detection in comparison to the non-modified SPE and the SPE modified with oGO. The results show that the SPE modification with oGO leads to low level Tyrosinase biofunctionality (although much higher than that of the SPE without oGO) while the modification with highly hydrophobic and conductive rGO leads to a higher level of biofunctionalization. This tuning capability of the biosensor response can be of interest for building several other biosensors, including immunosensors and DNA sensors for various applications.

Acknowledgments

MEC (Spain) for MAT2011-25870 grant is acknowledged. The technical support on graphene oxide characterization given by Pablo Garcia, Marcos Rosado, Guillaume Saufer and Javier Saiz Poseu from Institut Català de Nanociència i Nanotecnologia (ICN2) is also acknowledged.

References

- Acik, M., Lee, G., Mattevi, C., Chhowalla, M., Cho, K., Chabal, Y.J., 2010. *Nat. Mater.* 9 (10), 840–845.
- Belding, S.R., Campbell, F.W., Dickinson, E.J.F., Compton, R.G., 2010. *Phys. Chem. Chem. Phys.* 12 (37), 11208–11221.
- Cai, W.W., Piner, R.D., Stadermann, F.J., Park, S., Shaibat, M.A., Ishii, Y., Yang, D.X., Velamakanni, A., An, S.J., Stoller, M., An, J.H., Chen, D.M., Ruoff, R.S., 2008. *Science* 321 (5897), 1815–1817.
- Cheng, M., Yang, R., Zhang, L.C., Shi, Z.W., Yang, W., Wang, D.M., Xie, G.B., Shi, D.X., Zhang, G.Y., 2012. *Carbon* 50 (7), 2581–2587.
- Cuong, T.V., Pham, V.H., Tran, Q.T., Hahn, S.H., Chung, J.S., Shin, E.W., Kim, E.J., 2010. *Mater. Lett.* 64 (3), 399–401.
- Eda, G., Mattevi, C., Yamaguchi, H., Kim, H., Chhowalla, M., 2009. *J. Phys. Chem. C* 113 (35), 15768–15771.
- Fanjul-Bolado, P., Lamas-Ardizana, P.J., Hernandez-Santos, D., Costa-Garcia, A., 2009. *Anal. Chim. Acta* 638 (2), 133–138.
- Gao, X.F., Jang, J., Nagase, S., 2010. *J. Phys. Chem. C* 114 (2), 832–842.
- Geim, A.K., Novoselov, K.S., 2007. *Nat. Mater.* 6 (3), 183–191.
- Karuwan, C., Wisitsoraat, A., Phokharatkul, D., Sriprachuabwong, C., Lomas, T., Nacapricha, D., Tuantranont, A., 2013. *RSC Adv.* 3 (48), 25792–25799.
- Marciano, D.C., Kosynkin, D.V., Berlin, J.M., Sinitskii, A., Sun, Z.Z., Slesarev, A., Alemany, L.B., Lu, W., Tour, J.M., 2010. *Acs Nano* 4 (8), 4806–4814.
- Martin-Fernandez, I., Wang, D.B., Zhang, Y.G., 2012. *Nano Lett.* 12 (12), 6175–6179.
- Mathkar, A., Tozier, D., Cox, P., Ong, P.J., Galande, C., Balakrishnan, K., Reddy, A.L.M., Ajayan, P.M., 2012. *J. Phys. Chem. Lett.* 3 (8), 986–991.
- Morales-Narvaez, E., Merkoci, A., 2012. *24(25)*, 3298–3308.
- Park, S., An, J.H., Piner, R.D., Jung, I., Yang, D.X., Velamakanni, A., Nguyen, S.T., Ruoff, R.S., 2008a. *Chem. Mater.* 20 (21), 6592–6594.

- Park, S., Lee, K.S., Bozoklu, G., Cai, W., Nguyen, S.T., Ruoff, R.S., 2008b. *ACS Nano* 2 (3), 572–578.
- Peng, J., Gao, W., Gupta, B.K., Liu, Z., Romero-Aburto, R., Ge, L.H., Song, L., Alemany, L.B., Zhan, X.B., Gao, G.H., Vithayathil, S.A., Kaiparettu, B.A., Marti, A.A., Hayashi, T., Zhu, J.J., Ajayan, P.M., 2012. *Nano Lett.* 12 (2), 844–849.
- Ping, J., Wang, Y., Fan, K., Wu, J., Ying, Y., 2011. *Biosens. Bioelectron.* 28 (1), 204–209.
- Ping, J., Wang, Y., Ying, Y., Wu, J., 2012. *Anal. Chem.* 84 (7), 3473–3479.
- Salas, E.C., Sun, Z.Z., Luttge, A., Tour, J.M., 2010. *ACS Nano* 4 (8), 4852–4856.
- Shang, J.Z., Ma, L., Li, J.W., Ai, W., Yu, T., Gurzadyan, G.G., 2012. *Sci Rep.* 2.
- Shao, Y.Y., Wang, J., Wu, H., Liu, J., Aksay, I.A., Lin, Y.H., 2010. *Electroanalysis* 22 (10), 1027–1036.
- Shen, J.F., Hu, Y.Z., Shi, M., Lu, X., Qin, C., Li, C., Ye, M.X., 2009. *Chem. Mater.* 21 (15), 3514–3520.
- Song, W., Li, D.-W., Li, Y.-T., Li, Y., Long, Y.-T., 2011. *Biosens. Bioelectron.* 26 (7), 3181–3186.
- Stankovich, S., Dikin, D.A., Piner, R.D., Kohlhaas, K.A., Kleinhammes, A., Jia, Y., Wu, Y., Nguyen, S.T., Ruoff, R.S., 2007. *Carbon* 45 (7), 1558–1565.
- Yang, J., Yu, J.-H., Strickler, J.R., Chang, W.-J., Gunasekaran, S., 2013. *Biosens. Bioelectron.* 47, 530–538.
- Zhang, Y., Zhang, J.Y., Huang, X.L., Zhou, X.J., Wu, H.X., Guo, S.W., 2012. *Small* 8 (1), 154–159.
- Zhu, Y.W., Murali, S., Cai, W.W., Li, X.S., Suk, J.W., Potts, J.R., Ruoff, R.S., 2010. *Adv. Mater.* 22 (35), 3906–3924.

Water Activated Graphene Oxide Transfer Using Wax Printed Membranes for Fast Patterning of a Touch Sensitive Device

Luis Baptista-Pires,[†] Carmen C. Mayorga-Martínez,[†] Mariana Medina-Sánchez,[†] Helena Montón,[†] and Arben Merkoçi^{*,†,‡}

[†]Catalan Institute of Nanoscience and Nanotechnology (ICN2), CSIC and The Barcelona Institute of Science and Technology, Campus UAB, Bellaterra, Barcelona 08193, Spain

[‡]ICREA, Barcelona 08010, Spain

S Supporting Information

ABSTRACT: We demonstrate a graphene oxide printing technology using wax printed membranes for the fast patterning and water activation transfer using pressure based mechanisms. The wax printed membranes have 50 μm resolution, longtime stability and infinite shaping capability. The use of these membranes complemented with the vacuum filtration of graphene oxide provides the control over the thickness. Our demonstration provides a solvent free methodology for printing graphene oxide devices in all shapes and all substrates using the roll-to-roll automatized mechanism present in the wax printing machine. Graphene oxide was transferred over a wide variety of substrates as textile or PET in between others. Finally, we developed a touch switch sensing device integrated in a LED electronic circuit.

KEYWORDS: graphene oxide, wax printed membranes, patterning, transfer, touch sensor



Printed electronics paved the way to a new type of low-cost technologies over plastics and organic substrates for building electrical and electronic devices. Using a wide variety of materials conjugations such as inorganic¹ and organic^{2–4} semiconductors, metals⁵ or insulators⁶ enabled building devices such as Radio Frequency Identification (RFID) systems, light emitting diodes (LED), supercapacitors, thin film transistors, resistors or solar cells. Industry equipment in this area is mainly based on screen-printing technology, flexography, gravure, inkjet and lithography (also as developers of microcontact stamps).^{7–9} More exactly, lithography, flexography and gravure exhibit high setup costs and are advantageous only for high production rates. Additionally, lithography is mainly a chemical or photochemical process with the need for clean room facilities and consumable and expensive photoresists and developers. In the case of screen-printing and inkjet printing, the need for ink development is an issue in terms of viscosity and polymerization. For the singular case of inkjet printing, additionally to the ink development there is the substrate treatment and printing temperature. Despite this, the last two techniques are cost-effective for smaller quantities of printed products. All these technologies possess the need of know-how and specialized personnel as

common characteristic for the development of simple electronics devices.

Fast prototyping rise in the “Maker” or “Do It Yourself” communities have opened venues for fast integration in electronic industry of creative and original devices of all types integrated with the internet of things.^{10–12} This process is done mainly using the techniques described below which become hard in terms of versatility and price for low quantities of prototyping production. Despite 3D printing paving the way for different type of technologies in these areas, great efforts are still needed for the development of new processes for fast printing technologies that can integrate communities making a step forward to knowledge and technology transfer for society.

The importance of graphene oxide (GO) and derivatives such as reduced GO (rGO) has raised in recent years substituting a wide variety of materials for the production of supercapacitors,^{13–18} LED,¹⁹ RFID,²⁰ solar cells²¹ and (bio)-sensors.^{22–25} The ability to pattern and transfer GO without the use of organic toxic compounds (as in lithography), surfactants or polymer based solutions and as in inkjet or screen

Received: September 22, 2015

Accepted: December 21, 2015

Published: December 21, 2015

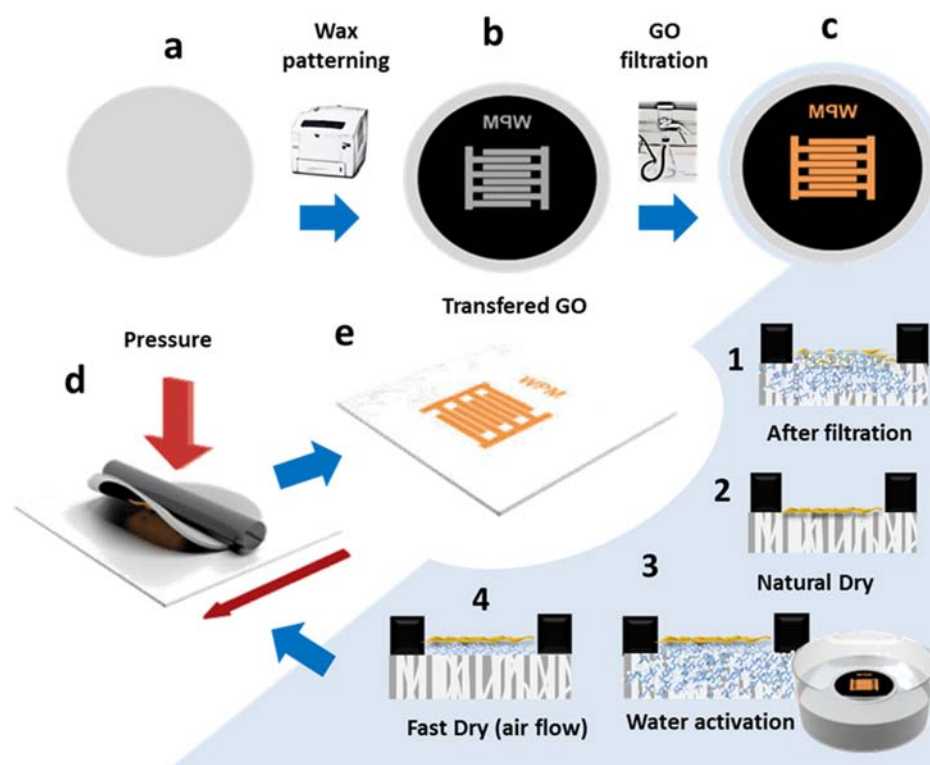


Figure 1. Schematics of the patterning and transfer of GO. (a) Nitrocellulose membrane; (b) WPM; (c) WPM modified with GO, (c1) sheets right after filtrations, (c2) after natural dry, (c3) after water activation, (c4) after fast dry with air flow; (d) transfer of GO by pressure to the substrate; (e) transferred GO pattern.

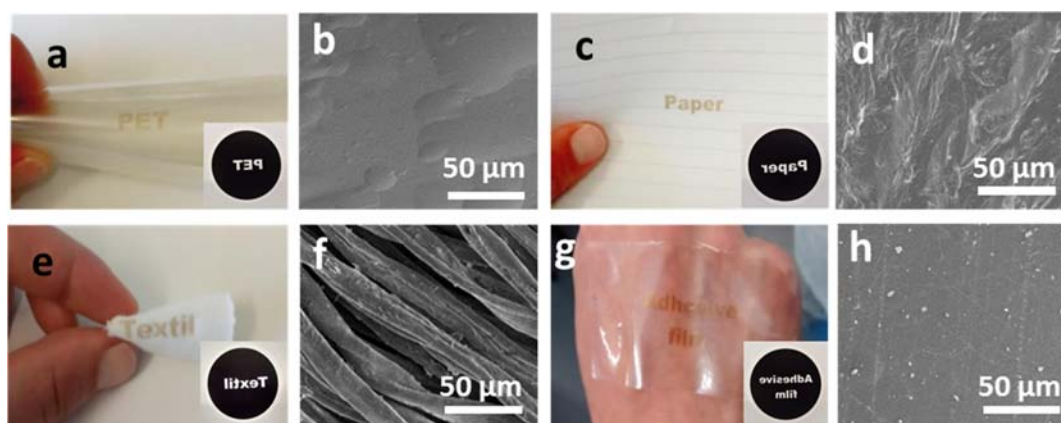


Figure 2. Patterning and transfer over different materials. (a) Patterned GO over PET (inset, WPM for PET); (b) SEM image of patterned rGO over PET. (c) Patterned GO over paper (inset, WPM for paper); (d) SEM image of patterned rGO over paper. (e) Patterned GO over textile t-shirt (inset, WPM for textile); (f) SEM image of patterned rGO over textile. (g) Patterned GO over adhesive film (inset, WPM for adhesive film); (h) SEM image of patterned rGO over the adhesive film.

printing is required given the influence that these compounds can have onto the optoelectronic properties.^{8,9,26–31} In this way, vacuum filtration makes a step forward in this development and has been used for various applications either for transferring thin films of rGO using liquid–air exfoliation leaving a suspended film that can be “fished” by the target substrate;³² or for transferring thin films with nanometer resolution onto substrates by dissolving the nitrocellulose membrane with acetone when in contact with the target substrate.³³ Despite the great advances over the transfer of GO thin films using vacuum filtration described before, patterning technologies are still the handicap/bottleneck of the whole process. Existing transfer technologies do not solve problems

such as GO ink preparation²⁸ or the need for lithographic²⁷ patterning and physical erasure.²⁶ Filling this gap that would lead to an automatized process that controls the thickness and enables the direct patterning of controlled GO structures onto various substrates, in a fast and chemically free transfer mode, without any requirement for ink treatment and being at the same time simple and cost-effective is still a challenging objective in GO printing technologies.

Herein, we propose a methodology for fast patterning and transfer of GO using water activated wax printed membranes (WPM). Wax printing technology is a green, low cost and versatile technology that can be easily performed using the desired shape or image chosen by the user with micrometer

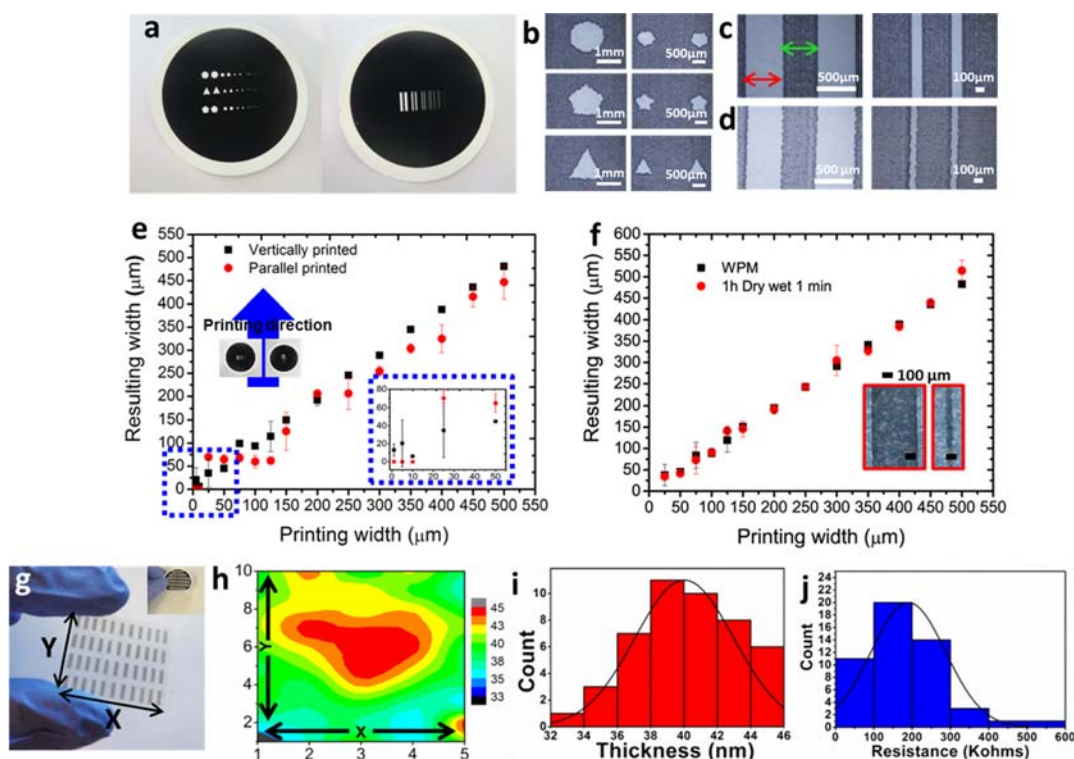


Figure 3. Reproducibility of WPM and transferred patterns. (a) WPM with different forms (left side) and lines (right side). Optical microscope image of the WPM for (b) forms, (c) lines vertically printed, (d) lines parallel printed. (e) Evaluation of vertically and parallel printed WPM of printing width (designed in the computer) and resulting width (patterned onto the NCM). (f) Evaluation of the transferred GO in comparison with WPM widths (inset: optical microscope image of patterned GO lines with 50 and 300 μm). (g) Photo of the patterned lines with 1×4 mm (inset: photo of the transferred GO with the WPM). (h) Variation of the thickness of GO over the patterned substrate area. (i and j) Histogram of the thickness (GO) and resistance (rGO) distribution, respectively.

resolution.^{34,35} Its hydrophobic nature enables to drive GO water suspension over the membrane to the desired regions. This technology coupled with the vacuum filtration provides control over the shape and thickness of GO leaving a patterned GO mesh over the nitrocellulose membrane. In this way, we developed a water activated mechanism to transfer patterned GO over flexible substrates. The roll-to-roll mechanism that outfits the wax printer machine makes this technique suitable for rapid building of plastic, paper or textile electronic platforms. We have used this technique to produce a touch sensitive device over polyethylene terephthalate (PET) for switching a LED on and off.

RESULTS AND DISCUSSION

Figure 1 shows how a nitrocellulose membrane (Figure 1a) is patterned onto the desired shape (Figure 1b) using a wax printer machine. To form the GO pattern, the inverse pattern is printed onto the membrane surface. The wax clogs the pores of the membrane wherever it is printed leaving the nonwax containing regions (gray in the reverse pattern) unclogged. The WPM is set onto the filtering glass, and the suspension of GO (at a desired concentration) is filtered, leaving a GO mesh on top of the WPM (Figure 1c1). The WPM is left to dry (Figure 1c2), and then it is water activated by rewetting in a water bath (Figure 1c3), fast dried using air flow on the back part of the membrane (Figure 1c4), and transferred by pressure (Figure 1d,1e) to the desired target substrate.

When the GO mesh over the WPM is dried, which takes between 30 and 60 min (Figure 1c2), the interactions with the membrane are in their stronger phase which incapacitate the

transfer of GO. On the other hand, right after filtration (Figure 1c1), the transfer can, for instance, spread GO all over the substrate depending on the absorptive properties of the target material.

According to this, we have produced different WPMs through wax printing and modified them with GO (inset Figure 2a,c,e,g). We used the wax printer which is outfitted with roll-to-roll hardware for fast and automatized transfer of GO over different flexible substrates such as PET, textile t-shirt, paper and adhesive film as demonstrated in Figure 2 using procedure from Figure 1. As proof of concept, we transferred a modified WPM using a spatula (Figure S1) where a simple image of the Nobel coin can be transformed into a black and white WPM (Figure S1a–c) and transferred over a window glass by simple hand pressure of the spatula (Figure S1d).

To determine the resolution, we produced different WPMs composed of different geometric forms and lines (Figure 3a). The WPMs shown in Figure 3b exhibited acceptable designs over a range of 500 μm for circles, once the circle geometry gets degraded over lower size resolutions. The direction of the wax printing (parallel or vertical) was an important parameter to evaluate, as it affects the resolution and the shape of the patterned wax. Figure 3c shows wax lines printed vertically and Figure 3d shows lines parallel printed. The wax line, represented in Figure 3c as the green cross, has a minimum resolution of 100 μm which is consistent with literature—values under 100 μm are simply not patterned from the wax printing machine. We investigated the resolution of the unclogged space represented in Figure 3c as the red cross once will be the minimum resolution of the future GO pattern.

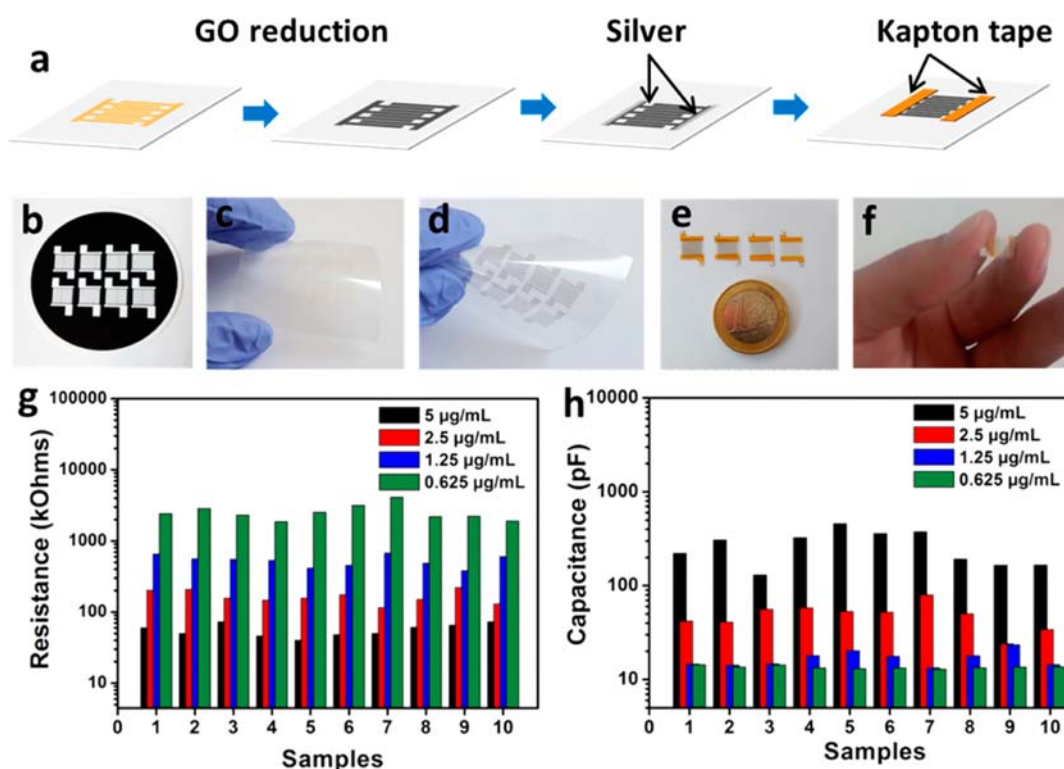


Figure 4. Electrical characterization of the IDE. (a) Schematics of the IDE fabrication. (b) WPM used for the design of GO IDE. (c) IDE transferred over PET in their oxidized form. (d) IDE transferred over PET in their reduced form. (e) Photo of all IDEs with different filtered volumes (5 mL of 5, 2.5, 1.25, 0.625 µg/mL, from left to right). (f) IDE with a filtrated volume of 0.625 µg/mL. (g) Resistance of 10 IDEs. (h) Capacitance of 10 IDEs.

A resolution of 50 µm (Figure 3e) was obtained when the WPM was printed vertically. For lines parallel printed, the variation in the line size is determined by the bumps and the printing and the resulting width are not consistent. According to this, to define long narrow lines it is better having them printed perpendicular to the printer feed direction (so one avoids poor line to line printer registration issues). According to the technology features described before, the resolution of the WPMs is mainly a hardware characteristic of our printing machine. We believe that hardware evolution will entail advances in resolution factors, and in this way, our technique could possibly in the future compete in the microelectronic device fabrication domain. On the other hand, the main principle of our process could be used, and the coupling between photolithography or inkjet printing could produce masks over the nitrocellulose membranes with the technical and cost losses associated with it (as described elsewhere in this work). The ink development such as using smaller GO sheet size should be performed so as to reach better resolution. Despite this, we believe that even the current printing resolution of the WPMs is still efficient for the production of devices such as supercapacitors, solar cells, sensors and biosensors. The lateral spreading of the wax across the WPM at room temperature was studied over 5 months (Figure S2) and any significant deformation or spreading was not observed and therefore we concluded that these WPMs are stable over the long-term. Each WPM has a filtration area that is dependent on the patterned design influencing the filtration rate (time) and the vertical size of GO film.

We used vertically printed WPMs (Figure 3a) for studying the transfer process over PET using the roll-to-roll mechanism

that outfits the wax printing machine due to the automation that it provides. Accordingly, 5 mL of a GO concentration of 0.01 mg/mL was placed into the filtering flask, filtered and left to dry for 1 h. After 1 h of drying followed by 1 min wetting and drying process, the WPM was placed in contact with PET substrate and transferred using the wax printer machine. The transfer efficiency to PET using the mass weight of the WPM before and after the transfer ($n = 10$) was calculated obtaining a transfer efficiency of 99.74%. The minimum resolution of GO transferred into PET was 50 µm (Figure 3f) which is in accordance with the resolution of the WPM described before in this work. The transfer mechanism can be understood under the focus of the interlayer distance between GO sheet upon filtration. Filtration of GO layers originates a compressive stacking forming a compact film with low quantity of water molecules in between the layers. According to this, while rewetting, the water is absorbed in the surface of the GO film due to the hydrophilic nature of GO causing the release of the GO film from the membrane. We studied this evolution during one month and the transfer was still effective as reported in Figure S3. The hydrophobicity of GO sheets quickly increased upon drying as determined in Figure S4 and slowed down upon 1 h to 1 month. It is also known that the reduction of GO is slow at room temperature and normal life conditions which opens to us a big time window to process the transfer. The transfer pressure should be suitable to reach the necessary strength to be applied between GO mesh and the target substrate to avoid the 25 µm wax height (which can be considered as the maximum vertical size that GO film can have, Figure S5) and make direct contact between the GO mesh and the target substrate.

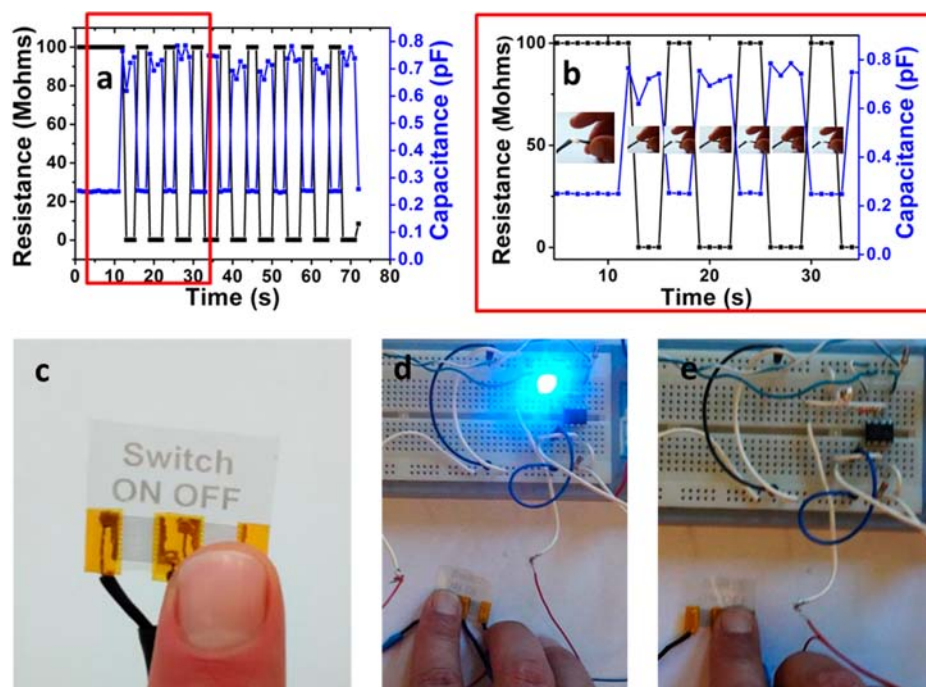


Figure 5. Touch sensitive device. (a) Variation of the resistance/capacitance upon touch. (b) Zoom of the initial 30 s of (a). (c) IDEs used for this experiment. (d) IDE turning on a LED upon touch. (e) IDE turning off a LED upon touch.

We have built a mask presented in Figure 3g (inset) to address the reproducibility of the transfer in terms of thickness and resistance. In Figure 3h, one can see the variation of the thickness of GO over the patterned substrate area. It has shown uniformity of the different lines printed with a medium thickness all over the substrate of 40 ± 3 nm (Figure 3i). The patterned GO films were reduced when immersed in 1 mg/mL of ascorbic acid at 30°C for 48 h (Figure 3g) and wired using silver ink. The sheet resistance was measured three times using a tester showing a mean distribution of 190.08 ± 97.15 k Ω (Figure 3j). The resistance and thickness variations of our methodology can be related to a myriad of factors such as the nature of our method by itself (the patterned wax should favor the fluidic movement over the membrane upon filtration), the circular filtration area and the round shape of the metallic sieve in the filtration flask which allows the GO to be filtrated in the central areas rather than in the surrounding areas, and the reduction methodology.^{36–41} We believe that all these aspects can, in the future, be optimized and developed accordingly and the scalability of the process could diminish and improve these factors. Additionally, we performed an adhesive-tape-peel-off wipe test⁴² in order to determine the stability of the conductive patterns (Figure S6 and Table S1). A different prepared film avoiding silver wiring was used in order to establish maximum contact between the adhesive tape and the rGO tracks area. The same GO concentration (0.01 mg/mL) was used, and after 5 peel-off counts, the resistance increased from 282.44 ± 93.02 to 326.75 ± 129.43 k Ω , which means an increase of 44.31 k Ω in mean resistance. This can be attributed to the consecutive peeling of few layer graphene⁴³ and the contact stretching of the tester connections with the rGO tracks. According to this, our conductive tracks appear to be stable, avoiding any treatments to substrate or to the patterned conductive tracks.

As reported in Figure 4a, we have developed interdigitated electrodes (IDE) using the mask presented in Figure 4b and filtered different concentrations of GO solutions in order to

determine the electrical properties dependence on the vertical size of GO film. Accordingly, GO IDEs were fabricated using the procedure developed before using 1 h of drying and water activation methodology over PET. The GO IDEs (Figure 4c) were reduced (Figure 4d) to improve the electronic properties, using ascorbic acid as a reducing agent. Using four different concentrations (5 mL of 5, 2.5, 1.25, 0.625 $\mu\text{g/mL}$; Figure 4e), we studied the evolution in terms of capacitance, resistance and vertical size.

According to this, with a decrease of a factor of 2 over the concentration of GO, the thickness was 38.9 ± 2.3 , 24.5 ± 0.7 , 19.8 ± 0.5 , and 14.9 ± 0.8 nm. The resistance varied from 57 ± 12 , 166 ± 34 , 531 ± 98 , and 2557 ± 679 k Ω with the decrease of concentration. The capacitance decreased from 270 ± 110 , 49 ± 15 , 17 ± 3 , and 13.2 ± 0.5 pF. We believe that the resistance and capacitance values would reach saturation with the consecutive increase of GO thickness (200 nm to 500 nm for instance), mainly due to the lack of effectiveness of our reduction methodology to achieve the intrinsic layers in the case of a thicker GO film (being the reduction process only effective on the uppermost layers).^{18,33} In this way, the variation of the capacitive properties over different electrodes with similar resistance can be related with the intrinsic properties of GO upon reduction once all the IDE where reduced submerged in ascorbic acid which can possibly alter the intrinsic properties such as the interlayer distance or the surface area exposed to the electrolyte. We expect that these properties can be tuned by the reduction method or either in the in situ development of GO foam-like materials to develop extreme capacitive characteristics.^{13,14,17,44,45}

Using the 60 nm IDE, we measured the resistance and capacitive properties upon the interaction with a human finger. As shown in Figure 5a,b upon touch, the circuit is closed and the resistance changes from >100 M Ω (cannot be read in a contact tester) to ≈ 110 k Ω . The capacitance is also changed from 0.25 pF to approximately 0.75 pF. We produced a touch

sensing device using an electronic circuit (Figure S7) with interest for real applications making the capacitive/resistive behavior of this IDE suitable for touch operations such as LED switcher (Figure 5c). Using this, we could operate a LED turning it ON (Figure 5d) and OFF (Figure 5d). A movie of the operation of the switcher was additionally obtained (can be seen in Movie S1). The possibility of having GO/rGO interfaces in one single device is also demonstrated. Despite similar circuitry development has been performed by inkjet printing,⁴⁶ when establishing a comparison with the proposed WPM-based printing, it demonstrates some advantages being a very simple patterning mode, avoiding optimization time of the ink (viscosity, printing temperature, GO concentration used and GO flake size), long chemical substrate treatment and coffee-ring effects. Our technology also can be used in the future for fast patterning of transparent conductive circuitry without the need to develop new GO matrix requested by inkjet printing or other printing technologies.

The proposed technology opens new venues for direct patterning of GO while filtering using a total green and biological friendly material such as wax and the possibility for long-term transfer using the water activation and roll-to-roll pressure. The methodology is automatized, with control over the *x*, *y* and *z* directions and easily scalable. The long-term stability that possesses opens the possibility for in-field applications. In addition, it can be tuned from a simple patterning methodology (the WPM itself can be turned into simple microfluidic or electronic device made of GO) to a transferring methodology (one could transfer GO without patterning for a wide variety of substrates just by a mechanical actuation using the water activation mechanism). Moreover, one can look at this technology as a nonchemical, clean and polymer free self-adhesive or water activated adhesive for direct patterning of GO devices. We believe a WPM could in the future perform multifunction's that are nowadays applications of lithography such as PDMS stamps molding.

The proposed patterning technique also can be adapted after right optimizations to a wide variety of materials such as silicon nanowires,^{47,48} carbon nanotubes⁴⁹ or 2D materials⁵⁰ (such as graphene, MOS₂, WSe₂ or boron nitride). The corresponding matrix of nanomaterial-based inks must avoid the hydrophobic forces of the wax, should not dissolve the membrane and have target substrate affinity. This could be achieved using aqueous solution (as in the current GO printing) or with adequate chemically modified materials, ion intercalated solutions or surfactant suspensions followed by optimization of the transfer process. The possibility to apply the proposed technology to other materials will open the way to fabrication of other devices and many other applications with interest for various fields. Despite the fact that further work will be needed in this area, we believe that the proposed technology will open new opportunities for GO (or other nanomaterials)-based devices. This novel and versatile WPM-based printing technology is advantageous and disruptive in comparison to existing/similar techniques reported earlier.^{32,33,51} The WPMs can in a near future open many other application fields taking advantages of each fabrication step of the current technology (presented in Figure 1) either separately or all together.

CONCLUSIONS

In summary, we have reported a new, versatile, low cost and customizable method for patterning GO onto a myriad of substrates through highly stable, microscale WPMs that can be

seen as water activated "adhesives". The ability and stability of these WPMs in consonance with the properties of GO makes this technique versatile and easy to handle. These masks enable controlled shaped filtration and transfer of different thickness's of GO in various shapes of interest for different applications with a minimum resolution of 50 μm . The GO-printing technology that we report here is advantageous over previously reported methods for fabrication of GO-based devices in terms of ease, versatility, cost and potential end-applications. This long-term transfer of GO is promising to implement in areas that are not suitable to have a laboratory such as underdeveloped countries, opening the way for in-field transfer of GO. This could enable future uses such as *in situ* transfer of supercapacitor, a solar cell or a LED among others, for wearable or portable applications. This methodology can pave the way for intuitive soft electronics and fast prototyping in the "maker" community, and finally, we believe the step toward industrial scalability can be easily demonstrated for disposable humanized sensing technologies.

METHODS

Wax Printing Characterization. The nitrocellulose membranes used are hydrophilic and have a pore size of 0.025 μm and a diameter of 47 mm. The wax was printed with a Xerox ColorQube 8570 printer (which is compatible with Windows, MacOS and UNIX). All drawings of the electrode patterns were done on Corel Draw. The high-resolution printing mode was always chosen and the membranes were used 5 min after printing, as a compromise to minimize spreading and maximize drying of the wax. Optical microscopy images of the wax-patterned membranes were obtained on a Nikon Eclipse LV100 microscope with a 20 \times /0.45 objective lens.

GO Characterization. All devices were reduced at the same time to avoid irreproducibilities and to make conductive structures, once GO is highly resistive material. The reduction efficiency was assessed by X-ray Photoelectron Spectroscopy (XPS) (Figure S8) and Scanning Electron Microscopy (SEM) (Figure S9).

The GO was provided by Angstrom Materials. When needed, it was reduced submerging the electrode in ascorbic acid vapor at 30 $^{\circ}\text{C}$ for 48 h. All GO electrodes were reduced at the same time to avoid reduction variations. Aqueous suspensions of GO at various concentrations using a 1 L vacuum-filtering flask, 300 mL glass filter holder and 47 mm SS screen (1/Pk). The WPMs were transferred using the wax printing machine described before. The thickness was determined using a Elipsometer Rudolph AutoEl III.

The samples were electrically characterized using Autolab302 potentiostat/galvanostat/frequency-response analyzer PGST30, controlled by GPES/FRA Version 4.9. The X-ray Photoelectron Spectroscopy (XPS) measurements were performed with a Phoibos 150 analyzer (SPECS GmbH, Berlin, Germany) in ultrahigh vacuum conditions (base pressure 1×10^{-10} mbar) with a monochromatic aluminum $K\alpha$ X-ray source (1486.74 eV). The energy resolution as measured by the fwhm of the Ag 3d5/2 peak for a sputtered silver foil was 0.58 eV. Scanning Electron Microscopy (SEM) was done on a FEI Quanta FEG (pressure, 70 Pa; HV, 20 kV; and spot, four).

ASSOCIATED CONTENT

Supporting Information

The Supporting Information is available free of charge on the ACS Publications website at DOI: 10.1021/acsnano.5b05963.

Transfer of WPM GO mesh to glass using a spatula; optical microscopy characterization of WPM; evaluation of printing and resulting width of the WPM before and after transfer and GO transfer onto PET at different drying time; hydrophobicity of GO film over time filtered on nitrocellulose membranes; SEM characterization of WPM; circuit applied for the touch sensor device; optical

characterization of GO and rGO; SEM characterization of GO and rGO (PDF)
Movie S1: A video of the working switcher (AVI)

AUTHOR INFORMATION

Corresponding Author

*E-mail: arben.merkoci@icn.cat.

Author Contributions

L.B.-P. and A.M. conceived and designed the study. L.B.-P. fabricated the devices and performed the experiments. C.C.M.-M. ran the electric measurements. M.M.-S. and H.M. conceived the different designed platforms.

Notes

The authors declare no competing financial interest.

ACKNOWLEDGMENTS

This work was supported by The European Commission Program, FP7-OCEAN, SMS Project (613844). ICN2 acknowledges support from the Severo Ochoa Program (MINECO, Grant SEV-2013-0295). Nanobiosensors and Bioelectronics Group acknowledges Generalitat de Catalunya for SGR support and the authors would like to acknowledge MICINN for funding this project (grant MAT2014-52485-P; grant MAT2011-25870 for BES-2012-056022).

REFERENCES

- (1) Fang, X.; Bando, Y.; Gautam, U. K.; Ye, C.; Golberg, D. Inorganic Semiconductor Nanostructures and Their Field-Emission Applications. *J. Mater. Chem.* **2008**, *18*, 509–522.
- (2) Fenwick, O.; Bozec, L.; Credgington, D.; Hammiche, A.; Lazzerini, G. M.; Silberberg, Y. R.; Cacialli, F. Thermochemical Nanopatterning of Organic Semiconductors. *Nat. Nanotechnol.* **2009**, *4*, 664–668.
- (3) Mathijssen, S. G. J.; Smits, E. C. P.; van Hal, P. A.; Wondergem, H. J.; Ponomarenko, S. A.; Moser, A.; Resel, R.; Bobbert, P. A.; Kemerink, M.; Janssen, R. A. J.; de Leeuw, D. M.; et al. Monolayer Coverage and Channel Length Set the Mobility in Self-Assembled Monolayer Field-Effect Transistors. *Nat. Nanotechnol.* **2009**, *4*, 674–680.
- (4) Zhang, Q.; Atay, T.; Tischler, J. R.; Bradley, M. S.; Bulovic, V.; Nurmikko, A. V. Highly Efficient Resonant Coupling of Optical Excitations in Hybrid Organic/Inorganic Semiconductor Nanostructures. *Nat. Nanotechnol.* **2007**, *2*, 555–559.
- (5) Dong, T.-Y.; Chen, W.-T.; Wang, C.-W.; Chen, C.-P.; Chen, C.-N.; Lin, M.-C.; Song, J.-M.; Chen, I.-G.; Kao, T.-H. One-Step Synthesis of Uniform Silver Nanoparticles Capped by Saturated Decanoate: Direct Spray Printing Ink to Form Metallic Silver Films. *Phys. Chem. Chem. Phys.* **2009**, *11*, 6269–6275.
- (6) Sivaramakrishnan, S.; Chia, P.-J.; Yeo, Y.-C.; Chua, L.-L.; Ho, P. K. H. Controlled Insulator-to-Metal Transformation in Printable Polymer Composites with Nanometal Clusters. *Nat. Mater.* **2007**, *6*, 149–155.
- (7) Suganuma, K. *Introduction to Printed Electronics*, 1 ed.; Springer-Verlag: New York, 2014; pp VI, 124.
- (8) Dua, V.; Surwade, S. P.; Ammu, S.; Agnihotra, S. R.; Jain, S.; Roberts, K. E.; Park, S.; Ruoff, R. S.; Manohar, S. K. All-Organic Vapor Sensor Using Inkjet-Printed Reduced Graphene Oxide. *Angew. Chem., Int. Ed.* **2010**, *49*, 2154–2157.
- (9) Lee, J. S.; Kim, N. H.; Kang, M. S.; Yu, H.; Lee, D. R.; Oh, J. H.; Chang, S. T.; Cho, J. H. Wafer-Scale Patterning of Reduced Graphene Oxide Electrodes by Transfer-and-Reverse Stamping for High Performance OFETs. *Small* **2013**, *9*, 2817–2825.
- (10) <http://www.nature.com/news/2005/050404/full/news050404-3.html> (accessed April 8, 2015).
- (11) <http://time.com/104210/maker-faire-maker-movement/> (accessed April 8, 2015).
- (12) Moorefield-Lang, H. M. Makers in the library: Case Studies of 3D Printers and Maker Spaces in Library Settings. *Library Hi Tech* **2014**, *32*, 583–593.
- (13) Zhu, Y.; Murali, S.; Stoller, M. D.; Ganesh, K. J.; Cai, W.; Ferreira, P. J.; Pirkle, A.; Wallace, R. M.; Cychosz, K. A.; Thommes, M.; Su, D.; Stach, E. A.; Ruoff, R. S.; et al. Carbon-Based Supercapacitors Produced by Activation of Graphene. *Science* **2011**, *332*, 1537–1541.
- (14) Zhang, L. L.; Zhao, X.; Stoller, M. D.; Zhu, Y.; Ji, H.; Murali, S.; Wu, Y.; Perales, S.; Clevenger, B.; Ruoff, R. S.; et al. Highly Conductive and Porous Activated Reduced Graphene Oxide Films for High-Power Supercapacitors. *Nano Lett.* **2012**, *12*, 1806–1812.
- (15) Niu, Z. Q.; Zhang, L.; Liu, L.; Zhu, B. W.; Dong, H. B.; Chen, X. D. All-Solid-State Flexible Ultrathin Micro-Supercapacitors Based on Graphene. *Adv. Mater.* **2013**, *25*, 4035–4042.
- (16) Gao, W.; Singh, N.; Song, L.; Liu, Z.; Reddy, A. L. M.; Ci, L.; Vajtai, R.; Zhang, Q.; Wei, B.; Ajayan, P. M.; et al. Direct Laser Writing of Micro-Supercapacitors on Hydrated Graphite Oxide Films. *Nat. Nanotechnol.* **2011**, *6*, 496–500.
- (17) El-Kady, M. F.; Kaner, R. B. Scalable Fabrication of High-Power Graphene Micro-Supercapacitors for Flexible and On-Chip Energy Storage. *Nat. Commun.* **2013**, *4*, 1475–1483.
- (18) Wu, Z. S.; Parvez, K.; Feng, X. L.; Mullen, K. Graphene-Based In-Plane Micro-Supercapacitors with High Power and Energy Densities. *Nat. Commun.* **2013**, *4*, 2487–2494.
- (19) Wang, X.; Tian, H.; Mohammad, M. A.; Li, C.; Wu, C.; Yang, Y.; Ren, T.-L. A Spectrally Tunable All-Graphene-Based Flexible Field-Effect Light-Emitting Device. *Nat. Commun.* **2015**, *6*, 7767–7767.
- (20) Lee, J. S.; Oh, J.; Jun, J.; Jang, J. Wireless Hydrogen Smart Sensor Based on Pt/Graphene-Immobilized Radio-Frequency Identification Tag. *ACS Nano* **2015**, *9*, 7783–7790.
- (21) Liu, J.; Kim, G.-H.; Xue, Y.; Kim, J. Y.; Baek, J.-B.; Durstock, M.; Dai, L. Graphene Oxide Nanoribbon as Hole Extraction Layer to Enhance Efficiency and Stability of Polymer Solar Cells. *Adv. Mater.* **2014**, *26*, 786–790.
- (22) Morales-Narvaez, E.; Perez-Lopez, B.; Pires, L. B.; Merkoci, A. Simple Forster Resonance Energy Transfer Evidence for the Ultrahigh Quantum Dot Quenching Efficiency by Graphene Oxide Compared to Other Carbon Structures. *Carbon* **2012**, *50*, 2987–2993.
- (23) Mannoor, M. S.; Tao, H.; Clayton, J. D.; Sengupta, A.; Kaplan, D. L.; Naik, R. R.; Verma, N.; Omenetto, F. G.; McAlpine, M. C. Graphene-Based Wireless Bacteria Detection on Tooth Enamel. *Nat. Commun.* **2012**, *3*, 763–770.
- (24) Yoon, H. J.; Kim, T. H.; Zhang, Z.; Azizi, E.; Pham, T. M.; Paoletti, C.; Lin, J.; Ramnath, N.; Wicha, M. S.; Hayes, D. F.; Simeone, D. M.; Nagrath, S.; et al. Sensitive Capture of Circulating Tumour Cells by Functionalized Graphene Oxide Nanosheets. *Nat. Nanotechnol.* **2013**, *8*, 735–741.
- (25) Morales-Narvaez, E.; Merkoci, A. Graphene Oxide as an Optical Biosensing Platform. *Adv. Mater.* **2012**, *24*, 3298–3308.
- (26) He, Q. Y.; Wu, S. X.; Gao, S.; Cao, X. H.; Yin, Z. Y.; Li, H.; Chen, P.; Zhang, H. Transparent, Flexible, All-Reduced Graphene Oxide Thin Film Transistors. *ACS Nano* **2011**, *5*, 5038–5044.
- (27) Pang, S. P.; Tsao, H. N.; Feng, X. L.; Mullen, K. Patterned Graphene Electrodes from Solution-Processed Graphite Oxide Films for Organic Field-Effect Transistors. *Adv. Mater.* **2009**, *21*, 3488–3491.
- (28) Lu, G.; Zhou, X. Z.; Li, H.; Yin, Z. Y.; Li, B.; Huang, L.; Boey, F.; Zhang, H. Nanolithography of Single-Layer Graphene Oxide Films by Atomic Force Microscopy. *Langmuir* **2010**, *26*, 6164–6166.
- (29) Jeong, H. Y.; Kim, J. Y.; Kim, J. W.; Hwang, J. O.; Kim, J. E.; Lee, J. Y.; Yoon, T. H.; Cho, B. J.; Kim, S. O.; Ruoff, R. S.; Choi, S. Y.; et al. Graphene Oxide Thin Films for Flexible Nonvolatile Memory Applications. *Nano Lett.* **2010**, *10*, 4381–4386.
- (30) Kim, T.; Kim, H.; Kwon, S. W.; Kim, Y.; Park, W. K.; Yoon, D. H.; Jang, A. R.; Shin, H. S.; Suh, K. S.; Yang, W. S.; et al. Large-Scale Graphene Micropatterns via Self-Assembly-Mediated Process for Flexible Device Application. *Nano Lett.* **2012**, *12*, 743–748.

- (31) Wang, S.; Ang, P. K.; Wang, Z. Q.; Tang, A. L. L.; Thong, J. T. L.; Loh, K. P. High Mobility, Printable, and Solution-Processed Graphene Electronics. *Nano Lett.* **2010**, *10*, 92–98.
- (32) Wang, X.; Xiong, Z.; Liu, Z.; Zhang, T. Exfoliation at the Liquid/Air Interface to Assemble Reduced Graphene Oxide Ultrathin Films for a Flexible Noncontact Sensing Device. *Adv. Mater.* **2015**, *27*, 1370–1375.
- (33) Eda, G.; Fanchini, G.; Chhowalla, M. Large-Area Ultrathin Films of Reduced Graphene Oxide as a Transparent and Flexible Electronic Material. *Nat. Nanotechnol.* **2008**, *3*, 270–274.
- (34) Carrilho, E.; Martinez, A. W.; Whitesides, G. M. Understanding Wax Printing: A Simple Micropatterning Process for Paper-Based Microfluidics. *Anal. Chem.* **2009**, *81*, 7091–7095.
- (35) Lu, Y.; Shi, W. W.; Qin, J. H.; Lin, B. C. Fabrication and Characterization of Paper-Based Microfluidics Prepared in Nitrocellulose Membrane By Wax Printing. *Anal. Chem.* **2010**, *82*, 329–335.
- (36) Zhang, J.; Yang, H.; Shen, G.; Cheng, P.; Zhang, J.; Guo, S. Reduction of Graphene Oxide via L-Ascorbic Acid. *Chem. Commun.* **2010**, *46*, 1112–1114.
- (37) Shin, H. J.; Kim, K. K.; Benayad, A.; Yoon, S. M.; Park, H. K.; Jung, I. S.; Jin, M. H.; Jeong, H. K.; Kim, J. M.; Choi, J. Y.; Lee, Y. H.; et al. Efficient Reduction of Graphite Oxide by Sodium Borohydride and Its Effect on Electrical Conductance. *Adv. Funct. Mater.* **2009**, *19*, 1987–1992.
- (38) Gao, W.; Alemany, L. B.; Ci, L. J.; Ajayan, P. M. New Insights Into the Structure and Reduction of Graphite Oxide. *Nat. Chem.* **2009**, *1*, 403–408.
- (39) Shin, K. H.; Jang, Y.; Kim, B. S.; Jang, J.; Kim, S. H. Highly Conductive Reduced Graphene Oxide Produced via Pressure-Assisted Reduction at Mild Temperature for Flexible and Transparent Electrodes. *Chem. Commun.* **2013**, *49*, 4887–4889.
- (40) Ping, J.; Wang, Y.; Fan, K.; Wu, J.; Ying, Y. Direct Electrochemical Reduction of Graphene Oxide on Ionic Liquid Doped Screen-Printed Electrode and its Electrochemical Biosensing Application. *Biosens. Bioelectron.* **2011**, *28*, 204–209.
- (41) Feng, H.; Cheng, R.; Zhao, X.; Duan, X.; Li, J. A Low-Temperature Method to Produce Highly Reduced Graphene Oxide. *Nat. Commun.* **2013**, *4*, 1539–1546.
- (42) Kim, S.-K.; Liu, T.; Wang, X. Flexible, Highly Durable, and Thermally Stable SWCNT/Polyimide Transparent Electrodes. *ACS Appl. Mater. Interfaces* **2015**, *7*, 20865–20874.
- (43) Novoselov, K. S.; Fal'ko, V. I.; Colombo, L.; Gellert, P. R.; Schwab, M. G.; Kim, K. A Roadmap for Graphene. *Nature* **2012**, *490*, 192–200.
- (44) Gao, W.; Singh, N.; Song, L.; Liu, Z.; Reddy, A. L. M.; Ci, L. J.; Vajtai, R.; Zhang, Q.; Wei, B. Q.; Ajayan, P. M.; et al. Direct Laser Writing of Micro-Supercapacitors on Hydrated Graphite Oxide Films. *Nat. Nanotechnol.* **2011**, *6*, 496–500.
- (45) Niu, Z.; Chen, J.; Hng, H. H.; Ma, J.; Chen, X. A Leavening Strategy to Prepare Reduced Graphene Oxide Foams. *Adv. Mater.* **2012**, *24*, 4144–4150.
- (46) Huang, L.; Huang, Y.; Liang, J.; Wan, X.; Chen, Y. Graphene-Based Conducting Inks for Direct Inkjet Printing of Flexible Conductive Patterns and Their Applications in Electric Circuits and Chemical Sensors. *Nano Res.* **2011**, *4*, 675–684.
- (47) Peng, C.; Gao, J.; Wang, S.; Zhang, X.; Zhang, X.; Sun, X. Stability of Hydrogen-Terminated Surfaces of Silicon Nanowires in Aqueous Solutions. *J. Phys. Chem. C* **2011**, *115*, 3866–3871.
- (48) Heo, K.; Cho, E.; Yang, J.-E.; Kim, M.-H.; Lee, M.; Lee, B. Y.; Kwon, S. G.; Lee, M.-S.; Jo, M.-H.; Choi, H.-J.; Hyeon, T.; Hong, S.; et al. Large-Scale Assembly of Silicon Nanowire Network-Based Devices Using Conventional Microfabrication Facilities. *Nano Lett.* **2008**, *8*, 4523–4527.
- (49) Wu, Z. C.; Chen, Z. H.; Du, X.; Logan, J. M.; Sippel, J.; Nikolou, M.; Kamaras, K.; Reynolds, J. R.; Tanner, D. B.; Hebard, A. F.; Rinzler, A. G.; et al. Transparent, Conductive Carbon Nanotube Films. *Science* **2004**, *305*, 1273–1276.
- (50) Nicolosi, V.; Chhowalla, M.; Kanatzidis, M. G.; Strano, M. S.; Coleman, J. N. Liquid Exfoliation of Layered Materials. *Science* **2013**, *340*, 1226419–1226437.
- (51) Hyun, W. J.; Park, O. O.; Chin, B. D. Foldable Graphene Electronic Circuits Based on Paper Substrates. *Adv. Mater.* **2013**, *25*, 4729–4734.

Supporting Information

Water Activated Graphene Oxide Transfer Using Wax Printed Membranes for Fast Patterning of a Touch Sensitive Device

Luis Baptista-Pires¹, Carmen C. Mayorga-Martínez¹, Mariana Medina-Sánchez¹, Helena Montón¹ and Arben Merkoçi^{1,2,}*

¹ Nanobioelectronics & Biosensors Group, Catalan Institute of Nanoscience and Nanotechnology, ICN2, Campus de la UAB, 08193 Bellaterra, Barcelona, Spain

² ICREA, Barcelona, Spain

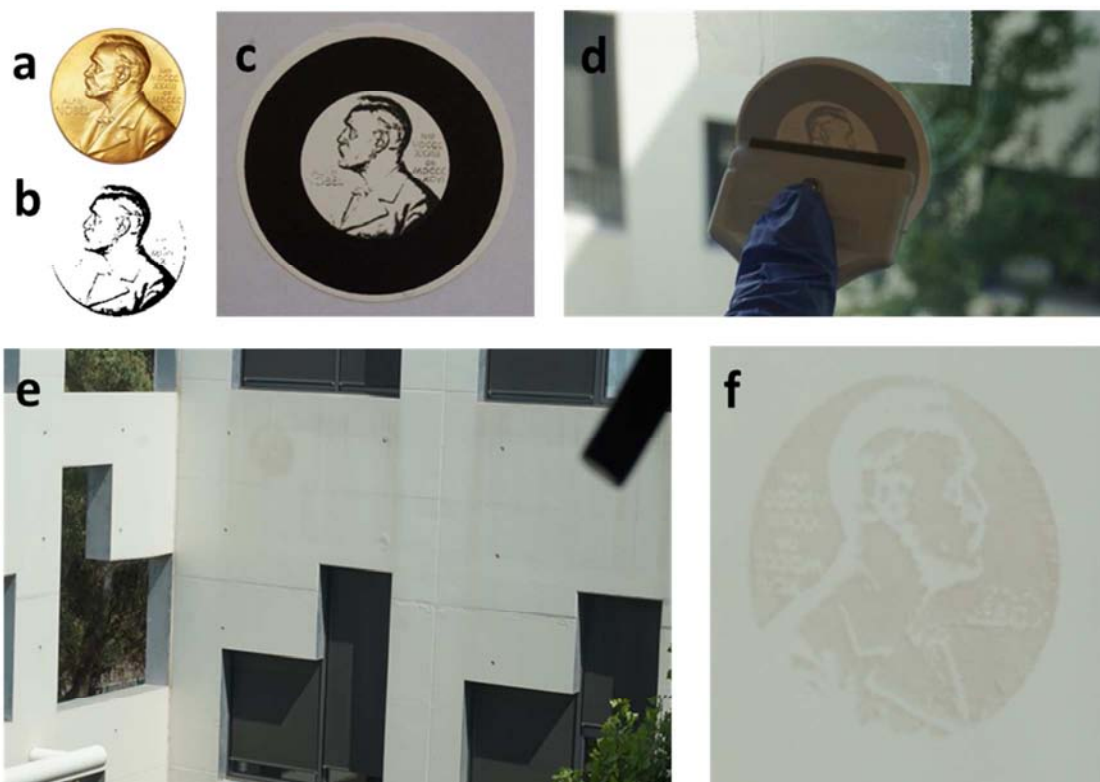


Figure S1. GO transferred over glass using a spatula.

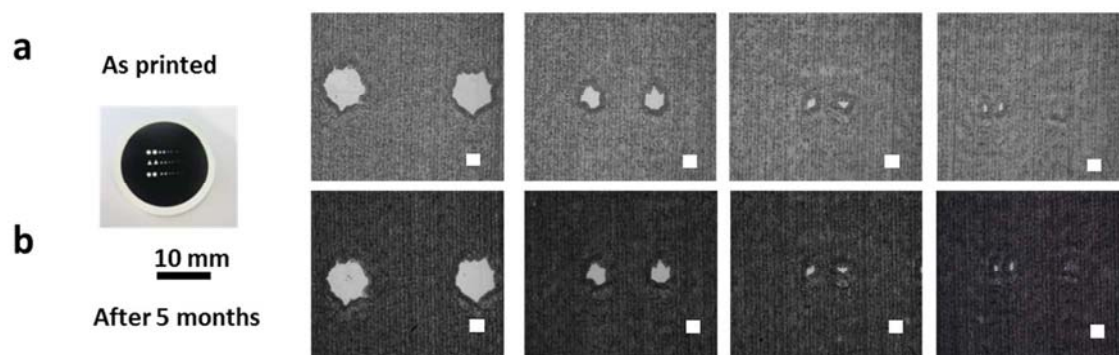


Figure S2. Optical microscopy characterisation of the WPM. a) immediately after printing and b) 5 months after printing.

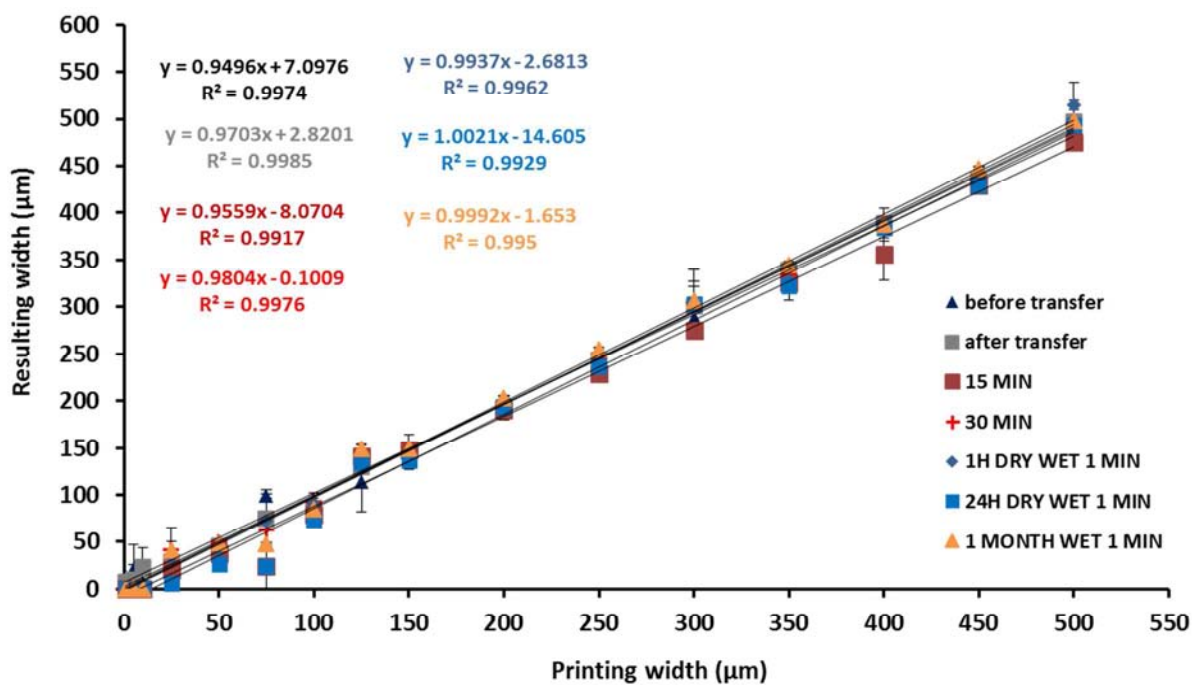


Figure S3. Evaluation of printing and resulting width of the WPM before and after transfer and GO transfer onto PET at different drying time.

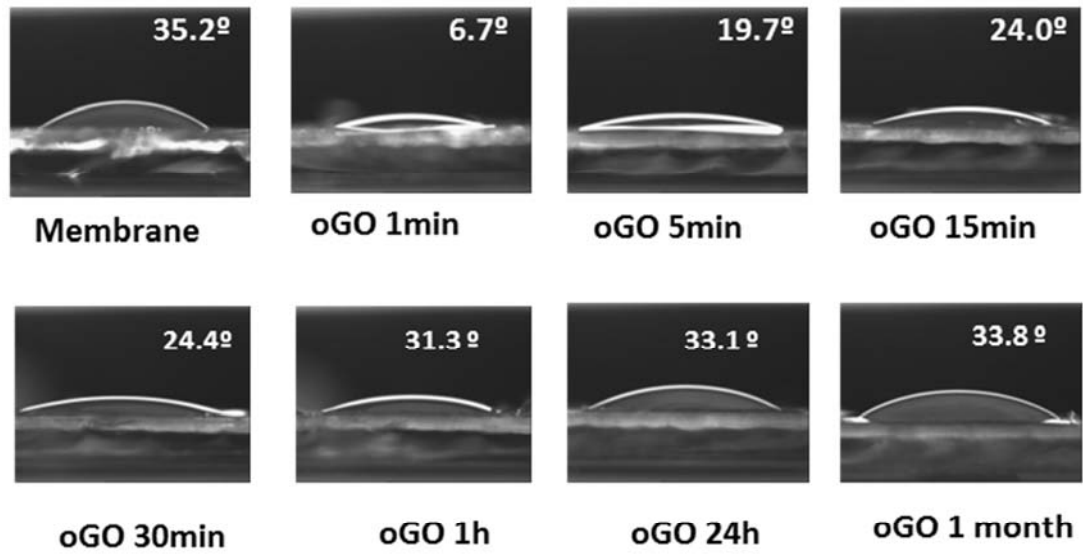


Figure S4. Hydrophobicity of GO film over time filtered on nitrocellulose membrane.

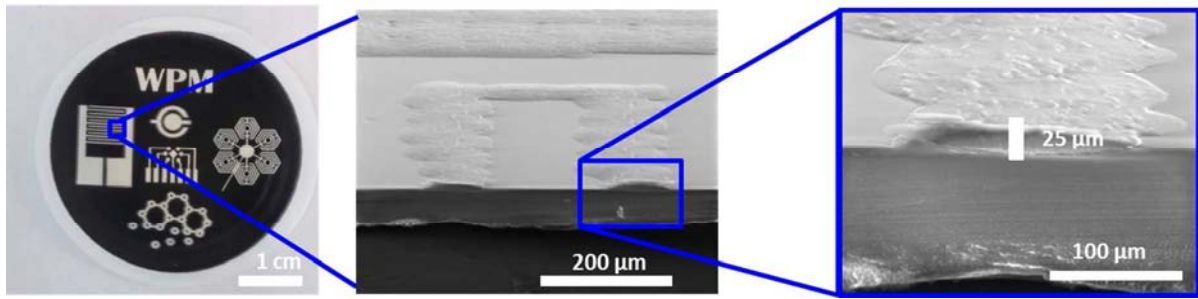


Figure S5. WPM with wax height.

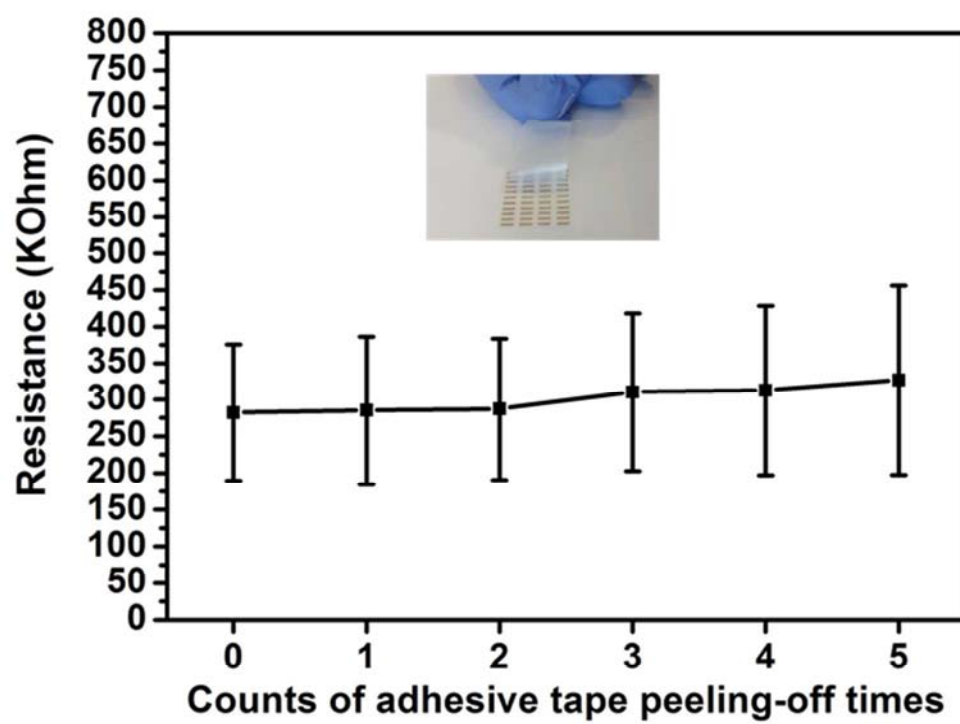


Figure S6. Adhesive peel-off wipe test. Inset: photo of conductive tracks after 5 peel-off counts.

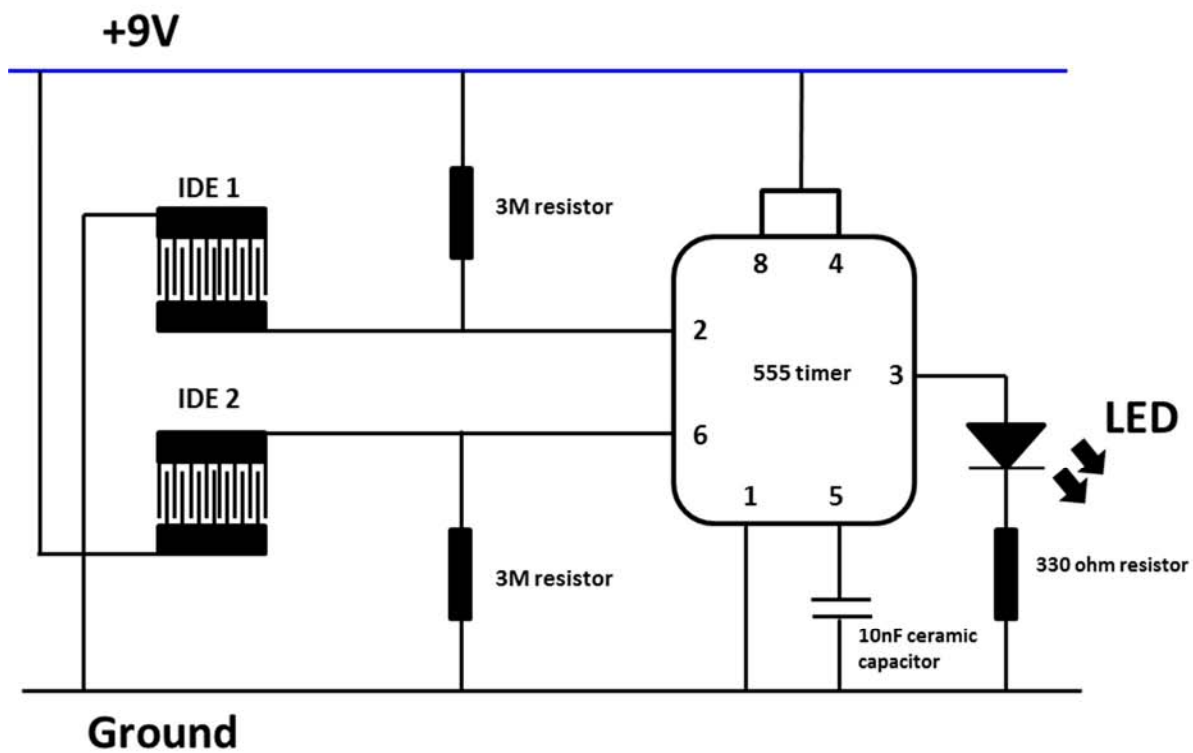


Figure S7. Electronic circuit used for the LED switcher.

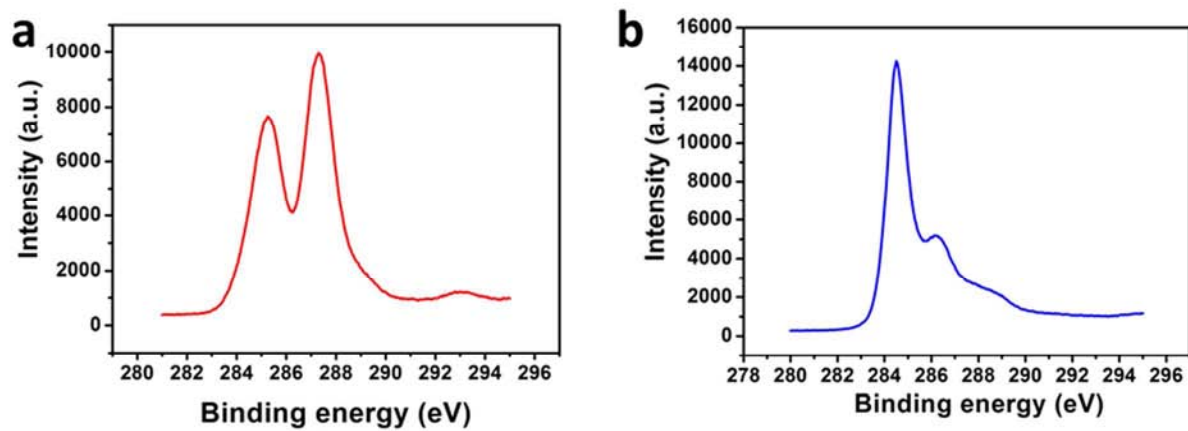


Figure S8. a) C1s spectra of GO and b) C1s spectra of rGO.

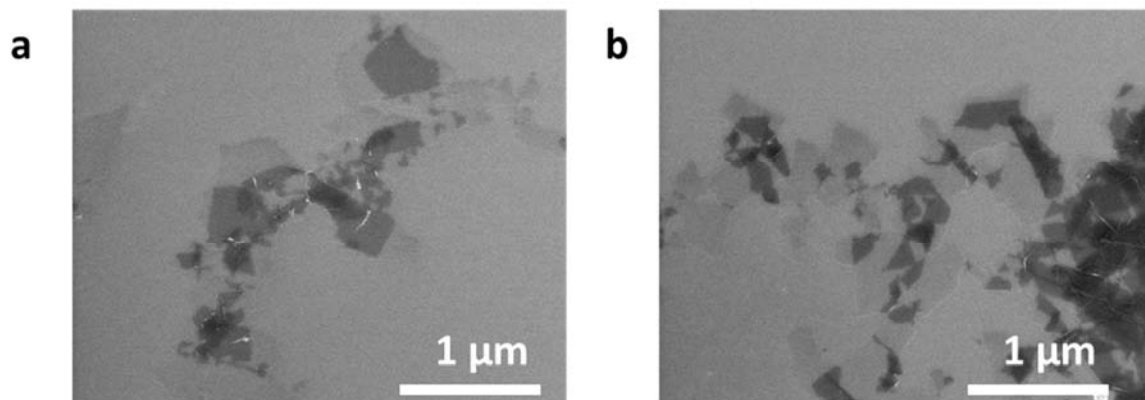


Figure S9. SEM characterization of a) GO and b) rGO.

The GO z-dimension (thickness) of the materials was *ca.* 1.0 to 1.2 nm. The maximum x-y dimensions were 554 nm. These data were provided by Angstrom Materials and are consistent with the SEM results (Figure S8).

Table S1. Resistance values evolution with adhesive peel-off wipe test.

	Initial	1st peel - off	2nd peel - off	3rd peel - off	4th peel - off	5th peel - off
Resistance/square (Kohms)	282.44 ±93.02	285.30 ±100.95	287.16 ±96.64	310.54 ±107.76	312.81 ±115.89	326.75 ±129.43

Acknowledgements

Tengo que empezar agradeciendo a **Anna Puig**, que ha contestado a ese email hace muchos muchos años de un chico que estudiaba en Aveiro y quería hacer unas prácticas en el grupo Nanobioelectronics and Biosensors. Sin ella no habría llegado aquí. Y más bonito todavía, fueran todos los años que compartimos enseguida, día-a-día con emoción y que me quedarán guardados para siempre en un rincón bonito en mi corazón.

A **Arben Merkoçi**, por me haber recibido y explicado que había una gente que estaba usando un lápiz para aislar un tal de grafeno y así empezó mi camino de investigación que resulta en esta tesis. Darte las gracias por la libertad que siempre me has dado para poder hacer mis mil y una “paranoias”, por haberme puesto los pies en la tierra cuando mi cabeza ya volaba por la luna, y por la buena onda con que llevas todo esto.

A **Briza Pérez**, que me recibió y guio en mi primeros años con su grande sonrisa y me enseñó todo lo que hay en investigación. Compartir su alegría en el laboratorio y en la vida fue un placer y sus consejos de madre y amiga fueron de grande importancia para ser lo que soy hoy.

A **Carmen Mayorga**, por su tranquilidad y amistad llevando conmigo todos los días (lo que nos es fácil), la alegría que era transformar algo en un electrodo para medir lo que fuera, y su buena onda siempre ahí para ayudarme. aaaa!!!!!!!!!!!!!! !!

Al gran asturiano, **Alfredo de la Escosura** que no es una persona tan seria como parece jejejeje pero que me ha acompañado todos estos años intentado que no bebiera toda la sidra que hay en Asturias.. ups.. intentado que enfoque y sea metódico para poder sacar las cosas adelante. Puxa Asturias.

Al loco **Parolo**, que es el más grande , más pancho y más listo – todo esto al mismo tiempo – que he conocido jamas! Sus trucos científicos los he aprendido de memoria, su tranquilidad para llevar el doctorado me han tranquilizado, y su gran capacidad para comer las sobras de la comida de los que están a alrededor se hecha de menos. Mil y unas birras hemos bebido y muchas mas beberemos aun que te hayas cambiado a vegeta y tengamos que beber birra de soja.

Al sol **Marisol**, a sus chuches, su risa que invadía todo el pasillo, sus uñas falsas, su locura y alegría! Una marquesa de las patatas, las birras y los chuches picantes. Como se te echa de menos.

A la Lena **Helena** células **Monton**, por la ayuda que me ha dado para crecer células en ambientes ultra contaminados bien a mi gusto, por juntarme con su gente, por haber estado ahí siempre que fue necesario, por haberme enseñado a escalar o a portarme bien jjejeje y por su stress animado que levantaba tempestades en un vaso de agua. Un gusto.

A **Gemma** madre **Aragay** con sus moléculas, seriedad, y trabajo arduo... jejejej..! la moral y confianza que me ha dado al principio en como lo podría hacer muy bien no la voy a olvidar.

A **Mariana Medina** y su capacidad para fabricar cualquier tipo de device, cualquier... todo es posible con Mariana poniendo las manos. Me ha enseñado muchísimo con todas sus infinitas herramientas, microfluidicas, sala blanca, plasma cleaner, screen printing y todo mezclado a la vez funcionando perfectamente era digno de clase de universidad que no había tenido.

A **Lourdes Rivas**, una professora de la química, a veces tranquila otras veces te pega tres hostias para que aprendas jejejeje me ha enseñado a hacer reacciones tan fáciles como una mezcla de mil acidos puros que resultan que hace chispas si les pones fibra de carbono. Siempre ha estado ahí, hay veces se esconde , pero cuando hace falta surge , te ayuda y te enseña con su buen corazon.

Al **Miquel Catalá**, que llevaba rocas en la mochila para hacer crecer la montaña que había en Terrasa y poder hacer excursiones todavía mas largas. Un personaje que no voy a olvidar.

A **Adaris**, con su música y juego de cadera bailoteando por el laboratorio! Alegría en persona.

A **Maria Guix**, siempre contenta y feliz por ahí, con sus micromotors y sus super videos. La chica mas feliz de todo el san Jordi!

A **Flavio**, que es todo un personaje por enseñar su propia lengua y a compartir pitis infinitos en la entrada.

A **Sergi** y su luisinho que nunca lo ha dejado de decir hasta el final jkejejeje

Al grande **Carlos**, buen amigo siempre ahí para ayudarte que me ha enseñado lo que es un asado argentino y un chimichurri que se come a cucharadas. El mas grande!

Al gran **Alex Chamo**, el tio mas buena gente que he conocido jamás, mi amigo y mi compi, el mejor viajero, el que te pone un laboratorio a funcionar el solo, el que se fuma un puro en el tejado de su casa, el que ha compartido y sigue compartido conmigo los mejores dias de mi vida, sea en Jaca, Menorca , Cerdanyolla o la Salut!!

A **Dani**, mi reportero fotográfico, el friki en persona, Dios de la química y de las moléculas con las mejores bromas científicas que he conocido y te dejan perplejo 5 segundos en silencio pensando donde habrá sacado este la broma. El que no bebe pero se traga un vaso de whisky en 2 segundos. El Mirkin del B2B.

A **Alex Zamora** al que he perdido el bus su casamento en un bonito dia de San Jordi jejejeje ¡!!

To **Deniz Baas** and **Amal Rabit** which I will allways keep their good friendship and discussion.

A **Marcos Rosado**, por crecemos juntos en esta caminata de los grafenos en los microscopios. Las mejores sesiones y las más animadas de SEM que he conocido.

Al señor **Onofre**, el gran capitán, el pirata de las baleares por sus enseñanzas.

A Alfonso del Rey, por haberme acompañado en nuevas rutas académicas.

A **Mireia Marti**, **Anabel Rodriguez** y a la Gran **ROSA JUAN** por toda la ayuda y buen corazón que han demostrado todo este tiempo.

Y a muchos otros que he compartido todos estos días .. que fueran bastantes..
algunos animados otros animados también =) .. como **Roque, Pablo, Carlos Carbonell, Jesus** ...etc.

Nos vemos por ahí ¡!